DEVELOPMENT OF A FIELD-BASED MOBILE PLATFORM FOR PLANT PHENOTYPING

A Thesis Submitted to the College of

Graduate and Postdoctoral Studies

In Partial Fulfillment of the Requirements

For the Degree of Master of Science

In the Department of Mechanical Engineering

University of Saskatchewan

Saskatoon

By

Mostafa Bayati

PERMISSION TO USE

In presenting this thesis/dissertation in partial fulfillment of the requirements for a Postgraduate degree from the University of Saskatchewan, I agree that the Libraries of this University may make it freely available for inspection. I further agree that permission for copying of this thesis/dissertation in any manner, in whole or in part, for scholarly purposes may be granted by the professor (Prof. Reza Fotouhi) who supervised my thesis/dissertation work or, in his absence, by the Head of the Department or the Dean of the College in which my thesis work was done. It is understood that any copying or publication or use of this thesis/dissertation or parts thereof for financial gain shall not be allowed without my written permission. It is also understood that due recognition shall be given to me and to the University of Saskatchewan in any scholarly use which may be made of any material in my thesis/dissertation.

Requests for permission to copy or to make other uses of materials in this thesis/dissertation in whole or part should be addressed to:

Head of the Department of Mechanical Engineering
University of Saskatchewan, College of Engineering
3B48 Engineering Building, 57 Campus Drive
Saskatoon, Saskatchewan S7N 5A9, Canada

OR

Dean
College of Graduate and Postdoctoral Studies
University of Saskatchewan
116 Thorvaldson Building, 110 Science Place
Saskatoon, Saskatchewan S7N 5C9
Canada

ABSTRACT

Design, implementation and performance verification of an affordable field-based high-throughput plant phenotyping platform[1] for monitoring Canola plants, including both data acquisition/visualization software and measurement system, was the main objective of this research.

The primary motivation for this research is the fact that breeders need a well-organized approach and efficient tool to monitor and analyze a number of plant traits to achieve a higher yield. At the moment, manual measurement is a conventional approach to gather the required information for plant analysis. Nevertheless, manual measurement has many limitations especially to study a large-scale field. To address this bottleneck, a high-throughput plant phenotyping platform (HTPP) was developed which consists of a data acquisition system, a data storage unit, and a data visualization and analysis software. Such an HTPP will be an essential asset for breeders to conveniently gather a comprehensive database which contains various information such as a plant height, temperature, Normalized Difference Vegetation Index (NDVI), etc.

To develop and implement such an HTPP, first, the overall system block diagram and required algorithms were drawn. Then to find the optimum set of equipment according to the requirement of this application, the performance of different sensors and devices were examined using literature search and experimental examinations in the laboratory setting. Then a mechanical boom was attached to the rear of a farm vehicle (a Swather) to carry different sensors, cameras and other measurement equipment (mechanical development of the boom structure was carried out by other members of the research team).

A control box containing power supplies, safety fuses, and a data logger unit was attached to the farm vehicle, and a program was developed for data logger to read sensors signals as well as GPS data for data geo-referencing and future retrieval purposes. The efficiency of different system architecture including different data transmission networks

[1] A robotic platform consisting of a set of hardware and software components for autonomous data collection

was examined by conducting several field tests to minimize existing errors such as delays in synchronizing different steps. Three programs were developed in MATLAB GUI for image acquisition via webcam and DSLR cameras as well as a central program for data processing and interactive data visualization.

The indoor tests were performed at the Robotics laboratory, University of Saskatchewan and outdoor experiments were performed on a Canola nursery at Cargill Canada, Aberdeen, SK, throughout spring-summer 2016 and 2017.

Finally, the performance and effectiveness of the developed field-based phenotyping platform was validated by various measures such as conducting some manual measurements and comparing the results with the values given by the platform. According to the achieved results, both hardware and software components of the proposed system meet the requirements of a field-based plant phenotyping platform as an essential asset for breeders for comprehensive study of Canola plants or any other cultivars as a result of some minor design modifications.

The main contributions of this study to plant phenotyping research are autonomous image acquisition capability, enhancement of the data acquisition cycle to minimize data geo-referencing error, development of a modular program for data visualization in MATLAB, and faster data collection in a high-throughput fashion (almost 125 times faster).

ACKNOWLEDGMENTS

I want to take the opportunity to thank my supervisor Prof. Reza Fotouhi who supported me in my research and gave me heartwarming guidance when I needed during my career as a graduate student. I am also thankful for the help of my advisory committee for the improvement and excellence of this research.

I also want to appreciate the time and provided groundwork that Dr. Katy Navabi, Ms. Amber Sawchuk, Mr. Michael Bateman and other staff at Cargill Canada dedicated to this research. I also want to thank my colleagues at Robotics laboratory, Dr. Rahim Oraji, Mr. Tyler Zhang and Mr. Farzam Ayatizadeh who helped me with my field experiments. Also, the technical collaboration of Mr. Matthew Conley at USDA, Arid-Land Agricultural Research Center is appreciated.

Last but not least, the help of other staff at the Department of Mechanical engineering and also college of graduate studies during my career at the University of Saskatchewan is greatly appreciated.

DEDICATION

This thesis is dedicated to my real life heroes, my mom, and dad,

who gave me pure love and sacrificed their dreams to make mines come true.

Being far from them during my studies was the hardest thing I've ever experienced in my life.

TABLE OF CONTENTS

LIST OF TABLES

Table Number page number

LIST OF FIGURES

Figure Number page number

LIST OF ABBREVIATIONS

HTPP	High-Throughput plant Phenotyping Platform
CO2	Carbon Dioxide
DSLR	Digital Single-Lens Reflex
FOV	Field of View
GIS	Geographic Information System
GPS	Global Positioning System
GUI	Graphical User Interface
HSI	Hyper Spectral Imaging
HTP	High- Throughput Phenotyping
IP	International Protection grading
IRT	Infra-Red Thermometer
LC	Light Curtain
LDS	Laser Distance Sensors
LIDAR	Light Detection and Ranging
NDVI	Normalized Difference Vegetation Index
NMEA	National Marine Electronics Association
QGIS	Quantum Geographic Information System
RGB	Red-Green-Blue
RTK	Real-Time Kinematic
SRS	Spectral Reflectance Sensor
TCP/IP	Transmission Control Protocol/Internet Protocol
ToF	Time-of-Flight
UAS	Unmanned Aerial System
UAV	Unmanned Aerial Vehicle
UGV	Unmanned Ground Vehicle

CHAPTER 1

INTRODUCTION

1-1- Background

According to the United Nations department of economics and social affairs, population division, continuously increasing human population will reach a remarkable number, over 9 billion, by the year 2050 [1]. Concretely, by considering this huge number of people and evaluating current state of available energy, water, and food resources, the first question comes to everybody's mind would be can enough food for next generations be surely supplied? Apparently, there is no exact answer for this question. However, the proper answer would be yes, as long as we start to manage available resources from now intelligently, and plan to competently increase the production by exploiting latest technologies to produce higher quality food and fewer leftovers, and then by taking the most advantage of restricted agriculture infrastructure.

To achieve and implement such a broad plan, plant science is focused on two main areas including genotyping and phenotyping. A genotype is a corresponding gene to some plant traits, e.g., height, and only can be determined by genetic tests, and hence needs special facilities and equipment to be studied. On the other hand, a phenotype is a plant physical characteristic and commonly can be observed and measured by human observations without the need of any extraordinary equipment.

The research on genotyping and phenotyping are technically two correlated subjects in plant science. Meanwhile, scientists need to know how genotypes are related to phenotypes and vice versa. In recent decades, many researchers have worked on genotyping in different means. Phenotyping; however, still has yet to be worked on because obtaining precise phenotypic data is always a challenging and problematic task which is primarily being done manually by a human. For example, to measure a plant height for studying the growth rate, researchers should go into the farm and measure this trait by a scaled bar or a tape measure. This can be a sustainable approach as long as a small-scale research is being directed in laboratory configuration. However,

it's not practicable if the farm is large and there are a significant number of plants to be studied in a short period of time.

Considering all needs and importance of phenotyping in plant science and current limitations to do this task with a reliable approach has stimulated the interest of many scholars. Indeed, not only researchers in agriculture and plant science but also in mechanical, electrical and computer engineering research are trying to define standard protocols and methods for designing and implementing such a high-throughput system to measure different plant characteristics in the most efficient way as possible.

The majority of previous works in this area has been proposed by utilizing sensors and imaging equipment to capture a limited number of characteristics of a plant in controlled environments and laboratory configuration. However, a few studies have been conducted for field-based phenotyping systems which offer the flexibly of scanning a notable number of plants in an actual field. That's why in this research an affordable field-based high-throughput plant phenotyping platform is developed to help breeders in data collection and visualization of a remarkable number of plants without any damage to crops in the actual field configuration. In next sections, different concepts for a plant phenotyping platform will be explained, and a literature review to examine the existing platforms for plant phenotyping is provided in section 1-7.

1-2- Plant Phenotyping Systems

The importance and significance of development of a plant phenotyping system were clarified in the last section. Having a closer look at existing plant phenotyping and trait measurement systems reveals that a plant phenotyping system consists of a mechatronic platform which physically or without any contact measures different traits using some sensors and also some pieces of program to create databases and more data analyses in the post-processing phase.

In fact, a plant phenotyping platform can be classified according to four criteria:

- Field-based vs. indoor platforms
- Mobile vs. stationary platforms
- Destructive vs. non-destructive platforms
- High-throughput vs. low-throughput platforms

A field-based plant phenotyping platform can be used in outdoor configuration and collects data in an actual field. Whereas, an indoor platform can only be used in a laboratory or a greenhouse. This constraint is mainly because of the utilized equipment specifications. For example, a sensor which is not water and dust resistant cannot be reliably used in the outdoor configuration.

A mobile plant phenotyping platform can travel all throughout the field while capturing data. While a stationary platform is a fixed structure that has to be attached predominantly inside a laboratory or a greenhouse. It is mentionable that a mobile platform is primarily intended to be used for rapid data collection in a large-scale field. Whereas, a stationary platform is more suitable for slower and higher accuracy measurements.

In a destructive plant phenotyping platform, the whole or part of a plant needs to be cut for more analysis. This means a plant will be lifeless after conducting measurements. However, a non-destructive platform doesn't damage the plant while measures different parameters. For example, an ultrasonic sensor can measure the height of a plant without any damage to plant itself.

Lastly, a high-throughput plant phenotyping platform can measure numerous parameters simultaneously (usually more than four) and stores a high volume of data in a database. On the other hand, a low-throughput platform provides a lower amount of data at the same time, and it is typically used when analysis of one specific characteristic of a plant is desired.

In next sections, plant phenotyping platforms will be classified in more in-depth categories according to the existing designs.

1-2-1- Manual and Hand-held systems

Hand-held systems are mobile, non-destructive, low-throughput and can be either field-based or indoor plant phenotyping platforms. The main idea of this design is moving a measurement device all over a canopy by a human and therefore there is no need for any complicated mechanical structure to carry scanning equipment [40]. This platform is the easiest and a cost-effective plant phenotyping system to capture different characteristics of a plant. Figure 1-1 illustrates a hand-held plant phenotyping platform.

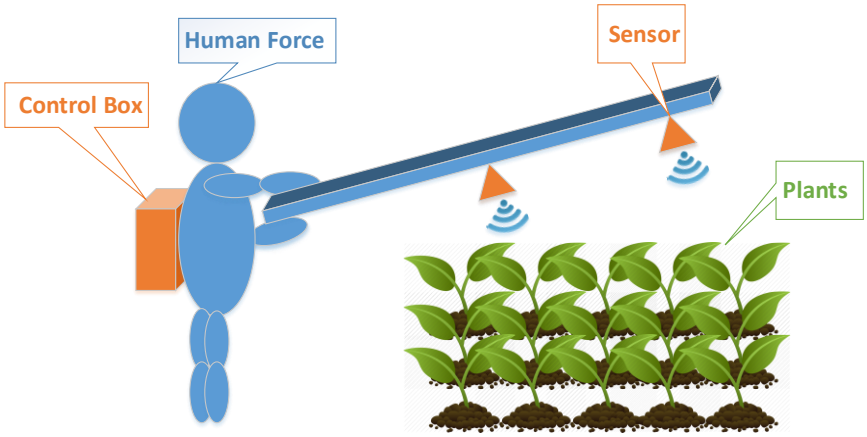

Figure 1-1: A hand-held plant phenotyping platform

Hand-held platforms are low-cost and can be conveniently transported. However, they are less advantageous for phenotyping of a large-scale field because the data collection process can be significantly time-consuming and the quality of measurements can be negatively affected by a human error.

1-2-2- Semi-Stationary Measurement Towers or Cranes

Another idea would be enhancing a hand-held platform by replacing a human with a crane or a tower which can be installed adjacent to the field and the sensors can be attached to tip of the tower to measure desirable traits [41]. Figure 1-2 illustrates an example of this scheme.

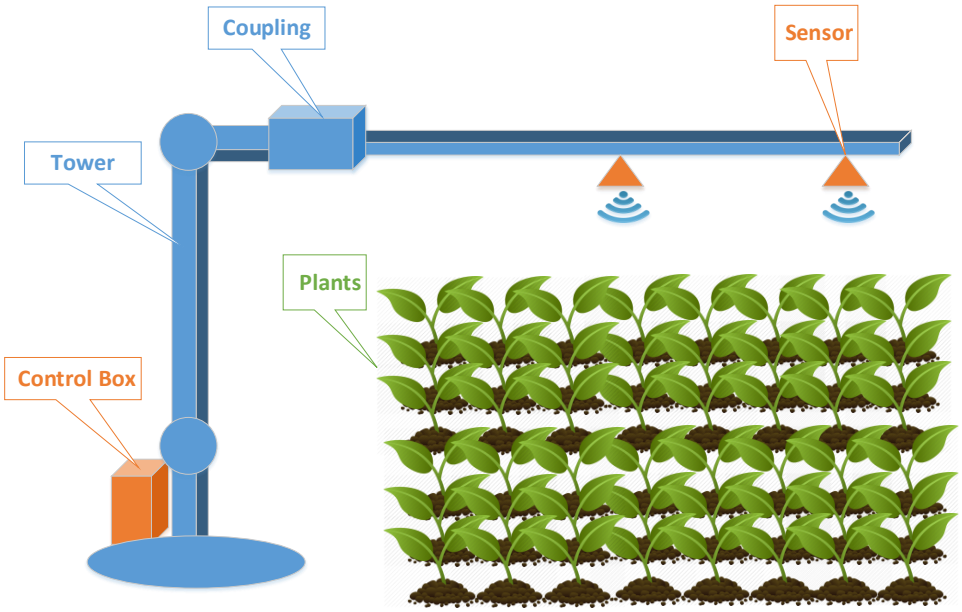

Figure 1-2: A semi-stationary plant phenotyping platform

This category of plant phenotyping platforms can be classified as field-based, stationary, non-destructive and low-throughput. It must be noted that the reason for being called "semi-stationary" is the fact that the utilized crane or the tower is immovable and fixed during the measurements, and it can be an effective choice to continuously analyze a small-scale field. However, this design is inherently costly because a sophisticated mechanical structure is needed. Also, this system cannot be used to scan a large area of plants at once because of the restricted field of view (FOV) of sensors.

1-2-3- Phenotyping Carts

Another cost-effective design of a phenotyping platform is taking advantage of a simple wheeled frame to carry different equipment such as sensors, power supplies and main computer [14]. According to the field condition, a one-wheel, two-wheel, three-wheel or a four-wheel frame can be used to carry scanning equipment. Figure 1-3 illustrates a typical two-wheel cart for phenotyping purposes.

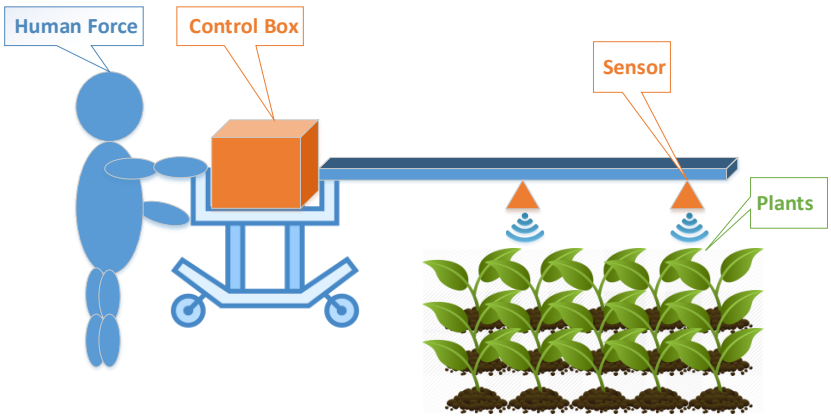

Figure 1-3: A phenotyping cart

Concretely, this design is more stable and is less prone to vibrations and measurement errors in comparison with a hand-held platform and also more cost-effective in comparison with a vehicle-carried plant phenotyping platform which will be discussed in next section. Apparently, a phenotyping cart still needs to be propelled by a human and this might not be quite convenient when phenotyping of a large-scale field is desired especially in summer. Lastly, a phenotyping cart can be categorized as a non-destructive, mobile, low-throughput, field-based platform.

1-2-4- Additional Boom Attached to a Vehicle

One of the most efficient approaches to design a powerful plant phenotyping platform would be taking advantage of existing farm vehicles and infrastructures such as tractors and sprayers [7]. This will considerably reduce the total cost of a phenotyping platform because there is no more need to build a complicated mechanical structure to carry different sensors and other scanning equipment.

Moreover, because of an existing suspension system in a farm vehicle, the scanning equipment are prone to a lower level of vibration and this feature helps to reduce the measurement errors. However, there is still a need for an additional mechanical boom to be attached to the front or rear of the vehicle as a fixing frame for different sensors. In other words, a farm vehicle needs to be retrofitted before being used as a plant phenotyping platform. Figure 1-4 illustrates an example for this design which was proposed in this research.

Figure 1-4: Using a farm vehicle and a boom for plant phenotyping

Last but not least, this design can be classified as a field-based, non-destructive, mobile, high-throughput platform.

1-2-5- Unmanned Aerial Vehicle (UAVs)

Unmanned Aerial Vehicles (UAVs) or drones are being used in many applications nowadays. More importantly, the attractiveness of using drones in agriculture has been significantly increased in past decades [18]. Indeed, drones are widely being used to identify pests and weeds, collect samples for laboratory tests, capturing aerial images, etc. Figure 1-5 illustrates a conceptual depiction of this design.

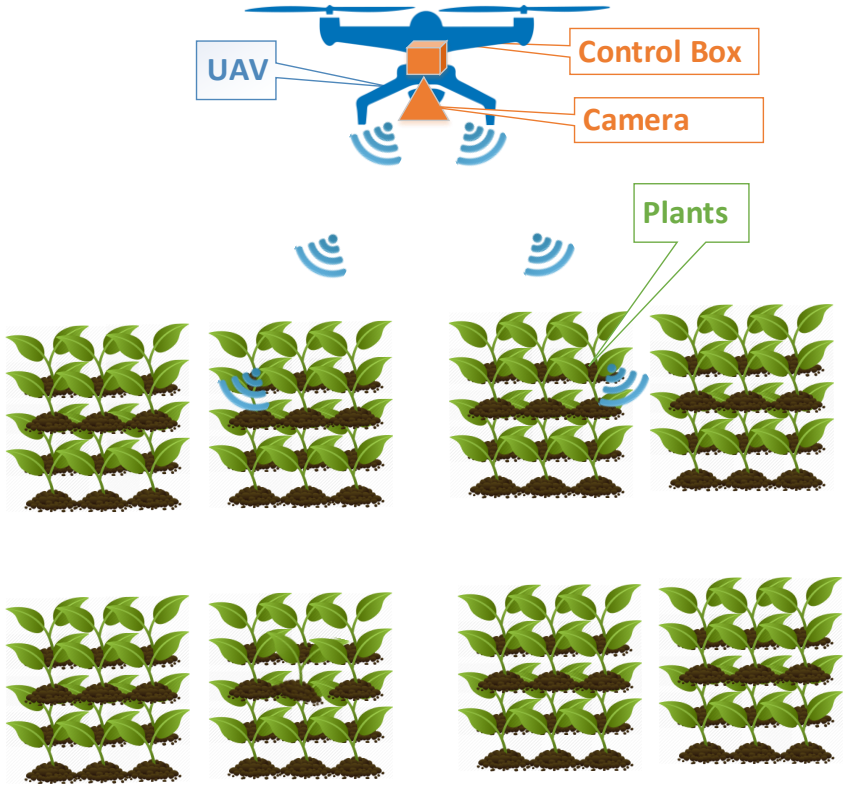

Figure 1-5: UAVs for plant phenotyping

Exploiting drones as a plant phenotyping platform seems a capable approach as they are agile and can easily maneuver in unreachable areas for ground vehicles. However, the following considerations should be taken into account before choosing a drone as a phenotyping platform. First of all, drones can only carry a limited number of sensors due to their payload capacity restriction. In fact, the more sensors are used, the more power is needed and a higher capacity battery is required which cannot be carried by many drones. Furthermore, speed and position

control of drones is more problematic than ground vehicle especially when they are being used in a not entirely calm and settled weather conditions such a windy day.

These field-based, non-destructive, mobile and high-throughput aerial vehicles can be a suitable choice for remote image acquisition especially spectral imaging, yet not advantageous for being used in near ground maneuvers or carrying other sensors such as ultrasonic or laser distance sensors due to their highly restricted payload.

1-2-6- Autonomously Navigated Robots

Development of agricultural robots has been a favorite topic in robotic research. Also, different methods and algorithms have been exploited to navigate a robot without need for a human observation and to control its operation in field conditions. In other words, robots can be tremendously advantageous in the agriculture industry for different purposes and more importantly for field-based plant phenotyping [16].

Figure 1-6: A typical autonomously navigated robot for plant phenotyping

In fact, the main idea of this design is using an autonomously navigated robot instead of a manually driven vehicle to carry scanning equipment to achieve a more accurate motion control and to decrease the dependency of the plant phenotyping platform to human intervention. Such a platform can be used in severe weather conditions and also is capable of carrying several sensors and scanning equipment simultaneously to minimize the required time for data collection in a high-throughput plant phenotyping platform. Figure 1-6 illustrates a mobile robot developed in the robotics laboratory at the U of S for the outdoor and agricultural applications.

1-2-7- Wireless Sensor Networks

Another idea to implement a plant phenotyping system would be taking advantage of wireless sensor networks to analyze plants. In other words, sensors and scanning equipment can be distributed all over a field, and then all data can be transmitted over a wireless network to a central database. Figure 1-7 illustrates a phenotyping system based on a wireless sensor network.

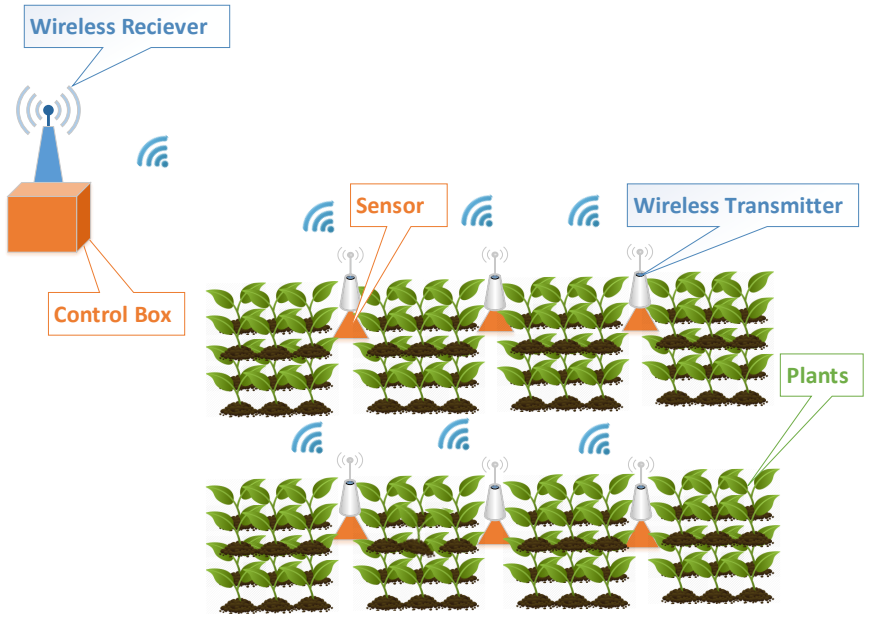

Figure 1-7: A plant Phenotyping System based-on wireless sensor networks

Apparently, this idea appears the most robust method to be used as a plant phenotyping platform because a real-time monitoring capability for every individual plant can be achieved. However, high cost and occasionally unfeasibility of implementing such a large-scale network in a real farm are among the weaknesses of this method as a plant phenotyping system.

1-3- Motivation of Study and Problem Statement

The need for a plant phenotyping platform to measure and capture different characteristics of a plant in a real field configuration has been comprehended. Considering existing solutions reveals that although some research have been devoted to design different plant phenotyping platforms with their distinctive capabilities, less attention has been paid to development of an all-inclusive program for data visualization and post-processing in a field-based high-throughput plant phenotyping platform. Moreover, none of the existing platforms

offer simultaneous data collection and autonomous image acquisition capability. So a measurement system consisting of different sensors and scanning equipment was developed and integrated, and also a customized program with an interactive graphical user interface was designed as a first generation field-based high-throughput plant phenotyping platform.

In this research project, the primary focus was on phenotyping of canola plants in a field consisting of 252 individual plots, and a farm vehicle (a swather) was used to carry scanning equipment. However, the proposed open-end system architecture is capable of being used for phenotyping of other plants by minor software and hardware modification. Figure 1-8 illustrates a drone captured image of a typical canola field containing many plots.

Figure 1-8: A drone captured image of a Canola field (Photo credit: Cargill Canada)

Furthermore, the proposed plant phenotyping platform is capable of being retrofitted to introduce a more advanced version of an entirely autonomously navigated plant phenotyping robot. In fact, advantages of mobile robots can be taken by replacing the utilized farm vehicle to carry sensors and measurement devices. Figure 1-9 a) and b) illustrate two versions of developed booms for the proposed plant phenotyping platform.

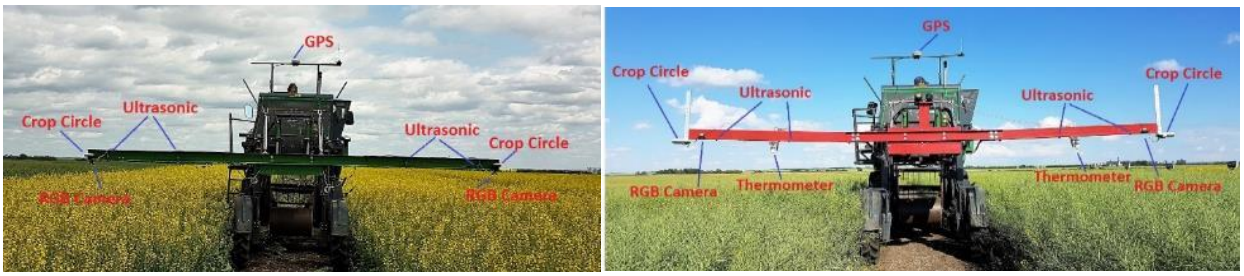

Figure 1-9: Developed phenotyping platform a) version one, un-foldable mechanical boom b) version two, foldable boom for convenient transportation

With design and development of such a plant phenotyping platform comes a series of challenges to be addressed, listed as follows:

1. There are many sensors and equipment to be used for measurement of different physical or chemical characteristics, but only a few of them meet the requirements of a field-based plant phenotyping platform. To select the most efficient components, similar researches and designs should be assessed, and their pros and cons should be identified. Indeed, firstly, a comprehensive study of literature should be done, and existing platforms should be evaluated. Secondly, the performance of each component in laboratory configuration needs to be examined before being employed in the actual field. This laboratory examination will significantly reduce spent time and budget to design the final version of the proposed plant phenotyping platform.
2. The data acquisition unit should be capable of communicating with a variety of sensors and equipment which use different protocols and standards when translating physical parameters to electronic signals. Also, spare inputs/outputs should be dedicated in design to offer the flexibility and capability of integrating more sensors or scanning equipment in future, if needed. Moreover, the operation system of the data acquisition unit should be able to handle numerous concurrent tasks to save all information in a data file without any misrepresentation or data distortion.
3. To be able to precisely associate data with corresponding plot and visualize them after data collection, all data points should be geo-referenced using an accurate global positioning system (GPS), but precise GPS units are costly and may not be affordable for many researchers to be used in a plant phenotyping platform. However, nowadays some farm vehicles are equipped with an accurate GPS for intelligent seeding and harvesting purposes. So there should be a solution to extract data out of an existing GPS on a farm vehicle to geo-reference collected phenotypic data and images without any interference with the normal operation of the vehicle itself. Furthermore, there is only one GPS antenna available on top of the vehicle, so a function should be developed to calculate the location of each sensor to the data given by GPS in the spherical coordinate system.

4. The plant phenotyping platform must be able to simultaneously collect all data including red-green-blue (RGB) images and other desired phenotypic data in only one traverse of the entire field. This is an essential capability if phenotyping of a large-scale field is desired, so it will be significantly time-consuming and frustrating to repeat data collection more than once. Hence, the data acquisition and image acquisition programs should be developed so that they can be executed concurrently and independently.
5. An inclusive software should be developed to visualize raw data files. Developing an interactive graphical user interface (GUI) can be a helpful tool for this purpose so that users will be able to monitor any desired plot by clicking on any available measurement points. Moreover, the software must be developed using an efficient and easy to use programming language and must be capable of customization and ability to add more features in future for advanced data analysis.
6. There should be a series of verification strategies to confirm the accuracy and reliability of the plant phenotyping platform with an acceptable level of measurement error. For example, using random manual measurements and placing visual signs next to each plot can be a right approach for confirming the validity of captured images and collected data.
7. To develop a mobile plant phenotyping platform, different mechanisms and solutions can be utilized to attach sensors and scanning equipment to a farm vehicle. The employed mechanical structure must be designed most finely so that it meets the requirement of each component to operate accurately, and also causes minimum damage to the plants while doing measurements. Moreover, the mechanical structure should be highly flexible to be used in future for phenotyping of diverse plant species with different height and density. The mechanical design of the structure was carried out by other members of our research group. However, to collaborate with the mechanical design team, I provided required inputs such as physical dimensions (weight, volume, etc.), operating conditions (field of view and range of operation, etc.) of measurement equipment to be attached to the vehicle.

1-4- Objectives

This study is looking for an answer for this research question: How can we exploit the automation technologies to capture different characteristics of a plant instead of the commonly used approach which is manual measurement? What set of sensors and equipment can be reliably used for this purpose?

This research has two main objectives in particular. ***First, to develop (design/fabricate) the electrical and software components of an efficient data acquisition and monitoring system for plant analysis (development of a new field-based high-throughput plant phenotyping platform). Second, to validate the effectiveness of the developed platform by studying a canola nursery during the plant growth season.*** These objectives can be broken down into the enlisted sub-objectives below:

1. To study the current status of plant phenotyping research, and to identify the advantages and disadvantages of existing designs. Also, the requirements of an efficient field-based plant phenotyping platform need to be specified to be considered in design phase.
2. To design and develop a measurement system, and to retrofit the electrical system of a farm vehicle for precision agriculture, and particularly for plant phenotyping purposes.
3. To develop different programs and customize them for real-time data and image acquisition in a field-based mobile platform to achieve the possibility of future retrieval of captured plant characteristics.
4. To find a reliable approach for mapping a field (extracting the latitude and longitude information), and to geo-reference the collected data using global positioning system.
5. To develop an inclusive program using MATLAB GUI for interactive data visualization to represent a significant amount of data to breeders in a user-friendly manner.
6. To validate the efficiency and accuracy of the developed plant phenotyping platform using different verification strategies, and to semi-autonomously analyze a canola field during the growing season (between June 23 and August 18) to create phenotypic databases (containing different characteristics of plants) for more advanced statistical analysis by breeders in future.

1-5- Methodology

This research was conducted in different steps that resulted in proposing and testing a new field-based high-throughput plant phenotyping platform to study canola cultivars primarily. These steps can be summarized as follows to achieve the mentioned objectives:

1. Several field visits and meetings were done with a senior breeder and farm technical experts from Cargill Canada to define breeders' needs and expectations from a plant phenotyping platform. These meetings and brainstorm sessions were carried out until end of the research to enhance the performance of the proposed system. Also, a thorough study was performed on almost all well-known existing plant phenotyping platforms, and their pros and cons were identified to define the current gap in this field.
2. Some conceptual drafts, system block diagrams, and required tasks and algorithms were drawn. Then a long list of candidate equipment and devices was made for an in-depth investigation. To find out more about the efficiency and performance of the chosen material, several communications were done with different manufacturers to make sure nominee equipment can be efficiently used in our application. Subsequently, the first set of equipment was purchased in fall 2016, and a series of preliminary experiments were performed in laboratory configuration before actual field experiments. For example, the performance of an ultrasonic sensor to measure the height of a plant was examined in robotics laboratory, University of Saskatchewan. Finally, the first generation of a plant phenotyping platform capable of height measurement and capturing the image was developed, and a series of experimental field tests were conducted in a canola field in fall 2016. This included design and fabrication of a long mechanical boom which carries four ultrasonic sensors. At the end of the first round of experiments, the result was inspected, and existing flaws in the early design and ways to improve the performance of the system were identified. Then more sensors were chosen, purchased and tested in the laboratory to be used in 2017.
3. Data and image acquisition programs were debugged and significantly enhanced for better performance. For example, different sources of error including the delay in synchronizing GPS data with the measurement points were identified, and a novel

software solution was proposed to minimize the negative effect of the existing issue. Finally, the enhanced plant phenotyping platform was assembled and prepared for field experiments in summer 2017.

4. Because there was no accurate hand-held GPS system, nor a local map to locate individual plots in the studied nursery, different approaches were used to create a customized map of the studied canola nursery and to offer an accurate geo-referencing capability. The same method can be extended in future to map other fields.
5. A program with a graphical user interface was developed to visualize all collected data and to offer the possibility of the future data analysis. In fact, the need for a software to interactively represent all collected data to the user was acknowledged, so that the collected data could be conveniently imported into the developed program and the available information for individual plots could be represented as some graphical objects.
6. The developed field-based plant phenotyping platform was used, and nine times field experiments were performed to collect data during summer 2017 between June 23 and August 18. Also, it was tried to continuously enhance the performance of the developed plant phenotyping platform after every field experiment by evaluating the results until the measurement system was re-assembled on a second-generation mechanical structure which was designed for convenient transportation of the platform as can be seen in figure 2-64. Finally, the result of measurements and geo-referencing were validated to examine the reliability and accuracy of the developed algorithms and collected data. For example, several visible signs were placed at the known locations in the field, and the performance of the developed program to locate those signs was examined during several experiments. Also, the result of several manual height measurements was compared with the height data collected by the platform to validate the accuracy of measurements.

1-6- Outline of the Thesis

This thesis consists of 5 chapters and 6 appendices. Current chapter, provides a background knowledge and overview of plant phenotyping platforms for better understanding of the person who reads about the subject to be able to follow up provided topics in next chapters. Also, problem definition, motivations, objectives and methodology of this research is discussed

in current chapter. Furthermore, a comprehensive literature review and examination of the existing designs in plant phenotyping research is provided at the end of current chapter in section 1-7. Chapter 2 gives the breakdown of developed hardware and measurement system for plant phenotyping platform and also provides an overview of different approaches to measure different characteristics of a plant. At the end of this chapter, the system block diagram of proposed phenotyping platform in 2016 and 2017 is provided. Chapter 3 describes the details of developed programs for data acquisition, capturing image and also data visualization. Also the detail of utilized data geo-referencing method is discussed in this chapter. Chapter 4 discusses experimental field examinations that were performed during fall 2016 and summer/spring 2017 and aimed to demonstrate the performance and efficiency of proposed plant phenotyping platform after explaining the results of phenotyping a canola nursery between June and August 2017. Also, the details of utilized methods to map a canola field is discussed in this chapter. Chapter 5 brings a conclusion of this research as well as some suggestions for enhancement of current design for future work.

1-7- Literature Review

Not many researchers have developed and published on the development of high-throughput plant phenotyping systems in field-based condition. However, a substantial amount of works have been done on different methods to automate and minimize the need for human power and observation to capture different characteristics of a single plant in laboratory configuration. In this section, the most sophisticated high-throughput plant phenotyping platforms and technologies have been introduced to the time being, as well as some previous studies on exploiting autonomous and semi-autonomous systems in agriculture is discussed. It was tried to focus on the utilized technologies for plant phenotyping rather than their results related to phenomics and crop science which is out of the scope of this research.

Before discussion and evaluation of the existing plant phenotyping platforms in this section, some reference publications are introduced in next three paragraphs for better understanding of the plant phenotyping research and its significance. These studies can be a valuable source for researchers who are about to start to develop a plant phenotyping platform.

Robert T. Furbank and Mark Tester explained why plant phenotyping research is essential and reviewed some of the existing plant phenotyping platforms [2]. Also, they explained what the concept of phenomics-genomics pipeline is and how phenotypes are correlated to genotypes. Moreover, they reviewed various possible methods to measure different plant traits including temperature, chlorophyll and a plant growth rate.

Juan M. Montes and others explored and clarified how novel plant phenotyping platforms could be useful and a crucial asset in genetic science [3]. They specifically concentrated on effectiveness and importance of spectral reflectance of plant canopy in genetic studies.

Joshua N. Cobb and others proposed a comprehensive study on the requirements of an efficient plant phenotyping system and explained how phenotyping could be useful in different genetic studies [4]. Moreover, they provided a list of nominated image analysis software and phenotyping platforms that was present at their time for various applications. They also discussed in-depth about the recommended procedure to extract, analyze and store phenotypic data for better performance.

Researchers at the Kansas State University proposed a field-based high-throughput phenotyping platform which was attached to a farm vehicle (a high clearance sprayer), and the performance of their system was evaluated on wheat and soybean plants [5]. In their design, canopy height, temperature, and reflectance were three target traits to be measured and analyzed. Their proposed data acquisition system consists of a National Instrument LabView software [6] and an interface hardware module to convert sensors analog signals to a readable digital data for a computer.

In fact, proposed plant phenotyping platform at Kansas State University was one of the primary references for the current design in this research, and it was an innovative design in high-throughput plant phenotyping research. Nevertheless, some fundamental issues can be perceived in their design which was tried to be addressed in this research. The main weakness in their design is the fact that there is no image acquisition system in their proposed high-throughput phenotyping platform. Concretely, capturing RGB images of cultivars is as important as collecting data using different sensors, and a single RGB image can be an informative source of data to analyze a plant. Besides, it is more convenient and reliable to validate the accuracy of the

proposed geo-referencing algorithm by taking a look at the pictures rather than comparing the numeric data with some random manual measurements. Indeed, relying merely on a human observation to capture field conditions at the time of data collection might not be accurate enough. The next issue with proposed design by researchers at Kansas State University is the resulting amount of positioning error. In fact, they achieved a maximum positioning error of 17.9 cm which appears a substantial level of error and seems unacceptable for a highly accurate plant phenotyping system. For example, if plants are arranged side by side in small plots (similar to the arrangement of the studied canola field in this research), this design doesn't seem reliable enough because collected data for each plot might be misrepresentative due to the positioning error. The third issue is using a laser sensor for height measurement which is not able to detect small objects including tiny branches of some plants such as canola. Also this sensor can be negatively affected by ambient light if it is not enclosed by a proper case and can significantly reduce the overall system performance. However, the laser scanner can be used in laboratory configuration to measure height of plants with a relatively large leaf area with no problem. So it is suggested to avoid using a laser sensor for height measurement purposes in a field-based high-throughput phenotyping system.

Another sophisticated high-throughput plant phenotyping platform is proposed by researchers from the University of Arizona, Cornell University and U.S. Department of agriculture, agricultural research service, Arid-Land agricultural research center [6]. In their design, a sprayer was retrofitted to carry measurement equipment. Canopy height, Normalized Difference Vegetation Index (NDVI) [7] and also temperature were target traits to be analyzed. Furthermore, they evaluated the performance of their proposed plant phenotyping platform by conducting field tests on Pima Cotton plants.

The most important aspect of their study was the diversity of the utilized test conditions and scenarios they have surveyed in their experiments. Indeed, their research was not only targeted the design of a high-throughput plant phenotyping system but also focused on plant science and phenomics aspect as well. For example, they designed and conducted their experiments on well-watered and water-limited conditions to study the behavior of the Pima Cotton plant in different situations. Moreover, they examined the performance of hand-held

measurement devices for plant phenotyping and also an externally mounted measurement package on a helicopter to capture near-infrared and thermal images.

Nonetheless, it seems there are some flaws and techniques to enhance the performance of the proposed phenotyping platform at the University of Arizona. In fact, their design can be improved by considering some points to achieve a highly efficient field-based high-throughput plant phenotyping platform. For example, the data collection architecture should be more integrated. Meanwhile, their proposed design is based on more than one datalogger unit to store sensors data, and apparently it is not entirely convenient to extract data files out of two or more data storage units in the field. This complicated structure significantly increases the dependency of the system on direct supervision of an expert user during and after field experiments to make sure everything is working well. If the memory capacity or communication protocols of a single datalogger is not adequate to meet the system requirements, it is better to use a dedicated data acquisition hardware module and software running on a high-end laptop to take over this task similar to the introduced design at the Kansas State University [4].

The second issue that can be addressed in the proposed design at the University of Arizona is the proposed visualization and data processing software. Indeed, they developed two plug-ins for Quantum Geographic Information System (QGIS) software package [8] for geospatial data processing and user interface which does not seem flexible enough for advanced data post-processing in a high-throughput plant phenotyping platform. For example, if MATLAB or LabView was used as the main software, their proposed phenotyping system could have had the capability of further post-processing on captured images and other available data. So, development of an extensive and integrated software which consists of different modules and can concurrently handle all these tasks will be significantly helpful, and it will be an essential feature in a highly efficient high-throughput plant phenotyping system.

Another improvement in the proposed design at the University of Arizona can be done through enhancing the algorithm for geo-referencing. In their design, raw data is processed and GPS string is broken down into useful pieces (e.g., longitude and latitude) in every data acquisition cycle in real-time. Nevertheless, any real-time processing of the GPS data at the time of data acquisition is time-consuming and significantly slows down the system response, and

should be done in post-processing programs after completion of data collection. In other words, if only raw GPS string were captured in real-time combined with sensors data, then it could be broken down into useful pieces for data geo-referencing in post-processing programs where processing time is not strictly constrained.

Furthermore, similar to the existing issue in the proposed design at Kansas State University, the absence of an image acquisition feature to capture RGB images at the time of data collection can be seen in the University of Arizona's design. However, they might obtain pictures after or before collecting data as an individual process, but this is not an acceptable approach if phenotyping of a large-scale field is desired because it can be quite time-consuming and frustrating to scan the whole field twice.

Another field-based high-throughput plant phenotyping platform was proposed by researchers in Germany [9]. In their research, the development of a tractor-pulled non-destructive phenotyping platform was proposed. Their system was named "BreedVision" and it was primarily intended to be used for phenotyping of small grain cereals.

As specified by authors, existing phenotyping platforms were not sophisticated enough at the time of their study, and they were typically using a single sensor to measure a specific characteristic of a plant but BreedVision overcame this drawback by using various sensors and utilizing data fusion concept.

In fact, BreedVision exploited four different type of sensors to measure diverse plant characteristics including a laser distance sensors (LDS) to provide the height of the plant and tiller density information. A 3D Time-of-Flight (ToF) camera to deliver three-dimensional details of plants. Light curtain (LC) imaging which was a linear set of stacked light barriers and was intended for height and tiller density measurement purposes. A hyperspectral imaging (HSI) camera which was a transmission spectrograph based on a line scan method, and was suitable for in-situ plant moisture content determination. Their HSI camera could cover the wavelengths between 970 nm and 1670 nm. More technical information about the utilized sensors such as power consumption and data transmission protocols were explained in their publication which can be a useful resource for other researchers who aim to develop a similar platform.

Moreover, it is stated that each sensor on BreedVision has its local processor to optimize the data communication traffic. All data sets were logged in a MySQL [10] database which was installed on a central computer. The developers of BreedVision platform declared two phases for phenotyping of a plant. Firstly at trait calibration stage, some data set, which were gathered manually, had to be imported into the software and then at trait determination stage, the software could calculate some phenotyping values according to the sensors data. Lastly, the performance of BreedVision was examined during two consecutive field experiments at Stuttgart, Germany in 2011 and 2012.

Despite all advancements and innovative ideas in the BreedVision development, some issues can be seen in their design that should be addressed to have a more robust and efficient high-throughput plant phenotyping platform. The first and most principal imperfection in their design is the fact that all sensors had to be enclosed in a black shield to avoid the effect of ambient light in operation of light curtain and laser sensors. Also, all sensors had to be lined up on top of the plants to be able to measure different traits. This can be only a practical approach for phenotyping of small plants, yet not applicable to be extended for larger plants which can be grown up to 1.5 meters (e.g., Canola).

The second ambiguity in BreedVision design is the developed algorithm for spatial data analysis and data geo-referencing. There are some figures that display their utilized positioning system offers highly accurate measurement with a millimeter accuracy without using an RTK GPS system. However, it is not well explained what the mapping algorithm was as they utilized a simple USB GPS unit that can only provide maximum 2.5 meter positioning accuracy according to the GPS manufacturer datasheet [11].

Last but not least, BreedVision was merely able to scan one plot at the same time due to its controlled mechanical and measurement system design, and it can be quite time-consuming if phenotyping of a large-scale field is desired.

Another field-based high-throughput plant phenotyping platform was proposed by researchers at the University of Nebraska-Lincoln [12] based on an existing proximal sensing cart which had to be propelled manually by human power [13]. Three different traits were targeted in their design including canopy height, temperature, and NDVI. Moreover, studies were

concentrated on phenotyping of soybean and wheat plants. Also, a RGB camera and a portable spectrometer were used in their design to calculate NDVI and greenness of plants.

Despite the fact that using NI LabView and development of a user-friendly interface was a notable result of the proposed plant phenotyping platform at the University of Nebraska-Lincoln, using stop-measure-go fashion to capture different parameters and take pictures was a principal problem. Meanwhile, it is not conceivable to use the stop-measure-go method to phenotype a field consisting of more than 500 plots. Besides, the utilized GPS unit was only able to provide 20cm positioning accuracy which is not acceptable for a highly accurate plant phenotyping system. Furthermore, a Spectral Reflectance Sensor (SRS) by Decagon Device [14] was used for spectral analysis which has a slow response time (600ms) and not quite suitable for a mobile plant phenotyping platform which needs to capture data in a fraction of a second while the carrying vehicle is moving. Moreover, using this sensor with slow response time and the stop-measure-go fashion design significantly restricted the maximum travel speed of the phenotyping platform. For example, it took 3 hours for them to scan a field consisting of 240 wheat plots in only one experiment and concretely this slow scan rate is not acceptable for phenotyping plants in large-scale fields. However, in proposed design in this thesis, it takes less than 20 minutes to scan a field consisting of 252 plots.

Another plant phenotyping platform is "BoniRob" which was proposed by Bosch Deepfield Robotics [15]. BoniRob is a multi-purpose autonomously navigated robot for an agricultural application which is based on a four-wheel drive mobile robot and utilized hydraulic components offer a highly flexible mechanical structure. Also, spectral imaging and 3D time-of-flight cameras and an RTK GPS were added to BoniRob for plant phenotyping purposes. Moreover, maize and wheat are two plants that primarily were considered for field experiments and performance assessment.

One of the interesting features of BoniRob is offering a 3D simulation environment based-on Gazebo software [16] which can communicate with a robot in real-time. Also, the mechanical design of this robot seems robust and efficient for outdoor and agricultural experiments. However, there is not enough information available about BoniRob software for data acquisition to assess the efficiency of this robot particularly as a high-throughput plant phenotyping

platform. The first ambiguity about using BoniRob as a high-throughput plant phenotyping platform is the data storage architecture which is not clear how data can be stored and conveniently retrieved for post-processing and future analysis. Furthermore, it is not clear what is the maximum scan time in one data collection cycle and whether there is any delay issue in data geo-referencing algorithm or not. Last but not least, there are many sophisticated robots armed with highly elegant features available at the market, but not many of them affordable to be used as a high-throughput plant phenotyping platform. So BoniRob, as a multi-purpose agriculture robot, appears to be a highly expensive product and should be explicitly retrofitted for plant phenotyping applications before being used as a high-throughput plant phenotyping platform.

Another study was presented by researchers at Aalborg and Copenhagen Universities for mapping weeds in sugar beet fields as a part of a more significant project [17]. They utilized an innovative method to detect weeds on a field by image processing and classification algorithms [18]. To do so, first an unmanned aircraft system (UAS) was deployed to capture aerial images from high altitudes, and after processing aerial photos and finding the candidate areas, an unmanned ground vehicle (UGV) was dispatched to the areas that need more courtesy and observation. Then UAS decreases the altitude to focus more closely on candidate areas and this process continues until the weed is verified and located on a customized map. Lastly, Genetic algorithm was used for path planning in UGV to scan the identified locations by UAS [19].

The proposed design at Aalborg and Copenhagen Universities can be a good idea in the development of a plant phenotyping platform specifically for capturing spectral images to measure NDVI and also for leaf area measurement. In fact, the advantages of drones and ground vehicles can be merged to propose a highly accurate collaborative measurement system.

Although, the proposed real-time image processing and classification algorithm on the UAS was not explained clearly to assess its performance because image processing is an inherently time-consuming task and more importantly can be a significant source of error when real-time image processing is required.

Another plant phenotyping platform was developed by the chair of plant nutrition, department of plant sciences at the Technical University of Munich and it was called PhenoTrac

4 [20]. Gero Barmeier and Urs Schmidhalter developed PhenoTrac 4 primarily for high-throughput phenotyping of winter wheat and barley plants in 2014. PhenoTrac 4 was armed with a RTK GPS, hyperspectral imaging sensors, temperature sensors and distance sensors for height measurement purposes. Moreover, Pablo Rischbeck and others took advantages of PhenoTrac 4 to capture height and thermal parameters over a four years study for yield prediction of drought-stressed spring barley [21]. They utilized multiple linear regression and partial least square models to improve yield prediction.

Another pant phenotyping robot was proposed by Thomas Bak and Hans Jakobsen for weed detection using image processing [22]. Their system was designed based on a PC 104 system [23] as the central computer to control the motion of the robot and running navigation algorithms, and a camera was used for row guidance and weed detection purposes. Also, a unique four-wheel drive mechanism was designed to make the robot flexible to maneuver and travel in any directions including parallel displacement during turns at the end of each rows.

Nonetheless, a main issue that can be addressed in their design is the size of the robot. Their robot doesn't seem a high clearance vehicle so it should be retrofitted to be used for high-throughput phenotyping of bigger plants such as Canola. For example, an additional robotic arm or mechanical boom could be designed to expand the workspace of the proposed robot.

Another design was proposed by Lin Haibo and others which was a wheeled robot for wheat precision seeding [24]. Their four wheels drive vehicle consists of four main components. The first part is the mechanical structure of the robot which includes wheels and steering motors and also motor drive system. The second part is an embedded controller which obtains commands from a user and also sensor system and accordingly controls the operation of the robot. Lastly, the seeding mechanism includes a vacuum fan and a motor for seeding wheat. They provided the kinematic model for their robot which is helpful for path planning purposes, and also validated the efficiency of their design by conducting field experiments in different scenarios including analyzing the seed distribution and seed space characteristics.

Their design seems a capable mobile robot as a carrying vehicle for field-based plant phenotyping. However, the size drawback still can be a restriction for phenotyping of larger plants including canola and the robot needs to be retrofitted for this purpose.

Huanhuan Wang and others proposed a low-cost scanning system for indoor phenotyping based-on a low-cost 2D laser scanner [25]. In fact, they attached two Light Detection and Ranging sensors (LIDAR) at the two far-ends of a fixing frame and then the frame was moved through the plant to reconstruct a 3D model of the plant based-on sensor information. Their proposed system can be an efficient choice to measure leaf surface area merely in laboratory configuration as their employed low-cost LIDAR is highly sensitive to ambient light. Moreover, the system is highly susceptible to movements. Meanwhile, the plant should be absolutely fixed while LIDAR sensors are performing the scanning task.

Another sophisticated plant phenotyping platform was proposed by LemnaTec [26]. LemnaTec is a pioneer company in plant phenotyping based in Aachen, Germany which commercially manufactures different plant phenotyping platforms for diverse research environments including laboratory, indoor greenhouses, and field-based experiments. The most important advantage of LemnaTec products is the accuracy of measurements in a small-scale trial and also a variety of parameters can be measured and analyzed including plant morphology, color, biomass, temperature, height and so on.

In fact, many researchers have taken advantage of LemnaTec phenotyping platforms in their studies. Noah Fahlgren and others developed a versatile phenotyping system called Bellwether Phenotyping Platform to analyze temporal responses of Setaria plant to water availability [27]. They also established the Bellwether Foundation Phenotyping facility at Donald Danforth Plant science center located in St. Louis, Missouri [28]. In their research, PlantCV, an open source plant phenotyping software using computer vision [29] was introduced, and also LemnaTec Scanalyzer 3D [30] were deployed to build their customized plant phenotyping platform. Overall, plant biomass, height, color, architecture and tissue water were the primary target traits in their studies and research.

Yufeng Ge and others also exploited LemnaTec Scanalyzer 3D to study temporal dynamics of maize plant [31]. In their study, they processed RGB images to define plant coverage area by separating the green areas from the soil in an image using image processing algorithms. Also, hyperspectral images were processed to determine leaf reflectance and accordingly water consumption of the maize plant.

Moreover, LemnaTec manufactures a field-based Scanalyzer for outdoor phenotyping applications which is based on a rigid motorized gantry and a measurement box [32]. The system consists of a near-infrared camera, a visible camera, CO2 and Chlorophyll fluorescence sensors, and is capable of measuring canopy height, biomass, NDVI and leaf geometry. Moreover, Pouria Sadeghi-Tehran and others utilized this platform to propose an automated method to determine heading and flowering stages of the wheat plant using image processing algorithms [33].

A. Muscolo and others utilized an indoor greenhouse Scanalyzer system to analyze the phenotypic response of lentil to drought and salinity [34]. They first germinated the seeds and then plants were grown and monitored in a 12 days experiments.

Another commercial product for plant phenotyping is called PlantEye by Phenospex, a company located in Heerlen, Netherland [35]. PlantEye transmits near-infrared laser line through the plant and receives the reflected beam by an integrated camera which is located at the end of the sensor to capture 3D point clouds of plants. In next step, sensor segments the resulting 3D model and computes several morphological plant parameters including height and leaf area.

Despite all advancements and efficiency of commercial plant phenotyping platforms, high cost is a big issue that should be addressed before widely being used by researchers in the academic world. For example, only one PlantEye unit costs more than 43 000 Euros at the time being and apparently this amount is affordable only for large-scale research centers. Moreover, they are mostly designed for indoor and stationary configuration and not suitable for field-based phenotyping applications. These two considerations were of those bottlenecks to be addressed in this thesis to develop a low cost yet efficient field-based plant phenotyping platform.

Alexis Comar and others proposed a semi-automatic system for high-throughput phenotyping of wheat cultivars located in Auzeville Tolosane, France [36]. In their design, a horizontal beam was attached to a tractor, and a hyperspectral radiometer and two RGB cameras were deployed to monitor plots. Using image segmentation algorithms, the green fraction was extracted from RGB images, and vegetation indices were derived from radiometer data. Moreover, their system was equipped with a RTK GPS which provides centimeter accuracy for accurate geo-referencing.

Jesper Svensgaard, Thomas Roitsch and Svend Christensen proposed a mobile multispectral imaging platform [37]. Their design consists of a small crane to carry an enclosed box on topmost of the plots. A spectral camera and a LED light panel were attached inside the box to eliminate the negative effect of wind and sunlight. Their targeted traits were NDVI and also vegetation coverage which was extracted using supervised classification processing on utilized spectral camera. It is mentionable that third-party companies developed both hardware and classification software of their system and the design process was not included in their research. Lastly, they conducted their experiments in four different dates to validate the efficiency of their proposed plant phenotyping system.

J.M. Montes and others at Institute of Plant Breeding, Seed Science and Population Genetics, University of Hohenheim, Stuttgart, Germany believed insufficient tools for non-destructive phenotyping of a large number of genotypes in a field is the main reason for existing delay in researching early growth in plants. For that reason, they proposed a high-throughput non-destructive phenotyping system to analyze biomass in maize field adapted to the climatic conditions of central Europe [38]. In fact, they utilized light curtain and spectral reflectance sensors and different biometric methods to determine early biomass. Last but not least, they attached sensors to a tractor as the base vehicle and collected data at three stages.

Despite the interesting results proposed by J.M. Montes and others, there is not enough information about their utilized software and geo-referencing algorithm. Besides, it is not clear that their data collection process was manually or autonomously.

Another plant phenotyping platform was developed by Jared L. Crain and others which is called PhenoCart [39]. Their design can be classified into portable and hand-held phenotyping platforms because a manually propelled cart was used to carry measurement equipment. In fact, they utilized a webcam to capture RGB images, a spectral reflectance sensor and an infrared thermometer sensor to measure canopy temperature and also NDVI as their target traits. Furthermore, a GPS system was used to geo-reference data for future retrieval. Lastly, they conducted their experiments at the Campo Experimental Norman E. Borlaug CIMMYT research center near Ciudad Obregon, Sonora, Mexico.

One of the most critical advantages of their proposed system is using a laptop and NI LabView software as the primary software which gives the flexibility of conveniently adding more features to the PhenoCart in future if needed. However, some issues can be seen in their design and should be addressed to have a higher performance plant phenotyping system. Firstly, their utilized GPS unit is a low accuracy USB device with provides only 10cm accuracy and appears not suitable for phenotyping of small plots in a large-scale field. The second issue can be seen in their mechanical design. Meanwhile, a manually propelled cart can be used only in small nurseries, because it is not possible for a human to carry all measurement equipment, laptop and also batteries for a long time especially in summer. However, they limited their field tests to merely 30 plots and specific weather conditions (not cloudy, not windy). The third issue can be addressed in their proposed image acquisition system. It is ambiguous how images were taken either manually or automatically while the cart is being moved through the plots.

Donald Rundquist and others proposed a simple hand-held phenotyping platform for plant phenotyping [40]. Their system consists of a human transported backpack system and two Ocean Optics 2000 Hyperspectral field radiometers [41] to capture spectral reflectance of plants. The spectral reflectance can be used to calculate different indexes such as NDVI which is an essential index for plant science researchers. Moreover, they used a wireless connection to transfer captured data over TCP/IP network to a stationary computer using a wireless router.

Phenoscope is another plant phenotyping platform proposed by Sebastien Tisn and others in France [42]. Their design was an indoor mobile robotic platform to move plants, adjust watering and take a picture of 735 individual pots over a table in a greenhouse. Their facility was intended to be used by large-scale experiments that would not be reproducible manually.

Another plant phenotyping platform in greenhouse configuration is called GROWSCREEN-Rhizo, proposed by Kerstin A. Nagel and others in collaboration with a third-party company who built the prototype [43]. Their proposed system was able to capture an image of plants roots and as a result, reconstruct the root structure under controlled conditions to allow breeders to select desired underground traits. They also validated their experimentations using six different plant species and more importantly for barley and maize plants.

CHAPTER 2

DEVELOPMENT OF THE PLATFORM - HARDWARE AND SENSORS

2-1- Introduction

A plant phenotyping platform is a mechatronics system which consists of different programs for data and image acquisition and post-processing, an electrical system including variety of sensors and measurement devices for converting physical or chemical characteristics of plants to meaningful electrical signals, and also a data storage unit to store all measured data in a readable and meaningful format for future retrieval and analysis. Moreover, a plant phenotyping platform requires a mechanical structure to carry sensors and measurement equipment as a fixing frame.

As stated before, one of the main objectives of this research project is to develop the electrical and software components for a non-destructive field-based high-throughput plant phenotyping platform. With design and development of such a field-based platform comes a series of challenges and problems to be considered.

In this chapter, the process of developing hardware and sensor system for proposed plant phenotyping platform is discussed. In fact, four different plant traits were targeted in this research. They are 1- plant height, 2- plant temperature, 3- NDVI index, and 4- canopy coverage (from RGB images). It is notable that when is being referred to a plant trait in this research, it means the average of several values captured in different locations within a plot (a plot consists of a group of vegetation planted in rectangular sections) not each individual plants in a field. Furthermore, other traits can be measured by adding more sensors to the current system as the result of future works which will be addressed in chapter five. It is tried to systematically explain different possible methods and approaches to measure various characteristics of a plant, and at the end of each section, the proposed measurement method is explained.

Last but not least, the detail of the software part of the proposed plant phenotyping platform for data and image acquisition and also for data visualization will be discussed in next chapter as an individual topic. Indeed, the developed algorithms and different programs to implement individual tasks will be explained in chapter three.

2-2- Canopy Height Measurement Methods

Height measurement is one of the essential features in a plant phenotyping platform. There are several methods to measure height of a plant with their pros and cons, but the most convenient methods can be classified as below:

2-2-1- Manual Measurement

Apparently, using a tape measure or a scaled bar is a primary solution and the most straightforward approach to measure height of a plant as can be seen in Figure 2-1.

Figure 2-1: Manual height measurement

The advantages of using this method for height measurement are:

- Can be implemented by everyone with no need to a specific background knowledge
- Lower cost in comparison with other methods
- Accurate as long as a few plants are expected to be studied

On the other hand, this approach is not reliable and efficient enough because firstly, the accuracy of measurements is in a straight line with the quality of human observer. In other words, different people can capture entirely different values for the height of a similar plant, and reading error can negatively affect the performance of height measurement experiment.

Secondly, this approach is not practical to be used as an efficient solution in a large-scale study because the process of data collection using this method is slow and can be frustrating especially during the summer when working on an outdoor field is required.

2-2-2- Using a Laser scanner Sensor

Laser scanners or laser rangefinders are being used in many industrial applications including distance and level measurement systems. The fundamental operating principle of this sensor is emitting a laser beam by a laser transmitter and analyzing the reflected signal as can be seen in Figure 2-2.

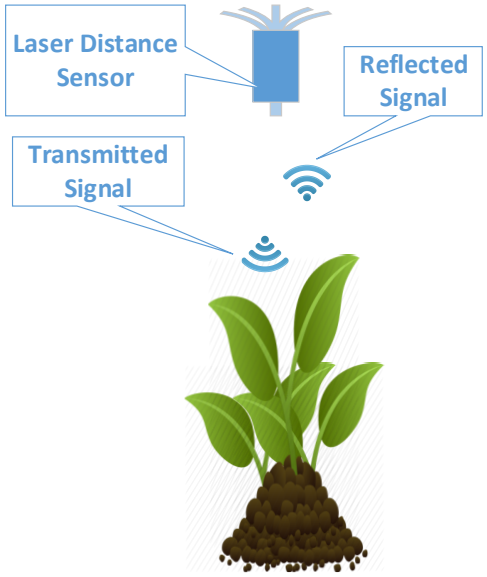

Figure 2-2: Laser distance measurement

Nevertheless, the main issue with laser distance sensors to measure the height of a plant is the insufficient field of view (FOV). Because this sensor uses an ultra-narrow laser beam to measure the distance, hence any tiny object can be unnoticed in the measurement process. Furthermore, this sensor is costly in comparison with other sensors such as ultrasonic distance measurement sensors. However, there are some lower-cost versions of this sensor, but they can be highly sensitive to ambient light, so they can be used in outdoor configuration only if the sensor is enclosed by a special cover to eliminate the adverse effect of sunlight.

2-2-3- Using a Camera and Image Processing

Image processing algorithms are widely being used in different applications including precision agriculture. Whether as a weed detection system or as a plant leaf area calculator, using a high-resolution camera can provide an in-depth information about a plant when the accuracy of a human observation is not sufficient.

In fact, another approach to measure the height of a plant would be taking advantage of image processing and more explicitly applying object detection algorithms on a digital image to compute the height of a plant. In this method, a camera is being used to take a picture of a plant from a known distance. Then the actual height of a plant can be calculated by analyzing the pixels of the captured image and using lookup tables and comparing the resulting values with the height of some known objects. Figure 2-3 illustrates a sample configuration for capturing a picture of a plant for further image analysis and height measurement purposes.

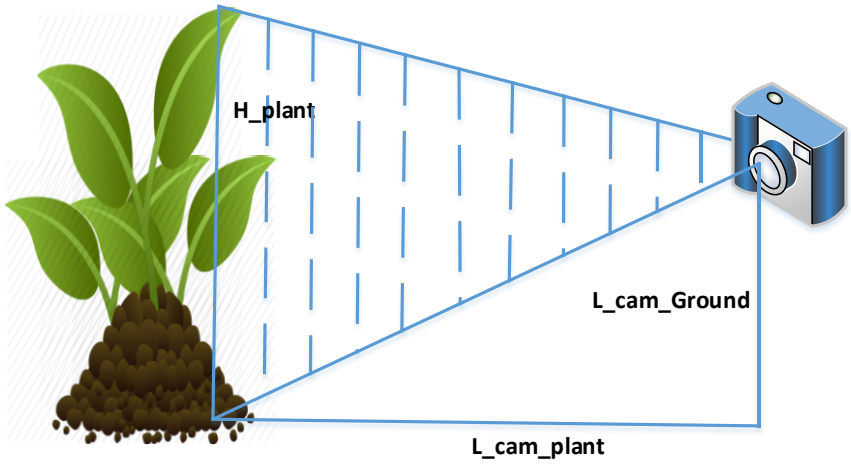

Figure 2-3: Using a camera to measure height of a plant

This solution can be a useful method for controlled and indoor experiments, yet not an optimum answer for field-based plant phenotyping because of two main reasons. Firstly, it needs a solid background knowledge in image processing, and secondly, the accuracy of measurements directly depends on specifications of the utilized camera and also is highly sensitive to environmental parameters such as sunshine, cloud coverage, and water vapor.

2-2-4- Using an Ultrasonic Sensor

Ultrasound is sound with frequencies above human audible range approximately above 20 kHz. Animals such as porpoises and bats use ultrasonic waves to locate their prey and also to avoid obstacles. Furthermore, ultrasonic sensors are widely being used in different industrial applications including distance and level measurement purposes.

Likewise to a laser rangefinder, the basic operating principle of an ultrasonic sensor is transmitting an ultrasound wave and receiving the reflected signal after running into an object

and passing through the air as can be seen in Figure 2-4. The distance between the object and the tip of the sensor can be calculated by analyzing the traveling time between transmitted and received signal.

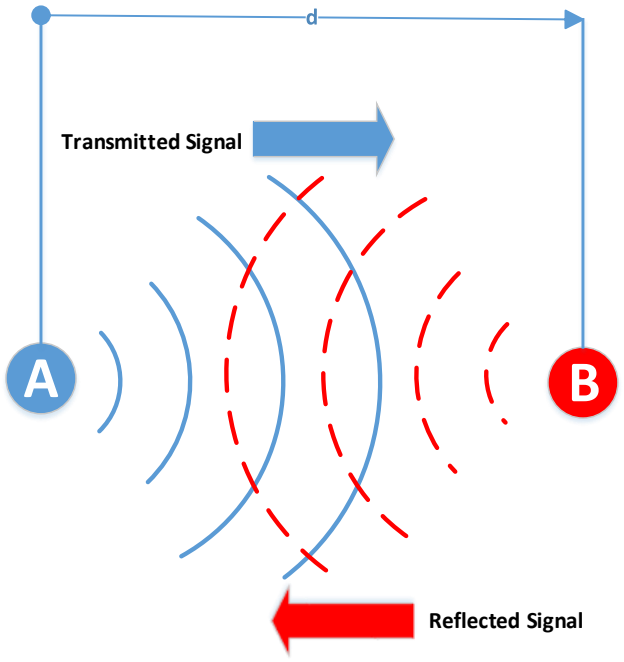

Figure 2-4: Operating principle of an ultrasonic sensor

In fact, the distance between point *A* and point *B* can be defined as:

$$D = \frac{1}{2}(S.t)$$ Equation 2-1

where *D* is the distance between point *A* and point *B*, *S* is the traveling speed of sound through the air (~ 344 m/s), and *t* is the time taken to send an ultrasound waveform from point A and receive the transmitted wave in point B.

Having a closer look at this working principle, it can be concluded that an ultrasonic sensor can be used to measure the height of an object and more importantly height of a plant as can be seen in Figure 2-5.

In fact, ultrasonic sensors are not primarily intended to be used for height measurement, but they are widely being used as a distance measurement sensor. However, as discussed before, they can be exploited for height measurement by subtracting the distance between the tip of the sensor and the ground from the distance between sensor and top of the plant.

Figure 2-5: Using ultrasonic signal to measure height of a plant

Indeed, if an ultrasound signal is emitted through its source and the reflected signal is received, then the canopy height can be derived by eliminating existing outlier numbers due to the possible unwanted measurements and averaging a group of valid sample points.

In comparison to laser rangefinders, ultrasonic sensors have a wider field of view (FOV), and hence they are more suitable to be used for plant height measurement because an ultrasonic sensor can notice relatively tiny leaves. This detection range; however, is limited according to the characteristic of each sensor and can be found on the provided datasheets by different manufacturers.

2-2-5- Proposed Height Measurement Method

In development of the proposed field-based high-throughput plant phenotyping platform, four ultrasonic distance sensors were used to measure the height of canola plants. The utilized sensor uses a 180 kHz carrier frequency and has 250 ms response time. IP67 sealing grade and also operation temperature range makes this sensor an excellent choice to be used for an outdoor configuration where sensor could be exposed to water spills and dust. Moreover, the detecting range of this sensor seems reasonable to measure height of a plant. Indeed, one of the most critical parameters that should be considered in design is the minimum allowable distance between tip of the sensor and a plant. As can be seen in the datasheet of this sensor, the distance between sensor and an object cannot be less than 200 mm. This limitation was observed in experimental tests as well. The full datasheet of this sensor can be found in Appendix F.

Before using the ultrasonic sensor in proposed plant phenotyping platform, the sensor has to be calibrated and the output signal should be scaled to be a true representative of the height of a plant. Moreover, the utilized sensor can be powered by a 15-30 VDC power supply and the output data is given as a 4-20mA current signal as can be seen in Figure 2-6. In the current arrangement, a 24 VDC power supply was used to power up this sensor; two 12 VDC batteries were dedicated to supplying the required power for all sensors and devices.

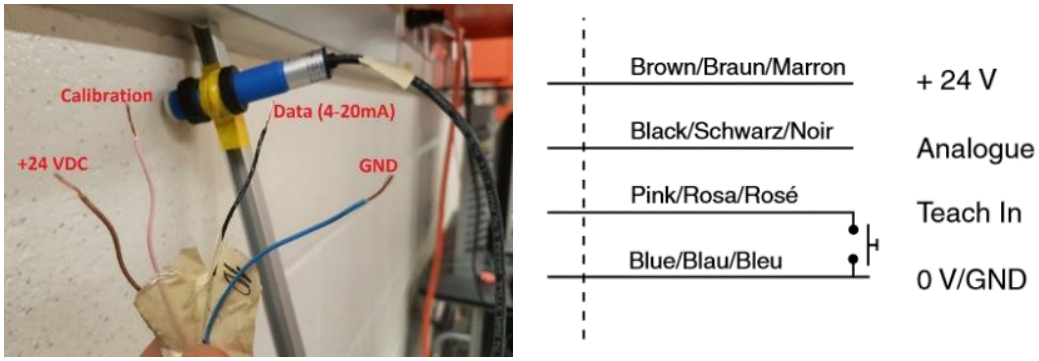

Figure 2-6: Wiring of utilized ultrasonic sensor

As mentioned earlier, the output signal should be adjusted before extracting meaningful data. In other words, it should be precisely defined what the minimum, and maximum output currents means for us. This particular sensor provides 4 mA as the minimum output current, and maximum current can be 20 mA according to the height of the object. So the sensor should be adjusted so that it delivers min/max output current corresponding to min/max distances being measured.

The process of output adjustment needs a precise observation and can be done by a user without any specific background knowledge. In other words, there are three LED lights on the back side of the sensor as can be seen in Figure 2-7 and according to the status of these three LEDs, the output signal can be adjusted or can be programmed, indeed.

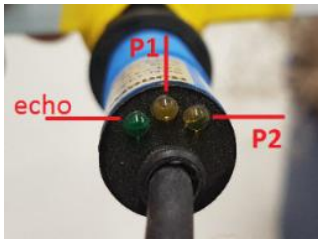

Figure 2-7: Guide LEDs for adjusting output signal

According to the datasheet provided by manufacturer, the output signal can be adjusted in two different modes as can be seen in Figure 2-8: a) positive slope, b) Negative slope. In the current design, the positive slope was chosen because it simplifies the calculations to extract height of the canopies.

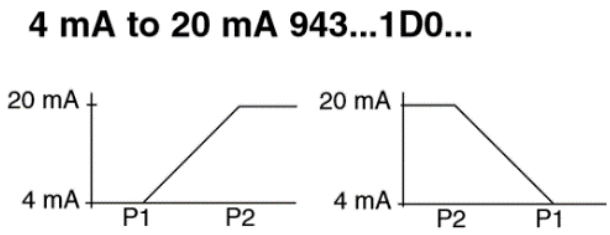

Figure 2-8: Utilized ultrasonic sensor adjustment graph

In other words, the process of output adjustment is defining point P1 and point P2 according to the Figure 2-8 as below:

1. First, the teach-in line (pink cable) should be connected to the ground until P1 LED started to flash with 2 Hz frequency. Now the line should be disconnected from ground and sensor should be pointed out to the distance that is desired to be represented by the sensor as a 4 mA signal. Now wire should be connected to the ground again for only one second. Now P1 point is set.
2. The procedure of setting P2 is the same as P1 but to start defining P2, the pink wire should be connected to the ground until P2 LED starts to flash with 2 Hz frequency. After P2 begins to flash, the sensor should be pointed out to the distance that is desired to be represented by the sensor with 20 mA, then the teach-in line should be connected and disconnected to the ground for one second, and now the sensor is adjusted. After adjusting the output signal, the sensor should be calibrated using some known objects to define the linear relationship between the height of an object and raw output values.

As discussed earlier, the main challenges to measure height of a plant are the adverse effect of environmental parameters such as ambient light and un-flatness of the traveling path on the validity of measurements. In fact, in the developed field-based plant phenotyping platform, unlike two other employed sensors which could measure canopy temperature and NDVI

regardless of the field condition, ultrasonic sensors are inherently sensitive to the distance between tip of the sensor and the ground. So, more in-depth investigations on the performance of this sensor needs to be done in laboratory before being employed in field configuration.

To assess and validate the effectiveness of the utilized ultrasonic sensor, a series of experiments were conducted at robotics laboratory at the University of Saskatchewan. Indeed, the employed sensor was attached to one side of an aluminum bar, and the other side of the bar was attached to a fixed frame as can be seen in Figure 2-9. The distance between the ground and the tip of the sensor was adjusted to 97 cm, which could be any other value within the acceptable range according to the datasheet provided by manufacturer.

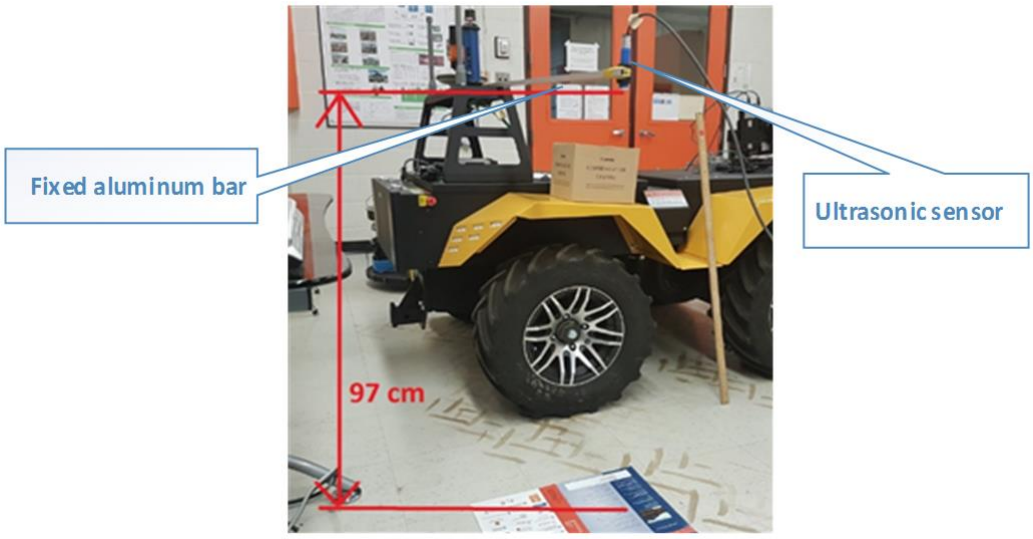

Figure 2-9: Sensor attachment for calibration

After powering up the sensor by a 24 VDC power supply, the sensor starts to stream a current signal which contains raw data according to different objects with dissimilar heights. Also, it is known that the relationship between the sensor output and height of various objects should be linear. So finding the linear correlation between sensor output and real height of the objects is desired. To do this, first the sensor output raw value (4-20 mA) was converted to a voltage value (by passing it through a highly accurate resistor) to be able to be connected to a data acquisition card, and then seven objects with different heights were stacked under the sensor tip, and corresponding values were captured and analyzed as can be seen in Table 2-1.

Table 2-1: Collected data for calibration of ultrasonic sensor

Object height (cm)	Output Raw value (mV)
21.0	2.880
29.5	4.203
36.0	5.241
44.5	6.620
51.5	7.802
60.0	9.041
77.0	11.870

As mentioned earlier, it is expected that the relationship between raw data and actual height should be a modeled by linear regression. This association can be verified after having a look at the Figure 2-10 which is a scatter graph of available data set in Table 2-1.

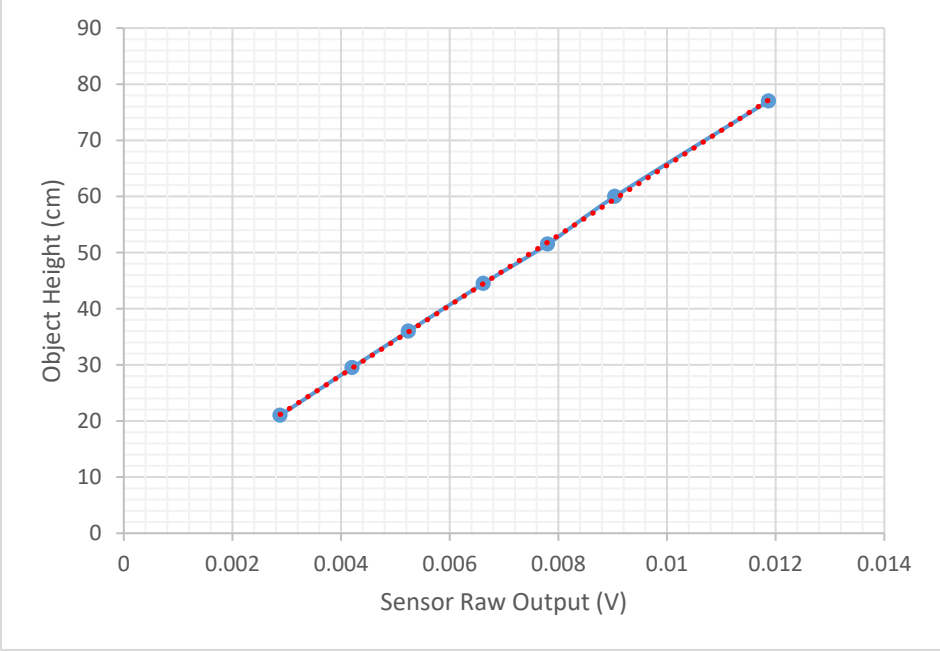

Figure 2-10: Ultrasonic sensor calibration graph

The solid blue dots represent the observed data and red dashed line represents the curve which fits the data for interpolation. The linear regression model can be derived as Equation 2-2:

$$y = 6768.4x + 1.9573$$ *Equation 2-2*

where y is the height of the object in cm and x is sensor raw value. So by using derived linear regression model, the output can be a reasonably accurate representative of the height of different objects and more importantly height of a plant.

Furthermore, before using the utilized ultrasonic sensor in the proposed field-based plant phenotyping platform, the performance of ultrasonic sensor was evaluated by conducting height measurement experiments in five different scenarios in laboratory configuration. In fact, it was tried to identify whether the employed sensor can reliably and accurately measure height of various objects with dissimilar shape or not.

- **Case Study 1- A stack of books as a test object**

As the first case study, a pile of varying number of books was used as a test object to assess the performance of the utilized ultrasonic sensor, as can be seen in Figure 2-11. It is mentionable that the same object was also used as known objects to calibrate the sensors because they have a full surface for reflecting strong signal.

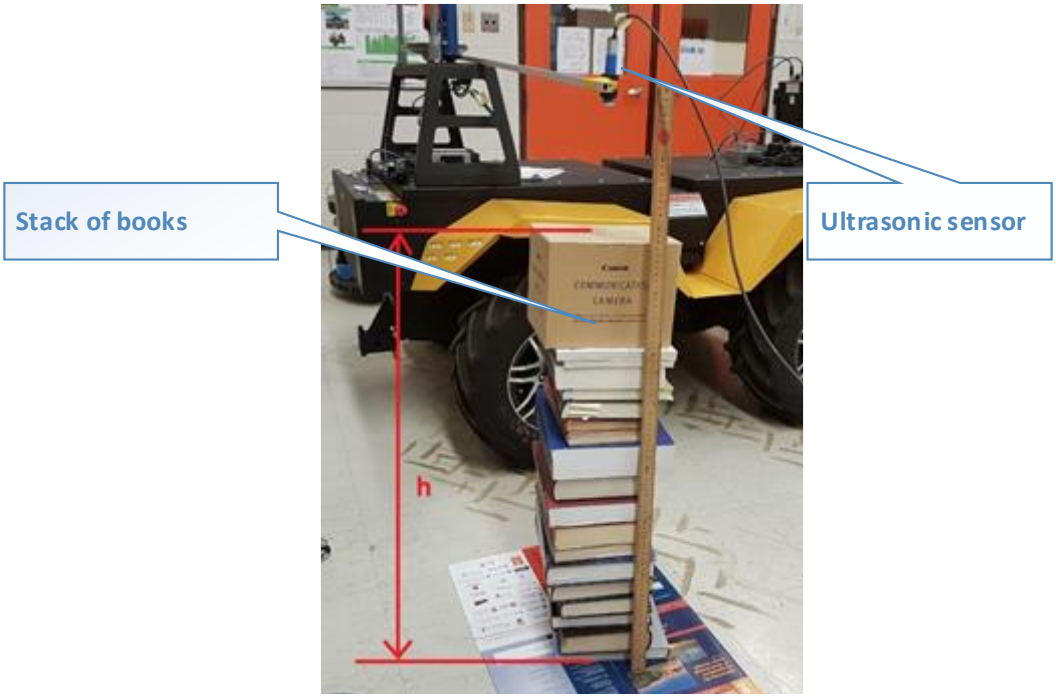

Figure 2-11: Case study 1- Measuring height of a stack of books with ultrasound sensor

To validate the measurements, different number of books were aligned with the tip of the sensor to achieve seven different heights, and ultrasound sensor was used for height

measurement in all seven cases. Also, a ruler was used to measure height of the stack of books manually for comparison with ultrasound measurements, and the result of experiments were summarized in Table 2-2.

Table 2-2: Measuring height of stacks of books

h_u (Ultrasonic Height in cm)	h_m (Manual Height in cm)	Diff= h_m - h_u (cm)	% diff $= \frac{Diff}{(hm+hu)/2}$
75.5	77.0	1.5	2.0%
59.0	60.0	1.0	1.7%
50.1	51.0	0.9	1.8%
44.4	44.5	0.1	0.2%
34.5	35.0	0.5	1.4%
27.2	27.5	0.3	1.1%
19.5	19.7	0.2	1.0%

As can be seen in Table 2-2, the result of measurements was reasonably accurate as was expected before. Also, Figure 2-12 illustrates the actual heights of different objects and measured heights of objects as solid dots in one axis. Furthermore, measurement errors (in cm) are mentioned on the graph beside each observation.

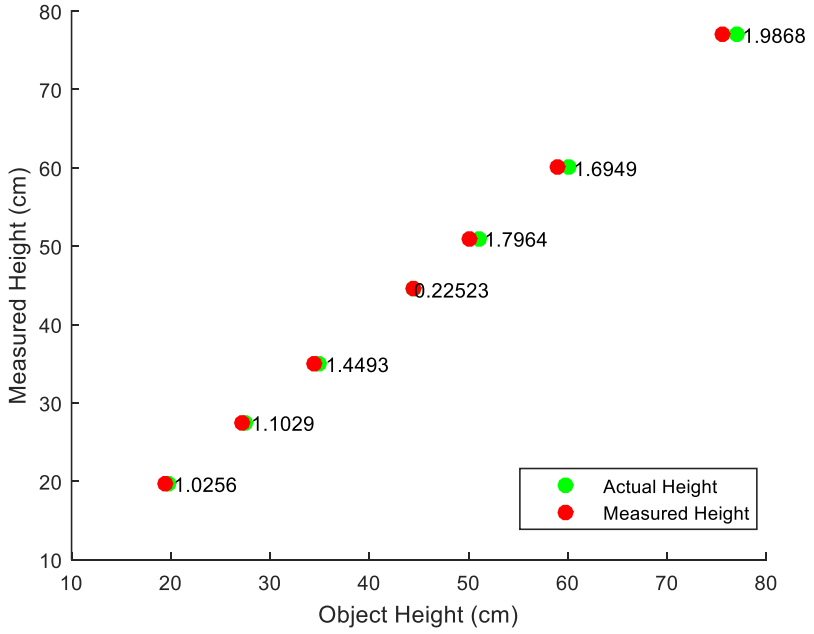

Figure 2-12: The result of height measurement for first case study

As can be seen, the minimum and maximum measurement errors were 0.2% and 2.0% which appears reasonably acceptable for a field-based ultrasonic height measurement system.

- **Case Study 2- A cylinder-shaped object as a test object**

The next case study was a cylindrical object with a diameter of 8.5 cm. The main difference between this case study and previous experiment is height measurement of an object with the smaller surface area to reflect ultrasonic signal as can be seen in Figure 2-13.

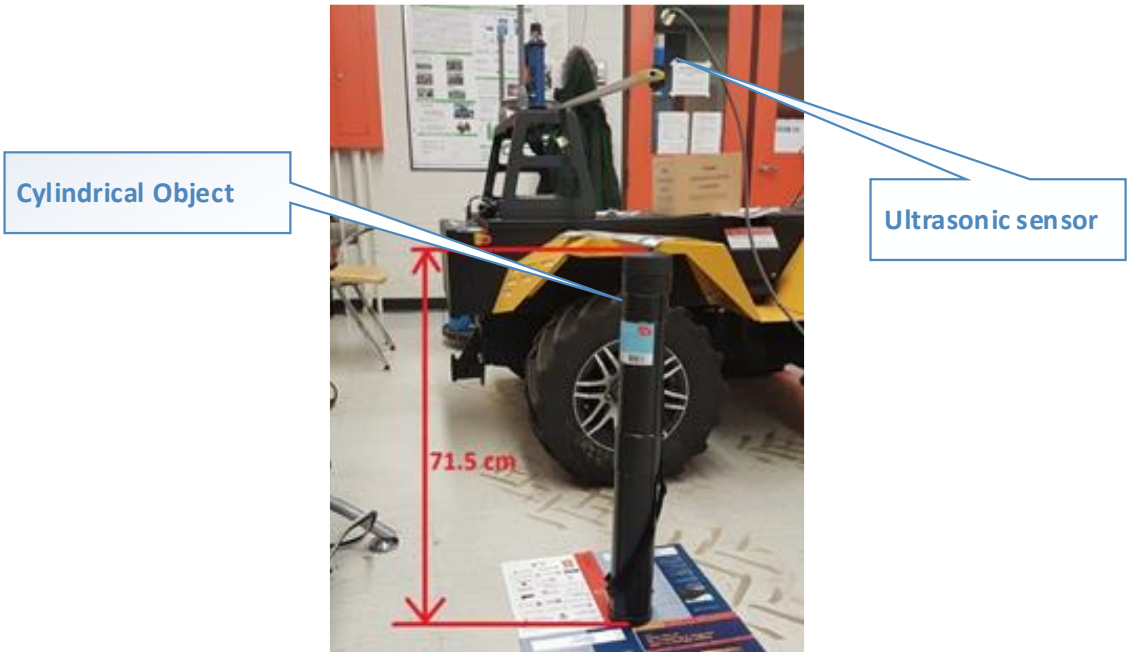

Figure 2-13: Case study 2- Measuring height of a cylindrical object

Likewise, the height of cylinder was adjusted in three different values for a better assessment. The result of measuring the height of this object in three various cases can be seen in Table 2-3.

Table 2-3: Collected data for measuring height of the cylinder

h_u (Ultrasonic Height in cm)	h_m (Manual Height in cm)	Diff= h_m - h_u (cm)	% diff $= \frac{Diff}{(hm+hu)/2}$
75.5	77.0	1.5	2.0%
59.0	60.0	1.0	1.7%
50.1	51.0	0.9	1.8%

Also, Figure 2-14 summarizes the result of this case study and illustrates a plot of actual object heights versus measured values and also demonstrates the errors in one axis.

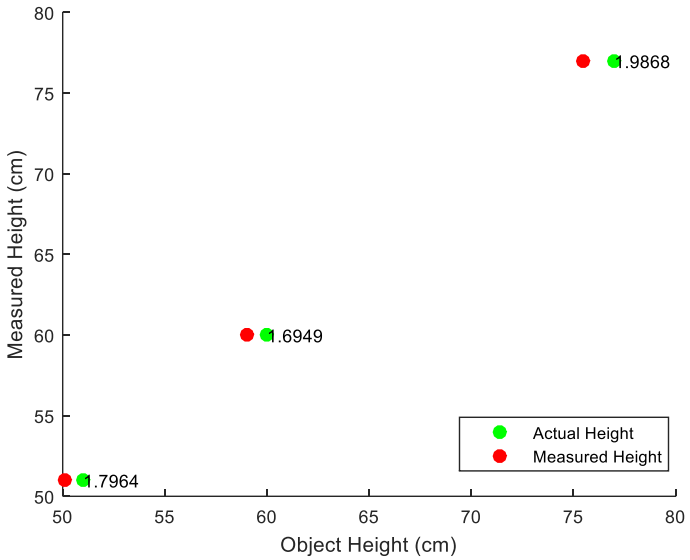

Figure 2-14: The result of height measurement for second case study

Despite the fact that the utilized cylindrical object has a smaller surface area to reflect ultrasound signals, it appears the ultrasonic sensor was able to measure height of this object without any problem. As can be seen, the maximum height measurement error was 1.9868 cm and this error value is reasonably acceptable for height measurement in a plat phenotyping system.

In next case studies, more objects with the smaller surface area will be examined to see how ultrasonic sensor is efficient and reliable to measure the height of different objects.

- **Case Study 3- An air pump as a test object**

In this case study an air pump was used as an object because of its unique shape. As can be seen in Figure 2-15, the examined object has a narrow surface area to reflect signals and seems a challenging case for evaluating the performance of the ultrasonic sensor in height measurement of different objects.

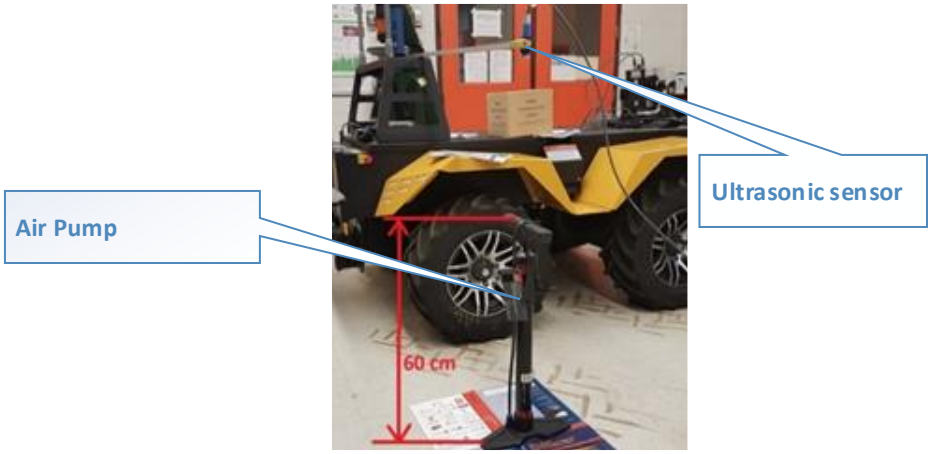

Figure 2-15: Case study 3- air pump as a test object

Interestingly, the ultrasonic sensor still could efficiently measure the height of such an object as can be seen in observations according to Table 2-4.

Table 2-4: Collected data for measuring height of the air pump

h_u (Ultrasonic Height in cm)	h_m (Manual Height in cm)	Diff= h_m - h_u (cm)	% diff $= \frac{Diff}{(hm+hu)/2}$
58.9	60.0	1.1	1.9%
63.8	65.0	1.2	1.9%
69.0	70.0	1.0	1.4%

Furthermore, Figure 2-16 summarizes the result of measurements as a graph.

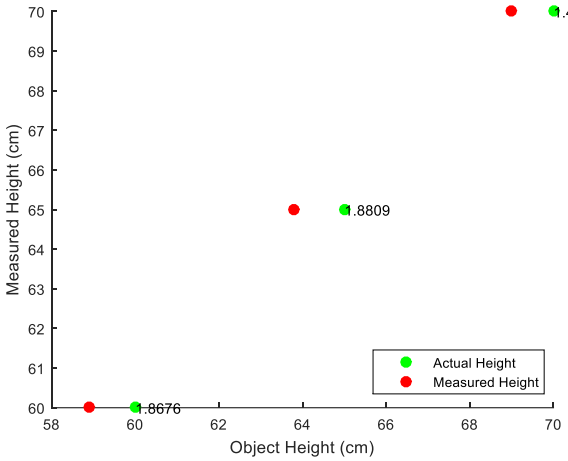

Figure 2-16: The result of height measurement for third case study

As can be seen in Figure 2-16, the ultrasonic sensor could successfully measure the height of such an object with only 1.4 cm measurement error.

- **Case Study 4- A radiator as a test object**

  In this case study, a radiator with some narrow blades on top was designated as a test object. This object was chosen to assess the performance of the ultrasonic sensor in detecting tiny objects. As can be seen in Figure 2-17, the width of top blades is undoubtedly narrow (less than 0.3 cm).

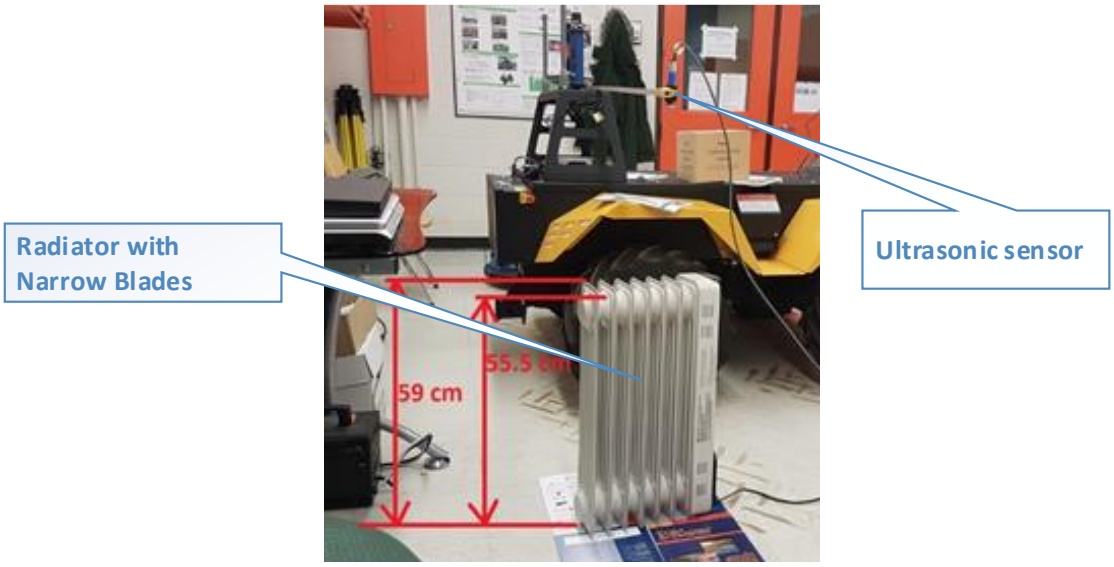

Figure 2-17: Case study 4- a heater with narrow edges as a test object

Table 2-5 illustrates the result of height measurement for this object.

Table 2-5: Collected data for measuring height of the heater

h_u (Ultrasonic Height in cm)	h_m (Manual Height in cm)	Diff= h_m - h_u (cm)	% diff $=\frac{Diff}{(hm+hu)/2}$
54	55.5 Middle	1.5	2.7%
NA	59.0 Top	NA	N/A

Having a closer look at the test results on Table 2-5 reveals that the ultrasonic sensor was able to measure the height of the heater from middle part to the ground with an acceptable measurement error. Whereas, the sensor could not notice narrow blades.

- **Case Study 5- A plant as a test object**

After examining the performance of ultrasonic sensor for measuring the height of different objects, in this section, the result of height measurement of a plant in laboratory configuration is discussed. First of all, it should be declared what it exactly means when we refer to a plant height because different people might have a different interpretation of this broad term. Indeed, a plant consists of various tiny branches, and they are not necessarily arranged uniformly. Also, the height of each branch can be significantly varied. However, what breeders expect from a height measurement system, which could be measured manually or using an electronic sensor, is defining the height of a plant from where most branches get together and a reasonable area to measure height can be observed. For example, as can be seen in Figure 2-18, there are many tiny branches on top of the plant, but as a rule of thumb, they are not the actual representative of the height of this plant.

Figure 2-18: Case study 5- A plant height measurement trial in laboratory configuration

As we observed in the previous section, the ultrasonic sensor was not able to detect the tiny blades on top of the heater. However, the height of the heater from middle top part of the heater to the ground could be successfully measured. So for our experiments, using an ultrasonic sensor can be challenging, and a precise investigation needs to be done before further assessment.

The next phase of performance evaluation was cutting height of the plant from 79cm to 71cm. This trial was repeated for 65cm and 51cm to achieve different heights and to examine how accurate and valid our measurements are. Finally, Table 2-6 illustrates the result of measurements using ultrasonic sensors and also using a ruler as an alternative height measurement method.

Table 2-6: Collected data for measuring height of plants

h_u (Ultrasonic Height in cm)	h_m (Manual Height in cm)	Diff= h_m - h_u (cm)	% diff $=\frac{Diff}{(hm+hu)/2}$
79.0	79.0	0.0	0.0%
70.0	71.0	1.0	1.4%
63.5	65.0	1.5	2.3%
50.0	51.0	1.0	2.0%

As can be seen in Figure 2-19, the ultrasonic sensor was able to measure the height of the plant in laboratory configuration with a minimum error of 0% and maximum error of 2.3%.

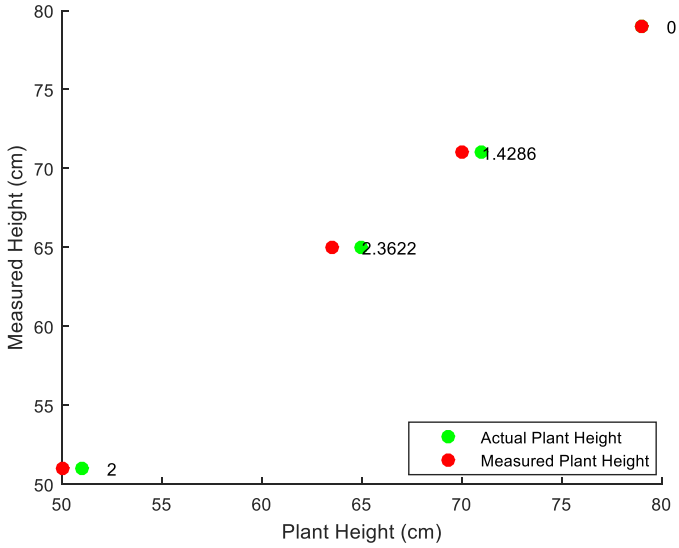

Figure 2-19: The result of height measurement of plants

By summarizing the results achieved after examining the performance of an ultrasound sensor to measure height of five different objects with dissimilar shape, we can conclude that this sensor can effectively measure height of different objects with a few considerations. First of all, tiny objects with a width of less than ~0.4cm cannot be detected by the utilized ultrasound sensor. So if height measurement of a plant is desired, the canopy should be dense enough to reflect a strong signal to achieve higher measurement precision. Secondly, the distance between the ground and the utilized frame to hold sensors on top of an object for height measurement purposes should be reasonably fixed. Otherwise, measurement error can be higher depends on the amount of deviation of the fixing frame in comparison to the ground.

After verifying the effectiveness of an ultrasonic sensor for height measurement purposes, in the developed plant phenotyping platform four ultrasonic sensors were used to measure the height of canola plants as can be seen in Figure 2-20. Indeed, sensors were arrayed in two different groups. Two sensors on the right wing and two sensors on the left provided the capability of simultaneously measuring the height of two different canopies.

Figure 2-20: Utilized ultrasonic sensors on the proposed HTPP

Furthermore, Figure 2-21 illustrates a closer view of installed ultrasonic sensors on the right wing of the mechanical boom.

Figure 2-21: Closer view at utilized ultrasonic sensors on the boom

2-3- Canopy Temperature Measurement Methods

The capability of temperature measurement is another important feature in a high-throughput plant phenotyping platform. In fact, the temperature of a plant is a representative

parameter of the water status, water usage and can be a fundamental factor in determining if a plant needs to be irrigated more or less. Also by analyzing a plant temperature, the ability of vegetation to handle heat stress can be determined. So breeders are highly interested in measuring and studying on this trait to achieve a better and more tolerable yield.

Temperature measurement systems can be classified in different aspects. These classifications; however, can be narrowed down into two main categories according to the fundamental operation principle they use, as follow:

2-3-1- Contact Method

A temperature measurement device which is in direct contact with a plant can be categorized in contact methods. In fact, in a contact temperature measurement method, a temperature sensitive device which can be a thermocouple, thermistor, resistance temperature detectors (RTDs), bimetallic thermometer, etc. is used to determine the temperature of a plant. Figure 2-22 illustrates an example of a contact temperature measurement device which uses a probe to measure the temperature of a plant.

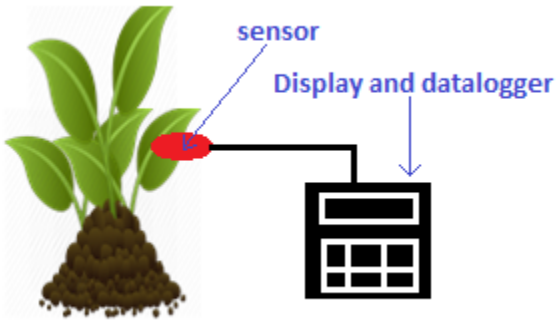

Figure 2-22: A contact temperature measurement device

Contact methods are easy to use and usually inexpensive. On the other hand, they have a slow response time because they have to be in direct contact with a plant for a specific amount of time and a stop-measure-go fashion should be utilized in a field experiment. Therefore they are hardly ever been used in a non-destructive high-throughput plant phenotyping platform. Furthermore, it is not possible to use this method in a large-scale field, and it is mostly being used merely for indoor experiments.

2-3-2- Non-Contact Method

Non-contact temperature measurement systems are widely being used in industry to measure the temperature of different objects for various applications where a contact method cannot be used, e.g., hazardous areas with extremely high heat or unreachable objects. Indeed, heat can be uniquely a valuable parameter to demystify concealed signs of a problem in any system. For example, a continuous temperature monitoring system in a high-voltage power generator can significantly decrease downtimes and avoids power outage and interruption due to malfunctionality of a component of the generator.

In fact, new improvements in infrared technologies have reduced costs and amplified reliability and lead to non-contact infrared thermometers offering smaller and lighter sensors with highly accurate measurement capability. More importantly, IR thermometers can be impressively useful in precision agriculture and in a plant phenotyping platform to measure a plant temperature because there is no risk of contamination or physical damage to plant itself when a non-contact IR thermometer is used. Figure 2-23 illustrates a hand-held IR thermometer when measuring canopy temperature in a canola field.

Figure 2-23: A portable non-contact temperature measurement device

2-3-3- Proposed Temperature Measurement Method

Despite the fact that temperature measurement is a crucial feature, there are some problematic challenges to be addressed in the design process of a temperature measurement system in a field-based plant phenotyping platform. Indeed, the adverse effect of environmental parameters such as ambient temperature as well as the impact of temperature of unwanted objects such as soil on the target plant should be considered. In other words, the proposed

temperature measurement system should be able to measure the temperature of a plant in outdoor configuration efficiently and should be able to eliminate the effect of soil temperature on the measurements with an acceptable level of measurement errors.

In the development of proposed field-based high-throughput plant phenotyping platform, two IR radiometers were used to measure the temperature of canola cultivars. One of the most critical advantages of the utilized sensor is the fact that it does not need a major field calibration because manufacturer provides a product-specific calibration parameter list to be used in programming and target temperature calculation. As can be seen in Figure 2-24, an excitation voltage needs to be applied to the sensor to operate and then a differential and single-ended analog inputs can be used to read the sensor output signal.

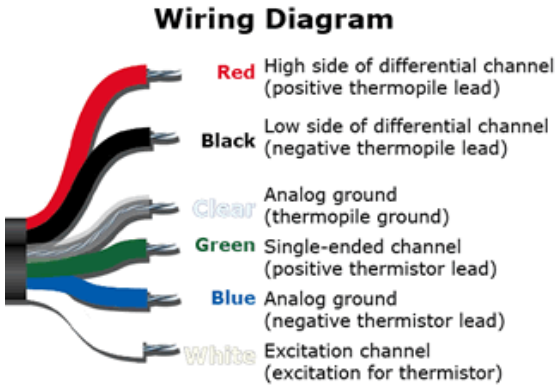

Figure 2-24: IR thermometer wiring diagram

Furthermore, the utilized sensor provides 20 µV per each degree centigrade as an analog output signal and has a ±0.2 C° uncertainty. Also, the sensor is only sensitive to 8-14 µm wavelength (atmospheric window) to eliminate the influence of unwanted carbon dioxide and water vapor on the measurements accuracy, so it can be an efficient choice to be used in a field-based plant phenotyping platform where water exposure is highly imaginable.

Moreover, as can be seen in Figure 2-25, the utilized sensor has a narrow field of view (FOV) that helps to measure only the temperature of the surface of the plant instead of the soil. Indeed, Θ which is called half angle for IR thermometers is specifically 14° for the utilized sensor.

Figure 2-25: Field of view of the utilized thermometer

Figure 2-26 illustrates the internal circuit diagram of utilized IR thermometer which is a half bridge. It is important to understand how this internal circuit works to be able to convert the output raw value into the corresponding temperature value.

In fact, the sensor consists of a high accuracy resistor (24900 Ω) and a thermistor to measure the target temperature. Usually, a 2.5 VDC excitation voltage should be applied to the sensor to avoid self-heating and current drain effects.

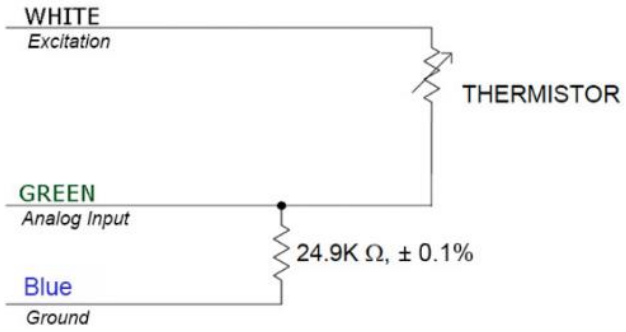

Figure 2-26: Internal circuit diagram of IR thermometer

The resistance value of the thermistor can be calculated as below:

$$R_T = 24900\left(\frac{V_{EX}}{V_{OUT}} - 1\right)$$ Equation 2-3

Where V_{EX} is the value of excitation voltage and V_{OUT} is output voltage. From Steinhart-Hart equation and thermistor specific coefficients we can derive the relation between the temperature and resistance as bellow:

$$T_K = \frac{1}{A + Bln(R_T) + C(\ln(R_T))^3}$$ Equation 2-4

Where $A = 1.129241 \times 10^{-3}$, $B = 2.341077 \times 10^{-4}$, and $C = 8.775468 \times 10^{-8}$ (Steinhart-Hart coefficients).

Also, the Stefan-Boltzmann equation can be used to calculate the target temperature as below:

$$T_T^4 - T_D^4 = m.S_D + b \qquad \text{Equation 2-5}$$

Where T_T is target temperature in Kelvin, T_D is detector temperature in Kelvin, S_D is the millivolt signal from the detector, m is slope, and b is intercepted.

Coefficients m and b are defined during the calibration process at each detector temperature set point. At the end a second-order polynomial is fitted to derive the equation that determines m and b and also T_D as below:

$$m = C2.T_D^2 + C1.T_D + C0 \qquad \text{Equation 2-6}$$

$$b = C2.T_D^2 + C1.T_D + C0 \qquad \text{Equation 2-7}$$

Where $C2$, $C1$, and $C0$ are the custom calibration coefficients listed on the calibration datasheet that comes with every thermometer. Finally, the target temperature in degree centigrade can be calculated as below:

$$T_T = (T_D^4 + m.S_D + b)^{\frac{1}{4}} - 273.15 \qquad \text{Equation 2-8}$$

Equations 2-6, 2-7, and 2-8 are needed to be used in the developed program for the datalogger to measure the temperature of canola plant canopies which will be discussed in section 3-2 of chapter three. Also, the source code for the mentioned program can be accessed in Appendix A for more investigations.

Moreover, the utilized IR thermometer was assembled in the robotics laboratory at the University of Saskatchewan as can be seen in Figure 2-27, and a test configuration was used to verify the operation of the sensor before being employed in the actual field condition.

In fact, it was tried to debug and improve the developed program in the datalogger to convert the sensor output raw values into the corresponding temperature values in degree centigrade.

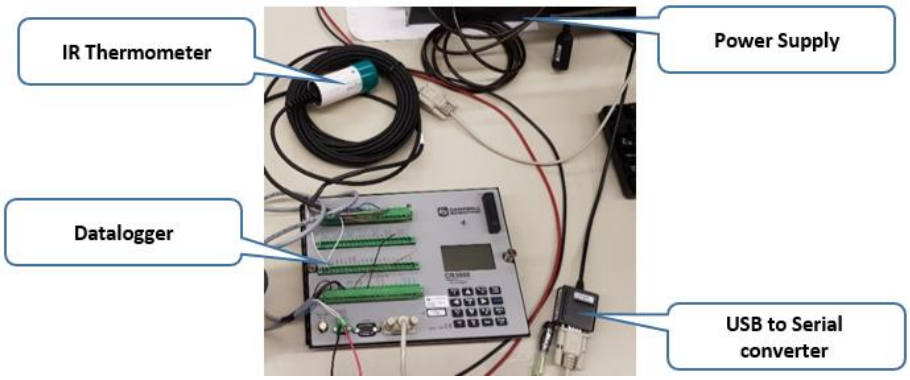

Figure 2-27: Testing IR thermometer in laboratory configuration

The utilized IR thermometer was aligned on top of an electric kettle to see whether it can reliably detect the variation in temperature of the water or not. Figure 2-28 illustrates the result of the experiment in laboratory configuration to measure the temperature of water using the utilized IR thermometer. In this figure, the numbers on the line graph represent the temperature of the water in C° and the horizontal axis represents the time of data sampling.

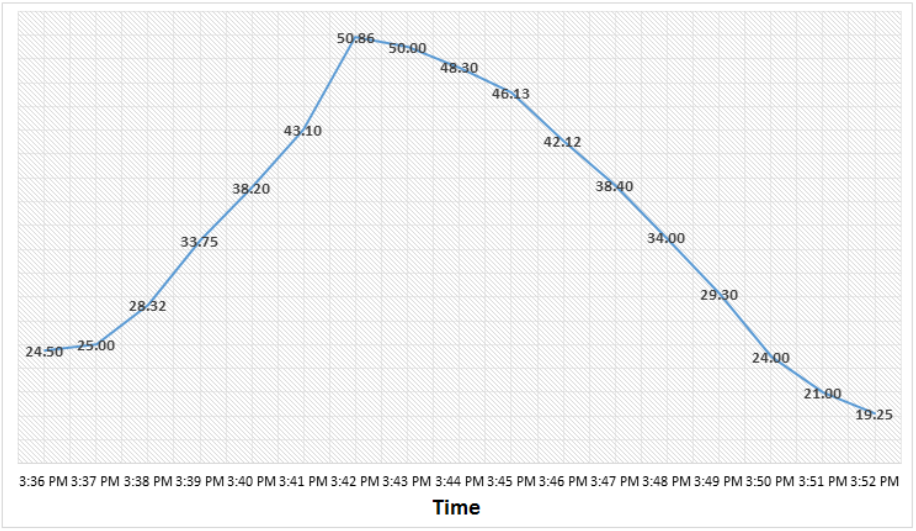

Figure 2-28: Variation in the temperature of the water captured by IR thermometer

Indeed, two glasses of water were poured into the kettle, and the heater was turned on around 3:36 pm. Then the temperature of the water increased until the heater was turned off after five minutes. Then a glass of cold water was slowly poured into the kettle to decrease the temperature of the heated water, and as can be seen in Figure 2-28 the employed sensor could successfully follow the variation in the temperature of the water during the experiment.

Finally, in the developed plant phenotyping platform, two IR radiometers were used to measure the temperature of canola cultivars as can be seen in Figure 2-29.

Two thermometers were arrayed in two different sets on the boom. Indeed, one sensor on the right wing and one sensor on the left provides the capability of simultaneously measuring the temperature of two different canopies.

Figure 2-29: Utilized IR thermometers on the proposed HTPP

Figure 2-30 illustrates a closer view of the utilized IR radiometer attached to the left wing of the boom, near the ultrasonic sensor, to measure canopy temperature. As can be seen, the sensor was installed on an adjustable-angle plate to achieve a different field of view, if needed. It was found that the sensor could give the required information without any distortion when it was facing down to the canopies.

Figure 2-30: Closer view at utilized thermometer on the boom

2-4- Proposed Image Acquisition Methods

In a plant phenotyping platform, the capability of capturing RGB images of a plant can be significantly useful because a single RGB image can be an informative source of information for breeders. For example, getting a glimpse of an RGB image can give an impression of different characteristics of a plant such as a leaf area index, NDVI and any possible suspicious sign of a disease in a plant.

Nonetheless, most of the existing field-based plant phenotyping platforms either do not offer an image acquisition capability or merely utilize a basic manual approach to capture images of cultivars because of two main reasons. First, the existing GPS unit in a camera does not offer the required position accuracy for a mobile plant phenotyping platform. Hence, an external GPS should be used to geo-reference captured images using an image acquisition software, and the synchronization of GPS data and captured images is a challenging task to have a valid geo-referencing system for the possibility of future image retrieval. Secondly, the quality of captured images on a mobile platform can be destructively affected by the vibration and instability of camera base. So the proper camera should be carefully chosen and used for this purpose.

In the development of proposed field-based high-throughput plant phenotyping platform, a novel approach was introduced to capture RGB images and geo-reference them using real-time GPS data for future retrieval. In fact, two image acquisition programs were developed in MATLAB, which will be explained in next chapter, to first capture images using a low-cost webcam and second to capture images using a DSLR camera. However, as results persisted, using a webcam was chosen that will be discussed in section 3-3 of chapter three.

With the development of such an image acquisition system for a field-based plant phenotyping platform comes a series of challenges described below:

- The utilized camera should offer the capability of remote controlling over one of the known communication protocols for convenient data access.
- A device driver or a software development kit (SDK) should be available for the utilized camera to be able to communicate with a programming language.
- The camera should be able to be powered up either by a USB cable or an accessible power source on a farm vehicle. Usually, a 12 VDC or 24 VDC is available on a farm vehicle.

- The utilized camera should offer a fast response time when capturing an image to avoid any conflict for synchronizing acquired images with corresponding GPS data for geo-referencing and possibility of future retrieval.
- The resolution of the camera lens and quality of captured images should be adequate to deliver a thorough visual information when a breeder gages images after field experiments.

In fact, there are many cameras available at the market for entirely different applications, and in the proposed plant phenotyping platform, a webcam and a DSLR camera were used as mentioned earlier.

2-4-1- Using a Webcam

The primary method to capture RGB images was introduced in a field-based plant phenotyping platform by employing two USB webcams to autonomously acquire visual data from two individual plots at the same time while the vehicle is passing through the entire canola field. In fact, a program was developed in MATLAB to first send controlling commands to webcams to take images when needed, and second to communicate with GPS unit for image geo-referencing and future retrieval. The detail of developed software for image acquisition will be discussed in next chapter.

In fact, in the developed field-based plant phenotyping platform a high definition webcam was preferred because of some promising reasons.

First of all, most webcams can conveniently communicate with almost all programming languages including MATLAB, so there will be less obstacles to access image frames in a central computer running image acquisition program. Secondly, a webcam does not need any external power supply to operate. Indeed, a 5 VDC can be supplied by USB port, and this helps to simplify the overall electrical system architecture. Thirdly, nowadays high-resolution webcams are available that offer 1080p and up to 30 frames per second (FPS) so there will be no substantial concern with the insufficient quality of captured images by a webcam and also its response time for synchronization with GPS data.

To choose a high-performance camera, several webcams were tested in laboratory configuration, as can be seen in Figure 2-31 (Logitech Pro, C920 and C615 webcams were examined). It was tried to weigh the selected cameras according to three primary criteria: 1) the

quality of captured images 2) the response time between sending controlling commands and taking a picture and 3) the ability to communicate with MATLAB.

Figure 2-31: Examining the performance of different webcams

To identify the difference between a regular webcam and a high definition webcam, some images were captured from the same object and with the same environmental conditions including ambient light in laboratory configuration and the resulting images were compared. As can be seen in Figure 2-32 a substantial difference can be perceived by having a look at the resulting images.

It is mentionable that no additional filter was applied to these images and for sure the quality of images can be enhanced more by using some filters on these photos.

a) Resulting image by Logitech Pro

b) Resulting image by Logitech C615

Figure 2-32: Test images captured by two different webcams

In fact, Figure 2-32 a) illustrates the captured image by an HD webcam with an image dimension of *1920*1080* pixels which successfully offered a vibrant picture, while the Figure 2-32 b) was obtained by another regular webcam with an image dimension of *1280*1024* pixels and as can be seen, the resulting image was not acceptable because the second webcam could not handle the adverse effect of ambient light. Figure 2-33 illustrates two image histograms for the captured RGB images with two different webcams which are illustrated in Figure 2-32 a) and b).

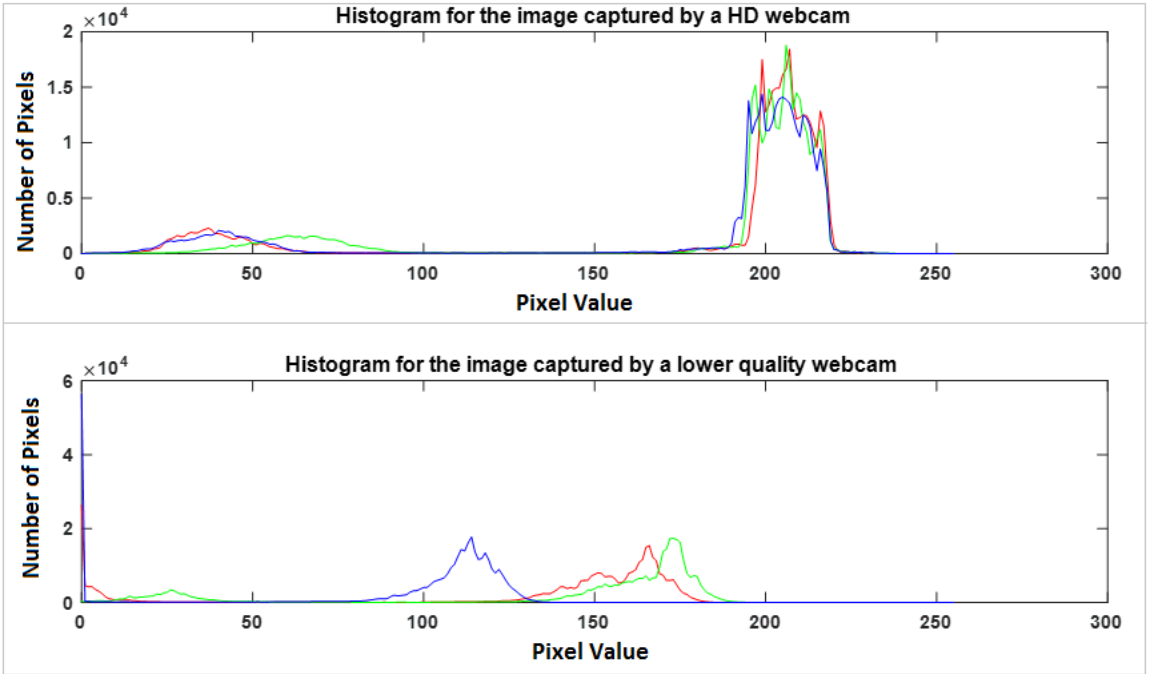

Figure 2-33: Image histograms for the captured images by two different webcams

As can be perceived, the histogram for the captured image by the HD webcam is more uniform in comparison with the histogram of the captured image by the regular webcam. In other words, the majority of image pixels for all three red, green and blue channels in a high quality image have a value around 210, while most of the pixels values in a lower quality image is dispersed between 90 and 180. Moreover, there are significant number of pixels with zero value in a low quality image which is due to the obscurity of the resulting picture. Obviously, applying some filters to remove the existing noises will significantly enhance the quality of these images and more advanced image processing and classification algorithms can be employed to analyze the plant characteristics such as leaf area. So choosing the optimal webcam can offer a higher resolution RGB image and hence more in-depth visual data about a plant in a plant phenotyping platform.

Furthermore, to evaluate the performance of utilized webcam in the fast image capturing, a test configuration was set up as can be seen in Figure 2-34.

In fact, an emulated GPS data string was generated by a first computer program and was sent through a RS232 data link, and the emulated GPS data was received by a second computer running image acquisition program. Then two webcams were aligned to capture a screenshot of

two monitors that was displaying a counting-up timer. Then an image capturing loop with a predefined scan rate as a part of image acquisition program was executed for almost 10 minutes to assess response time and to observe if an image is missing or not.

Figure 2-34: Assessing response time of the utilized webcams

Table 2-7 illustrates the result of time analysis for a single image capturing cycle. As will be discussed more in detail in next chapter, an image acquisition loop consists of four steps. This included sending controlling commands to cameras to take pictures, reading GPS raw data string from a serial port, breaking down the GPS string into meaningful pieces (extracting longitude, latitude and vehicle heading) and finally saving captured images by corresponding GPS data as an image filename for the possibility of future retrieval.

Table 2-7: Assessing existing delays in an image capturing loop

operation	**Time to complete the process (Second)**
Sending command to two cameras to take pictures	0.0030
Reading GPS data from serial port	0.0024
Parsing GPS data and extracting Longitude and latitude	0.00087580
Saving the first image as a *.*png* image	0.7128
Saving the second image as a *.*png* image	0.5837

Figure 2-35 illustrates the bar graph for time analysis of an image capturing loop in the developed image acquisition program.

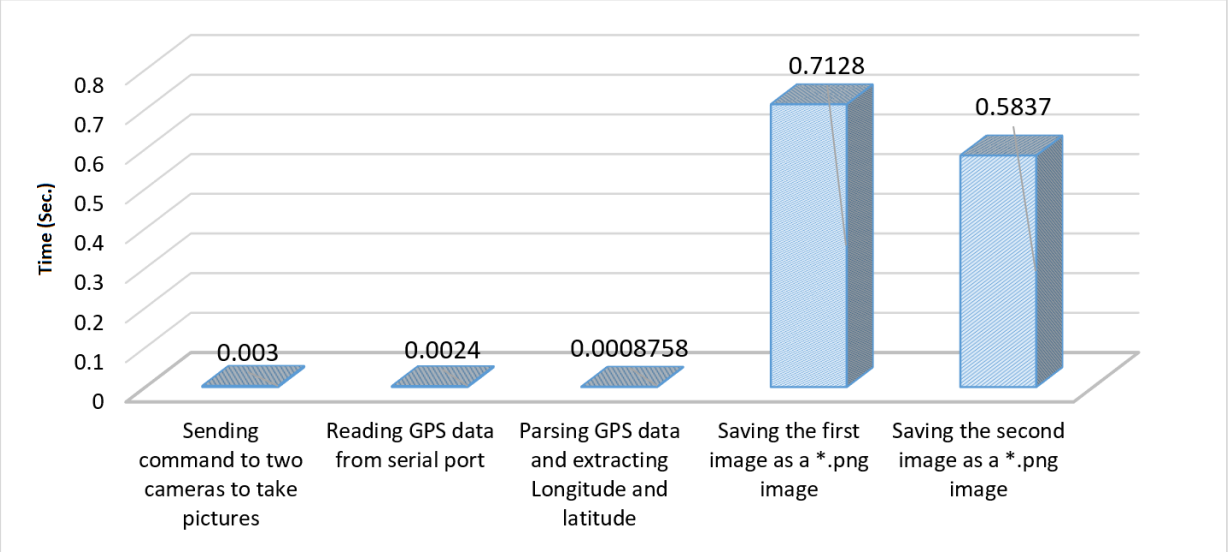

Figure 2-35: bar graph for time analysis of an image capturing loop

As can be perceived from the bar chart, the most time-consuming task is saving both images where 0.7128 second was consumed to save the first image and 0.5837 second was spent to save the second image. However, other three tasks took only 6.28 milliseconds. So as it will be explained in detail in next chapter, a novel approach was proposed to capture images using the developed image acquisition program such that instead of taking a picture and saving it at the end of each loop, images were saved in temporary memory during data collection. Then the contents of temporary memory were stored on the hard drive after capturing all images to avoid any conflict in synchronizing between GPS data and corresponding image for geo-referencing and future image retrieval.

It is mentionable that the time analysis was achieved using MATLAB *tic* and *toc* commands before and after each line in the developed program. This investigation is a crucial study for any other camera because a field-based plant phenotyping platform cannot offer an accurate data geo-referencing capability if there is a substantial delay in either image or data acquisition loops.

Finally, Figure 2-36 illustrates the location of cameras at two far ends of the boom to offer the capability of simultaneously capturing two images of individual plots.

It is notable that the same as other measurement devices, the location of each camera with respect to the GPS antenna on top of the vehicle is known so the required data for geo-referencing images can be calculated by developed functions as will be discussed in next chapter.

Figure 2-36: The location of utilized cameras on the boom

Also, Figure 2-37 illustrates a closer view of utilized webcam attach to the boom near the ultrasonic sensor and facing down to have a broad look of canola cultivars.

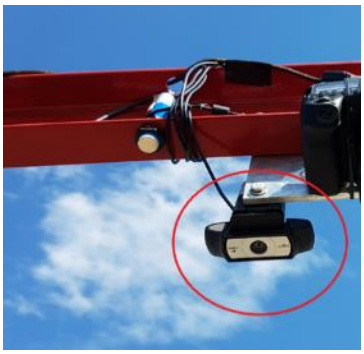

Figure 2-37: A closer look of utilized webcam on the mechanical boom

2-4-2- Using a Digital Single-Lens Reflex (DSLR) Camera

Despite the fact that a webcam could successfully deliver required RGB images of canola cultivars with some minor considerations, a novel approach was introduced to use DSLR cameras in the developed field-based plant phenotyping platform. In fact, a high-resolution DSLR camera can offer an informative and in-depth data about any plant. Furthermore, there are many custom-built lenses for these type of cameras that are specifically designed for plant analysis.

Also, there is more flexibility to eliminate intrusive ambient conditions on the quality of RGB images especially in outdoor configuration. This feature can be significantly useful in a field-based mobile plant phenotyping platform to suppress any possible movement and vibration on the boom.

a) Auto mode

b) AV mode

c) TV mode

Figure 2-38: DSLR camera different mode

As can be seen in Figure 2-38 the performance of a DSLR camera can be significantly enhanced by choosing the correct mode, and more importantly, it can capture images of any fast-moving objects in TV mode. However, the camera could not focus on the target, and the resulting picture was blurry when the automatic mode was used. Also using the camera in AV mode was not a good choice for outdoor configuration and the quality of the captured image was negatively affected by ambient light.

It is mentionable that in this test, some sample images were captured when the camera was facing down and was moved rapidly through a straight line. This analysis was conducted at University of Saskatchewan campus near engineering building during the daytime.

As will be discussed in next chapter, a software solution was used to control a Canon 70D DSLR camera using MATLAB and Canon software development kit (SDK). In fact, a program

was developed to take control of the camera shutter, and the utilized program could remotely control any capturing parameter including shutter speed and aperture value.

Also, to enhance the battery lifetime limitation and to power up the camera by an external power supply for extended time field experiments, a dummy battery and a high capacity battery pack were used instead of the original camera battery. Furthermore, a voltage converter was used to supply 9VDC for the camera when powering up the camera using the vehicle battery is desired.

Nevertheless, using a DSLR camera in the development of proposed plant phenotyping platform was not as successful as utilizing a webcam, because a problem was observed in the process of synchronizing GPS data with the location where images were taken. The reason for this issue is the fact that saving an image could not be controlled programmatically to avoid synchronization with GPS data problem. However, this feature could be controlled in a webcam.

Figure 2-39 illustrates a closer view of utilized Canon DSLR camera attached to the back boom for capturing RGB images. As can be seen, DSLR camera was installed at the far end of the boom and the same location as webcams; two DSLR cameras could simultaneously capture images of two individual canola plots.

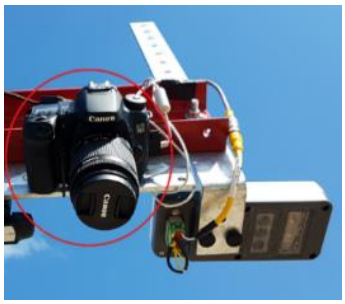

Figure 2-39: A closer view of utilized DSLR camera on the boom

2-4-3- Using a Wireless Camera

Another novel approach for image acquisition in the development of first generation of field-based plant phenotyping platform was deploying two wireless cameras in 2016 experiments. In fact, a particular filter was added to a Nikon Coolpix camera to be able to capture vegetation images.

One of the most advantageous features of the employed wireless camera is the fact that the utilized camera is based-on Android operation system and offers the flexibility of

communicating with different devices over a wireless network and also most of smartphone applications can be executed on this camera. Moreover, a wireless router was used to establish a local network between the central computer, the camera, and a smartphone or tablet if remote control is desired. Figure 2-40 illustrates a closer view of the utilized wireless camera in the first generation boom.

Figure 2-40: A closer look at utilized wireless camera in 2016

Using wireless cameras can be advantageous in the development of a field-based plant phenotyping platform because there will be no need for additional wiring to communicate between image acquisition program running on the central computer and different cameras. However, there is a concern about the battery lifetime limitations and also possible delays for synchronizing GPS data and captured images for georeferencing purposes.

To summarize, after studying the performance of three different type of candidate cameras (webcam, DSLR and wireless cameras), it seems a webcam is the optimum choice to be utilized in the proposed field-based plant phenotyping platform to capture RGB images of plant canopies because of some promising reasons. Firstly, a webcam has a shorter response time, and individual steps for capturing an image can be controlled programmatically. Hence, some programming solutions can be used to minimize the existing delay issue in synchronizing image filenames and GPS data for possibility of future retrieval. Secondly, unlike other cameras which need an additional battery or power supply to operate, a webcam doesn't need an additional power supply. So, it can be used continually for capturing RGB images in a large-scale field without battery lifetime issue. Thirdly, the quality of provided images by a HD webcam appears to be adequate for a field-based trial to analyze a plant canopy. Last but not least, the cost of a webcam is significantly lower than other cameras, so the overall cost of the developed field-based plant phenotyping platform will be less.

2-5- Proposed NDVI Measurement Method

Different objects absorb the different level of a solar radiation in each spectral regions, and hence reflectance data can be extracted from emitting spectral signals on an object and analyzing the reflected signal.

In a plant canopy, many indexes can be derived from this reflectance information. NDVI or Normalized Difference Vegetation Index is one of the most important indicators and demonstrates merely whether an area encompasses green vegetation or not.

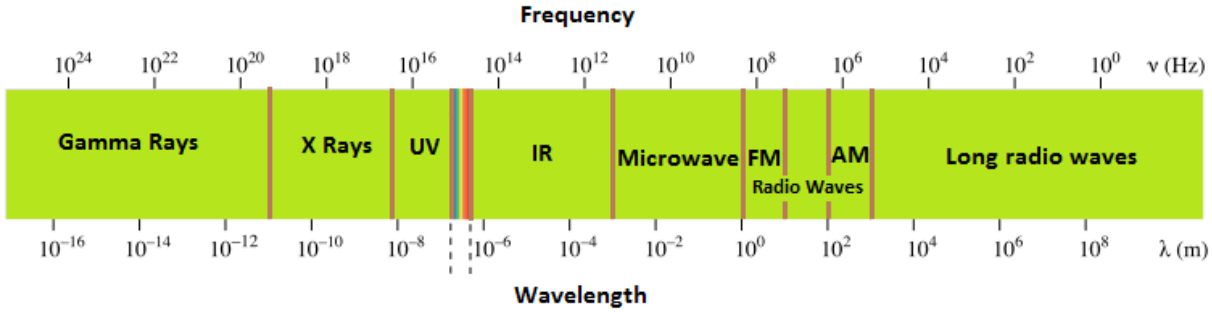

Figure 2-41: The electromagnetic spectrum

Indeed, in plant science, NDVI is a ratio and can be represented by a number between 0-1 and is being used in remote sensing and also plant science research. The closer this number to 1, the greener the area of study is. However, this number can be negative in rare circumstances.

For example, if an area contains some green plants so that they cover exactly half of the area and rest is bare soil, the NDVI can be roughly estimated by 0.5. NDVI=0 means there is no green vegetation in the observed area.

Furthermore, NDVI is calculated by Equation 2-9 using two basic reflectance information about live green plants:

$$NDVI = \frac{NIR - Red}{NIR + Red}$$ Equation 2-9

Where *Red* and *NIR* are spectral reflectance measurements in red and near-infrared (NIR) regions of the electromagnetic spectrum.

In fact, the capability of NDVI measurement is a crucial feature in a plant phenotyping platform because this indicator is an essential parameter for breeders to analyze the plant in different time of the year.

NDVI can be measured using passive or active measurement devices. Unlike passive radiometric light sensors, active devices are not limited by environmental conditions such as ambient light and cloud coverage. Moreover, active sensors don't need to be frequently calibrated and also are less sensitive to the distance between the sensor and the plant.

In the development of proposed field-based plant phenotyping platform, an active crop canopy sensor was utilized which not only provides NDVI but also delivers essential reflectance data from a plant. The employed sensor is also capable of offering measurements regardless of time of the day due to its spectacular light source technology.

Figure 2-42 illustrates top and bottom view of the utilized measurement unit which was used to measure NDVI in a Canola field.

Figure 2-42: Utilized active crop canopy sensor

As can be seen, the sensor uses three optical measurement bands (670 nm, 730 nm, and 780 nm) and a three-channel silicon photodiode array with a spectral range of 320 nm to 1100 nm which is used to measure reflected signals. Also, the sensor is lightweight (less than 0.43 kg) so can be easily used in a mobile plant phenotyping platform. The rugged IP68 packaging makes this device an excellent choice to be used in the outdoor configuration. Moreover, the sensor is capable of delivering ten samples per second in the auto-send mode for fast moving measurement purposes.

The output data can be conveniently extracted from a serial RS232 or RS485 link as can be seen in Figure 2- 43 and also a 12 V battery can be used to power up the sensor. The full datasheet of utilized crop canopy sensor can be accessed in appendices.

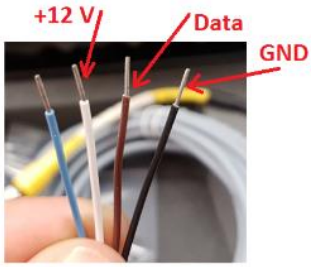

Figure 2- 43: NDVI sensor wiring

To evaluate the performance of selected measurement device to measure NDVI in a canola field, a test platform was configured in the laboratory to make sure the sensor works with no problem. There was some inconvenience to extract data out of the output serial port at the beginning, but the problem was solved after communicating with manufacturer and troubleshooting skills. For example, the default communication port for this sensor was RS485, but a RS232 link was needed to be able to connect this sensor to the utilized datalogger. Also, the sensor was not set to auto-send mode by default to stream the data continuously every 20 ms. And finally, the serial port communication baud rate had to be set to a value which was consistent with the supported values by the employed datalogger to avoid data distortion or loss.

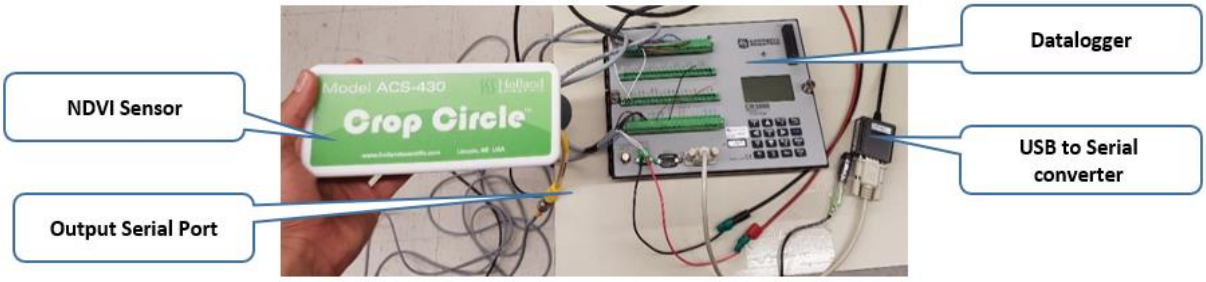

Figure 2-44: Performance assessment of the utilized sensor in laboratory configuration

To verify the effectiveness of the employed NDVI sensor, some objects with a different level of greenness were aligned with the sensor, and the measured values were observed. Because NDVI inherently is a relative index, not an absolute value, there is no exact solution to calibrate or test a NDVI sensor in laboratory configuration, and they are predominantly shipped pre-calibrated by the manufacturer. The essential factor in tests is the ratio of changes. In other words, the greener area, the closer NDVI to 1 is expected to be observed, and this matter was confirmed in the laboratory.

Furthermore, the field of view of the sensor can be determined according to the distance between tip of the sensor and the plant by Equation 2-10 as can be seen in Figure 2-45.

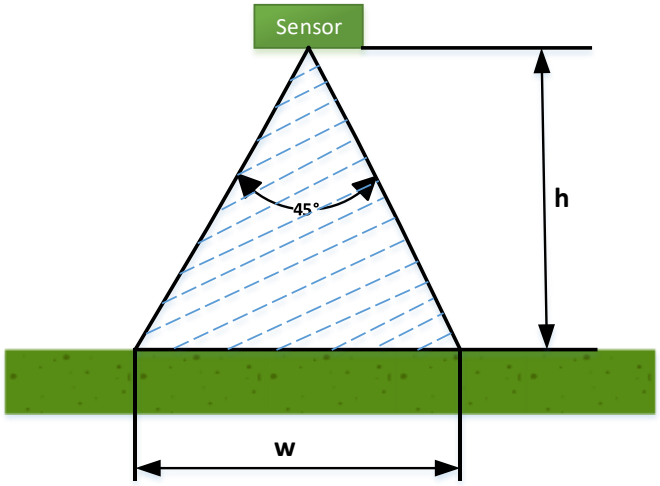

Figure 2-45: Calculating FOV of crop canopy sensor

$$W = 2.h.tan(\frac{\theta}{2}) = 0.82.h$$ Equation 2-10

Where Θ is an angular field of view (~45 degrees for the utilized sensor), W is the projected beam width, and h is the distance between the tip of the sensor and the plant. As can be perceived, the field of view can be adjusted by changing the distance between the boom and canopies and this feature can be undoubtedly helpful to eliminate unwanted measurements.

Figure 2-46 illustrates the location of two NDVI sensors on the right and the left side of the back boom. As can be seen, a bracket was used to adjust the distance between sensor and canopies to achieve the desired FOV.

Figure 2-46: Location of NDVI sensors on the back boom

Figure2- 47 illustrates a closer view of the utilized NDVI sensor. As can be seen, the sensor was rigidly fixed to the far end of the boom to have a better spacing and field of view.

Figure2- 47: Utilized crop canopy sensor on the boom

2-6- Proposed Data Storage System

Two databases were dedicated to the proposed plant phenotyping platform to store phenotypic data. The first database which is located in a central laptop contains all captured images by developed image acquisition programs. This will be discussed in detail in next chapter as a part of developed image acquisition programs. The Second database encompasses all measured values by sensors as well as GPS information for data geo-referencing. In fact, a datalogger was used to communicate with sensors and to store them into a database which can be exported as an Excel file for convenient access by the user. The utilized datalogger appears an ideal choice for a plant phenotyping platform because it can communicate with a variety of sensors with different protocols including a voltage/current analog signals, RS232/485, TCP/IP, DNP3 and more. The full datasheet of utilized datalogger can be accessed in appendices.

Figure 2-48 illustrates the utilized control panel which contains a datalogger, two batteries to provide 12 V and 24V DC power supplies to power up sensors and datalogger and also safety fuses to protect the system form possible short circuits.

Figure 2-48: Utilized datalogger inside a control panel

The cycle time for each data acquisition loop was adjusted to 250 ms which was found as the safe zone for datalogger for reliable operation without any distortion in captured data.

Meanwhile, four samples per second can be acquired by this configuration which seems ideal for the proposed plant phenotyping platform.

It is notable that the data collection is an entirely autonomous process and there is no need for an expert user to operate the vehicle during the field experiments. Indeed, a user can conveniently start the data/image acquisition programs, and at the end of data collection, data can be extracted out of data logger as an Excel file.

To extract data out of data logger at the end of data collection, according to Figure 2-49 a-d, first press *Enter* to enter into the main menu. Then select the *Run/Stop Program* and then select *Stop, Retain Data*. Now datalogger stops reading sensors and no more data will be stored in the database.

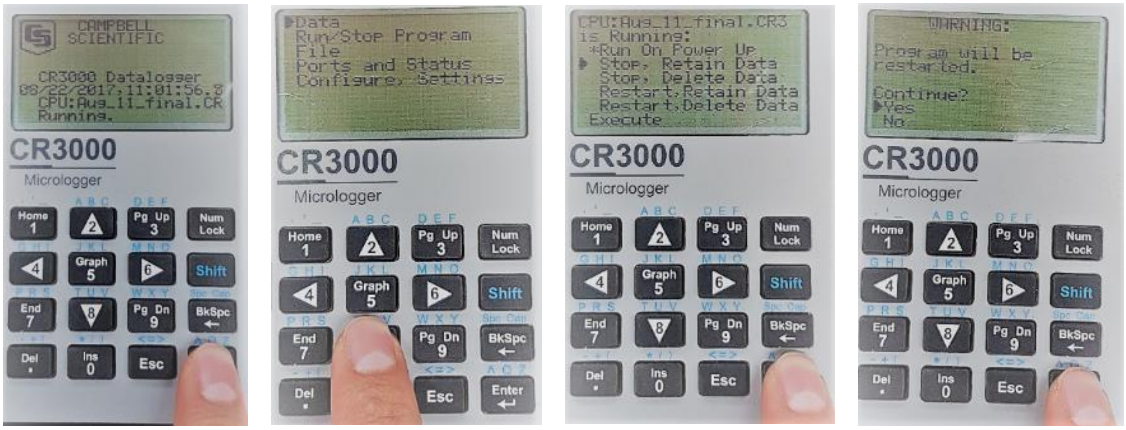

a) b) c) d)

Figure 2-49: Navigating into datalogger menu

At this time database can be extracted out of datalogger instantly or later in the laboratory if needed. To do so, *LoggerNet 4.4.2* should be used to connect to the datalogger over a RS232 link or any other desired communication media. As can be seen in Figure 2-50, this software has a user-friendly graphical interface and makes it easier for convenient data extraction. After opening the software, merely select *Connect* to establish a connection to datalogger.

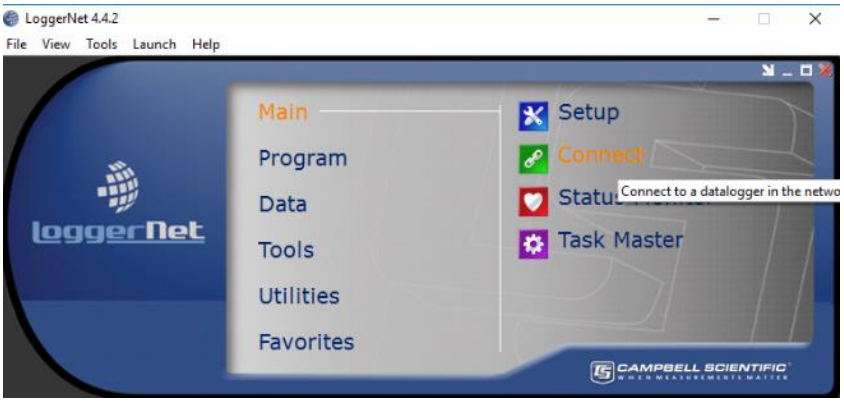

Figure 2-50: LoggerNet software to communicate with utilized datalogger

As can be seen in Figure 2-51, after a connection is established between the datalogger and the computer, different options are available to operate the datalogger. To extract the collected data after field experiments, merely select *Collect Now* and depends on the database volume, the database will be transferred to a computer for further data manipulation.

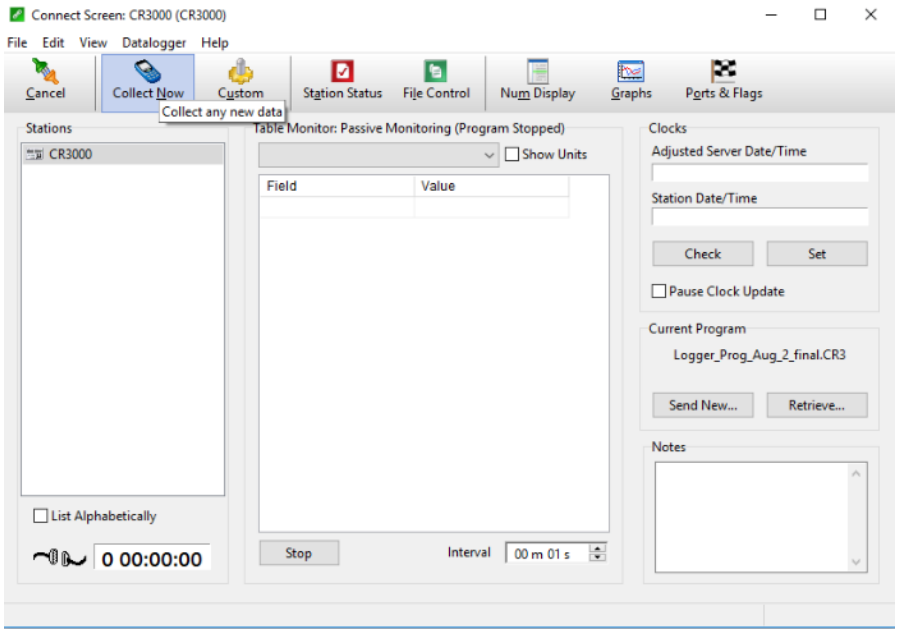

Figure 2-51: Starting data extraction out of datalogger

To customize the format of collected data, select Custom. Also, the software provides a comprehensive help system which can be useful to find different programming commands and operating datalogger remotely.

2-7- Utilized GPS system

There are several global navigation satellite systems to provide geospatial positioning information, and GPS is one of the most commonly used systems around the world. In fact, every single place on the globe can be addressed by a set of unique numbers including longitude and latitude. Because a single GPS receiver cannot provide a highly accurate information for precise geo-referencing purposes, several techniques have been used to enhance the accuracy of GPS receivers. For example, real-time kinematic GPS or RTK GPS is a favorite and efficient technique being used to improve the precision of position data delivered from a regular GPS.

In fact, an RTK GPS utilizes a base station, as can be seen in Figure 2-52, to send some data corrections to the rover GPS and is capable of enhancing the precision up to sub-centimeter which is highly desirable in robotics and more importantly in precision agriculture.

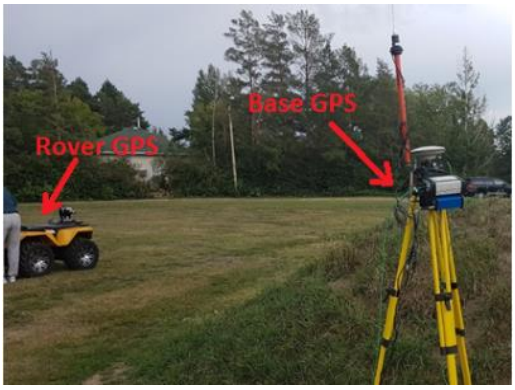

Figure 2-52: An RTK GPS system

Furthermore, there are other enhanced techniques which utilize cell towers as the base station to correct the delivered data by rover GPS. This technique is more common in farming because it is not convenient to carry a base station in different fields.

There are other lower cost techniques such as RTX which doesn't need any additional devices such as modems to correct the information using cell towers. Indeed, RTX utilizes more than one satellites as the data correction method. However, the accuracy of RTK GPS is more than RTX and also RTX has more limitations such as the inability to deliver a repeatable information some of the time and even requires long initialization time to correct the precision of given data.

Another novelty proposed in the developed plant phenotyping platform is utilizing the existing RTK GPS on a farm vehicle to not only access a highly accurate geospatial information

for data geo-referencing but also to reduce the total cost of the proposed platform. In fact, nowadays most of the farm vehicles are equipped with RTK GPS for precision seeding, harvesting, and auto-piloting purposes, and they have the capability of exporting real-time data to third-party devices as well. This ability has rarely been used with other researchers or farmers.

As can be seen in Figure 2-53, the existing GPS system on the utilized farm vehicle in the development of proposed plant phenotyping platform consists of a receiver and a display which runs required software to control the operation of the vehicle including auto-steering during seeding and harvesting seasons.

Figure 2-53: Utilized GPS receiver and display

Also as can be seen in Figure 2-54 the GPS antenna is located on top of the vehicle to provide a stable signal without any distortion. The full datasheet of utilized GPS can be accessed in appendices.

Figure 2-54: Utilized GPS antenna on the farm vehicle

In fact, existing GPS was set up to stream real-time geospatial information as a NMEA RMC data string over a serial RS232 link. Then a laptop which runs image acquisition program, and a datalogger which runs data acquisition program, read sensors signals and stores them in a database, to provide the possibility of using a highly accurate GPS data for georeferencing purposes.

A RMC string can be broken down into different pieces as provided in example below:

[d0,d1,d2,d3,d4,d5,d6,d7,d8,d9,d10,d11]

*Example: $GPRMC,123519,A,4807.038,N,01131.000,E,022.4,084.4,230394,003.1,W*6A*

Where *d0* is message ID or *$GPRMC*, *d1* is UTC of position fix, *d2* illustrates the status of GPS unit which can be *A*=active or *V*=void, *d3* and *d4* represent latitude, *d5* and *d6* represent longitude, *d7* is speed over the ground in knots, *d8* is track angle in degrees, *d9* is date, *d10* is magnetic variation in degrees and *d11* is the checksum data.

Utilizing this approach in the proposed data geo-referencing method, significantly reduced the total cost of the platform because not only an additional accurate RTK GPS was not needed to be purchased, but also no external inertial measurement unit (IMU) was added to the farm vehicle because RMC string contains the heading information of the vehicle which is necessary to obtain for data retrieval.

Finally, to obtain the actual location of each sensor and measurement devices during data collection using a single antenna on top of the farm vehicle, the relation between the GPS and each sensor should be found. As can be seen in Figure 2-55, which is the top view of the developed platform, every single distances and angles can be measured or calculated.

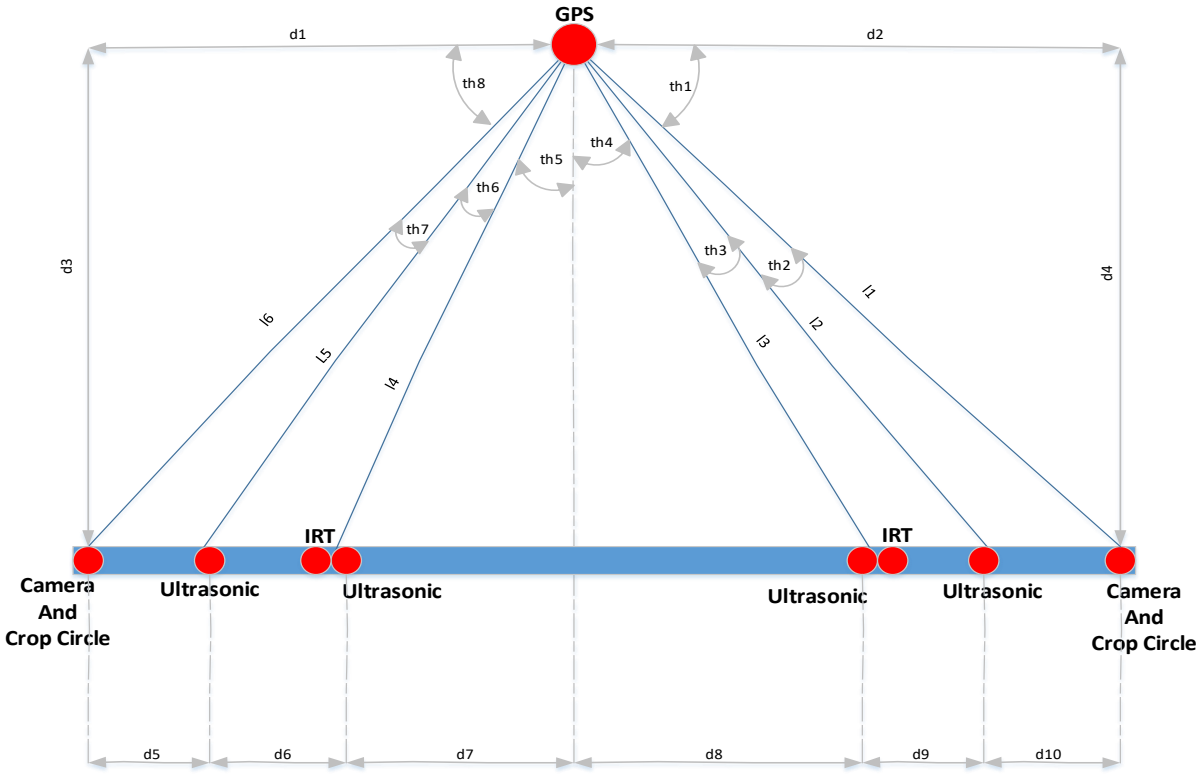

Figure 2-55: Correlation between GPS location and sensors

In fact, *d1*, *d2*, *d3*, *d4*, *d5*, *d6*, *d7*, *d8*, *d9* and *d10* are known parameters according to the mechanical structure of the vehicle and the boom. Because of the symmetrical arrangement of the platform, only a few settings needed to be calculated using Pythagorean theorem as follows.

Starting by *th4*, we can say:

$$\tan(th4) = \frac{d8}{d3} \qquad \textit{Equation 2-11}$$

Also:

$$\tan(th4 + th3) = \frac{d8 + d9}{d3} \qquad \textit{Equation 2-13}$$

And hence:

$$\tan(th4 + th3 + th2) = \frac{d8 + d9 + d10}{d3} \qquad \textit{Equation 2-14}$$

And apparently we can also conclude that:

$$th1 = \frac{\pi}{2} - th2 - th3 - th4 \qquad \textit{Equation 2-15}$$

Now to define the *l1*, *l2* and *l3* we can say:

$$\sin(th4) = \frac{d8}{l3} \quad Or \quad l3 = \frac{d8}{sin(th4)} \qquad \textit{Equation 2-16}$$

Using the same approach, *l1* and *l2* can be defined as below:

$$\sin(th4 + th3) = \frac{d8 + d9}{l2} \quad Or \quad l2 = \frac{d8+d9}{sin(th4+th3)} \qquad \textit{Equation 2-17}$$

$$\sin(th4 + th3 + th2) = \frac{d8 + d9 + d10}{l1} \quad Or \quad l1 = \frac{d8+d9+d10}{sin(th4+th3+th2)} \qquad \textit{Equation 2-18}$$

Now that the relation between the location of each sensor and the GPS antenna on top of the vehicle is found, the latitude and longitude at sensors location according to the latitude and longitude of the GPS antenna can be calculated. Because the relation between the latitude/longitude of two points is not linear, this has to be done in spherical coordinates.

To do so, we assume there are two points (P1, P2) on the earth and the latitude/longitude of the first point is known and finding the latitude/longitude at the second point is desired as can be seen in Figure 2-56.

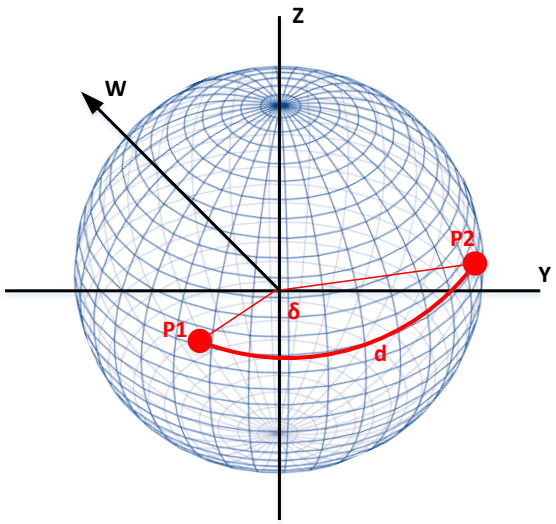

Figure 2-56: Distance between two points on spherical coordinates

Now parameters listed below should be defined to proceed:

Lat1 = latitude at point 1

Lon1 = longitude at point 1

Lat2 = latitude at point 2

Lon2 = longitude at point 2

θ = vehicle heading angle with respect to the North Pole

d = distance between point 1 and point 2

δ = angular distance (δ =d/R, which R is the earth's radius, assuming earth is a complete sphere)

By the spherical law of cosines, we can say:

$$cos(\delta) = sin(Lat1)sin(Lat2) + cos(Lat1)cos(Lat2)cos(Lon2 - Lon1) \qquad \textit{Equation 2-19}$$

Now if we assume a triangle in spherical coordinates between P1, P2 and the North Pole, and we define the angles between points and the North Pole as ψ1 and ψ2, again according to the spherical cosine law can be said:

$$cos(\psi 2) = cos(\psi 1)cos(\delta) + sin(\psi 1)sin(\delta)cos(\theta)$$ *Equation 2-20*

Hence:

$$cos(\theta) = \frac{cos(\psi 2) - cos(\psi 1)cos(\delta)}{sin(\psi 1)sin(\delta)}$$ *Equation 2-21*

Using $\psi_i = \pi/2 - Lat_i$, we can conclude that:

$$cos(\theta) = \frac{sin(Lat2) - sin(Lat1)cos(\delta)}{cos(Lat1)sin(\delta)}$$ *Equation 2-22*

Or:

$$sin(Lat2) = cos(\theta)cos(Lat1)sin(\delta) + sin(Lat1)cos(\delta)$$ *Equation 2-23*

$$Lat2 = Arcsin(cos(\theta)cos(Lat1)sin(\delta) + sin(Lat1)cos(\delta))$$ *Equation 2-24*

The Equation 2-24 defines the relation between the latitude at P2 according to the latitude at P1, vehicle heading and the distance between P1 and P2. With the same manner, the relationship between the longitude at P2 according to the longitude at P1, vehicle heading and the distance between P1 and P2 can be defined as below.

According to the Equation 2-19 we can say:

$$cos(Lon2 - Lon1) = \frac{cos(\delta) - sin(Lat1)sin(Lat2)}{cos(Lat1)cos(Lat2)}$$ *Equation 2-25*

Also, θ can be represented without angular distance using Equation 2-26:

$$tan(\theta) = \frac{sin(Lon2 - Lon1)cos(Lat2)}{cos(Lat1)sin(Lat2) - sin(Lat1)cos(Lat2)cos(Lon2 - Lon1)}$$ *Equation 2-26*

And we know that:

$$tan(\theta) = \frac{sin(\theta)}{cos(\theta)}$$ *Equation 2-27*

So:

$$sin(\theta)[cos(Lat1)sin(Lat\ 2) - sin(Lat\ 1)cos(Lat\ 2)cos(Lon2 - Lon1)] = sin(Lon2 - Lon1)cos(Lat2)cos(\theta)$$ *Equation 2-28*

By substituting Equation 2-22 and Equation 2-25 into the Equation 2-28, we can conclude:

$$sin(Lon2 - Lon1) = \frac{sin(\theta)sin(\delta)}{cos(Lat2)} \qquad \textit{Equation 2-29}$$

Now by having Equation 2-25 and Equation 2-29 we can say:

$$tan(Lon2 - Lon1) = \frac{sin(Lon2 - Lon1)}{cos(Lon2 - Lon1)} = \frac{cos(Lat1)sin(\theta)sin(\delta)}{cos(\delta) - sin(Lat1)sin(Lat2)} \qquad \textit{Equation 2-30}$$

And solving for Lon2 we get:

$$Lon2 = Lon1 + arctan(\frac{cos(Lat1)\, sin(\theta)\, sin(\delta)}{cos(\delta) - sin(Lat1)\, sin(Lat2)}) \qquad \textit{Equation 2-31}$$

Which defines the longitude at the point P2 according to the longitude and latitude at the point P1, vehicle heading and the distance between two points P1 and P2. Equation 2-24 and Equation 2-31 were implemented as a function in MATLAB to be used in both field mapping and visualization programs and will be discussed in detail in section 3-4-1 of chapter three.

For better understanding of practicality of the derived equations, consider the top view of the developed platform which was illustrated earlier in Figure 2-55. As noted before, the only available GPS antenna is located on top of the vehicle. However, we need to achieve the geospatial information at the location of each sensor to be able to associate the collected data with the corresponding plot. For example, to define the longitude and latitude at the location of the camera on the right wing of the mechanical boom, we can simply substitute *l1* and *th1* into the developed function in MATLAB to implement Equation 2-24 and Equation 2-31. In other words, the longitude/latitude of the mentioned camera can be calculated according to the longitude/latitude which is delivered by existing GPS antenna on top of the vehicle.

2-8- Proposed System Block Diagram for the Early Generation of the Platform

After investigating the utilized devices and methods to capture different characteristics of a plant using the proposed field-based high-throughput plant phenotyping platform, in this section and next section the proposed system architecture for experiments in 2016 and 2017 is discussed. Figure 2-57 illustrates the schematic of the proposed electrical system during 2016 experiments.

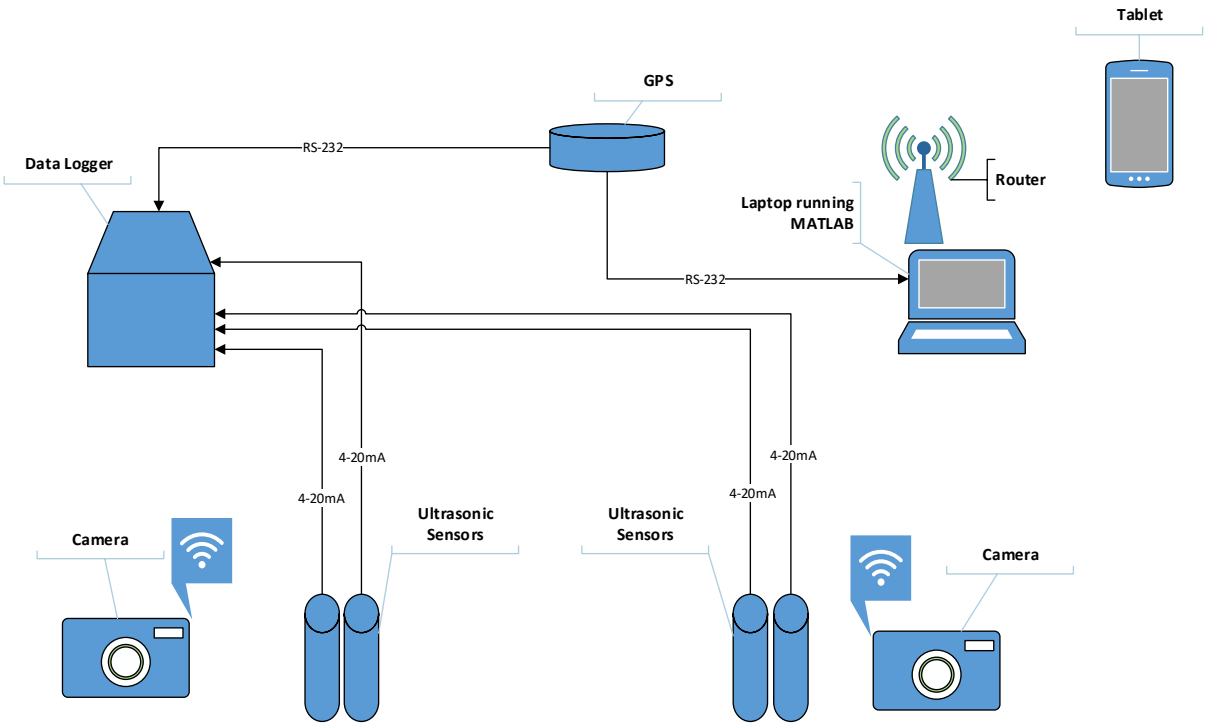

Figure 2-57: Proposed system architecture in 2016 trials

Indeed, four ultrasonic sensors were arranged on the mechanical back boom to measure the height of the plant canopies. Two sensors were used on each side of the boom as can be seen in Figure 2-58 to collect two data samples at the same time from the left side and middle part of each plot.

Also, the output signal of the ultrasonic sensors was chosen to be 4-20 mA because a relatively long cable was needed to connect sensors to the datalogger, so the system was prone to a lower level of noises and distortion.

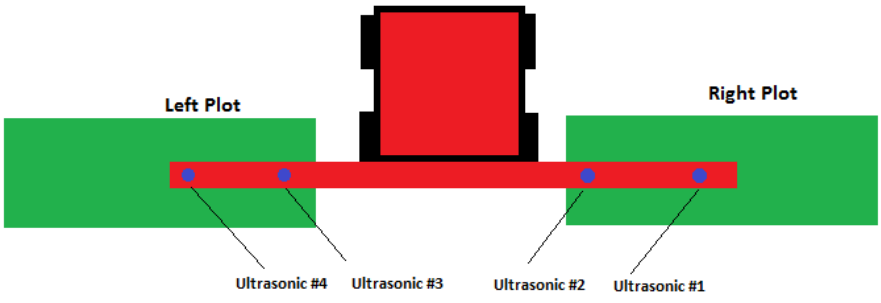

Figure 2-58: Ultrasonic Sensors on the back boom

Also existing GPS antenna exists on the farm vehicle was able only to export one data string at the same time, but to geo-reference both images and measured data by sensors, two outputs was needed. So a serial port splitter was used to expand the number of serial ports of GPS receiver.

Furthermore, the utilized cameras were connected to the central laptop running image acquisition program using a wireless router to capture RGB images as can be seen in Figure 2-59. In fact, both cameras and laptop were connected to this router and could communicate with each other because they were on the same IP pool.

Figure 2-59: Utilized Wireless router

Also, Figure 2-60 illustrates the location of utilized wireless cameras on the back boom to be able to capture two RGB images at the same time from the left side and middle part of each plot.

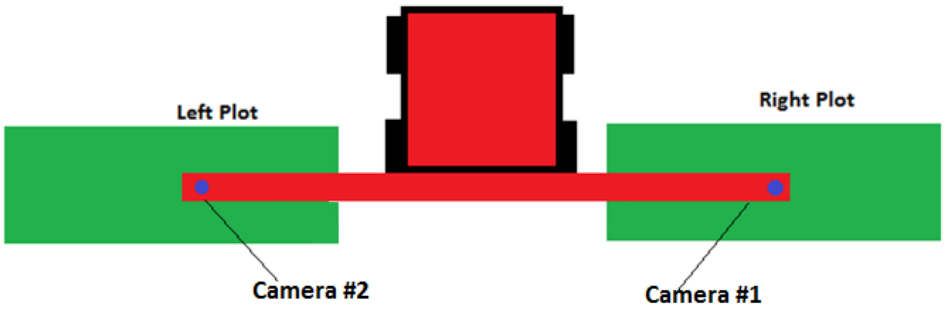

Figure 2-60: Wireless cameras on the back boom

Finally, Figure 2-61 illustrates the proposed field-based plant phenotyping platform during 2016 experiments.

Figure 2-61: Proposed platform in operation during 2016 trials

2-9- Proposed System Block Diagram for 2017 Experiments

After initial field experiments in 2016, the system bottlenecks and flaws were identified, and it was tried to resolve them in 2017 design as much as possible. As can be seen in Figure 2-62 a significant improvement was suggested in proposed system by adding more sensors to the system including thermometer and NDVI sensors in 2017. Furthermore, different causes of delays in a system including the wireless connection between cameras and laptop were replaced to achieve higher performance. The detail of results of each experiment will be discussed in chapter four.

In fact, two infrared thermometers which provide the canopy temperature as a voltage signal were added to the system. Also, Two NDVI sensors which provide a digital output over serial RS232/485 were attached to the far ends of the back boom, next to the cameras.

Furthermore, instead of wireless cameras which were identified as significant sources of delay in synchronizing captured data and GPS information for future retrieval, two USB cameras were used for first fast response time and second to eliminate the battery lifetime issue which was observed in 2016 experiments. In fact, a USB camera was found an effective choice to be used in a field-based plant phenotyping platform as an image acquisition device with some minor considerations.

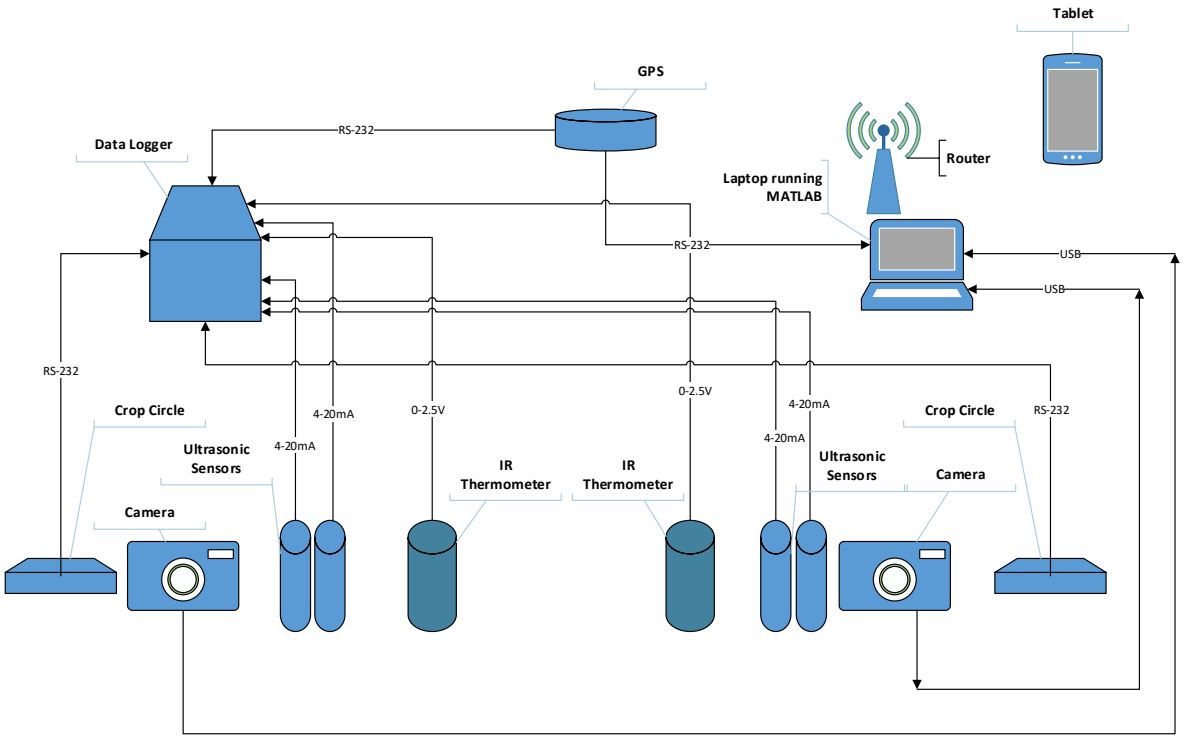

Figure 2-62: Proposed system architecture in 2017 experiments

Furthermore, the modularity of the system was improved by utilizing waterproof connectors to provide the possibility of easy removal of the electrical and instrumentation system from the farm vehicle, if needed.

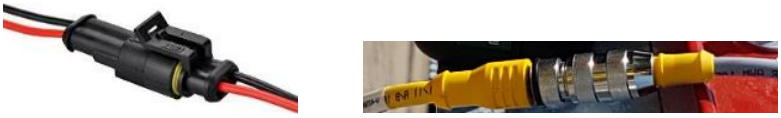

Figure 2-63: Utilized waterproof connectors

It is notable that, mechanical design team designed two different mechanical booms and after wiring sensors and measurement devices on each boom as two individual sets of experiments, their performance was tested in 2017. As can be seen in Figure 2-64 the first generation of the boom was not foldable for convenient transportation because of its long length. However, as can be seen in Figure 2-65 the second generation boom was designed such that offers the ability to fold on each side using two revolute joints. Also, the distance between the NDVI sensors and top of the canopies could be adjusted in second generation boom.

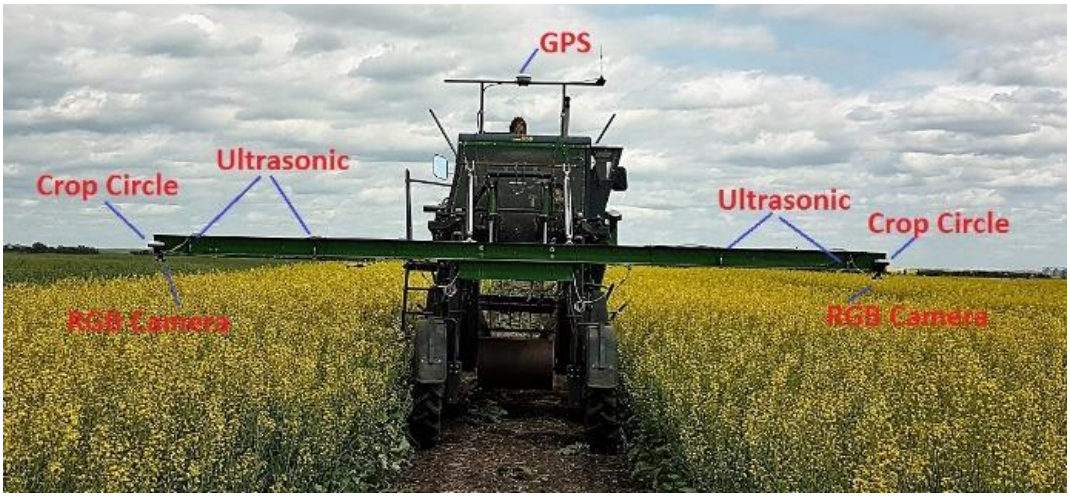

Figure 2-64: First platform (long and un-foldable boom) in operation during 2017 experiments

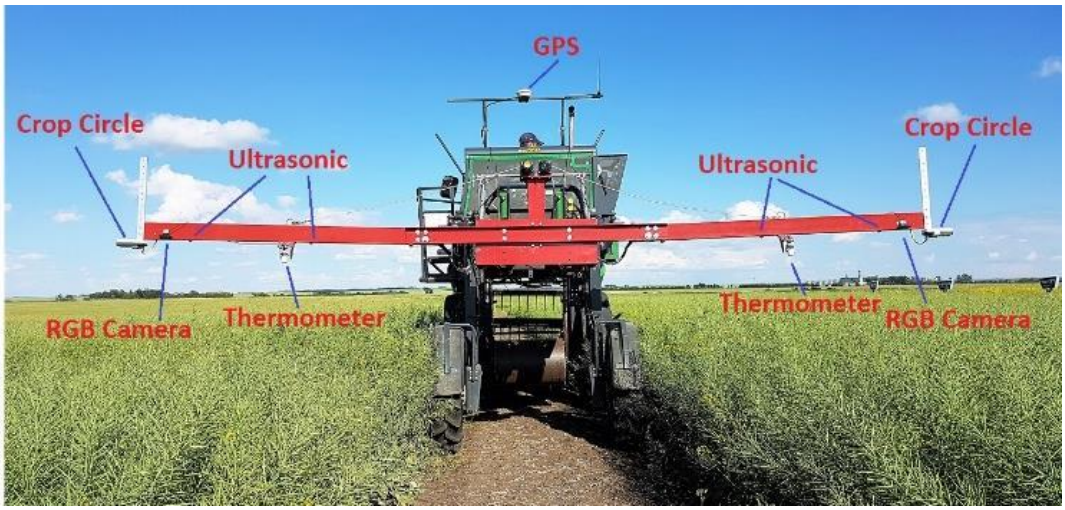

Figure 2-65: Second platform (with foldable boom) in service during 2017 experiments

2-10- Summary

To summarize, the hardware part of the developed field-based plant phenotyping platform was explained in this chapter. As explained, canopy height, temperature, NDVI, and photographic information (by RGB image) were target traits in the proposed platform. However, more sensors can be easily added to the current system to obtain more characteristics of a plant as the result of future works.

To verify the accuracy of measurements delivered by the utilized sensors, a series of experiments were conducted in the laboratory configuration. It was shown that an ultrasonic

sensor could effectively measure the height of different objects including the height of a plant with a few considerations.

Also, the performance of three different type of cameras including webcams, DSLR, and wireless cameras was examined, and it was found that the webcam appears the optimum choice to be used in a field-based mobile plant phenotyping platform to capture RGB images of plants. The reasons for this verdict can be summarized as fast response time, adequate image quality, convenient data communication and finally lower cost. In fact, it was found that the most time-consuming step in an image acquisition loop is saving an image, and a webcam was found the only camera which offers to be entirely controlled programmatically to minimize the existing delay in synchronization of captured images and GPS data to achieve an accurate geo-referencing algorithm.

Moreover, after a discussion about the utilized methods to capture canopy temperature and NDVI, as well as the structure of the data storage system, the proposed data/image geo-referencing method using a single GPS antenna was explained. Indeed, two equations were derived in spherical coordinates to correlate the latitude/longitude at point A with latitude/longitude at point B. These equations were needed to define the geo-spatial information at the location of each sensor according to the information obtained from the GPS antenna on top of the vehicle. The implementation of the resultant equations in MATLAB will be discussed in next chapter.

CHAPTER 3

PROGRAMS DEVELOPED FOR DATA ACQUISITION AND VISUALIZATION

3-1- Introduction

Apart from hardware development of the proposed field-based high-throughput plant phenotyping platform (HTPP) that was explained in the previous chapter, the most challenging achievement in this research is the development of programs for an effective field-based mobile HTPP. In fact, the three essential programs needed for an HTPP can be categorized as below:

- A data acquisition program to read different sensors data, geo-reference every single piece of data using an accurate GPS and then to create a phenotypic database that contains meaningful information about all plant canopies in a field.
- An image acquisition program to autonomously capture images of plant canopies, geo-reference them and store them on a computer hard drive for further assessment and future investigation.
- A data visualization program to read all collected data and images and represent them using a graphical user interface for convenient access by breeders.

With the development of each program mentioned above for a field-based mobile platform comes a series of challenges and problems to be addressed by assessing the performance of a variety of candidate solutions. For example, how can we create a custom map to localize individual plots in a field when an accurate hand-held GPS is not available? How can we define which group of data amongst thousands of collected dataset belongs to which individual plots? How the collected data can be synchronized with geospatial information to achieve a highly accurate geo-referencing method? How can we evidently represent available data to a user who doesn't have technical (programming or engineering) background? These few examples are amongst the challenges which in this chapter will be discussed in detail.

Despite the fact that there are many programming languages with their pros and cons, in this research MATLAB was used as the primary programming language for data visualization for the first time in a field-based HTPP because of several reasons.

First of all, MATLAB is widely accepted and is being used in the engineering community. This significantly reduces the consumed time to learn a new programming language, so other researchers can easily understand and continue the development of the proposed programs.

Secondly, MATLAB offers a variety of toolboxes and functions for advanced data analysis. For example, the quality of captured images by proposed HTPP can be easily enhanced, and different image analysis can be implemented using MATLAB Image Processing Toolbox. Also, different statistical data analysis and modeling toolboxes can be used to conveniently model and analyze collected data.

Thirdly, there will be no need for an additional geographic information system (GIS) software such as ArcGIS or QGIS for geospatial data representation which is being used in most of the existing field-based plant phenotyping platforms.

In following sections, developed programs for the proposed field-based HTPP will be explained. The hardware aspect of each section was discussed in chapter two. Also, this chapter doesn't focus on the results achieved by using the proposed programs, and the results are discussed in details in chapter four.

3-2- Data Acquisition Programs

As discussed in chapter two, a datalogger was used to communicate with a variety of sensors and to store collected data as an Excel database for future access. Figure 3-1 illustrates a schematic of the proposed data acquisition system.

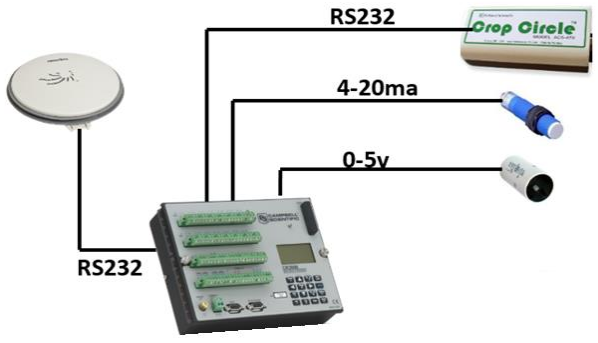

Figure 3-1: Data acquisition system consists of four ultrasonic sensors for height measurement, two IR thermometers for temperature measurement, and two Crop Circle sensors for measuring NDVI

The utilized programming environment for data acquisition, LoggerNet, was provided by the manufacturer of datalogger as can be seen in Figure 3-2.

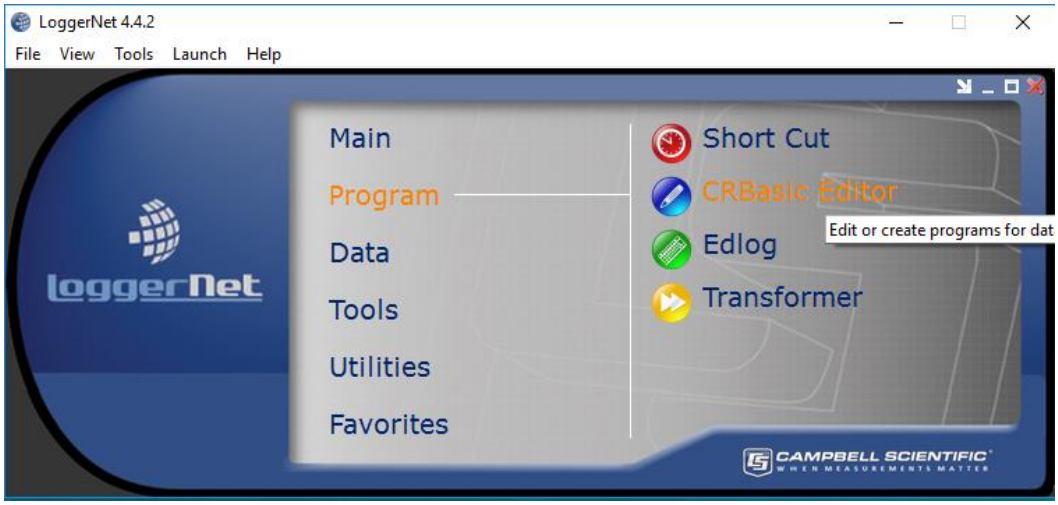

Figure 3-2: Utilized programming environment for DataLogger

In fact, a pseudo code for the developed data acquisition program can be summarized as below:

Declaring Variables

Defining the structure of Database (or data tables)

Start of the Program and initializing all Objects

Start of Data Capturing Loop

Reading Sensors Data

Data Manipulation if Needed

Call Data Tables and Save Collected Data

Repeat Data Capturing Loop

Final Operations before ending the Program

End of the Program

As can be perceived, the first step is declaring required variables which are meant to be used next during programming. For example, some variables with different data types should be defined to temporarily store collected data by sensors before saving them into the Excel file.

The second block is defining the structure of the database which is an Excel file to encompass all phenotypic data. This structure can be defined as needed with a variety of customized formats. In the proposed plant phenotyping platform, the structure of the phenotypic database is designed as Table 3-1. This table contains two typical data as an example for better intuition.

Table 3-1: The structure of Phenotypic Database

Record #	Date and Time	IRT #1	IRT #2	NDVI Sensor #1	NDVI Sensor #2	GPS NMEA String	Ultrasonic sensor #1	Ultrasonic sensor #2	Ultrasonic sensor #3	Ultrasonic sensor #4
1	Jan 1, 2017 3:00 pm	23	22.5	0.5	0.99	GPS1*	90	93	110	114
2	Jan 1, 2017 3:05 pm	24	27.2	0.7	0.1	GPS2**	85	82	121	123

* $GPRMC,162148,A,5220.28776661,N,10617.11092988,W,-0.0,91.3,180817,15.1,E*43

** $GPRMC,162150,A,5220.28776552,N,10617.11092693,W,0.0,91.3,180817,15.1,E*61

In fact, each column represents a specific data, and a row represents a complete data point. Record # is the number of data point in a whole database and can go up to 5000 depends on the size of the field and the data acquisition program execution time. Date and time illustrates the information about the data collection day. IRT#1 and 2 encompass the acquired data by inferred thermometers.

Likewise, NDVI sensor #1 and 2 show the captured data by each NDVI sensors. GPS NMEA string which is the most important column, represent geospatial information of the location where data was obtained to provide the possibility of future retrieval. Also, ultrasonic sensor #1-4 represent the canopy height which was collected by ultrasonic sensors.

The next step in a program for data acquisition is the primary data collection loop which aims to communicate with different sensors, manipulate raw data if needed and then store them in the database.

Figure 3-3 illustrates the algorithm developed for data acquisition. The complete program developed for data acquisition can be found in Appendix A.

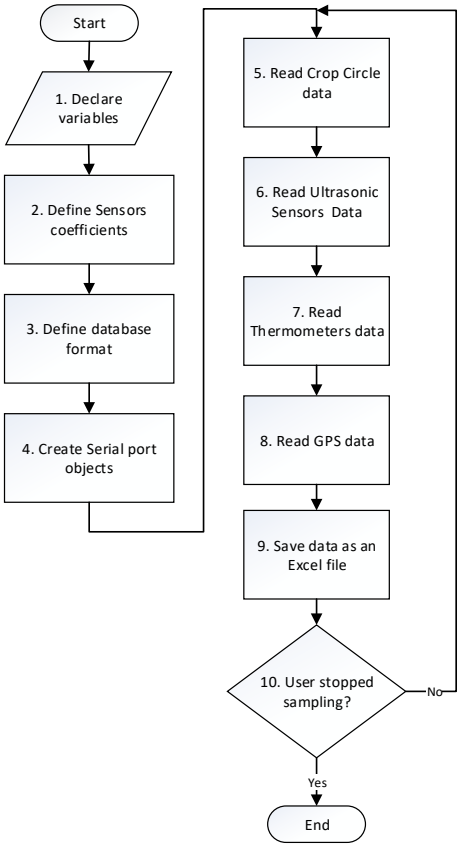

Figure 3-3: Flowchart of Data acquisition program algorithm developed

As can be seen in Figure 3-3, after declaring variables to temporarily hold values during data collection loop and defining the desired structure of the database, serial port objects were created. Indeed, one serial RS232 port was created to communicate with GPS string, and two other RS232 ports were used to read NDVI sensors data. The baud rate of 38400 bps was found the optimal and reliable data communication rate for all three serial RS232 ports to minimize data loss and to achieve a fast data transmission between datalogger and measurement devices.

Then ultrasonic sensors raw values were obtained as 4-20 mA signals and were converted to corresponding canopy height using a regression model which was discussed in chapter two. Then the infrared thermometers raw data were acquired as voltage signals and were transformed into the corresponding canopy temperature according to the functions developed for this purpose as was discussed in chapter two.

Also, the GPS information was captured as the last step to avoid synchronization issues in data geo-referencing. In fact, it was found that if GPS information is captured before reading

sensors data, an internal delay can cause a fundamental issue for data geo-referencing. Finally, all captured data were stored into an Excel file as the central phenotypic database.

It is mentionable that the data acquisition cycle was programmed to be executed every 250ms to capture four sample points per second. This capturing speed offered to collect around seven data per plot according to the vehicle traveling speed (~ 1.8 mph or 0.8 m/s). This number was found as the reliable zone for datalogger and sensors to avoid data loss or misrepresentation.

Finally, the developed program was compiled and downloaded into the datalogger as can be seen in Figure 3-4 and Figure 3-5.

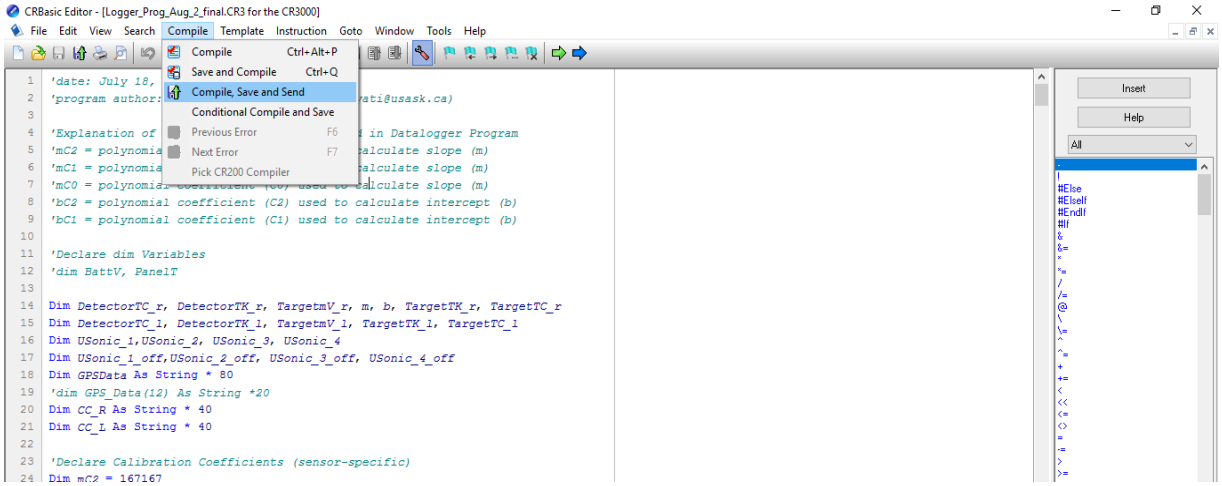

Figure 3-4: Compiling the data acquisition program

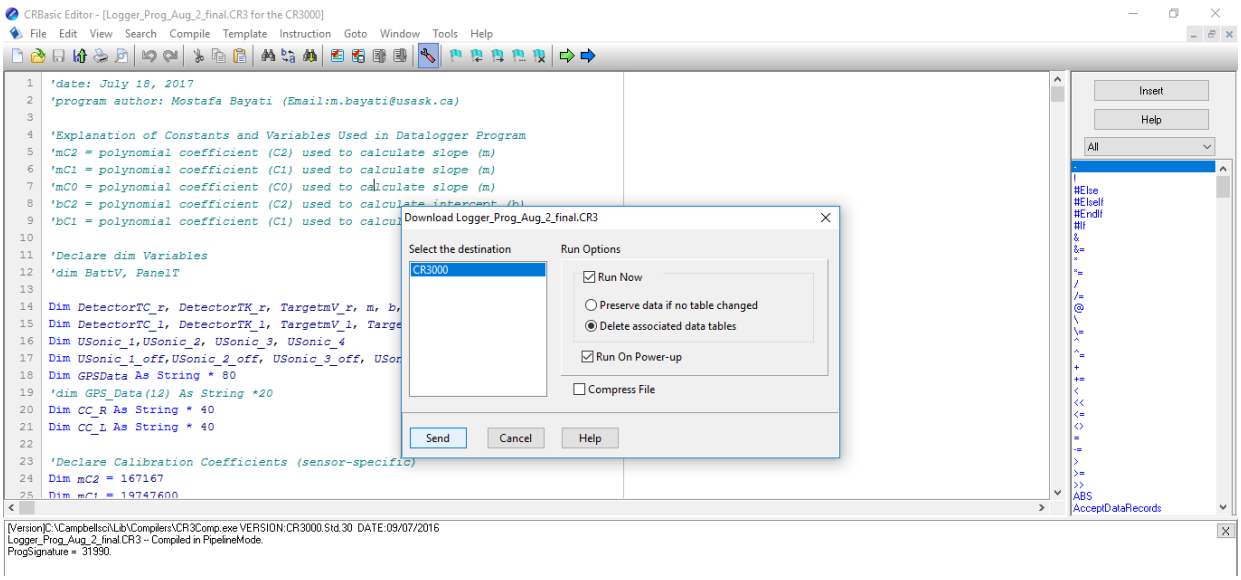

Figure 3-5: Downloading the data acquisition program into the DataLogger

Last but not least, it was tried to avoid any unnecessary data manipulation during data collection to minimize existing delays in synchronizing GPS information and sensors data. For example, GPS NMEA string was saved without any manipulation, and as will be discussed in future sections, raw data was broken down into meaningful pieces in data visualization program where delay cannot be a significant source of the error.

3-3- Image Acquisition Programs

In the previous section, it was explained how a program was developed for a datalogger to produce phenotypic databases which encompass a variety of information about plant canopies. Dataloggers are based-on a customized real-time operation system to read standard signals such as 4-20 mA or 0-5 V, and they are only used to store numeric or string data on their limited amount of memory as a text file. However, they cannot store high volume RGB images or other data files. So the image acquisition program has to be developed and executed on a laptop with Windows/Linux operation system instead of a datalogger.

As mentioned earlier, one of the novelties proposed in the developed field-based high-throughput plant phenotyping platform is the capability of autonomously capturing images of plant canopies while the vehicle is passing through the field. At the time being, none of the existing field-based HTPPs are reported to offer this feature. Figure 3-6 illustrates a schematic of the proposed image acquisition system.

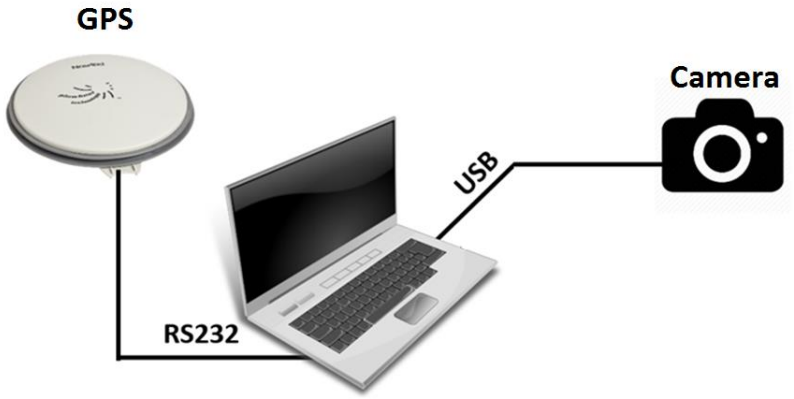

Figure 3-6: Image acquisition system consisting of a laptop to run the developed image acquisition program, a camera for capturing RGB images and a GPS for geo-referencing captured images

In fact, three different image acquisition programs were developed and their performance was evaluated during field experiments in 2016 and 2017. In the next three sections, details of each program will be explained and the complete source code of the final image acquisition program can be found in Appendix B.

3-3-1- Image Acquisition Program using Wireless Cameras

As discussed in chapter two, the performance of two wireless cameras to capture RGB images in the early generation of the proposed HTPP was evaluated during field experiments in 2016. Indeed, a program was developed in MATLAB GUI to communicate with two IP cameras as can be seen in Figure 3-7.

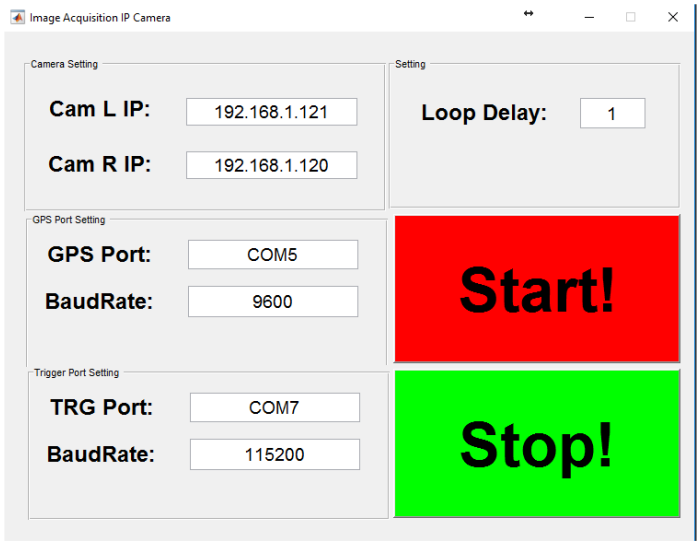

Figure 3-7: User interface for image acquisition using IP camera program.

Moreover, two different algorithms were developed to capture images as can be seen in Figure 3-8 a) and b). In fact, image acquisition loop was executed in two different modes to minimize the existing errors in synchronizing captured images and GPS data for georeferencing purposes.

As can be perceived from Figure 3-8 a), initially images were captured in a time-basis approach and image capturing loop was executed every 500 milliseconds or any other value assigned by the user during field experiments until the user stops the program. This approach was found inefficient due to a remarkable delay in a wireless network.

On the other hand, an external trigger signal coming from the vehicle GPS receiver box was used to define whether is needed to capture a picture or not as can be seen in Figure 3-8 b). Indeed, GPS receiver box was adjusted to send a trigger signal every 1.8 meters while the vehicle was passing through the field. Then after receiving this signal, the program was assigned to send the controlling commands to cameras to capture images at the center of each plot. This approach was used to avoid continuously sending commands to wireless cameras every 500ms to prevent data loss.

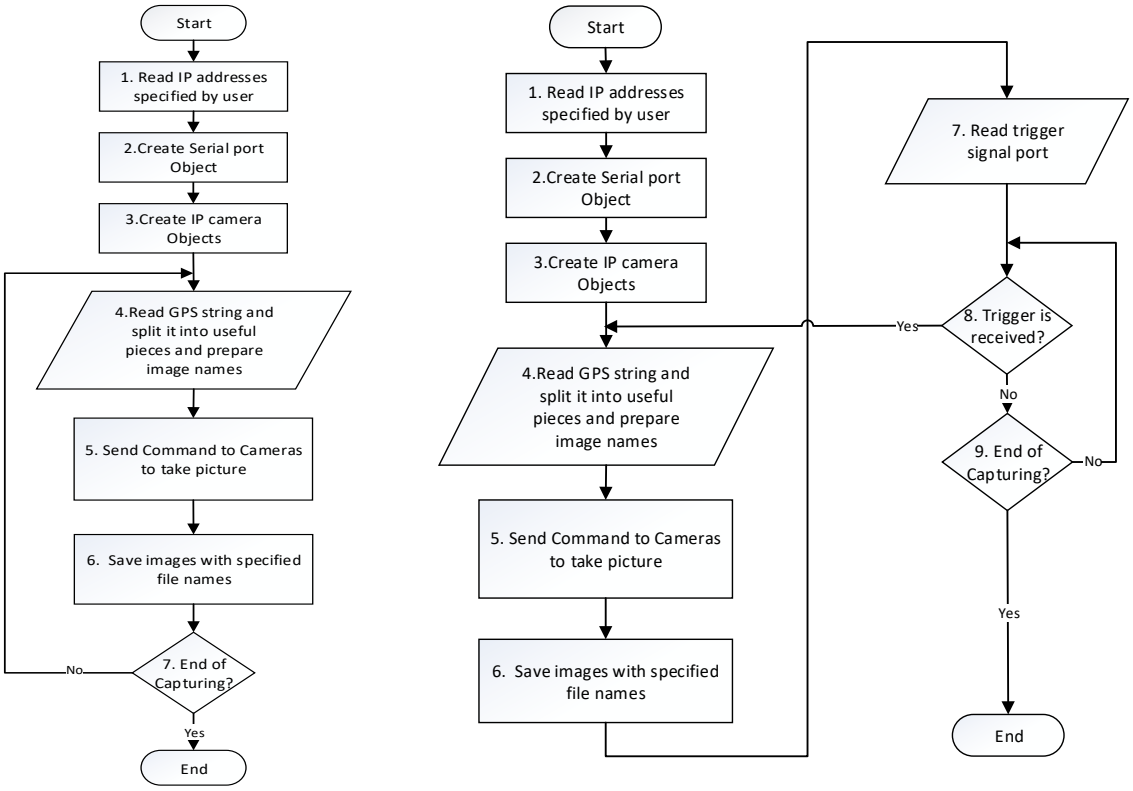

a) Triggering based-on time b) Triggering by GPS signal

Figure 3-8: Algorithm for image acquisition using wireless camera program

3-3-2- Image Acquisition Program using Webcams

Another novel approach to capture images of plant canopies is utilizing low-cost webcams to autonomously capture RGB images while the vehicle is scanning a large-scale field. As can be seen in Figure 3-9, a graphical user interface was developed for convenient user interaction to control the operation of image acquisition program.

Figure 3-9: User interface for image acquisition using webcam program

Figure 3-10 illustrates the algorithm for the developed image acquisition program using webcams.

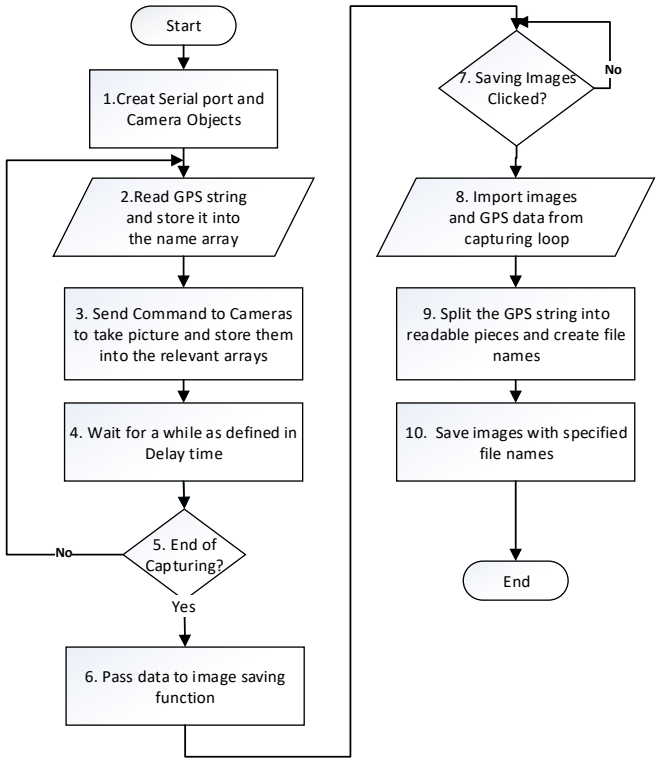

Figure 3-10: Flowchart of Image acquisition program using webcam

As can be seen from Figure 3-10, and as was discussed in Section 2-4 of Chapter two, a novel method was proposed to significantly reduce the existing delays in an image acquisition cycle and improve the geo-referencing process by storing images in temporary memory during data collection, and saving them on the hard drive after all images were captured.

In fact, using webcams offers the flexibility of controlling every single step in an image acquisition loop including sending commands, receiving the captured image, creating a custom file name and saving an image on the hard drive. However, other cameras such as DSLR cameras don't appear to offer this capability as it will be discussed in next section.

3-3-3- Image Acquisition Program using DSLR Cameras

As was discussed in section 2-4 of chapter two, DSLR cameras can be useful in a plant phenotyping platform because of the superior quality of their delivered images. Despite the fact that webcams could successfully capture images of plant canopies in the proposed field-based plant phenotyping platform, the performance of high-quality DSLR cameras for this application was evaluated in this research.

In fact, Canon offers a software development kit (SDK) to provide the capability of communicating with their DSLR camera using different programming languages. Moreover, digiCamControl is a customized software to control Canon DSLR cameras in MATLAB over USB port which was exploited for the development of an image acquisition program in the proposed plant phenotyping platform. Figure 3-11 illustrates the graphical user interface of the developed program for capturing image of plant canopies using DSLR cameras.

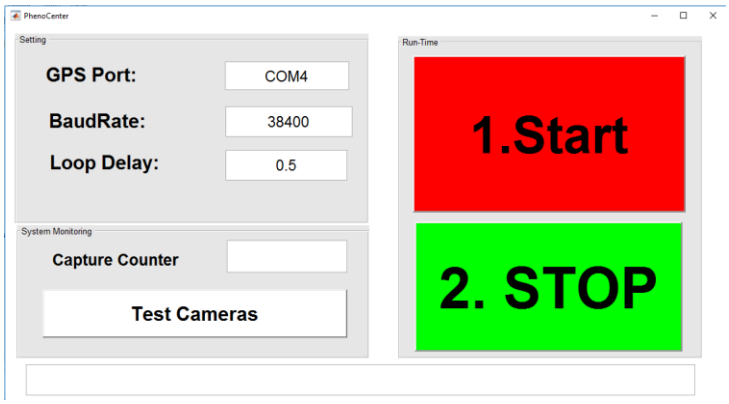

Figure 3-11: User interface for image acquisition using DSLR camera program

As can be seen from Figure 3-11, the developed program has a user interface to conveniently set up the GPS communication port, and to start/stop the image acquisition cycle during field experiments. Moreover, some captured images can be seen in "capture counter" section to make sure about the proper operation of the program during data collection.

Figure 3-12 illustrates the proposed algorithm to capture RGB images of plant canopy using two DSLR cameras.

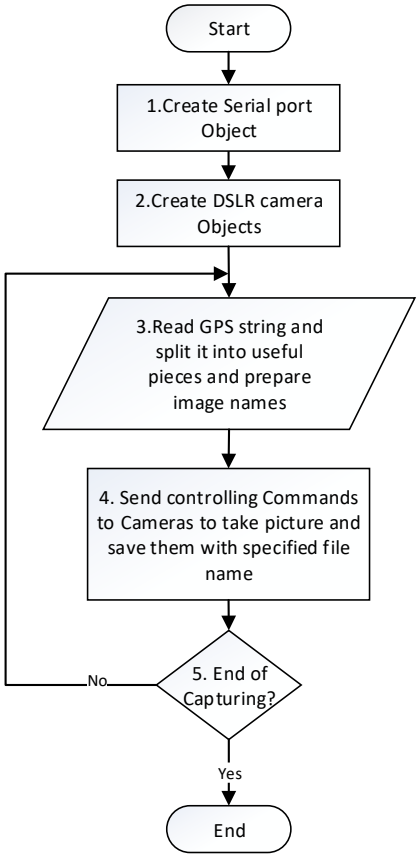

Figure 3-12: Flowchart of algorithm for image acquisition utilizing DSLR camera program

As can be seen, an image acquisition loop is quite straightforward, and the most critical and problematic task is accurately correlating GPS information to individual captured images to provide the possibility of future retrieval in the developed visualization program.

3-4- Data Visualization Program

As mentioned earlier, one of the most important achievements of this research is development of a highly flexible visualization program to represent and summarize a significant amount of collected data and images using the proposed field-based mobile HTPP.

Indeed, a breeder can monitor individual plots located on a field using the developed program by having a glimpse on the dedicated user interface for this purpose.

The majority of existing field-based HTPPs utilize the scripting feature offered by existing GIS software packages such as ArcGIS or Qgis for geospatial data analysis. In fact, these commercialized software are two dominant geographic information systems for geospatial analysis purposes and a special knowledge is needed to implement a geoprocessing module using supported programming languages. However, the proposed program in this research for data visualization and further data analysis is based-on MATLAB which offers a variety of functions for different purposes. Moreover, the developed program can be employed in both windows and Linux operation systems without any limitation.

The proposed features of the developed visualization program can be summarized as below:

- The possibility of drawing a custom map of any field which accurately depicts the location of individual plots.
- The possibility of reading phenotypic database after data collection and represent them as some meaningful and graphical objects for convenient user access.
- The possibility of importing all captured images for every single plot and visualizing them as graphical objects.
- The possibility of working offline or online to utilize available mapping and GIS tools such as Google maps, if needed.
- The possibility of zooming and panning into the desired plots located on the field for closer investigation of individual plots.
- The possibility of monitoring a specific data/image point available for a plot by simply clicking on the specified object.
- The possibility of conveniently expanding the capabilities of the developed program by exploiting other MATLAB toolboxes for data/image analysis and future development.

Figure 3-13 illustrates a screenshot of the main screen of the developed program for data/image visualization after importing a map of a canola field located in Aberdeen, SK. The complete source code for this program can be found in Appendix C.

Because this program consists of several functions to implement different tasks, Appendix C is provided in different sections with a brief explanation of each function.

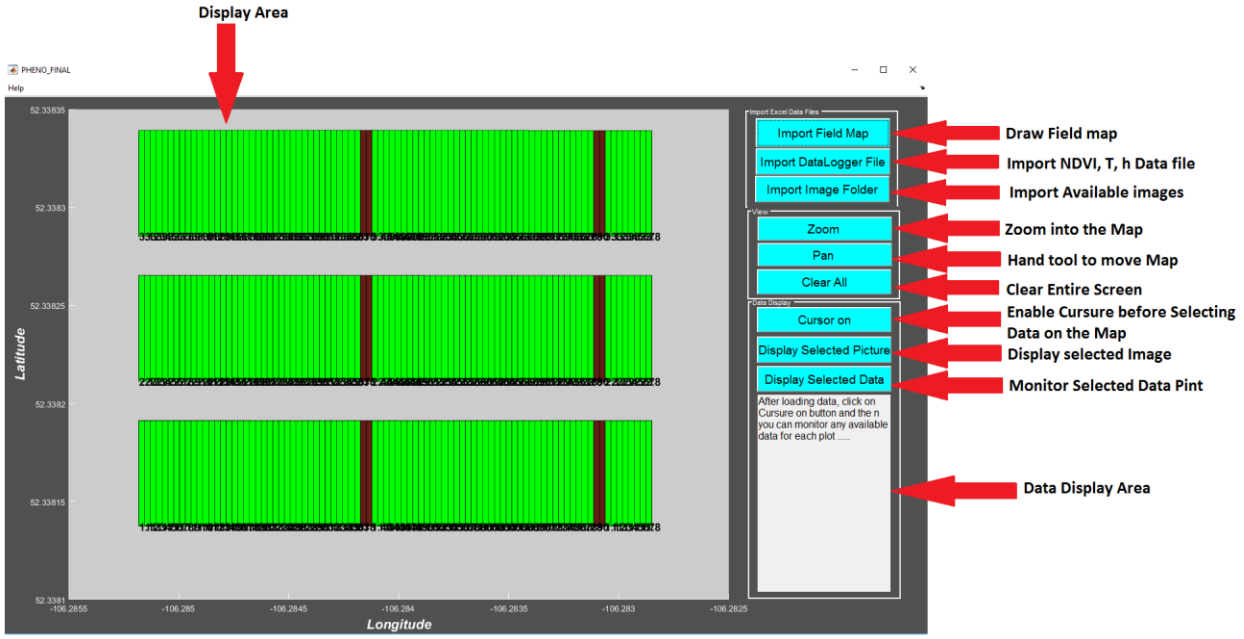

Figure 3-13: User interface for developed data visualization program

As can be seen from Figure 3-13, the graphical user interface consists of two main sections. The display area in the middle of the window illustrates the map of the field and also graphical objects to represent available data/images. On the right side, different push buttons can be selected to execute a variety of functions when needed. For example, the user can conveniently import a phenotypic database or a folder containing captured images. Also, there is the possibility of zooming or panning into the specific area of the map for closer investigations.

Concretely, monitoring the available data/image is the most important task and can be done by first, selecting a desired data/image point and second, clicking on display push buttons on the right side of the window.

Last but not least, developed visualization program encompasses several functions to fulfill different tasks which will be explained in details in next sections. This includes creating a map for the field, importing phenotypic data file and the folder containing captured images, and finally monitoring a desired data/image point by exploiting search algorithms.

3-4-1- Importing Field Map Data File Into the Program

Because an accurate hand-held GPS unit was not accessible during field experiments, nor a local map for the studied fields, the first challenge was finding an effective solution to create a map of the studied field with the only available GPS receiver on top of the vehicle. In fact, to correspond collected data with individual plots, longitude and latitude of every plot had to be defined before actual data collection trials.

In fact, three different approaches were examined to create a map of the field including using a trigger signal coming from GPS receiver, using a manual push button and using interpolation. The details of performance assessment of these three methods will be discussed in section 4-3 in chapter four. As will be discussed, it was found that the most efficient approach to creating map of a field seems to be using a software solution to estimate or interpolate the location of all plots according to some known points, preferably four corners of the field. So the software solution was chosen as the main method to map and localize all plots in the studied fields.

Indeed, as can be seen in Figure 3-14 the spatial information of the first plot was captured using the available accurate RTK GPS unit as a starting point. Subsequently, because of the fact that the size of all rectangular plots and the distance between two adjacent plots were known, the location of all plots could be calculated using the starting point and the determined equations in chapter two (Equations 2-24 and 2-31). In Figure 3-14, a green rectangle represents a plot, black dots represent the center of each plot, and the red lines illustrate the known distances between each plot and the starting point.

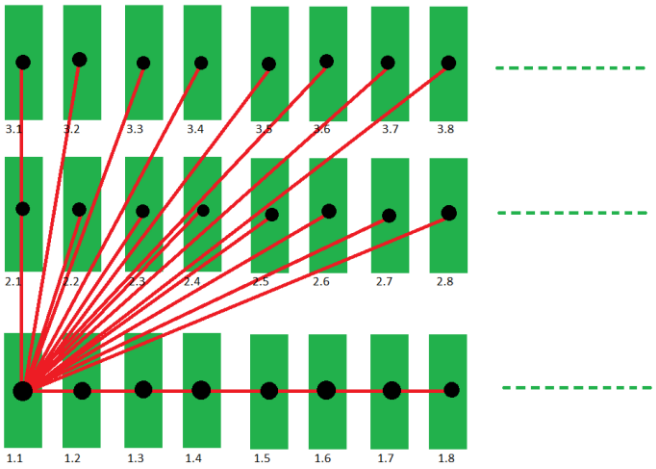

Figure 3-14: Calculating the location of all plots using a starting point to create a map for the field

A function called "Boom.m" was developed based on the Equation 3-1 and Equation 3-2 to not only define the longitude and latitude of individual plots according to the starting point as discussed before but also to correspond collected data/images to each plot according to the mechanical structure of the boom and farm vehicle.

$$Lat2 = Arcsin(cos(\theta)cos(Lat1)sin(\delta) + sin(Lat1)cos(\delta)) \quad \text{Equation 3-1}$$

$$Lon2 = Lon1 + arctan(\frac{cos(Lat1)\, sin(\theta)\, sin(\delta)}{cos(\delta) - sin(Lat1)\, sin(Lat2)}) \quad \text{Equation 3-2}$$

In these equations, Lat1 and Lon1 are the latitude and longitude at point 1, Lat2 and Lon2 are the latitude and longitude at point 2, θ is the vehicle heading angle with respect to the North Pole, δ is angular distance (δ =d/R, which R is the earth's radius, assuming earth is a complete sphere and d is the distance between point 1 and 2). More discussion about the details of these equations can be found in section 2-7 in chapter two. The developed function (Boom.m) in MATLAB to implement these formulas and to find latitude and longitude at point 2 according to the latitude and longitude at point 1 is as follow:

```
function [lat2,long2]=Boom(lat1d,long1d,d,thd)
    %This code was written by Mostafa Bayati on April 19, 2017
    format longG
    R=6371000;
    thr=deg2rad(thd);
    lat1r=deg2rad(lat1d);
    long1r=deg2rad(long1d);
    lat22=asin(sin(lat1r)*cos(d/R)+cos(lat1r)*sin(d/R)*cos(thr));
    long22=long1r+atan2(sin(thr)*sin(d/R)*cos(lat1r),cos(d/R)-sin(lat1r)*sin(lat22));
    lat2=rad2deg(lat22);
    long2=rad2deg(long22);
end
```

Where *lat1d* is the latitude at point 1, *long1d* is the longitude at point 1, *d* is the distance between two points in meters *thd* is the angle in respect to the North Pole in degrees.

As can be seen, the function has four input arguments and two outputs where *lat2* and *long2* are the latitude and longitude at point 2, *lat1d* and *long1d* are the latitude and longitude at point 1, *d* is the distance between point 1 and 2 in meters and finally *thd* is the heading or the angle between the true north and the line which connects point 1 and 2 in degrees.

Now using the developed function, the longitude and latitude at the center of each plot can be generated and a file called "field map" can be achieved as can be seen in Figure 3-15.

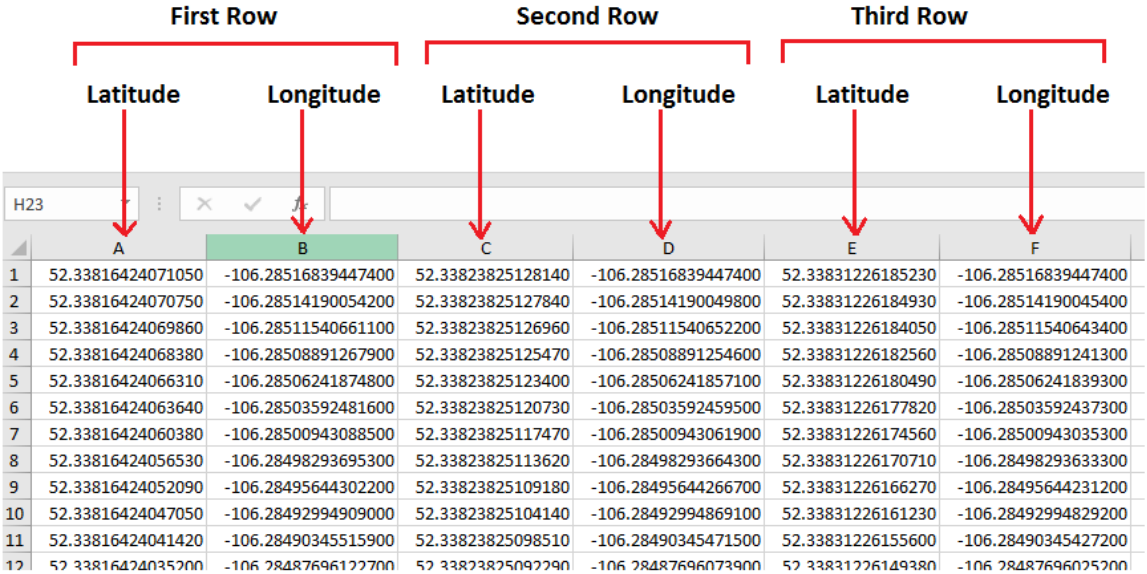

Figure 3-15: A screenshot of a part of the generated field map data file

Because studied canola field consists of 252 plots arranged in three rows, the resulting field mapping file contains six columns or three pairs of data, where the first pair represent the latitude and longitude at first row, the second pair represents the latitude and longitude at second row and likewise third pair represents required information about plots located on the third row.

Concretely, this field map file needs to be created only once for every field and can be used in the developed visualization program. In fact, the first step to use proposed visualization program is to import field mapping file. The user can conveniently click on the "Import Field Map," and the developed function to draw a map of the field will be executed. The algorithm for this function can be found in Figure 3-16. As can be seen, this function first, extracts the information available in field map file and second, arranges them into three different groups for each row. Then according to the size of each plot, the function calculates the information needed

for four corners of each plot. This will be used in next step, and some rectangles will be drawn as a representative of each plot on a field. In the end, plot numbers are assigned to each plot which can be based on any desired format.

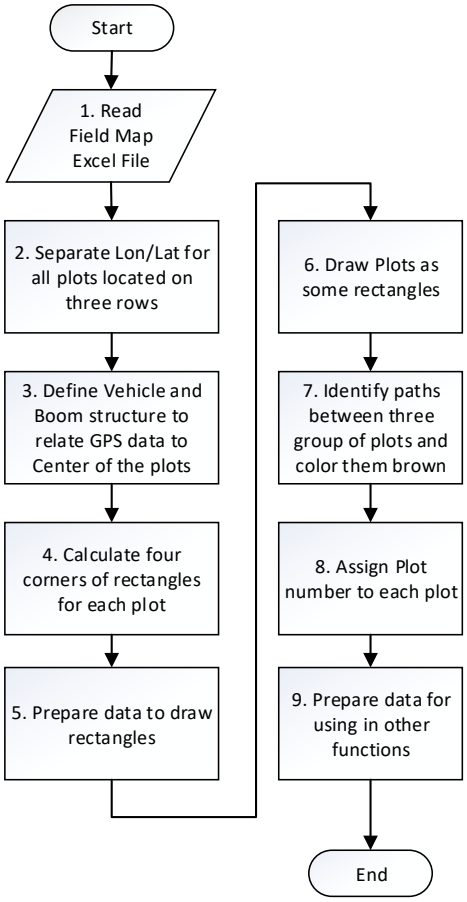

Figure 3-16: Field mapping program algorithm

It is mentionable that field map file should be located in the current directory of the program. Otherwise, program cannot find the file, and a window will appear and asks for the location of this file on the hard drive as can be seen in Figure 3-17.

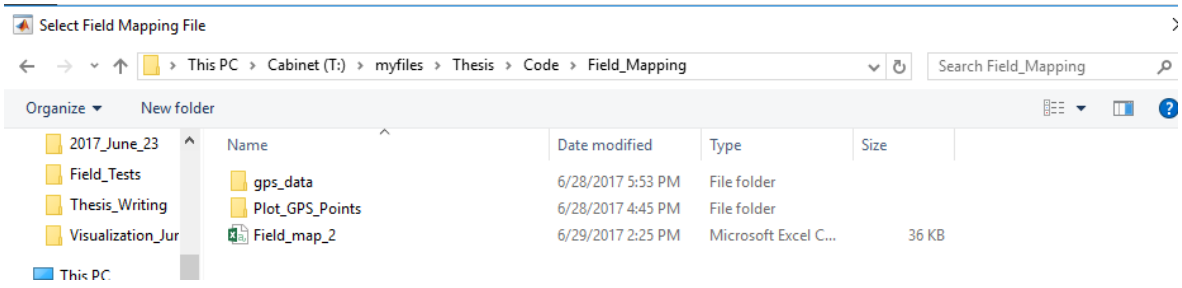

Figure 3-17: Importing field map file

Finally, Figure 3-18 illustrates a screenshot of the developed visualization program after field map file is successfully imported.

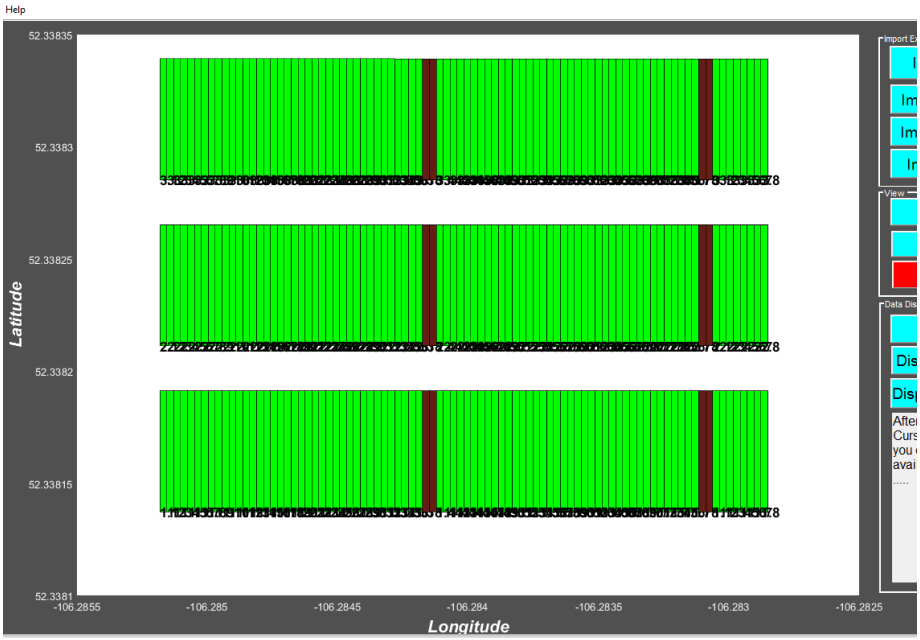

Figure 3-18: Generated map of the field

A closer view of individual plots can be achieved by zooming into the map as can be seen in Figure 3-19. To activate the zoom option, Zoom button should be clicked on the right side of the window and mouse scroll can be used to zoom in/out to the map.

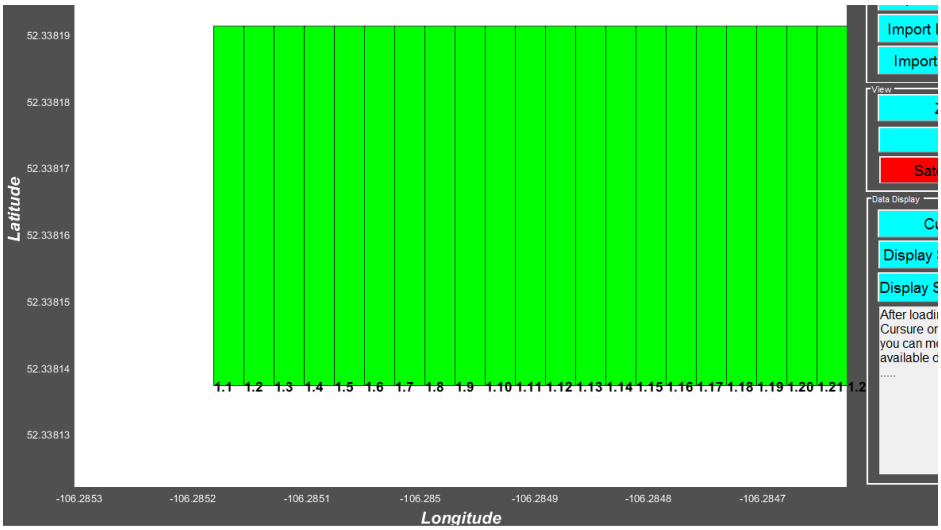

Figure 3-19: A closer view of map of the field and plot numbers

3-4-2- Importing Phenotypic Data File

At this step, a map of the field is created and can be seen in visualization program as was explained in the previous section, and collected data and images can be imported into the program for closer investigations. As discussed earlier, the phenotypic data file was designed to encompass collected data by different sensors to measure plant canopy temperature, height, and NDVI as well as corresponding GPS string to provide the possibility of future retrieval. Figure 3-20 illustrates a screenshot of first 23 datasets available in a sample phenotypic data file. This data file can length up to 5000 datasets depends on the scale of the studied field and the data acquisition program execution time.

	A	B	C	D	E	F	G	H	I	J	K	L	M	N	O	P	Q
1	21:03.7	839	18.54596	13.03494	0.23,0.27,0.21,0.0770,0.1344	0.21,0.32,0.07,0.2139,0.6452	$GPRMC,212045,A,5220.28773250,N,10616.98656852,W,1.4,90.2,230617,15.1,E*6E										
2	6/23/2017 15:21	840	18.54596	13.03192	0.23,0.27,0.21,0.0770,0.1327	0.21,0.33,0.05,0.2358,0.7249	$GPRMC,212046,A,5220.28773295,N,10616.98642336,W,1.5,90.0,230617,15.1,E*6B										
3	21:04.5	842	18.51517	14.37064	0.23,0.26,0.21,0.0586,0.1125	0.21,0.33,0.06,0.2248,0.6908	$GPRMC,212046,A,5220.28774026,N,10616.98605039,W,1.4,89.9,230617,15.1,E*69										
4	21:04.7	843	18.47354	15.01321	0.23,0.27,0.20,0.0727,0.1451	0.21,0.32,0.07,0.2171,0.6463	$GPRMC,212046,A,5220.28773432,N,10616.98592605,W,1.3,89.9,230617,15.1,E*6C										
5	6/23/2017 15:21	844	18.32083	16.18719	0.23,0.27,0.21,0.0886,0.1399	0.21,0.32,0.08,0.2018,0.5992	$GPRMC,212047,A,5220.28773748,N,10616.98578763,W,1.4,90.1,230617,15.1,E*61										
6	21:05.2	845	18.0983	17.58145	0.24,0.26,0.20,0.0415,0.1171	0.21,0.31,0.09,0.1822,0.5640	$GPRMC,212047,A,5220.28773828,N,10616.98566589,W,1.4,90.3,230617,15.1,E*63	$GPRMC,212047,A,5220.287									
7	21:05.5	846	18.05649	18.32687	0.23,0.26,0.20,0.0615,0.1286	0.23,0.28,0.15,0.1016,0.2886	$GPRMC,212047,A,5220.28773784,N,10616.98541253,W,1.5,90.3,230617,15.1,E*6E										
8	21:05.7	847	18.19571	18.62601	0.23,0.26,0.20,0.0592,0.1328	0.24,0.25,0.20,0.0169,0.1102	$GPRMC,212047,A,5220.28773659,N,10616.98528897,W,1.3,90.4,230617,15.1,E*63										
9	6/23/2017 15:21	848	18.27762	19.01053	0.23,0.27,0.21,0.0709,0.1327	0.24,0.25,0.20,0.0123,0.1024	$GPRMC,212048,A,5220.28773338,N,10616.98516920,W,1.3,90.5,230617,15.1,E*6F										
10	21:06.2	849	18.26373	19.47076	0.24,0.26,0.20,0.0523,0.1421	0.24,0.26,0.20,0.0449,0.1252	$GPRMC,212048,A,5220.28773247,N,10616.98506000,W,1.3,90.5,230617,15.1,E*6C	$GPRMC,212048,A,5220.287									
11	21:06.5	850	18.24832	19.74219	0.24,0.26,0.21,0.0488,0.1074	0.24,0.26,0.20,0.0372,0.1198	$GPRMC,212048,A,5220.28773774,N,10616.98478401,W,1.4,90.1,230617,15.1,E*67										
12	21:06.7	851	18.26221	19.74072	0.24,0.26,0.21,0.0423,0.1072	0.24,0.26,0.20,0.0559,0.1342	$GPRMC,212048,A,5220.28773522,N,10616.98466782,W,1.4,90.0,230617,15.1,E*60										
13	6/23/2017 15:21	852	18.27457	19.65793	0.24,0.26,0.20,0.0521,0.1281	0.24,0.26,0.20,0.0376,0.1143	$GPRMC,212049,A,5220.28773312,N,10616.98456302,W,1.3,90.2,230617,15.1,E*6E										
14	21:07.2	853	18.28845	19.50861	0.24,0.26,0.21,0.0339,0.0994	0.24,0.26,0.20,0.0490,0.1288	$GPRMC,212049,A,5220.28773527,N,10616.98442802,W,1.3,90.4,230617,15.1,E*66	$GPRMC,212049,A,5220.287									
15	21:07.5	854	18.37183	19.33035	0.23,0.28,0.20,0.1046,0.1581	0.24,0.26,0.20,0.0359,0.1146	$GPRMC,212049,A,5220.28773720,N,10616.98416081,W,1.5,90.4,230617,15.1,E*67										
16	21:07.7	855	18.45358	19.09726		0.24,0.26,0.21,0.0403,0.1100	$GPRMC,212049,A,5220.28773553,N,10616.98403210,W,1.5,90.0,230617,15.1,E*6B										
17	6/23/2017 15:21	856	18.46744	18.91977	0.24,0.26,0.21,0.0552,0.1159	0.23,0.27,0.20,0.0707,0.1500	$GPRMC,212050,A,5220.28773330,N,10616.98391688,W,1.4,89.9,230617,15.1,E*69										
18	21:08.2	857	18.39807	18.94708	0.24,0.26,0.21,0.0370,0.0996	0.23,0.26,0.20,0.0607,0.1295	$GPRMC,212050,A,5220.28773946,N,10616.98377171,W,1.4,90.0,230617,15.1,E*6A	$GPRMC,212050,A,5220.287									
19	21:08.5	858	18.38266	19.12305	0.23,0.28,0.20,0.0958,0.1648	0.24,0.26,0.20,0.0442,0.1274	$GPRMC,212050,A,5220.28773848,N,10616.98351632,W,1.5,89.7,230617,15.1,E*6F										
20	21:08.7	859	18.43817	19.2034	0.24,0.26,0.21,0.0454,0.1106	0.24,0.25,0.21,0.0102,0.0869	$GPRMC,212050,A,5220.28774104,N,10616.98338028,W,1.4,89.3,230617,15.1,E*6E										
21	6/23/2017 15:21	860	18.56299	19.24277	0.23,0.27,0.19,0.0812,0.1680	0.24,0.25,0.21,0.0239,0.1019	$GPRMC,212051,A,5220.28774681,N,10616.98326803,W,1.4,89.3,230617,15.1,E*6B										
22	21:09.2	861	18.6861	19.24277	0.23,0.28,0.20,0.0942,0.1562	0.24,0.26,0.21,0.0403,0.1126	$GPRMC,212051,A,5220.28774796,N,10616.98314362,W,1.4,89.7,230617,15.1,E*65	$GPRMC,212051,A,5220.287									
23	21:09.5	862	18.78293	19.26855	0.24,0.26,0.20,0.0422,0.1171	0.24,0.26,0.20,0.0483,0.1295	$GPRMC,212051,A,5220.28774939,N,10616.98288445,W,1.4,90.3,230617,15.1,E*64										

Figure 3-20: Screenshot of a sample phenotypic database (details was explained in Table 3-1)

The next crucial function needed to be developed in the proposed visualization program is extracting explicit and meaningful information out of the raw data file and interactively represent the information to breeders as some graphical objects.

In fact, GPS raw string had to be broken down into meaningful pieces to achieve longitude and latitude at each data sampling point. Then any available data associated with individual locations had to be correlated with each other before visualization. Also, the result had to be represented as a second layer on top of the field map layer for better perception.

Figure 3-21 illustrates the algorithm developed for implementing this function to visualize raw data files.

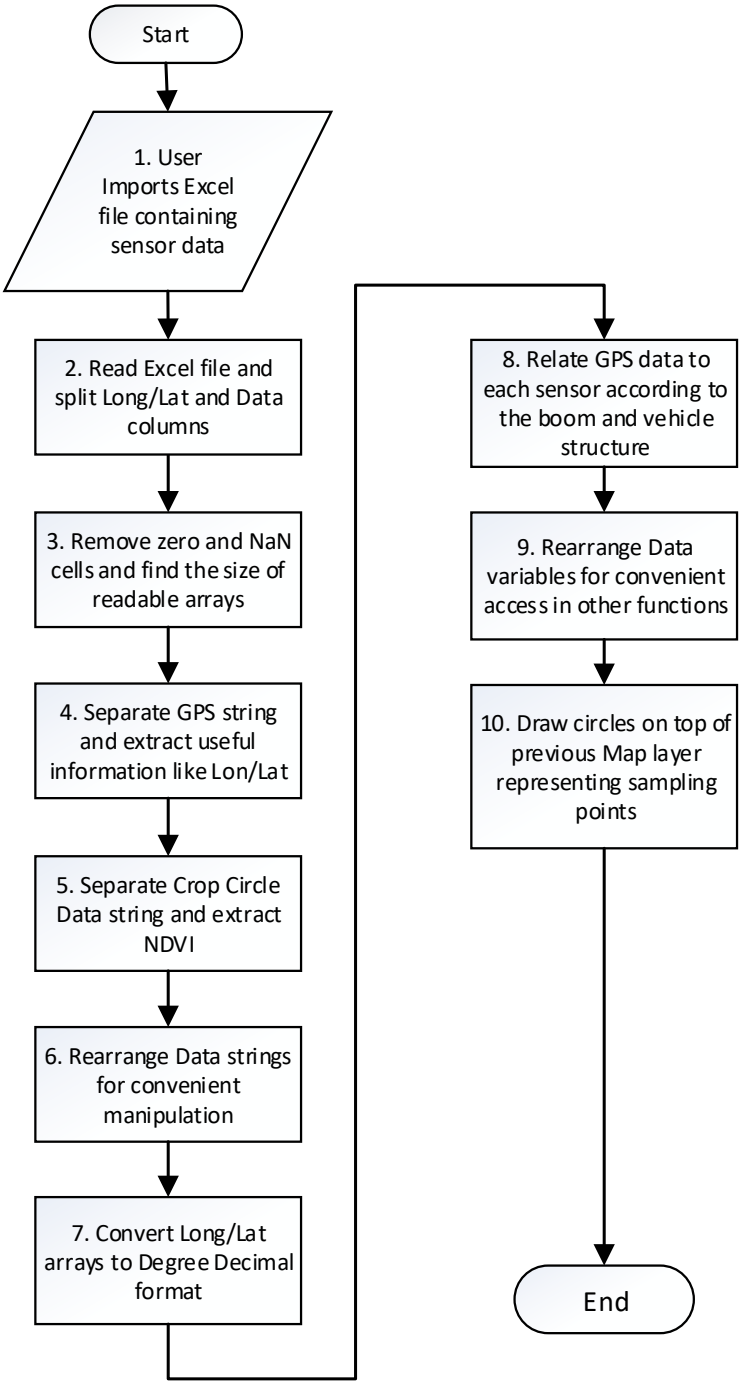

Figure 3-21: Algorithm for visualizing collected data

As can be seen from Figure 3-21, firstly, a data file which was extracted out of datalogger after a data collection trial must be imported into the program. To do so, the user should click on "import DataLogger file" button on the right side of the window and data file can be chosen as can be seen in Figure 3-22.

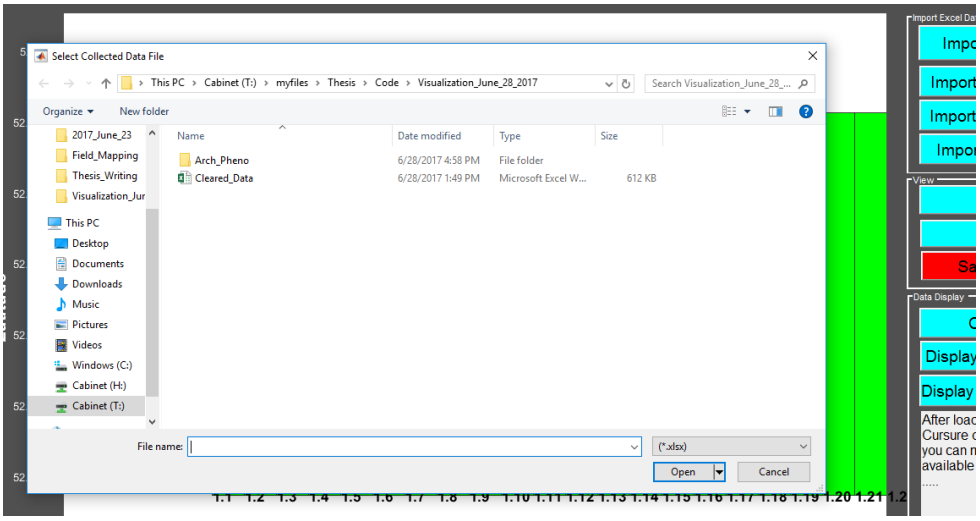

Figure 3-22: Importing phenotypic data file

Consequently, the developed program reads the imported data file and splits different columns and temporarily stores them in dedicated arrays. Because there might be corrupted data in the data file, the developed program removes all meaningless data and updates data arrays at this step. In next step, GPS raw data is broken down into different pieces and longitude, latitude and vehicle heading will be extracted for further processing. Likewise, raw data obtained from NDVI sensor needs to be parsed, and useful parts are extracted at this step.

Because raw GPS data provides longitude and latitude in degrees and decimal minute format (Lat_{DM}/Lon_{DM}), they need to be converted to decimal degrees (Lat_{DD}/Lon_{DD}) using Equations 3-3 and 3-4 to be manipulated as floating point numbers.

$$Lat_{DD} = \left(\frac{Lat_{DM} - 5200}{60}\right) + 52 \qquad \text{Equation 3-3}$$

$$Lon_{DD} = \left(\left(\frac{Lon_{DM} - 10600}{60}\right) + 106\right) * (-1) \qquad \text{Equation 3-4}$$

For example, after parsing a sample raw GPS string, we can extract the latitude and longitude as below:

Lat_{DM} = 5220.187369

Lon_{DM} = 10617.00265

So, using the Equations 3-3 and 3-4 we can find the equivalent latitude and longitude values in decimal degrees format as below:

$Lat_{DD} = 52.3364561441667$

$Lon_{DD} = -106.283377549167$

After converting the GPS string and extracting longitude and latitude in the desired format, the longitude and latitude of the location of each sensor need to be calculated according to the structure of the mechanical boom and vehicle using the Equation 3-2 and Equation 3-2 as was explained in section 2-7 of chapter two.

At this step, longitude/latitude at the location of each sensor and also collected data by each sensor can construct data matrices, and graphical objects can be drawn as a representative of each data sample point as can be seen in Figure 3-23.

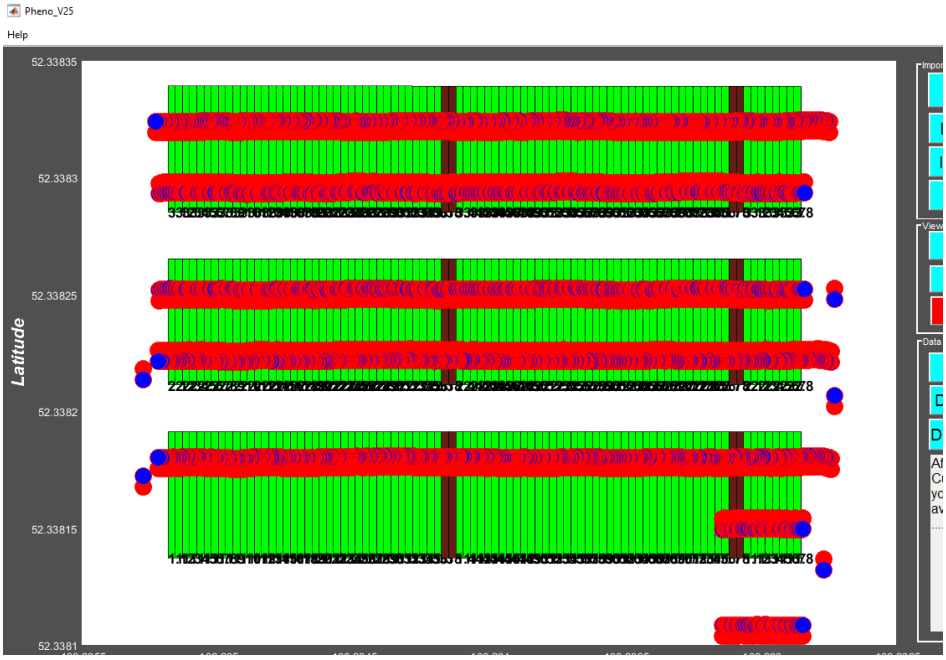

Figure 3-23: Visualization program after importing phenotypic data file

As can be seen in Figure 3-23, a second layer was added on top of the first graphical layer (map of the field which was previously drawn) and different graphical objects with distinct colors can be seen. This view might not be as informative as it should be and user needs to zoom into the desired section of the map for closer examination, as can be seen in Figure 3-24.

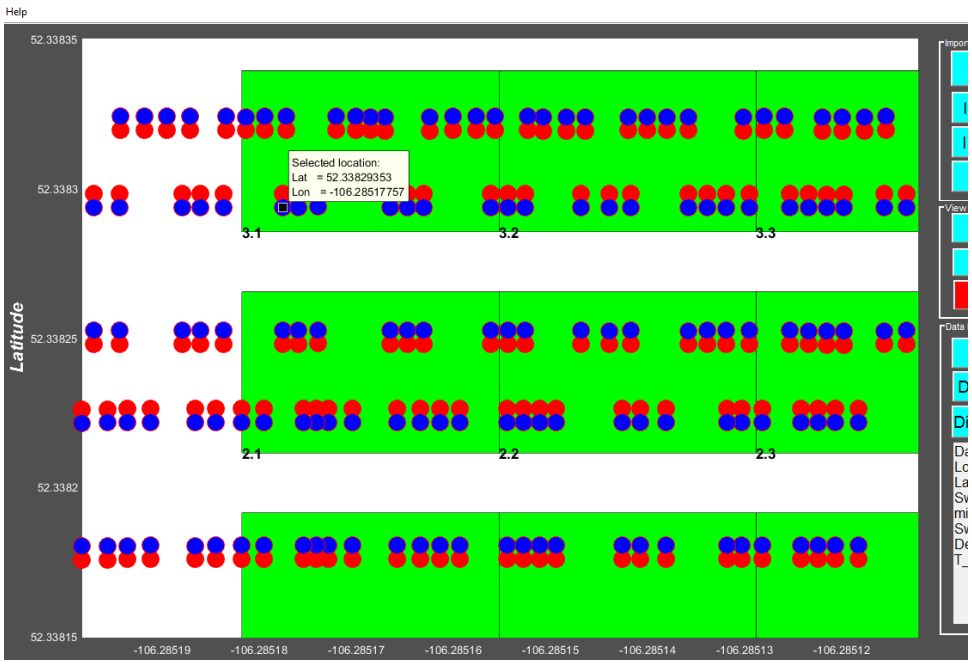

Figure 3-24: A closer view of imported phenotypic data file (blue dots represent ultrasonic and red dots represent thermometer data points)

Indeed, to zoom into the desired section of the map, "Zoom" button should be selected on the right side of the window and then the desired view can be achieved using mouse cursor.

It is notable that every graphical object was drawn is active and can be clicked, and the user can monitor the desired data point which will be discussed in next sections.

3-4-3- Importing Captured Images

As stated before, every captured image is geo-referenced by GPS information with the following format:

Latitude,Longitude,Heading,R/L

Example: 5209.831304,10631.087072,79.0,L.jpg

In fact, the file name of the individual image contains the information about the longitude, latitude, vehicle heading angle at the time of image capturing and also the last letter (can be R or L) which determines the camera captured the image on the right side of the boom or the left camera. Using mentioned final letter and the vehicle heading angle provides the capability of autonomously capturing images while the vehicle is passing through the entire field in different directions.

The algorithm developed for the proposed function to import captured images into the visualization program and to retrieve every single image as user needed can be seen in Figure 3-25. As can be perceived from this figure, after the folder contains captured images is imported into the program by selecting "Import Image Folder" on the right side, all available images will be scanned, and an array will be created which contains file names of all images.

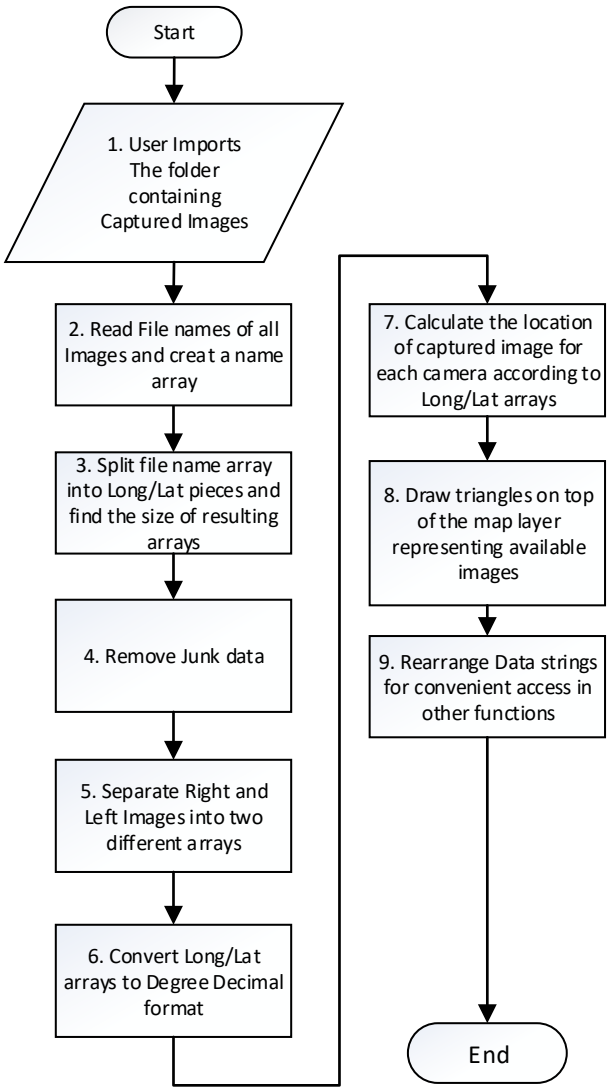

Figure 3-25: Flowchart of Algorithm for visualizing captured images

Now, because the available spatial information is captured at the location of the GPS antenna on top of the vehicle, the information needs to be transformed to the location of each camera as was explained in details in section 2-7 of chapter two.

Then the developed program checks whether there is any corrupted file name or not. If so, the damaged files will be removed from the name array.

Finally, some triangles will be drawn as the representative of available images for each plot as can be seen in Figure 3-26.

At this step, both the collected data file and captured images are imported into the visualization program, and graphical objects are drawn on the field map layer. So the user can conveniently click on any desired data/image point and monitor the available data for individual plots.

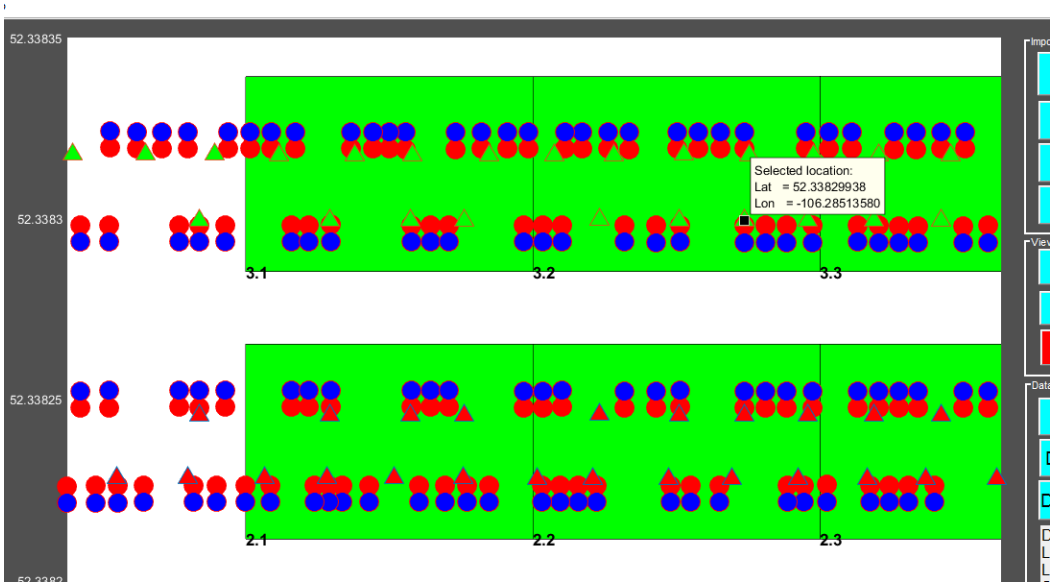

Figure 3-26: A close-up view of visualization program after importing all data (red and green triangles represent an available RGB image and the rest as explained in Figure 3-24)

3-4-4- Map View Options

As mentioned earlier, different options are designated in the developed visualization program for convenient data access by the user. For example, clicking on "Zoom" button provides the possibility of zooming into the desired section of the map. Likewise, "Pan" or hand tool can be selected to pan on the map.

The most important option is "Data Cursor" which has to be selected to provide the possibility of selecting a data/image point and will be explained with an example in next section.

3-4-5- Monitoring an Available Data Point

After "Data Cursor" button is selected, user can click on every graphical object to monitor available phenotypic data including plant canopy temperature, height, and NDVI or any available image for individual plots by selecting "Display Selected Data" or "Display Selected Image" depends on the selected object by user (data object or image object).

In fact, a function was developed to search into the data file or image folder, and to visualize associated data/image with the selected object by the user. The developed algorithm to implement this function can be seen in Figure 3-27.

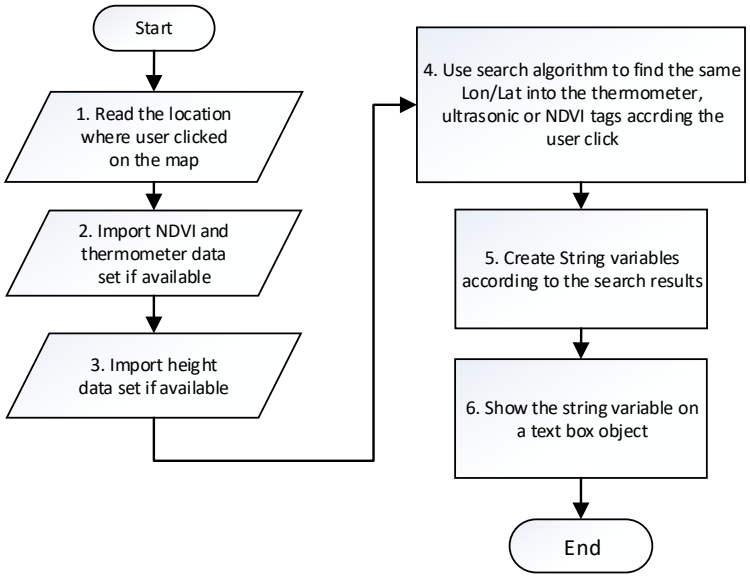

Figure 3-27: Algorithm for monitoring an available data point

As can be perceived, the developed function reads the location on the map where was clicked by the user. Then the phenotypic data which was stored in specified arrays in "Import DataLogger File" function, will be imported as an input argument to be used in next steps. Now the utilized search algorithm finds the corresponding element in phenotypic data array to the selected object by the user. At this stage, the result of search algorithm is prepared to be displayed to the user as a string array variable in a graphical display object on the lower right side of the window.

Figure 3-28 illustrates three example for monitoring a) height of a plant canopy, b) NDVI and c) temperature of a plant canopy.

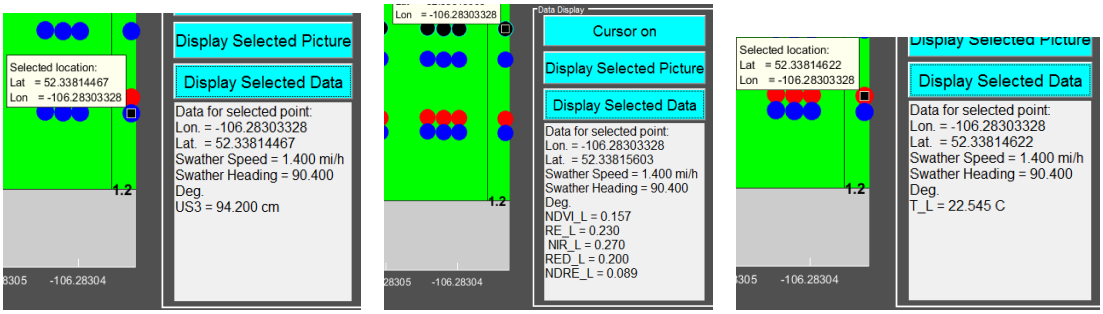

a) Height b) NDVI c) Temperature

Figure 3-28: Monitoring three sample temperature data points

3-4-6- Monitoring an Available Image

Similar to the process of monitoring an available phenotypic data point which was explained in the previous section, captured images of plant canopies are visualized as triangles on the field map. Then available images can be monitored by selecting the desired image and clicking on "Display selected Image" button on the right side of the window.

In fact, an algorithm was developed to implement this task as can be seen in Figure 3-29.

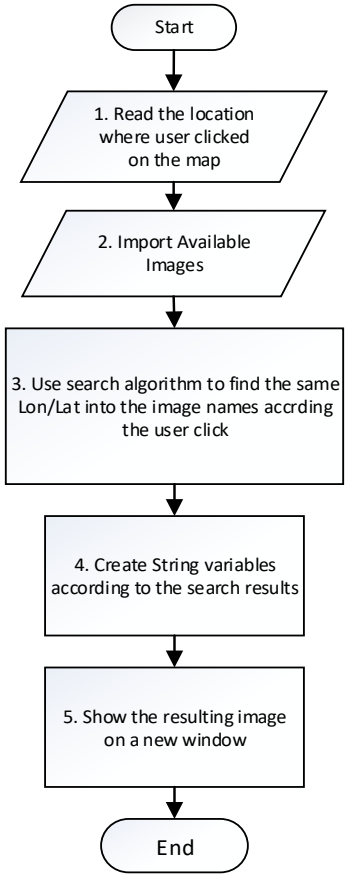

Figure 3-29: Algorithm for monitoring an available image

The only difference between the algorithm for monitoring a data object and an image object is the fact that all available images will not be loaded in temporary memory the same as collected phenotypic data. This is because of the fact that the size of image folder can be up to five gigabyte, and this can significantly slow down the program and the whole computer. On the contrary, the search process will be done on image file names array, and then after finding the desired image, the image will be shown to the user by opening from the hard drive.

Figure 3-30 a) and b) illustrate two images of a sample plot (plot number 2.30) in two different days. It will be explained how we can use the developed program to extract meaningful information to analyze the growth rate of the desired plot in section 4-5-3 in chapter four.

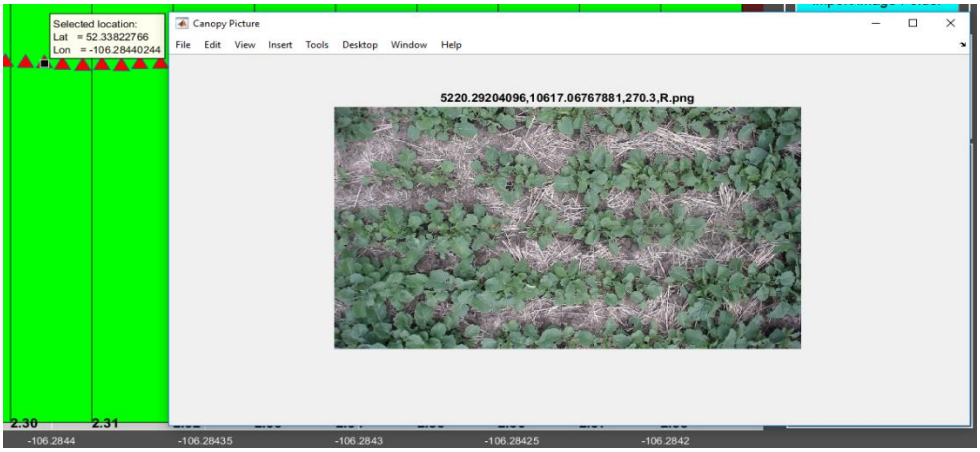

a) Plot # 2.30 on June 23

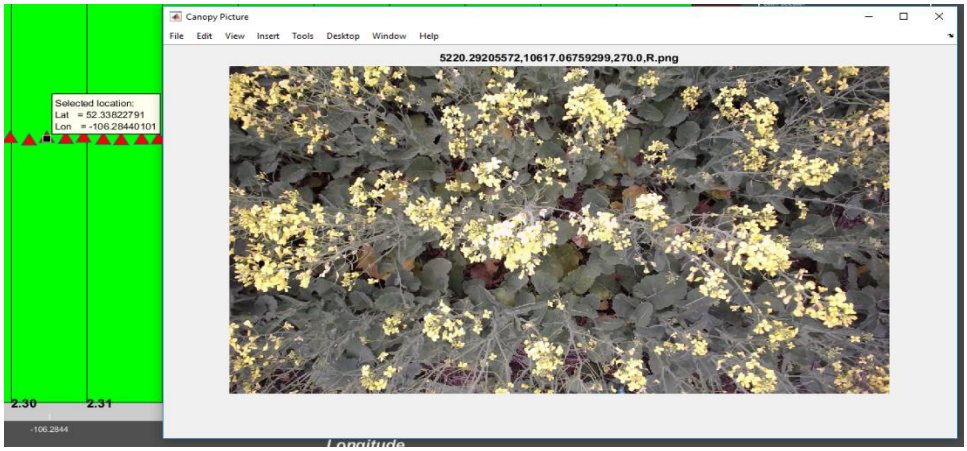

a) Plot # 2.30 on July 18

Figure 3-30: An example to show how an image data point can be used to investigate into a particular plot in different days

3-5- Summarizing Collected Data for Individual Plots as one Output file

In the last two sections, it was discussed how the developed data visualization program with a graphical user interface can be used to investigate the collected data and captured images for individual plots. This capability is significantly useful when a breeder needs to observe the collected information in different regions of a particular plot. For example, a breeder can study the greenness of a plot (NDVI values) at each corner or at the center of a plot to find out any possible disease using the graphical interface and some simple clicks.

On the other hand, sometimes it is desired to statistically analyze the collected data for the entire field or for a particular set of plots. In this case, a breeder can either exploit the graphical user interface to extract the required information as explained before, or more conveniently can analyze an excel file containing all information available for individual plots.

In other words, a breeder will be able to conveniently explore the available data for individual plots for more statistical analysis if we could somehow sort all collected information according to the plot numbers and associate a set of data to their matching plots, and save the result as a single excel file. This matter was an incentive point to sort all available data for each plot as an output file for each trial. Figure 3-31 illustrates the format of a sample output file which was generated to summarize all collected data and associate each data record to individual plots.

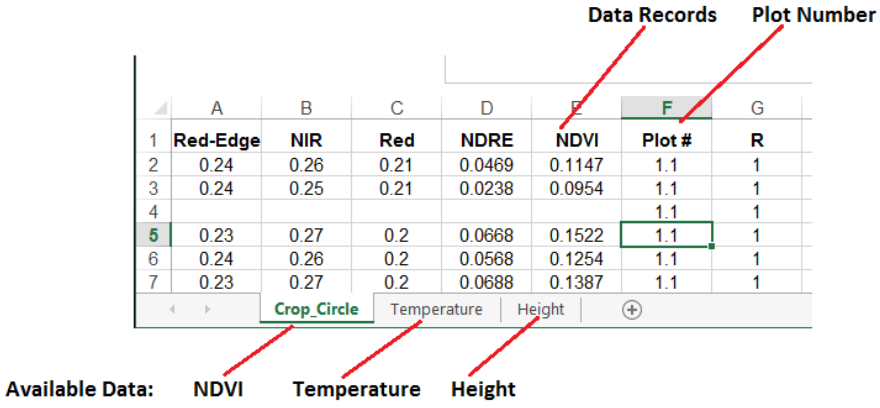

Figure 3-31: The format of output file to sort all collected data according to plot numbers

As can be seen in Figure 3-31, the output file consists of a number of sheets, depends on the number of employed measurement devices and sensors, (three sheets in this example) to represent the entire available data. Each sheet in an output file consists of a "plot number"

column, and at least one "data column". For example, having a closer look at the sample output file illustrated in Figure 3-31 reveals that five NDVI values (0.1147, 0.0954, 0.1522, 0.1254 and 0.1387) were captured for plot number 1.1. The same approach can be used to observe the available information for any other desired plot. Figure 3-32 illustrates another example to investigate into the "temperature sheet" in the generated output file.

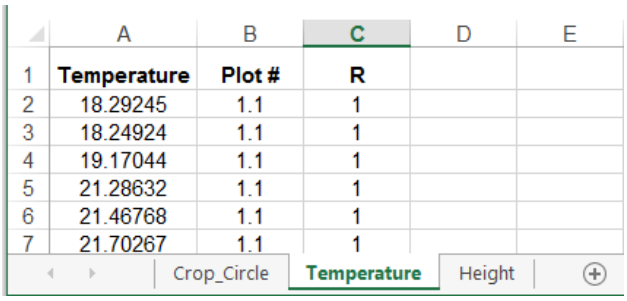

	A	B	C	D	E
1	**Temperature**	**Plot #**	**R**		
2	18.29245	1.1	1		
3	18.24924	1.1	1		
4	19.17044	1.1	1		
5	21.28632	1.1	1		
6	21.46768	1.1	1		
7	21.70267	1.1	1		

Crop_Circle | Temperature | Height

Figure 3-32: Investigating into the collected temperature values for plot 1.1

3-6- Summary

To summarize, the software components and developed programs for the proposed field-based plant phenotyping platform were discussed in this chapter. It was explained how a program was developed for a datalogger to communicate with different sensors and to store data in a database with a predefined format for convenient future access. Also, three different programs developed for capturing RGB images of plant canopies using a wireless camera, a webcam and a DSLR camera were explained. It was shown that how a webcam appears to be the optimum choice to be used in a field-based mobile HTPP because of the fact that webcam offers more flexibility in programming and interaction with the central laptop. Moreover, the details and different components and functions of the developed program to visualize the entire collected data and images was explained. In fact, the process of generating a local map for the studied fields, and the procedure to import collected data file and captured image folder into the program, and consequently monitoring some sample data points were elucidated. Last but not least, it was also discussed why generating an output file to summarize all collected data as a single excel file can be useful for breeders.

In next chapter, the outputs and experimental results achieved by using the developed field-based HTPP will be explained.

CHAPTER 4

EXPERIMENTAL TESTS AND RESULTS

4-1- Introduction

This chapter discusses the experimental results achieved after conducting several field tests during summer 2017 and fall 2016 to examine the performance of the developed field-based mobile platform for high-throughput plant phenotyping.

In fact, exploiting an existing farm vehicle and designing a measurement system including several sensors besides some programs to take control of the hardware components offers the possibility of autonomously capturing various characteristics of plant canopies. Such a system helps breeders to continuously monitor their entire field to achieve a better yield with minimum dependency to an expert human observation.

As mentioned in previous chapters, the design of the mechanical boom used as a fixing frame to attach the measurement system to the farm vehicle was an individual research, and the evaluation of its performance including the stress and vibration analysis was not part of the objectives of this study. Other parts, including software and hardware development, was the main goal of my research project.

Indeed, the required equipment list for the hardware and software development was prepared, a remarkable amount of external communications with apparatus manufacturers and authorized distributors were done, and several quotes were received to purchase the selected set of components. The list of utilized equipment and their datasheet can be found in Appendix F.

After gathering up all the equipment together, their performance was tested in a laboratory setting one-by-one, and they were assembled on the mechanical boom attached to the farm vehicle during several field works. The process of assembling and wiring the equipment was repeated three times because of the improvements and replacement of the mechanical boom.

Finally, a series of tests were designed to not only collect different characteristics of the plant canopies but also to validate and verify the accuracy and reliability of the proposed plant phenotyping platform. The result of these tests are explained in this chapter.

4-2- Studied Canola Filed

Field experiments were performed on a canola field at Cargill Canada canola research center close to the city of Aberdeen, Saskatchewan during summer 2017 as can be seen in Figure 4-1. Also, the performance of the system was verified in a wheat field located near University of Saskatchewan crop science field laboratory as well, but because the study of the wheat was not part of the objectives of this research, the focus of this chapter will be only on canola cultivars.

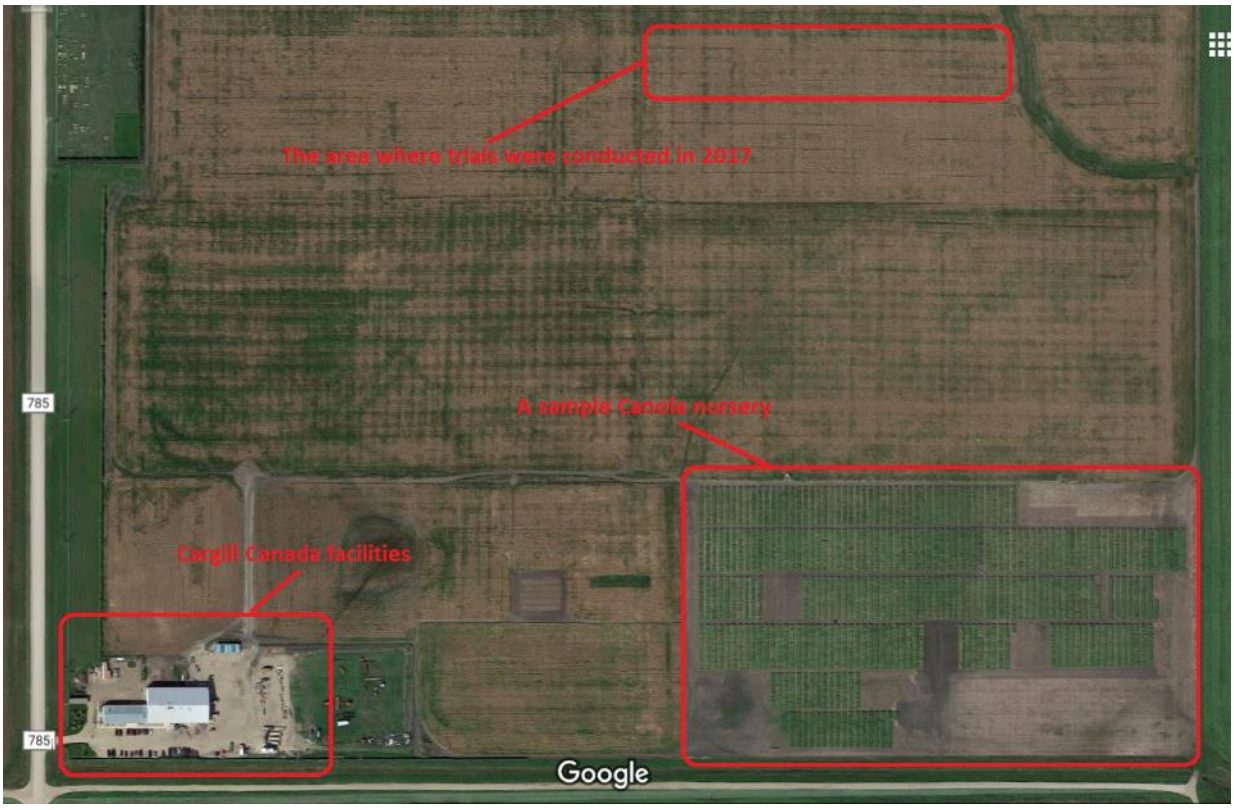

Figure 4-1: Location of studied field at Cargill Canola research center (Photo extracted from Google Map)

The studied Canola field comprises of 252 rectangular plots which were arranged in three different rows based-on different genotypes. Also, the length of a single plot was 6 m, and the width of a plot was 1.8 m. Winter canola cultivars (with darker leaf color) were planted between two adjacent plots to create a visible boundary for each plot. Also, Figure 4-2 illustrates a closer view of a part of the canola field which red rectangles represent individual plots.

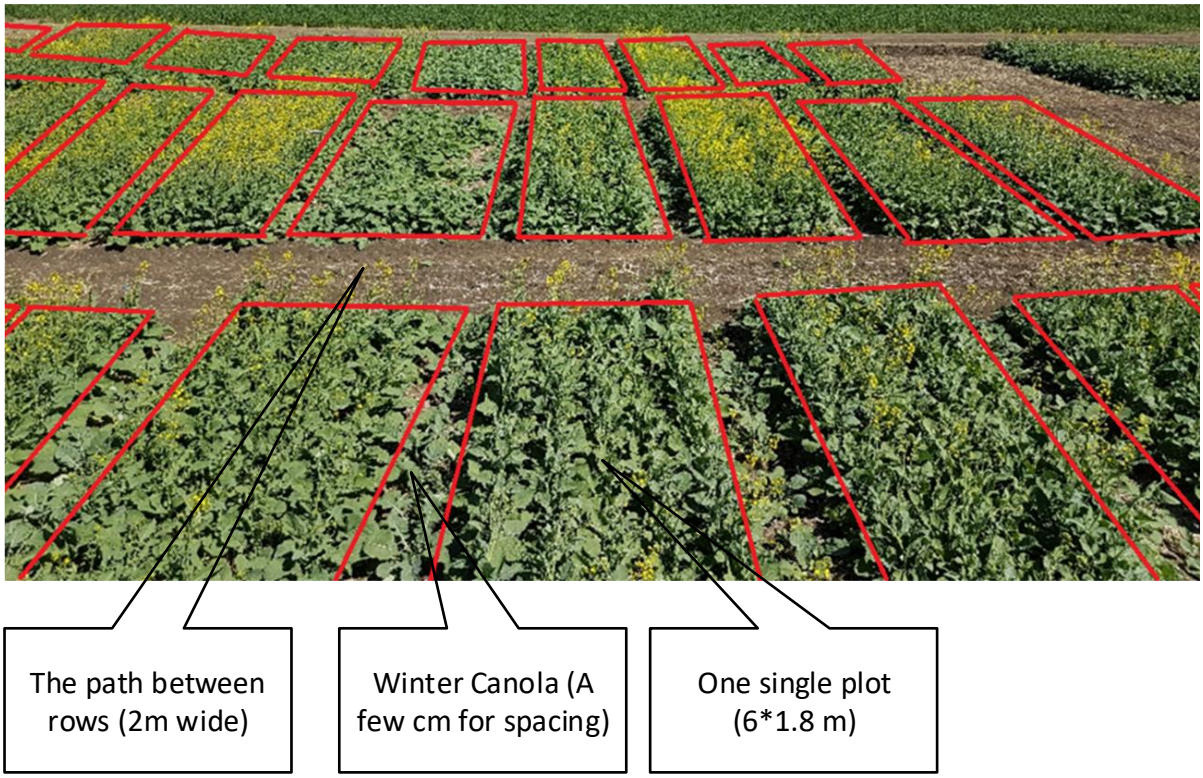

Figure 4-2: Studied Canola field near Aberdeen consisting of 252 plots

Moreover, Figure 4-3 illustrates the top view of the plots arranged in three different rows in the studied nursery. In fact, each row consists of 84 individual plots, and as mentioned earlier; each plot (or each group of plots) is based-on diverse genotype which correlates to particular phenotypes or a characteristic of a plant.

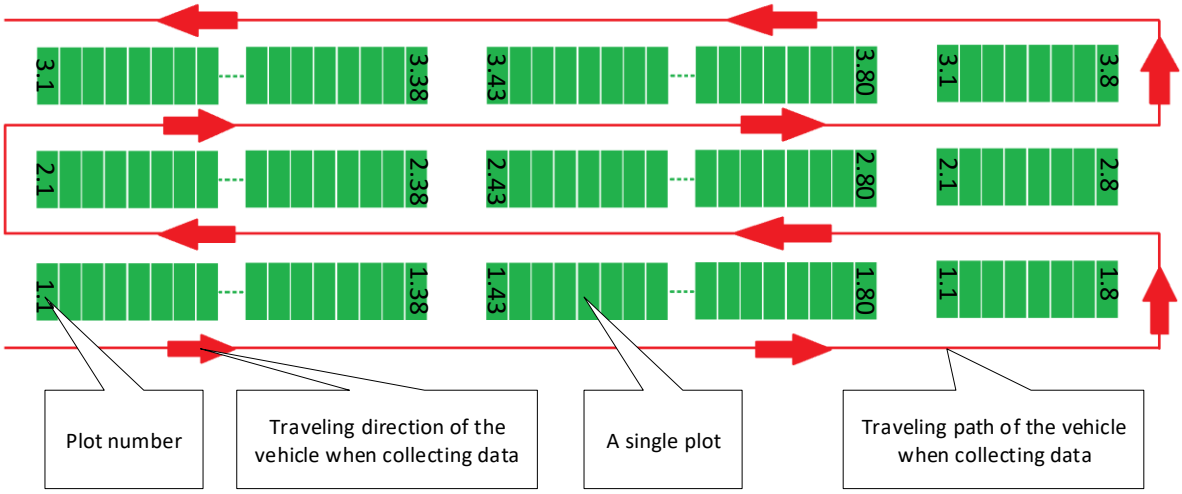

Figure 4-3: Top view of the investigated Canola nursery

With the mentioned configuration, the farm vehicle could carry measurement equipment all throughout the field as can be seen in Figure 4-4 to collect both phenotypic data and also RGB images of plant canopies. The black arrows illustrate the direction of the movement of the vehicle during the data collection.

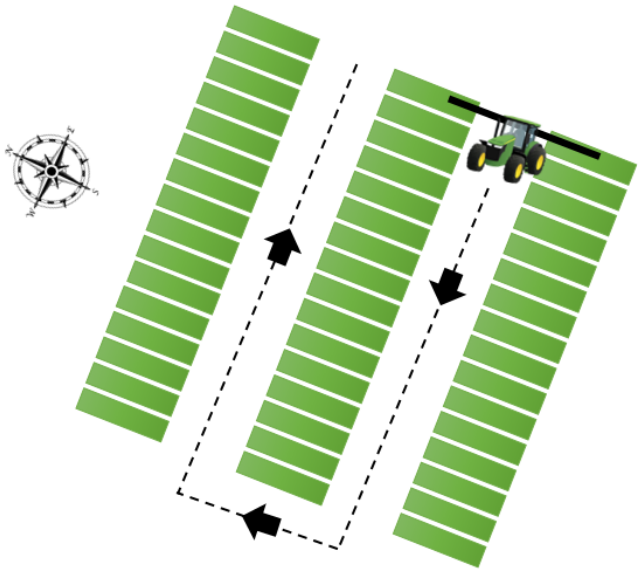

Figure 4-4: Vehicle traveling path during the data collection

The traveling speed of the vehicle was set to around 1.9 mph (3 km/h) during the data collection for two main reasons.

Firstly, the vehicle was prone to less level of vibrations when traveling at this speed. Hence, the measurement equipment including RGB cameras could reliably deliver data without any distortion. Secondly, as mentioned before, the width of a single plot was 1.8 m, and data collection rate in the data acquisition program was adjusted to 250 ms. So we can calculate the resulting number of sampled data per plot as follows:

$$3\ km/h = 0.833\ m/s \qquad \text{Equation 4-1}$$

So the time taken for the vehicle to pass through a single plot was about 2.16 sec. Hence, we can conclude that:

$$\frac{1 sec}{2.16\ sec} = \frac{4\ samples}{X} \qquad \text{Equation 4-2}$$

Where X is the number of data sampled per plot with the designated traveling speed which is 8 samples per plot. However, the performance of the system was tested with a higher speed, 3.4

mph (5.5 km/h), as well, and no major problem was observed, but the number of captured data was decreased to ~4 samples per plot. It is mentionable that, this number of data samples per plot is also a function of other parameters such as the response time of the sensors and also the availability of GPS signal. In other words, after data collection, some plots might be found with less amount of available sampled data due to the GPS signal fading or inability of sensors to respond every 250 ms. Furthermore, the width of the traveling path between two rows is 3 m which was wide enough for the selected vehicle to travel through without any damage to the plants as can be seen in Figure 4-5.

Figure 4-5: The traveling path between two plot rows

The ground was well constructed and relatively flat, and had to be assumed as an entirely flatten surface which was found one of the reasons for some concerns observed for height measurement using ultrasonic sensors. This matter will be discussed further in future sections.

Apart from several field trips to prepare all equipment, nine data collection trials (in nine different days) were conducted during summer 2017.

4-3- Evaluating Proposed Field Mapping Methods

As mentioned in previous chapters, there was no geospatial information available for the studied canola field, nor an accurate portable GPS to conveniently acquire required information about the location of individual plots to map the entire field as a requirement for data visualization program. So a reliable solution had to be found to obtain necessary information using the only GPS available on top of the farm vehicle.

In fact, the ultimate goal of mapping the field was to find the longitude and latitude values at the center of all 252 plots, and then to visualize every plot and paths by some symbolic rectangles as can be seen in Figure 4-6.

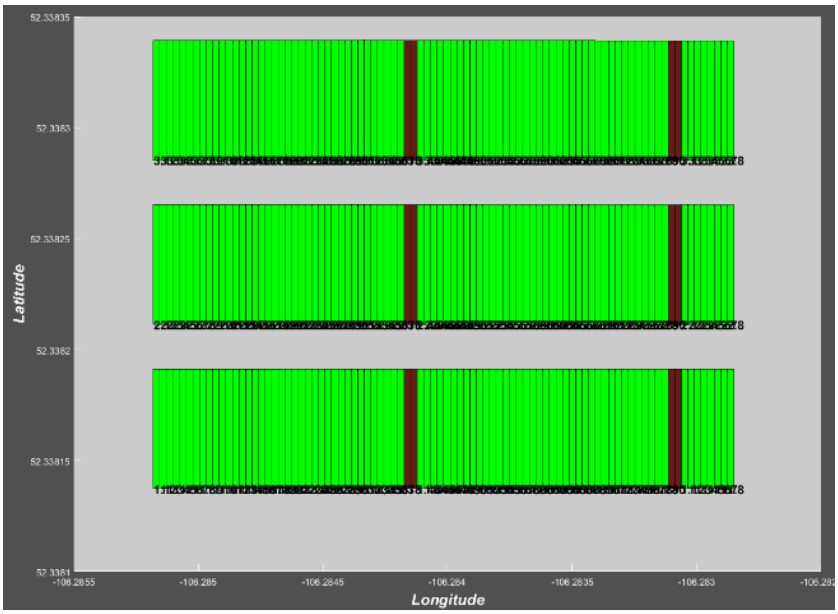

Figure 4-6: Map of the field in the developed visualization program

To obtain the desired information, three different tests were carried out and the performance of each approach was evaluated to find out the most reliable and accurate solution for mapping the entire field as will be discussed in next three sections. It will be explained why using interpolation and math appears the most efficient approach for this purpose, indeed.

4-3-1- Using a Manual Push Button

In the first approach, while the vehicle was passing through the entire field, a push button was manually pushed when the vehicle was aligned to the center of each plot. In other words, I had to push a trigger switch 252 times to capture longitude and latitude at the center of each plot.

Figure 4-7 illustrates a graph for a part of the resulting GPS data file after field trials. In this figure, X-axis represents longitude, and Y-axis represents latitude, and each red sign represents the center of a single plot in the field. Nevertheless, it was found that pushing a manual push button for 252 times doesn't seem practical. Because as can be perceived from Figure 4-7, there were some missing points amongst the captured data due to the inability of the user to activate the trigger signal at the right time to capture the required GPS information.

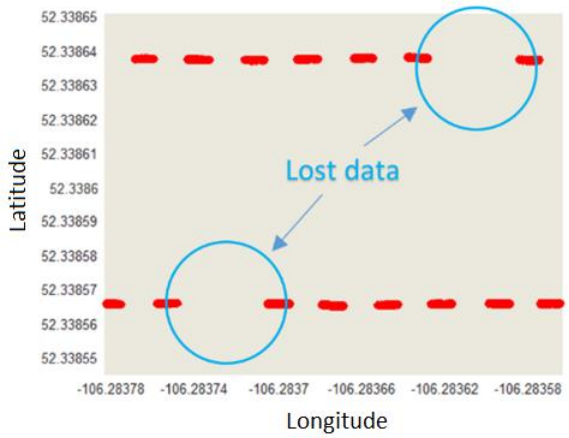

Figure 4-7: Acquired GPS data for mapping the field using a push button

However, this approach can be useful to map a field with a few plots. So the next approach was to use a trigger pulse coming from GPS receiver box as a command signal to store required information at particular locations in the field.

4-3-2- Using GPS Trigger Signal

It was found that the existing GPS receiver box was running a software which could calculate the distance traveled by the vehicle over a particular period of time. So the GPS was set up to send an electrical signal every 1.8 m (the distance between centers of two adjacent plots). Then this trigger signal was connected to a digital input of a datalogger, and a program was developed for the datalogger to store GPS data when the trigger pulse was received.

Figure 4-8 illustrates a graph for the recorded GPS data after field trials. In this figure, red dots represent the center of an individual plot located in the field.

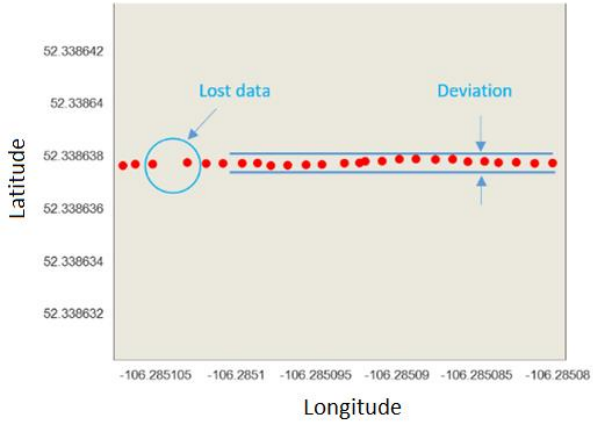

Figure 4-8: Acquired GPS data for mapping the field using a GPS trigger signal

As can be seen in Figure 4-8, similar to the previous approach, a few lost data can be found amongst the collected data. The number of lost information; however, is significantly less than the previous method, but it still happens due to the GPS signal lost at the particular time when the datalogger was trying to read the GPS data.

Moreover, this approach was found to be more prone to a problematic issue which is a miscalculation of the traveled distance when the GPS signal fades during the experiments. So the software was unable to back-calculate the traveled distance according to the starting point, and if GPS signal is lost at the beginning, the entire data will be distorted.

4-3-3- Using Interpolation

The last and most efficient approach to determine the geospatial information about the location of each plot in the field was using interpolation and math. In fact, the center of a few candidate plots, preferably four plots located on each corner of the field, should be precisely captured using the existing GPS. Then the geospatial information of the rest of the plots could be accurately calculated using the function developed to correlate GPS data to the location of each sensor, which was explained in chapter three.

Figure 4-9 illustrates a graph for the result of calculating center of each plot in the studied field using a few sample points. In this figure, X-axis represents the longitude and Y-axis represents the latitude and also, red dots demonstrate the center of each plot in the field.

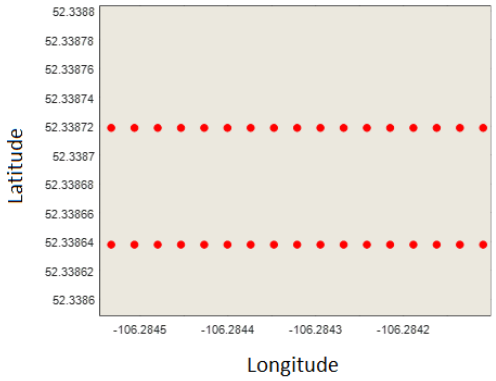

Figure 4-9: Acquired GPS data for mapping the field using interpolation

As can be seen, using this approach eliminates the issues related to GPS signal lost and also there is no deviation from the straight line due to the inability of the driver to drive through a straight line, as was observed in the previous method.

At this point, the required information to map the studied field is obtained and the desired set of data can be collected to be visualized in the developed program with an acceptable accuracy. In the next sections, the results of data collection trials are discussed.

4-4- Results of Field Experiments in 2016

During 2016 trials, the proposed plant phenotyping platform was at its earliest stage for the majority of plants were harvested when the platform was fabricated, and only a small section of plots was left for experiments. In fact, the primary purpose of the field tests in fall 2016 can be summarized as follows:

- To extract GPS National Marine Electronics Association (NMEA) string out of GPS receiver box for data/image geo-referencing
- To examine the performance of ultrasonic sensors for plant height measurement
- To assess the quality and performance of a wireless RGB camera to capture pictures of plant canopies in outdoor configuration
- To attach a mechanical boom to the back of the farm vehicle as a fixing frame for different measurement equipment
- And finally, to identify unforeseen existing flaws in the design of the platform

Overall, teamwork ended up with a field-based plant phenotyping platform as can be seen in Figure 4-10, and only one data collection trial was conducted in fall 2016. However, several on-site experiments were done to achieve objectives of the experiments.

Figure 4-10: The proposed HTPP for tests in fall 2016

It was found that the existing RTK GPS on the farm vehicle has the capability of streaming required geospatial data including longitude and latitude as a standard NMEA string over a serial port so that any third-party device could use this data for georeferencing purposes. As mentioned before, in the proposed setup a datalogger was used to collect phenotypic data coming from different sensors, so GPS output port was connected to the datalogger for geo-referencing every single data. Nevertheless, the existing GPS could only provide a single data output, but to geo-reference both collected data in datalogger and also captured images in laptop, two outputs were required. This problem was solved by using a serial port splitter and no major issue, e.g., weakening the quality of the GPS signal, was observed after adding this element to the system.

Figure 4-11 illustrates a screenshot of the collected data in 2016. As can be seen, this data file encompasses 12 columns (A-L), and the number of rows depends on the duration of the data collection. In fact, column A illustrates the date and time of the data collection; columns C-F represent the captured height values by four ultrasonic sensors (sensor 1-4 respectively) in millimeter. Columns G-L illustrate the captured GPS data where column I is latitude, and column K is the longitude of the sampling point.

	A	B	C	D	E	F	G	H	I	J	K	L
1	TIMESTAMP	RECORD	USonic_1	USonic_2	USonic_3	USonic_4	GPS_Data(1)	GPS_Data(2)	GPS_Data(3)	GPS_Data(4)	GPS_Data(5)	GPS_Data(6)
2	9/22/2016 18:08	57	741.6	806	546	533.8	$GPGGA	831	5220.118831	N	10617.00263	W
3	9/22/2016 18:08	58	730.5	682	740.2	503	$GPGGA	833	5220.119497	N	10617.00263	W
4	9/22/2016 18:08	59	628.6	804	635.9	515.4	$GPGGA	835	5220.120144	N	10617.00263	W
5	9/22/2016 18:08	60	493.4	693.5	640.1	37.96	$GPGGA	837	5220.120828	N	10617.00265	W
6	9/22/2016 18:08	61	791.8	806	683.8	34.06	$GPGGA	839	5220.121485	N	10617.00265	W
7	9/22/2016 18:08	62	706.5	746.5	505	341.9	$GPGGA	841	5220.122135	N	10617.00267	W
8	9/22/2016 18:08	63	674.8	773.5	775.7	738	$GPGGA	843	5220.122793	N	10617.00266	W
9	9/22/2016 18:08	64	586.5	38.27	775.5	469.3	$GPGGA	845	5220.123484	N	10617.00267	W
10	9/22/2016 18:08	65	53.82	475.7	559.7	554.7	$GPGGA	847	5220.124119	N	10617.00266	W
11	9/22/2016 18:08	66	439.3	521.5	775.6	551.7	$GPGGA	849	5220.124797	N	10617.00266	W
12	9/22/2016 18:08	67	673.9	571.4	697.5	614.5	$GPGGA	851	5220.125548	N	10617.00266	W
13	9/22/2016 18:08	68	517	634.4	655.5	54.06	$GPGGA	853	5220.126269	N	10617.00267	W
14	9/22/2016 18:08	69	731.7	758	775.5	577.1	$GPGGA	855	5220.126991	N	10617.00266	W
15	9/22/2016 18:08	70	629.8	548.4	775.7	576.2	$GPGGA	857	5220.127746	N	10617.00266	W
16	9/22/2016 18:08	71	570.4	770.8	656.4	502.3	$GPGGA	859	5220.128463	N	10617.00265	W
17	9/22/2016 18:08	72	38.21	557.9	481.2	430.7	$GPGGA	901	5220.129178	N	10617.00265	W
18	9/22/2016 18:09	73	430	495.3	587.1	678.3	$GPGGA	903	5220.129905	N	10617.00264	W

Figure 4-11: A screenshot of phenotypic data file collected in 2016

With the utilized data file structure in 2016, it was found that a remarkable amount of delay occurred when the GPS string was being processed within the data collection loop to break down the GPS string into the individual parts. In other words, the datalogger required some time

to analyze the GPS data, and this made a problem in geo-referencing collected data for future retrieval. It will be explained how this issue was solved in the final design during 2017 trials by saving the raw GPS string and processing the raw values in the developed data visualization program where there is no critical time limitation for data processing.

Moreover, it was found that ultrasonic sensors could operate in the outdoor configuration without any problem, and could reasonably measure the height of the plants. Indeed, ultrasonic sensors could distinguish the variation in the height of the plant canopies after being calibrated. Figure 4-12 illustrates a graph based on the collected data by one of the ultrasonic sensors when the vehicle was traveling with a speed around 4.5 mph (7.24 km/h) to reconstruct three adjacent canopies profile.

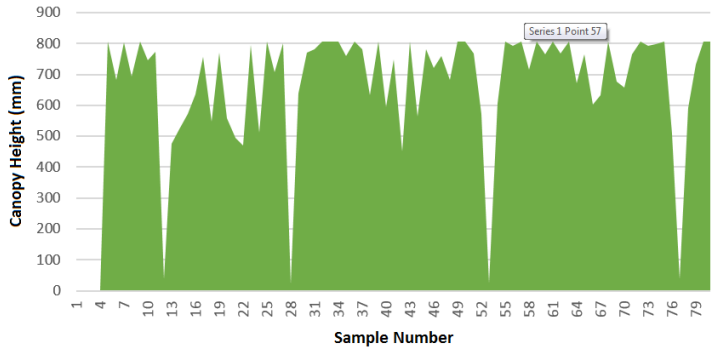

Figure 4-12: Canopy profile reconstruction using ultrasonic data collected in 2016

In this graph, the Y-axis represents the canopy height in millimeter. As can be seen, the surface of the canopies seems wide-ranging because as mentioned earlier the set of plots dedicated for field experiment was shattered in late September 2016. In fact, the four sharp gaps in Figure 4-12 represent the boundary between two adjacent plots.

As discussed in chapter two, two wireless cameras were used to capture images of canola cultivars in the proposed field-based plant phenotyping platform in 2016. The primary incentive to utilize wireless cameras was to avoid additional wiring to connect cameras to the laptop. However, it was found that it is better to use wired cameras instead of the wireless cameras to eliminate the occurred delays in synchronization of the image acquisition program, GPS data and captured images by cameras. This problem was addressed in the proposed design in 2017.

Because initially it wasn't clear whether there is a local map for the studied field or not, it was tried to include as much information as possible in the file name of the captured images. Figure 4-13 illustrates a screenshot of part of the final folder containing all captured images on the laptop hard drive.

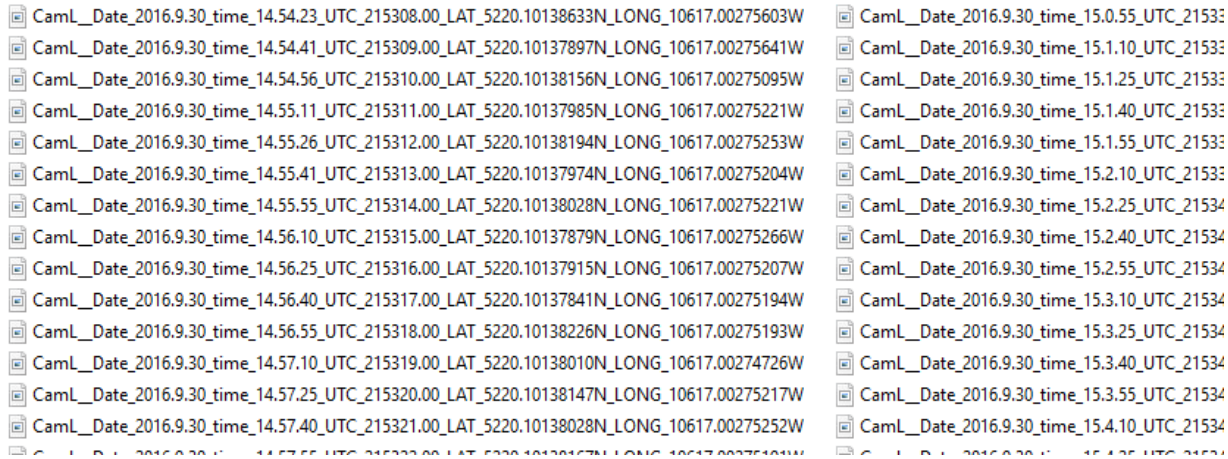

Figure 4-13: A screenshot of the folder enclosing captured images in 2016 experiment

As can be perceived, the format of the image file name corresponds to the location and the time when images were captured. In fact, a general form for a sample image name can be represented as below:

$$Camx_1\_Date\_x_2\_time\_x_3\_LAT\_x_4\_LONG\_x_5$$

Where *X1* is either R or L which represents whether the image was captured by the right or left side camera, *X2* and *X3* are the date and time of image acquisition, and finally, *X4* and *X5* are latitude and longitude of the location where the image was captured. However, it was found that it is not necessary to add in date and time to the filename of the image because this information was already available by default Microsoft Windows features. Indeed, as was explained in the previous chapter, it meets the requirements for future image retrieval if longitude and latitude of the location where the image was captured are used in the filename. Moreover, if the vehicle turns into the different directions during the data collection, it is necessary to include the vehicle heading into the filename of the images to be able to correlate captured images and data to the corresponding plots accurately.

Figure 4-14 illustrates two sample images of canola cultivars which were captured in 2016 using two wireless cameras.

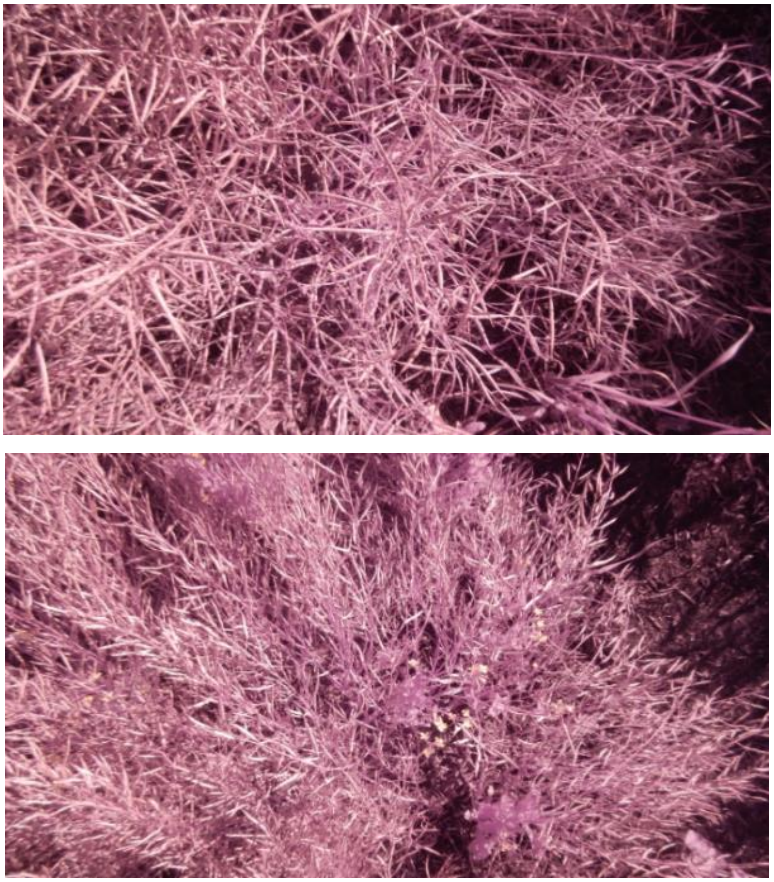

Figure 4-14: Sample captured images in 2016 experiment

The reason for the dominance of the red color in these pictures is the fact that an additional filter was initially added to the RGB cameras to achieve an estimated value for NDVI. However, it was found that the utilized filters could not give a useful information, and it is better to capture intact RGB images instead.

Overall, the employed approach to capture images of plant canopies in 2016 did not successfully pass the performance evaluation tests because of existing delays in a wireless network for camera-laptop interaction. So it was not possible to associate each image with the corresponding plot using captured GPS data. Furthermore, the utilized wireless camera couldn't handle the assigned task to capture images every 500ms because of its slow response time, and the time was needed to recover after taking an image.

4-5- Results of Field Experiments in 2017

After the experience was gained through experimental tests in 2016, as well as more in-depth study of the existing and similar designs and evaluating their pros and cons, a considerably improved field-based plant phenotyping platform was proposed in 2017 as can be seen in Figure 4-15.

Figure 4-15: The proposed HTPP for experiments in 2017

The details of the hardware and software components of the proposed system were explained in chapters two and three. As discussed before, four different plant traits were targeted in the proposed field-based plant phenotyping platform including canopy height, temperature, NDVI and also plant growth were captured by RGB cameras.

Moreover, different programs were developed including an inclusive program for interactive data and image visualization.

Overall, the field trials for 2017 experiments can be summarized in Table 4-1 , which gives an explanation of field tests and visit during 2017 growing season. However, to be able to achieve the desired objectives, more site visits had to be occasionally done, which are not included in the table.

Table 4-1: List of conducted field visits/trials during 2017 growing season

Date	Tasks
May 31, 2017	- The first generation of the mechanical boom was assembled - Vibration test was done by mechanical team
June 8, 2017	- Ultrasonic sensors and other components were assembled on the boom - Electrical system including sensors and datalogger were wired - A communication link was established with the vehicle GPS - Note: Couldn't collect any data on the field due to the irrigation and wet ground
June 15, 2017	- Required GPS data for field mapping was collected - Webcam and DSLR cameras were tested to see the effect of vibration on the quality of images - No phenotypic data were collected
June 23, 2017	- **1st data collection** was conducted on a partially cloudy day - Canopy NDVI and temperature were target traits - RGB images were captured by webcam. Visible signs were used to validate the geo-referencing
July 4, 2017	- **2nd data collection** was conducted on an entirely clear sky. Some plots were in flower - Canopy NDVI and temperature were target traits. RGB images were captured by webcam - Prof. Fotouhi examined the reliability of the system by sitting next to the driver - Data collection with higher speed was tried (3.2 mph)
July 7, 2017	- Ultrasonic sensors were assembled on the boom - **3rd data collection** was conducted in a relatively clear sky with a few scattered clouds - Canopy NDVI and temperature were target traits. Many tiny branches were observed - RGB images were captured by webcam
July 13, 2017	- **4th data collection** was conducted in an entirely clear sky - Canopy NDVI and temperature were target traits. **Almost all plots were in flower** - RGB images were captured by webcam. New visible signs were used to verify geo-referencing - Ultrasonic sensors were tested on-site and prepared for next data collections
July 18, 2017	- **5th data collection** was conducted on a partially cloudy day - **Ultrasonic sensors were used**. Canopy height, NDVI, and temperature were target traits - The height of random plots was measured manually. **Maximum flower observed** - RGB images were captured by webcam
July 25, 2017	- **6th data collection** was conducted on a partially cloudy day with intense sunshine - Canopy height, NDVI, and temperature were target traits - Flowers were shrank and less reflection area could be seen - RGB images were captured by webcam. It was found that sun location was moved to the south - The mechanical team conducted vibration test. All sensors were detached at the end
Aug. 2, 2017	- Second generation boom was assembled. Sensors and data logger was attached and wired - **7th data collection** was conducted in a fairly clear sky - Canopy height, NDVI, and temperature were target traits. No more flower could be seen - RGB images were captured by webcam
Aug. 11, 2017	- **8th data collection** was conducted in a relatively clear sky with intense sunshine - Canopy Height, NDVI, and temperature were target traits. - There were many seeds on top of the plants as if the height of canopies appeared to be shrank - RGB images were captured by webcam
Aug. 18, 2017	- **9th data collection** was conducted before the noon in an entirely clear sky - Canopy Height, NDVI, and temperature were target traits - RGB images were captured by webcam - DSLR cameras were tested again

As can be seen from Table 4-1, nine times data collection trials and three more field works were performed during summer 2017.

The first data collection was on June 23, 2017, which canopy temperature and NDVI were target traits to be measured, and RGB images were captured on the same day. The similar process was carried out until 5th data collection trial on July 18, 2017, when ultrasonic sensors were added into the system to measure canopy height beside temperature and NDVI. The reason for not capturing height notes before July 18 is the fact that breeders only need to study the height of a canopy when they are coming into flower. Also, before the mentioned date, canola plants were remarkably tiny and there were not enough leaf area to reflect ultrasonic signals. Finally, the 9th and last data collection was conducted on August 18, 2017 when the field was being prepared to be harvested.

The main focus of experiments during summer 2017 was on evaluating the performance of the developed high-throughput plant phenotyping platform through studying the growth of a population consisting of 252 Canola plots in a nursery located in a Canola research center in Saskatchewan.

In fact, the result of each data collection trial was an Excel file encompassing information about NDVI, temperature, and height of different plots, as well as a folder holding RGB images captured at different locations in the field. So in total, nine data file and nine image folders were collected, and the data can be visualized in the developed visualization program.

The detail of developed program was discussed in chapter three. In next sections, a briefer explanation of the results achieved by using the proposed field-based high-throughput plant phenotyping platform to study the Canola growth is provided.

4-5-1- Verifying the accuracy of geo-referencing algorithm by visible signs

The primary concern about the performance of the developed platform was the validity of the measurements. In other words, it had to be confirmed that the developed platform consisting of a GPS unit, data/image acquisition programs, and proposed visualization program provides an accurate set of information about individual plots.

Concretely, the main source of error that might challenge the validity of the collected data would be associating some information to a plot where they do not belong. This problem could simply happen due to either the inability of GPS unit to provide an accurate geospatial

information or an unseen problem such as a delay in synchronizing GPS data with information coming from different sensors for ge-oreferencing purposes.

To address this bottleneck, a novel approach was used to validate the performance of the developed platform. As can be seen in Figure 4-16-b, plot numbers were printed and placed next to individual plots in the field. In Figure 4-16-c, the border of the plot is marked by red lines and the sign can be seen as a white/red and yellow round object in Figure 4-16-a.

a) Two different type of signs were used

b) Placing visible signs next to the plots c) A sample plot and a visible sign next to it

Figure 4-16: Using visible signs next to individual plots to validate the geo-referencing algorithm

Now the reliability of the information provided by the developed plant phenotyping platform can be verified if the consistency of the plot numbers captured by cameras with the plot numbers on the field map of the visualization program is verified.

After investigating into the captured images during different trials, it was verified that almost every sign could be seen on the corresponding plot using the developed visualization program. Figure 4-17 illustrates a sample screenshot of the visualization program when an available image for the plot number 1.14 near the left edge is selected and observed by the user.

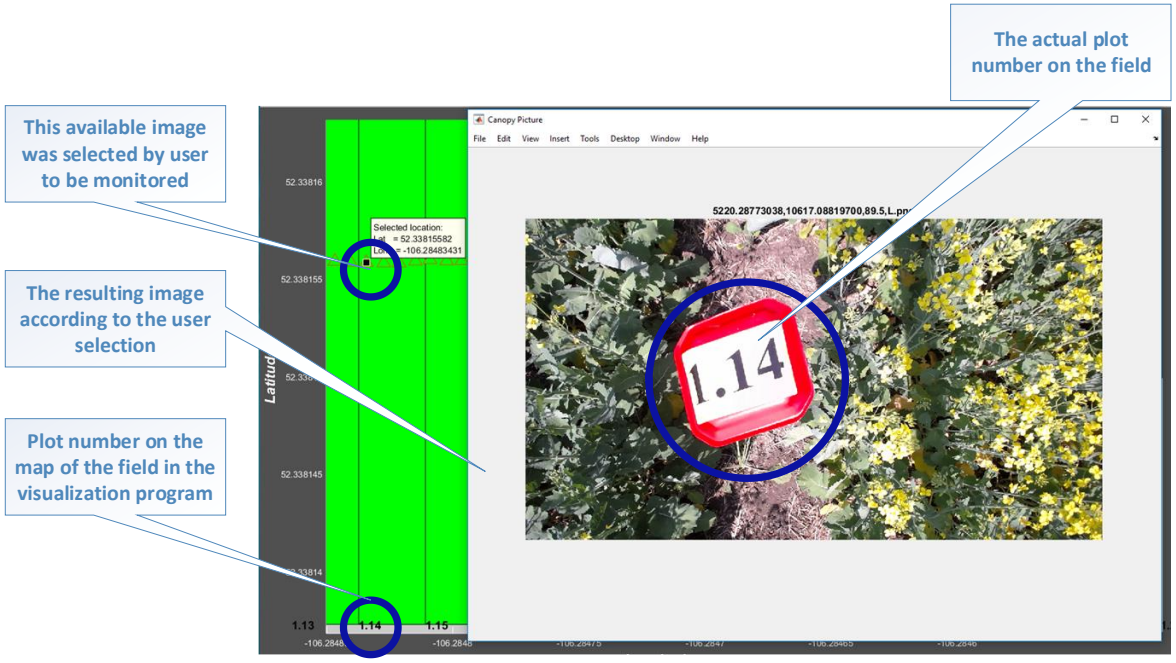

Figure 4-17: Verifying the accuracy of the geo-referencing using the developed visualization program

As can be seen in Figure 4-17, the visible sign which was placed on the field next to the plot number 1.14 can be seen on the corresponding plot which is being symbolized by the program. Furthermore, Figure 4-18 and Figure 4-19 illustrate the result of verifying the accuracy of geo-referencing algorithm by visible signs for two different plots.

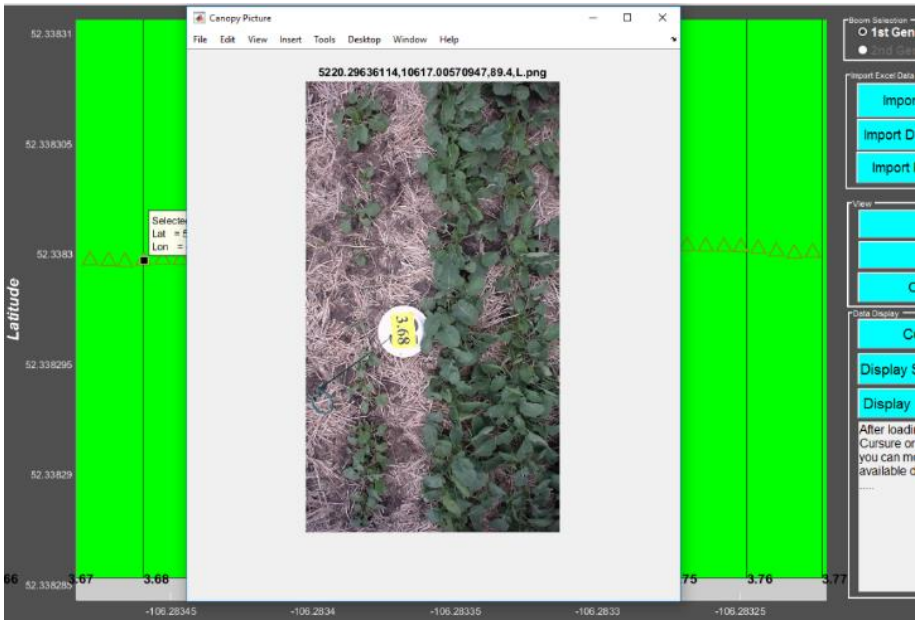

Figure 4-18: Result of verifying the accuracy of geo-referencing algorithm by visible signs based-on experiments on June 23, 2017 (plot # 3.68)

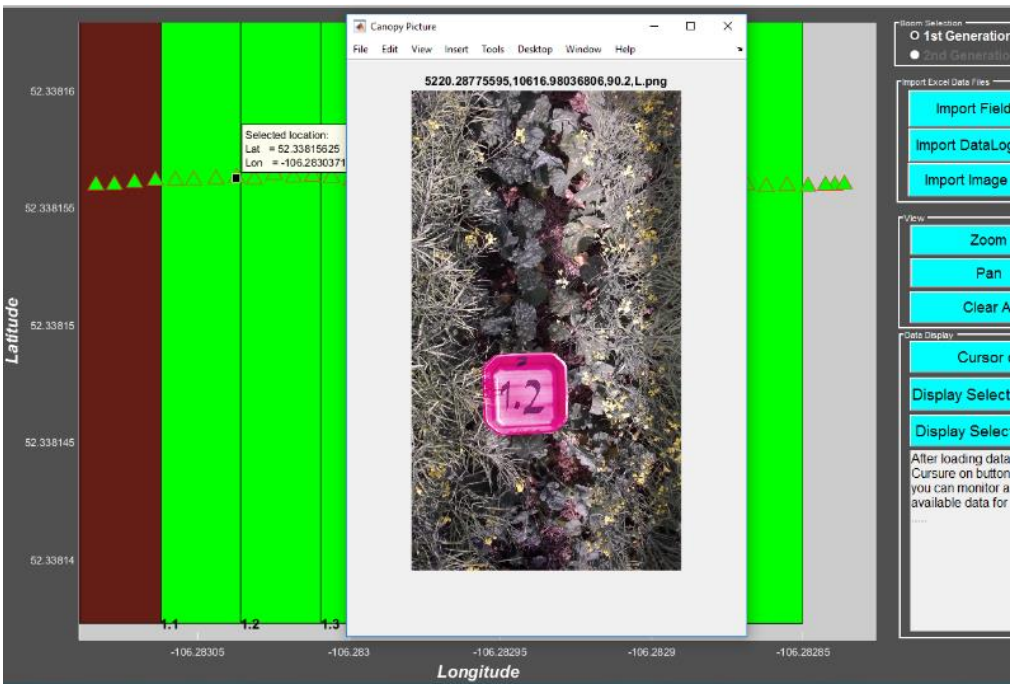

Figure 4-19: Result of verifying the accuracy of geo-referencing algorithm by visible signs based-on experiments on July 25, 2017 (plot # 1.2)

Using the same approach, other signs can be found using the developed visualization program to verify the effectivness of the georeferencing algorithm. The full result of this verification test is provided in Appendix D1-4. In fact, a screenshot of the output of the program based-on the collected data on June 23, July 13, July 25 and August 2 for three random plots can be observed in Appendix D1-4.

It is mentionable that some additional text boxes are added to the screenshot provided in Figure 4-17 for a better understanding of the main idea for verifying the accuracy of the geo-referencing algorithm. However, the results provided in Appendix D do not have any additional mark or comment to keep the originality of the images intact.

4-5-2- Analyzing the entire studied population (252 Canola plots) over summer 2017

As mentioned before, the proposed plant phenotyping platform was used to study a population consisting of 252 canola plots between June – August 2017. The focus of the study was on exploiting the developed platform to acquire information about canopy height, temperature, and NDVI. Also, RGB images of plant canopies were captured for more detailed investigations.

Indeed, using the proposed system with the selected traveling speed of the vehicle (~ 1.9 mph) to scan the entire field ended up with two main outputs. First, eight RGB images (four images on each side of a plot) were captured per plot. Second, 16 data points per each sensor (eight points on each side of a plot) for each plot were collected. However, due to the random GPS signal loss and occasional inability of the sensors to give out data signals, the number of recorded data for every plot was infrequently less than mentioned numbers.

One of the advantages of using a high-throughput plant phenotyping platform is the fact that the resulting database can be used in different approaches for different purposes. In fact, breeders have the flexibility to study both entire popultation and the individual plots for closer investigations. In this section a summary of the results achieved after studying a population consisting of 252 canola plots by the proposed plant phenotyping platform is provided. Figure 4-20 illustrates variation in the average canopy a) NDVI and b) temperature values of the studied population between June 23 – August 18, 2017.

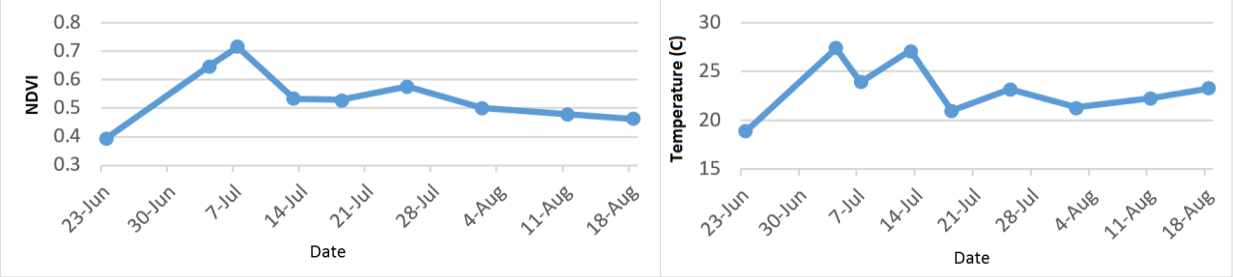

a) Average Canopy NDVI for Different Trials b) Average Canopy temperature for Different Trials

Figure 4-20: Variation in the entire studied population between June 23, 2017 and August 18, 2017

For example, it can be comprehended from Figure 4-20 that the average NDVI and temperature of the entire population (252 plots) are recorded to reach their maximum values on July 7 and July 4, 2017 respectively. So we expect that the majarity of the plant canopies should be in their maximum greenness on July 7, and this matter can be verified by investigating into the captured images during July 7 trial. Moreover, Figure 4-21 illustrates the histograms of the collected data for the entire population (252 plots) during nine edifferent days between June 23 – August 18, 2017.

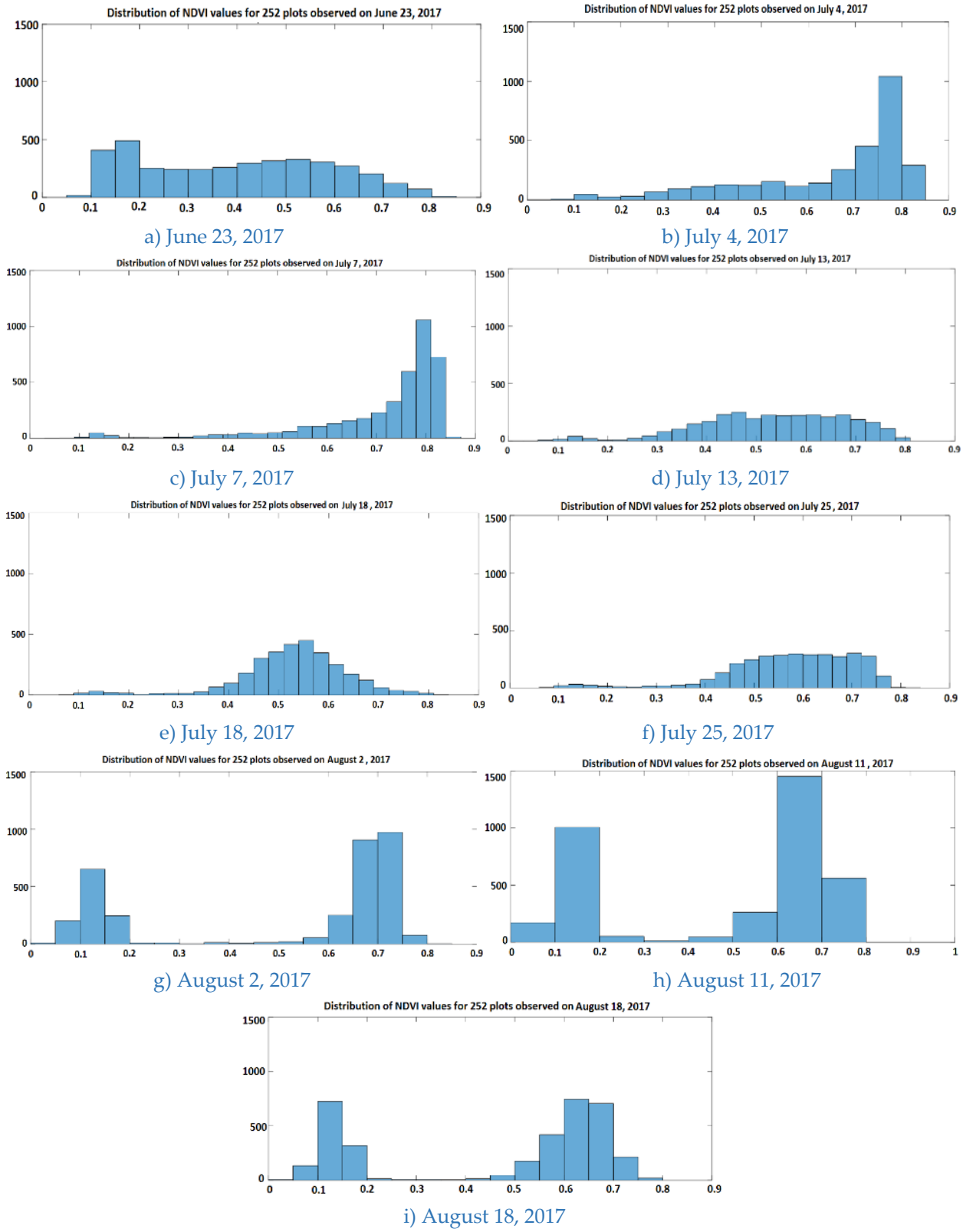

a) June 23, 2017

b) July 4, 2017

c) July 7, 2017

d) July 13, 2017

e) July 18, 2017

f) July 25, 2017

g) August 2, 2017

h) August 11, 2017

i) August 18, 2017

Figure 4-21: Histograms for NDVI values of the entire studied population (252 plots) between June 23 and August 18. (X-Axes and Y-Axes represent NDVI value and number of sample points respectively)

Having a closer look at the achieved histograms provided in Figure 4-21 gives the impression of distribution of NDVI values in the studied population consisting of 252 canola plots in different days. For example, from Figure 4-20 it was found that the maximum average NDVI value (~ 0.78) was recorded on July 7, 2017, so we expect that the majority of NDVI values should be around 0.8. This matter can be clearly perceived by having a look at the distribution of NDVI values in Figure 4-21 c)July 7, 2017, which clearly illustrates almost 1000 sample points were reported the value of 0.8 for NDVI.

4-5-3- Analyzing growth of individual plots over summer 2017

In previous section, the variation and distribution of different plant characteristics in a whole population consisting of 252 canola plots captured in different trials was discussed. So breeders can use the provided data to estimate a proper model to find a possible correlation between different traits to achieve a better yield.

In this section, it is tried to illutrate how the proposed plant phenotyping platform can be used to acquire information about individual plots. In fact, as can be seen in Figure 4-22, the studied canola plants were quite fast gowing during the experiments, so studying the growth of individual plots with diverse genotypes can be significanlty useful. Indeed, this helps breeders for better understanding of the correlation between genotypes and phenotypes.

a) June 15, 2017 b) July 13, 2017

Figure 4-22: Significant growth of plots in less than a month

As discussed before, the develoepd field-based high-throughput plant phenotyping platform provides information about a plant canopy NDVI, temperature and height as well as plant growth images.

However, more information could be collected by adding more sensors, if needed. Therefore, the proposed data visualization program can be used to study the behaviour of different characteristics of each plot as a member in a whole population of 252 canola plots.

In this section, a random plot (plot number 1.35) was selected to study the behaviour of its NDVI and temprature. In fact, the variation of these two parameters between June 23, 2017 (1st data collection trial) and August 18, 2017 (9th and the last data collection trial in 2017) was extracted using the proposed visualization program.

Table 4-2 illustrates summary of captured data for the plot number 1.35 in nine different days during summer 2017.

Table 4-2: Summary of captured data for plot number 1.35

Date	NDVI	Temp (C°)	Ambient Temp (C°) Ref: the weather network	Diff= Ambient Temp - Temp	Time of the data collection
June 23	0.4128	15.9	18.8	2.9	15:20 pm
July 4	0.7294	25.6	27.4	1.8	15:50 pm
July 7	0.7580	22.3	29.8	7.5	10:55 am
July 13	0.5504	26.1	29.3	3.2	14:30 pm
July 18	0.4989	20.5	22.9	2.4	14:35 pm
July 25	0.5614	22.7	25.7	3.0	14:45 pm
August	0.6686	22.1	24.7	2.6	16:30 pm
August	0.6340	23.2	27.1	3.9	12:05 pm
August	0.5935	23.1	27.3	4.2	10:20 am

As can be seen in Table 4-2, first column represents the date when the data collection was conducted. Columns two and three, represent the average NDVI and temperature values recorded for the mentioned plot respectively. Column four represents the ambient temperature at the time of data collection, column five illustrates the difference between the ambient temperature and the temperature of the canopy captured by IR thermometers, and finally column six illustrates the time of the day when trial was conducted on the studied canola nursery.
Moreover, Figure 4-23 illustrates two line graphs for better intuition of the variation of a) NDVI and b) canopy temperature of the plot number 1.35 during the summer 2017.

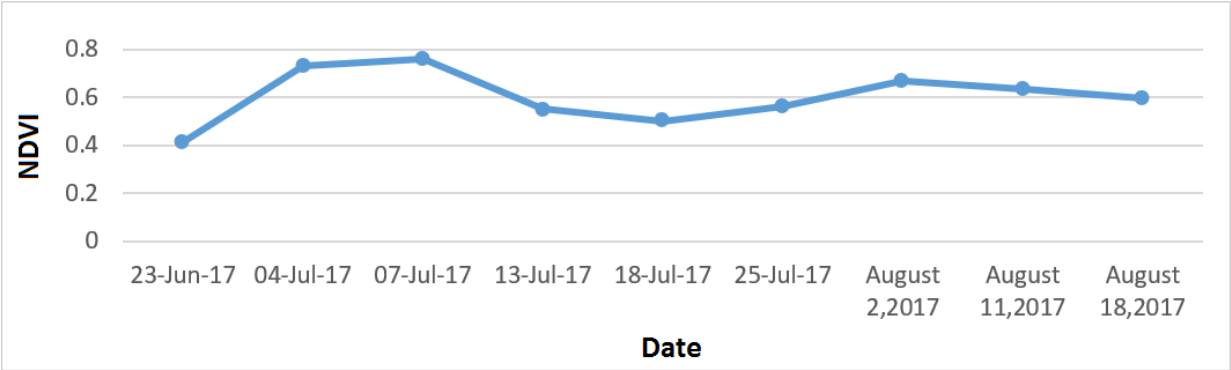

a)

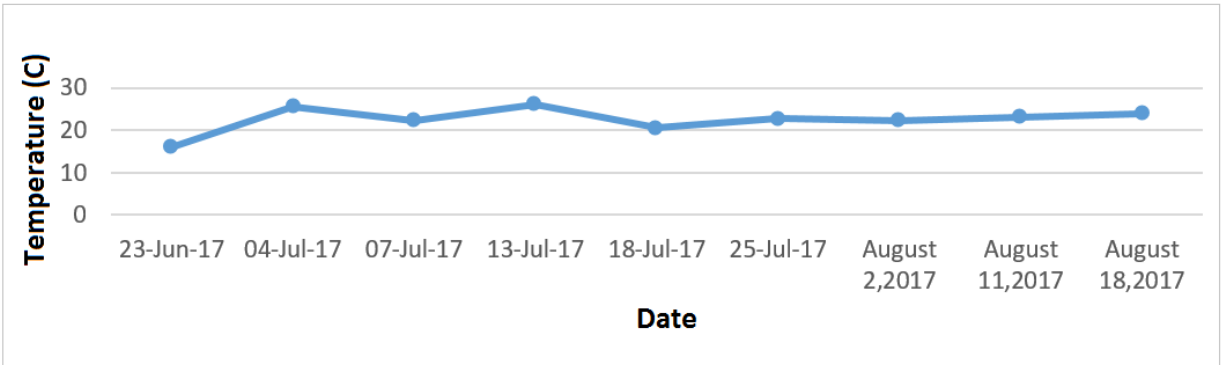

b)

Figure 4-23: Variation of NDVI and temperature of plot # 1.35 during summer 2017

As can be perceived, the temperature for the mentioned plot is recorded to be ~ 17 c^o on June 23, 2017 and after some ups and downs, it was settled around 22 c^o on August 18, 2017. It appears the study of variation in temperature of canola cultivars might be a good research topic to find out the relation between this trait and the final yield. No report could be found in this regard when the literature review was conducted.

On the other hand, NDVI value for the mentioned plot had a continous growth after June 23 untill the maximum NDVI value was captured on July 7, which is ~0.78. After July 7, the majority of plants came into flowers (with yellow color) so the NDVI value, which is an indication of the greenness level of a canopy, was decreased. A turning point can be perceived on July 18 because the plots were observed in their maximum flower on July 18 (yellow color was dominant to green color). After July 18, when flowers began to be shrank, the NDVI value started to increase because the green color was gradually becomming dominant to the yellow color.

It appears there were no significant up and downs in NDVI value after August 2 which is due to the fact that no flower or remarkable growth could be observed in cultivars.

One of the most powerful features of the proposed visualization program is the fact that not only all phenotypic data of different plots can be studied, but also photographic data of individual plots can be explored for better insight. Indeed, user can select an available image and monitor a desired section of any plot. For example, Figure 4-24 - Figure 4-32 illustrate captured images of plot number 1.35 in nine different days during summer 2017.

The provided screenshots are extracted from the propsoed visualization program for better understanding. As can be seen in Figure 4-24, an available image on the middle of the plot number 1.35 was selected for a closer investigation in this example. However, the plot can be observed from other views by selecting any other available images.

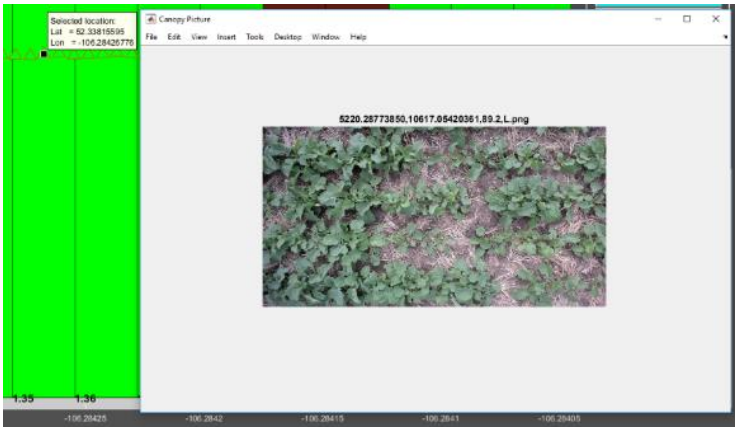

Figure 4-24: Plot # 1.35 on June 23

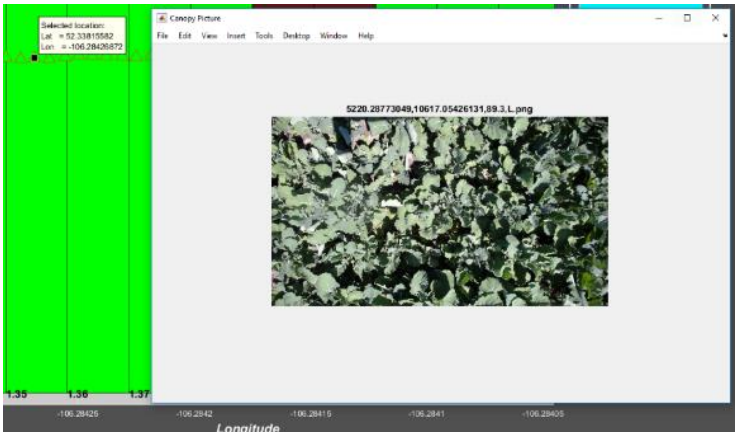

Figure 4-25: Plot # 1.35 on July 4

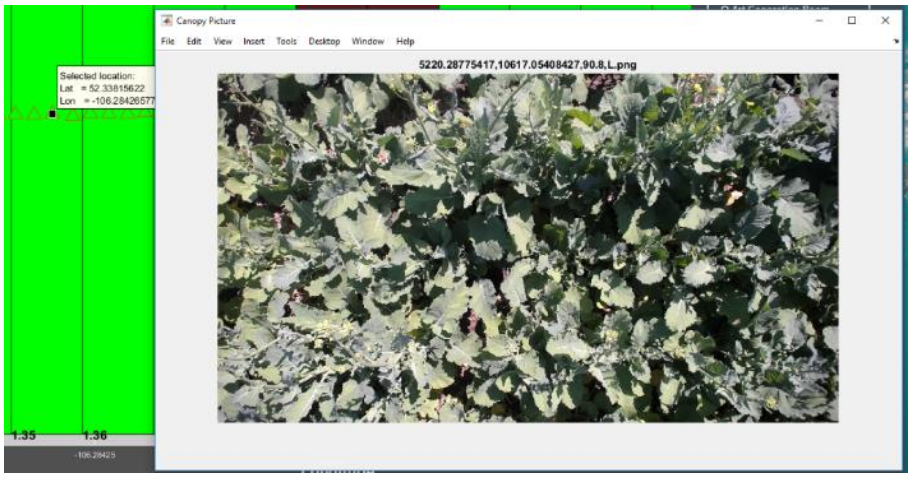

Figure 4-26: Plot # 1.35 on July 7

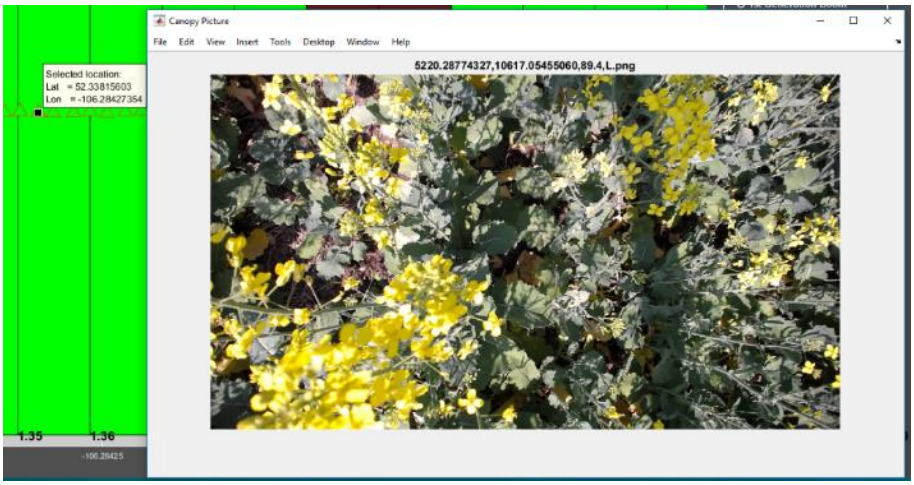

Figure 4-27: Plot # 1.35 on July 13

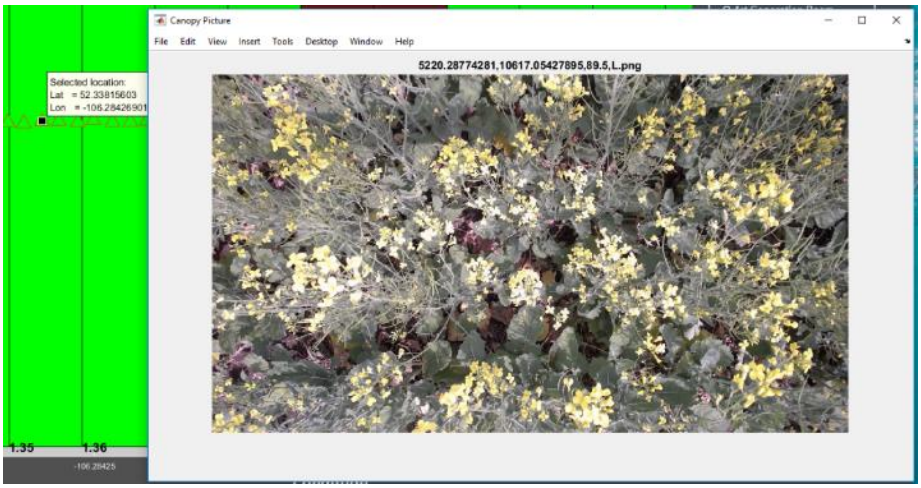

Figure 4-28: Plot # 1.35 on July 18

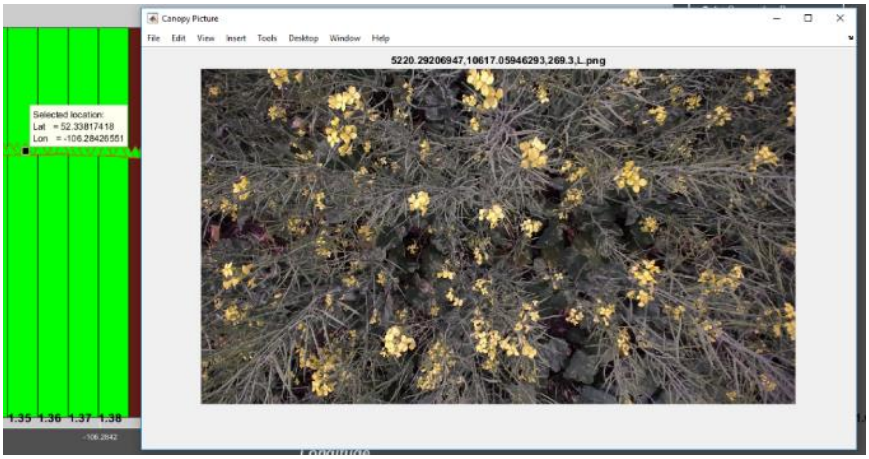

Figure 4-29: Plot # 1.35 on July 25

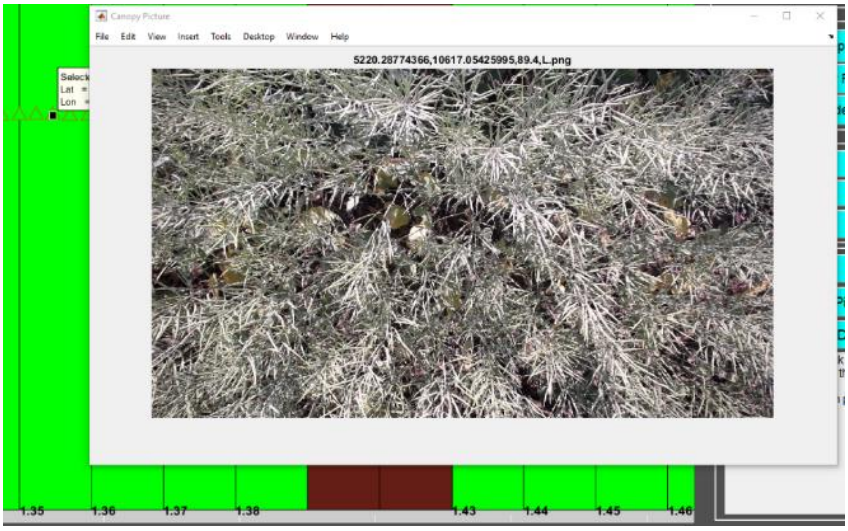

Figure 4-30: Plot # 1.35 on August 2

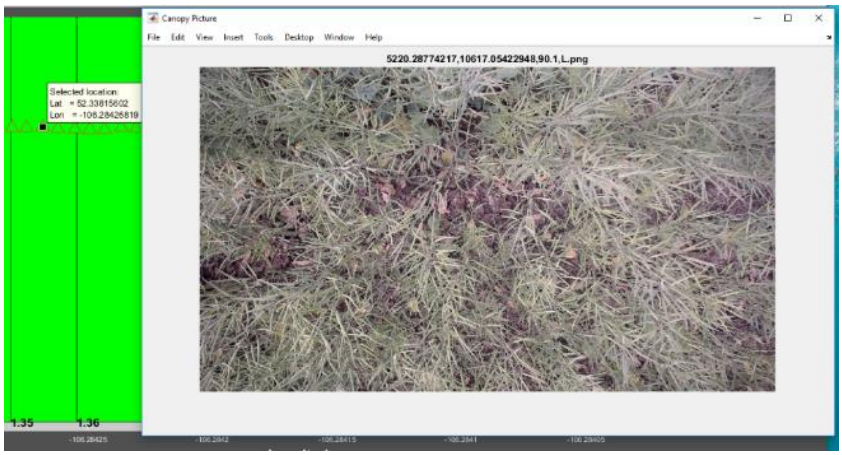

Figure 4-31: Plot # 1.35 on August 11

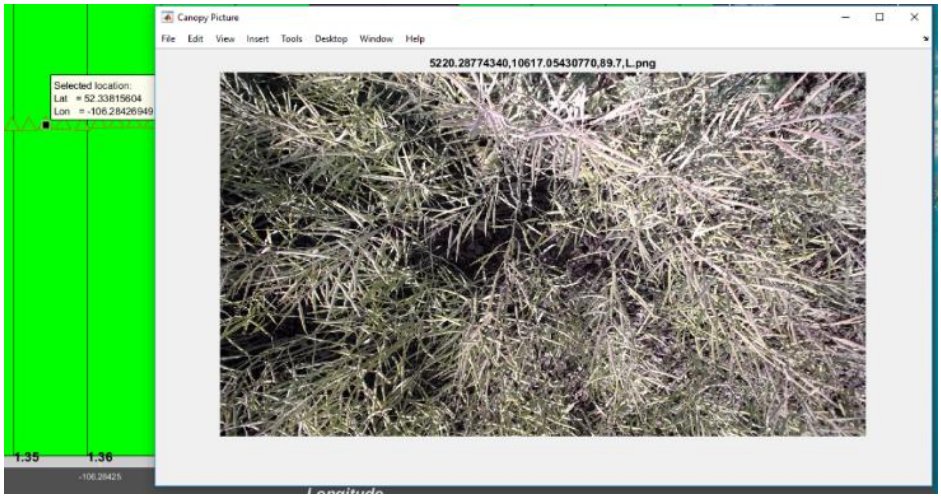

Figure 4-32: Plot # 1.35 on August 18

The growth rate of the plot number 1.35 can be clearly seen in last nine images, and breeders can combine these photographioc data with the acquired phenotypic data (NDVI, temperature and height in this example) to have a comprehensive study of different plots. For example, according to the Table 4-2, the maximum NDVI value of the plot 1.35 was 0.76 on July 7 so it is expected that the majority of this plot should be covered by green leaves on the mentioned day. Having a closer look at the previous images, it can be concluded that plot 1.35 was in its maximum level of greenness on July 7, 2017 as can be seen in Figure 4-26.

Likewise, the minimum NDVI value of the plot 1.35 was reported on June 23, 2017 which is 0.41. This NDVI value means less than half of the plot should be covered by plants, and this can be verified by having a look at Figure 4-24 which is an image on the middle of plot 1.35.

Last but not least, the behaviour of any other desired plot can be studied similar to the provided example. To observe more examples, refer to Appendix D where section D5 illustrates the result of analyzing growth of the plot # 1.75, section D6- for the plot # 2.30, section D7 for the plot # 2.80, section D8- for the plot # 3.5 and section D9 for the plot # 3.60 over summer 2017.

4-5-4- Height measurements

In chapter three, the performance and efficiency of an ultrasonic sensor to measure height of different objects and ultimately to measure height of a plant in laboratory configuration was examined and discussed. In this section, a brief discussion about the reliability of height measurement by ultrasonic sensors in the proposed HTPP is provided. Meanwhile, linearity,

repeatability and sensing distance range will be assessed and the result of comparing manual height measurement and the values given by ultrasonic sensors will be provided.

First of all, as numbers in datasheet reveal, linearity error of the utilized sensor is <0.3% (refer to Figure F-9 in Appendix F) which is adequate to measure height of a plant canopy. Furthermore, no nonlinear behavior was observed during measurements provided that the distance between tip of the sensor and top of the canopy is within the allowable range. Obviously, outside of this standard range, the sensor doesn't respond linearly and measurements are not acceptable. This fact was observed in experiments as well. Indeed, when the distance between the boom and top of the canopy was outside of the sensing range, the output signal was faded or unrelated to height of the plant.

The second important factor is repeatability. As stated in the datasheet of the utilized ultrasonic sensor, the repeatability error is 0.2% (refer to Figure F-9 in Appendix F) and doesn't appear to be an issue for a height measurement system. Besides, repeatability error was assessed in experiments by repeating the measurements with exactly the same measurement conditions over a period of time after turning off and on the main power for several times to see whether there is any significant difference between measurements or not. As experimental results persisted, there were no remarkable repeatability error because all data collected over a period of time were similar. However, there were a negligible error (less than one cm) in some cases which is acceptable in the current design because in a mobile and field-based measurement system, a few centimeters of absolute error in measurement is predictable and unescapable.

Additionally, to verify the accuracy and reliability of the measured canopies height by ultrasonic sensors in the proposed HTPP, manual height measurement were carried out for entire plots on certain days as can be seen in Figure 4-33.

Figure 4-33: Manual height measurement for verifying ultrasonic height measurements

Indeed, height of some plots were measured manually using a scaled bar and the result was stored in a pocket pc. Then the proposed visualization program was used to extract height information for individual plots, and the result was compared with the manual height measurements for the similar plots. The verification was done for two trial days on July 18, 2017 and August 2, 2017 and the results are provided in the next two sections.

4-5-4-1- Height measurements on July 18

Figure 4-34 illustrates a graph for comparison of manual and ultrasonic height measurement for 19 plots which was conducted on July 18, 2017.

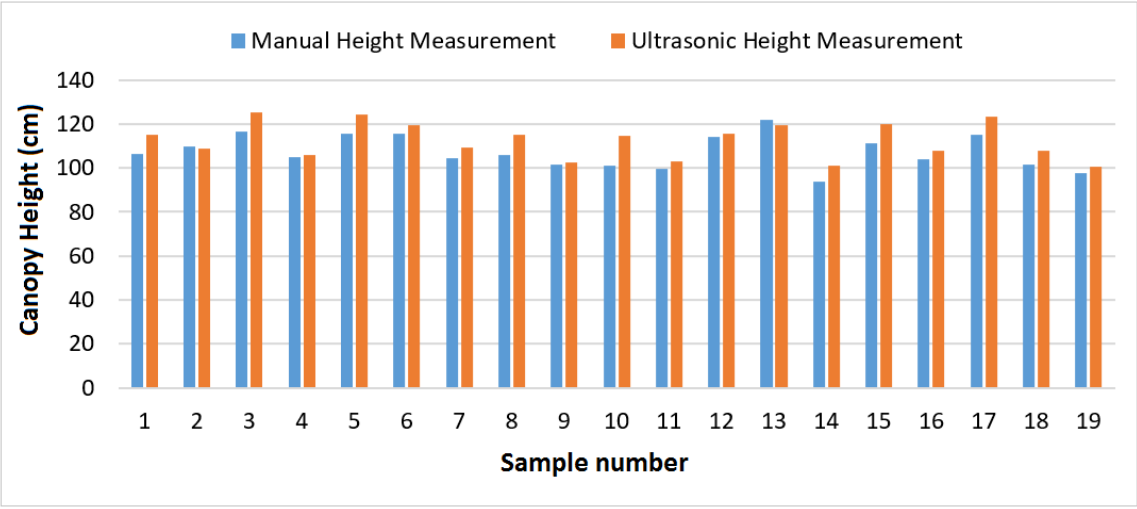

Figure 4-34: Comparison between manual and ultrasonic height measurements on July 18, 2017

Also Table 4-3 illustrates the detail of this experiment where column two represents the plot number, third and fourth columns represent manual and ultrasonic height measurements respectively and columns five and six give the impression of absolute and percent measurement errors.

Table 4-3: Coparison between manual and ultrasonic height measurement on July 18, 2017

R	Plot #	h_m (Manual Height in cm)	h_u (Ultrasonic Height in cm)	Diff= h_m - h_u (cm)	% diff $=\frac{Diff}{(hm+hu)/2}$
1	1.2	106.3	114.8	-8.5	-8%
2	1.3	109.7	108.5	1.1	1%
3	1.1	116.7	125.0	-8.3	-7%
4	1.17	104.7	105.8	-1.2	-1%
5	1.24	115.6	124.2	-8.6	-7%
6	1.29	115.7	119.2	-3.6	-3%
7	1.36	104.3	109.4	-5.1	-5%
8	1.44	105.7	115.3	-9.6	-9%
9	1.5	101.7	102.3	-0.6	-1%
10	1.62	101.0	114.6	-13.6	-13%
11	1.74	99.7	103.1	-3.5	-3%
12	2.2	114.0	115.7	-1.7	-1%
13	2.9	121.7	119.4	2.2	2%
14	2.24	93.7	101.1	-7.4	-8%
15	3.2	111.0	120.0	-8.9	-8%
16	3.8	104.0	108.0	-4.0	-4%
17	3.17	115.0	123.1	-8.1	-7%
18	3.29	101.3	107.9	-6.6	-6%
19	3.34	97.7	100.7	-3.0	-3%

As can be seen, the result of comparison between manual and ultrasonic height measurement is fairly promising as the difference between manual and ultrasonic height measurement methods ranges between -0.6 and -13.6. Also, the average percent error is only -5% and majority of percent errors are less than 7%, and the minimum error is reported to be only -1% for plot number 2.2.

In the same way, the verification experiment was repeated for a second day on August 2, 2017 for 41 random plots. The result of this experiment can be seen in next section.

4-5-4-2- Results based-on experiments on August 2, 2017

Table 4-4 illustrate the result of comparing manual and ultrasonic height measurements on August 2, 2017.

Table 4-4: Coparison between manual and ultrasonic height measurement on August 2, 2017

R	Plot #	h_m (Manual Height in cm)	h_u (Ultrasonic Height in cm)	Diff= h_m - h_u (cm)	% diff $=\frac{Diff}{(hm+hu)/2}$
1	1.11	116.0	105.1	10.9	10%
2	1.23	112.0	103.5	8.5	8%
3	1.17	114.0	95.0	19.0	18%
4	1.18	118.0	103.0	15.0	14%
5	1.27	122.0	103.4	18.6	16%
6	1.28	123.0	105.9	17.1	15%
7	1.3	125.0	102.5	22.5	20%
8	1.32	131.0	112.0	19.0	16%
9	1.33	123.0	109.9	13.2	11%
10	1.45	115.0	107.7	7.3	7%
11	1.75	122.0	105.3	16.7	15%
12	2.1	135.0	115.3	19.7	16%
13	2.2	123.0	113.2	9.8	8%
14	2.13	129.0	113.9	15.1	12%
15	2.31	122.0	113.2	8.8	8%
16	2.46	117.0	114.6	2.4	2%
17	2.53	118.0	112.7	5.3	5%
18	2.54	115.0	106.0	9.0	8%
19	2.57	109.0	111.1	-2.1	-2%
20	2.66	114.0	108.2	5.8	5%
21	2.7	102.0	107.8	-5.8	-6%
22	2.78	104.0	105.6	-1.6	-2%
23	2.79	119.0	112.7	6.3	5%
24	3.1	122.0	109.1	12.9	11%
25	3.11	123.0	105.4	17.6	15%
26	3.15	128.0	107.8	20.2	17%
27	3.18	127.0	108.4	18.6	16%
28	3.21	128.0	110.3	17.8	15%
29	3.24	119.0	108.4	10.6	9%
30	3.25	126.0	113.2	12.8	11%
31	3.27	127.0	110.8	16.2	14%
32	3.29	109.0	100.1	9.0	9%
33	3.32	117.0	101.3	15.7	14%
34	3.33	118.0	99.5	18.6	17%
35	3.37	117.0	98.9	18.1	17%
36	3.5	96.0	95.1	0.9	1%
37	3.57	111.0	98.6	12.4	12%
38	3.6	120.0	95.2	24.8	23%
39	3.66	119.0	101.0	18.0	16%
40	3.67	107.0	95.3	11.7	12%
41	3.72	115.0	107.2	7.8	7%

Also Figure 4-35 illustrates a bar graph to compare the result of manual and ultrasonic height measurement.

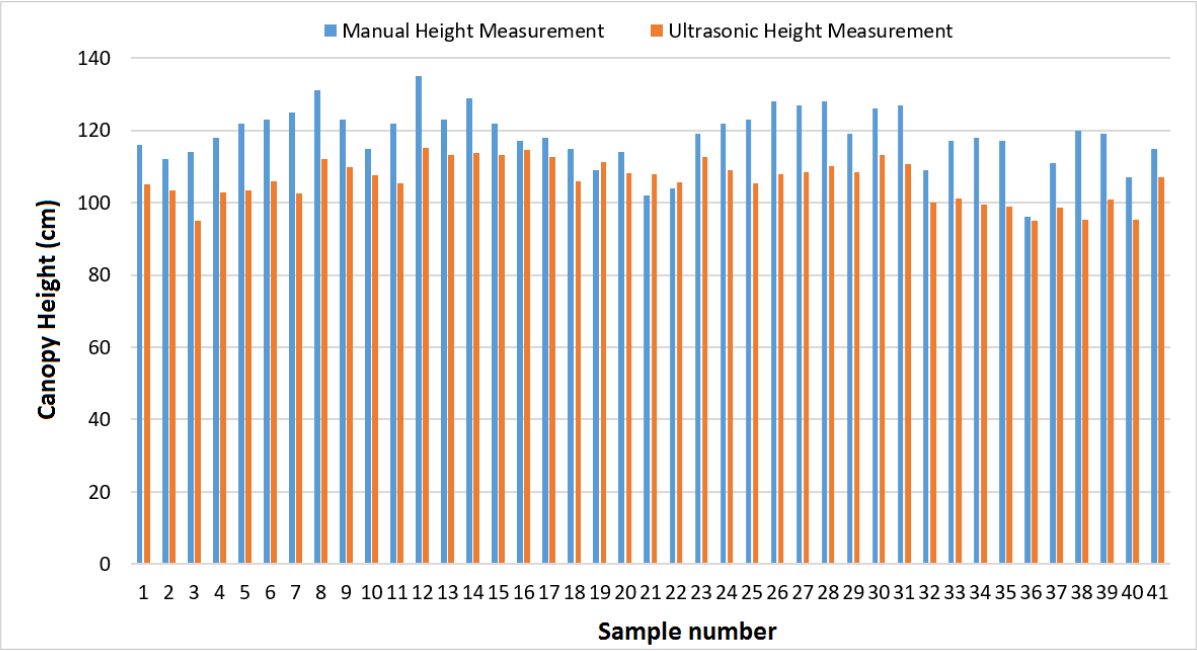

Figure 4-35: Comparison between manual and ultrasonic height measurements on August 2, 2017

As can be seen, the average percent error for this experiment was 11% which seems higher than the previous experiment. However, this amount of error for a height measurement system using a field-based mobile platform can be justified as there are some source of errors in height measurement of plants in the field configuration which will be discussed in next section. Moreover, the height values captured by manual measurement method appear to be consistently higher than the values given by ultrasonic sensors. The reason for this difference is the fact that labors were asked to pull the plants out when measuring the height. In other words, ultrasonic sensors could not recognize when plants were somewhat laid down due to the heavy seeds on top of the branches, and it appears there is no solution to solve this issue, unless using image processing algorithms to extract the stem angle.

4-5-4-3- Variation between manual and ultrasonic measurements

A number of promising conclusions can be drawn based on the results after examining the performance of the proposed field-based plant phenotyping platform for height measurement of a population connsisting of 252 canola cultivars.

First of all, unlike NDVI and temperature sensors which are height independent, the distance between tip of the ultrasonic sensors and the ground need to be relatively fixed. Otherwise, the accuracy of height measurement will be decreased. During the experiments, it was assumed that the groud where the platform was traveling is flat. This assumption was fairly acceptable as can be seen in Figure 4-36.

Figure 4-36: The traveling path of the HTP

Nevertheless, it was found that after a rainy day, some ups and downs could be seen on the ground which were challenging for the current height measurement system. However, as mentioned before in a field-based mobile platform, a measurement error of 5-10 % for height measurement is inevitable.

Also it was assumed that there is no significant vibration and displacement of the additional mechanical boom as a fixing frame to hold snsors. However, due to the vibration of the whole farm vehicle in driving mode, a slight amount of displacement of the mechanical boom could be seen during the data collection (displacements range was captured between 2cm and 10 cm).

To solve these two issues, it was found that an additional laser distance sensor can be exploited to continuously measure the distance between tip of the sensor and the bare ground. Then this distance can be incorporated to calculate height of the plants.

Secondly, as it was observed in laboratory tests, the ultrasonic sensor could accurately detect different objects which have sufficient surface area to reflect ultrasonic signals. Nevertheless, sensor was not able to detect thin substances, so an enough reflection area should be accessible withing the field of view of the sensor. Hence, an ultrasonic sensor can be highly effective to measure height of a plant provided that the plant is dense enough or has somewhat wide leaves. However, canola cultivars have many tiny branches when they are not in flower as can be seen in Figure 4-37. So if height measurement of canola cultivars is desired when they are not in flower, it is anticipated that a higher level of measurement error will be achieved.

Figure 4-37: Tiny branches which make height measurement problematic

The third source of error in height measurement of plants in field configuration, is unevenness of some plots. In other words, an average of some sample points can not be a true representative of these kind of plots. For example, Figure 4-38 illustrates an extremely uneven plot which was observed in studied canola nursery during summer 2017 experiments.

Figure 4-38: A sample uneven canopy (plot number 3.58)

In fact, height of a plant canopy represents the average of several sample points in different locations within a plot. For example, Figure 4-39 illustrates a sample plot (green rectangle) with nine sample points (red circles).

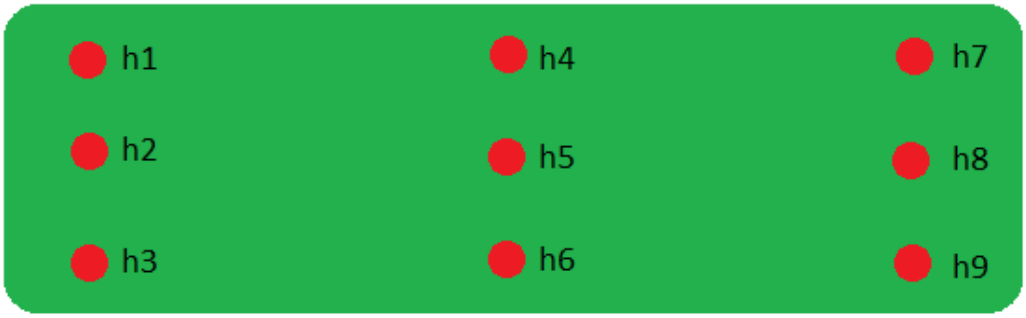

Figure 4-39: Height measurement of a plant canopy

So if a single number should be given as a representative of height of the mentioned plot, the average number can be calculate using Equation 4-3.

$$h_{Average} = \frac{\sum_{i=1}^{9} h_i}{9}$$ *Equation 4-3*

For the uneven plot number 3.58 which was shown in Figure 4-38, the resulting height values (unfiltered) given by ultrasonic sensors can be seen in Table 4-5.

Table 4-5: Ultrasonic height measurement for plot # 3.58 (Values in cm):

0	0	0	0	62.76	94.59	94.57	94.59	94.57	81.5	81.5	117	117	63.75
62.03	94.66	0	0	0	0	0	98.6	98.6	93.43	100.3	98.8	96.08	95.81
Average= **63.3** cm													

As can be seen, 28 sample points were captured for plot number 3.58 using four ultrasonic sensors which nine zero values can be observed amongst these numbers, and clearly this is due the fact that nearly half of the plot was covered by bare soil (or plant with height of zero). So if an average height value is needed for this plot, Equation 4-3 can be extended to calculate the average value which gives the value of 63.3 cm.

On the other hand, the three sample point values provided in Table 4-6 were manually captured by a human on August 2, 2017.

Table 4-6: Manual height measurement for plot # 3.58

1st value	2nd value	3rd value	Average
115 cm	99 cm	113 cm	**109 cm**

As can be seen, we cannot comprehend any unusual behavior or unevenness in the mentioned plot by merely having a look at these manual measurements. Subsequently in this case, if we compare the difference between manual and ultrasonic height measurements, the result will be unacceptable with a significant absolute error of 45.7 cm.

In this case, neither ulltrasonic sensors ,nor the person who conducted manual measurements could be blamed for this error. In fact, a plant height is a broad term, and the meaning of height of a plant canopy should be clearly defined for a human before conducting manual height measurement.

The last source of error observed in height measurement process was the significant variation in the surface of some plant canopies. In fact, apart from the occasional unevenness and unnoticeable tiny branches observed in some plots which was discussed in previsous paragraphs, the surface of some plots was remarkably bumpy. In other words, more than three or four rather different numbers could be remarked as the representative of the canopy heigh at different locations within the plot. So this is likely that a human and ultrasonic sensors observe the height from different point of views, and hence comparing the resulting numbers might give a missleading impression.

Figure 4-40 illustrates the histogram for the variation in manual height measurements in August 2, 2017. In fact, the difference between minimum and maximum values comprehended by a human for a single plot was calculated for 41 observations, and the mentioned histogram was drwan.

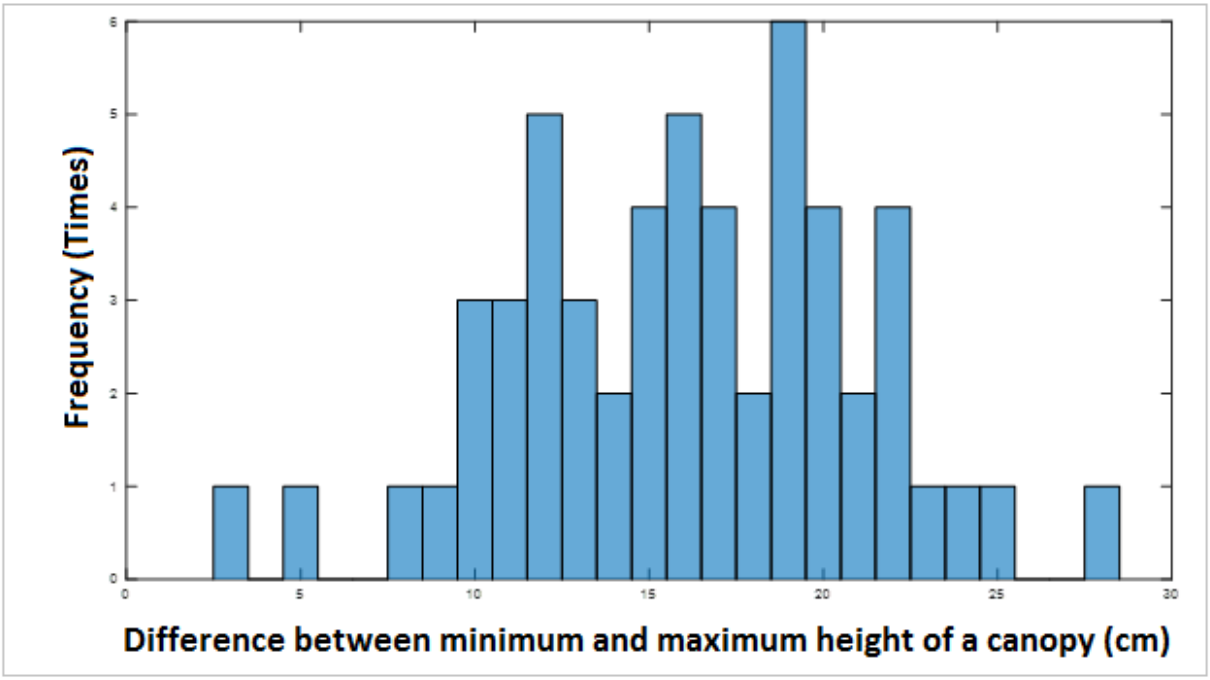

Figure 4-40: Histogram for the difference between minimum and maximum values manually captured for height of 55 different plots on August 2

As can be seen in Figure 4-40, for example the difference between minimum and maximum values manually captured by a human was 19cm for six different plots. Meanwhile, manual measurement recorded both 98cm and 111 cm for the plot number 1.17. So observing a wide-ranging numbers in ultrasonic measurements is also imaginable.

4-5-5- The quality of images captured by different cameras

As discussed in chapters two and three, not only a HD webcam was used to capture photographic data of plant canopies, but also the performance of DSLR cameras was examined to be used in a field-based plant phenotyping platform.

Figure 4-41 compares the quality of a) a webcam and b) a DSLR camera to capture photographic data of a similar plot. More examples can be accessed in Appendix D sections D10 and D11 for better comparisons of the quality of captured images in August 11 and August 18.

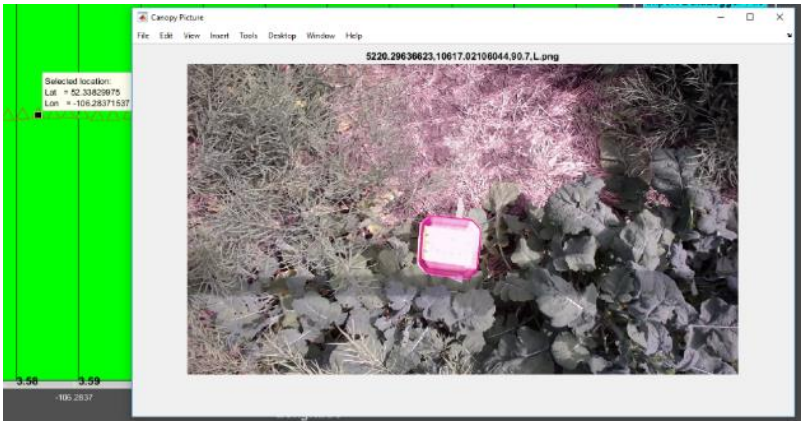

a)

b)

Figure 4-41: a) Webcam Image and b) Canon Image (File name: 5220.29636957,10617.01589084,L) (More examples can be accessed in Appendix D sections D10 and D11)

Figure 4-41-a is extracted using the developed visualization program. However, Figure 4-41-b is the image captured by DSLR camera and could not be associated with the corresponding plot (3.58). In fact, it was found that utilized software to communicate with DSLR cameras does not offer the flexibility of controlling all image acquisition steps. For example, as discussed in section 3-4-1 in chapter three, the main source of delay to synchronize GPS data with captured images for geo-referencing is the time consumed to save images after receiving the image frame. Unlike the exploited webcams which a novelty in the developed program offered the possibility of saving images in temporary memory during data collection to reduce the existing delays, the image saving process of DSLR camera could not be entirely controled.

So a remarkable amount of delay was inevitable to save every image during data collection, and hence associating an accurate geospatial data with the corresponding images was not possible to achieve a highly efficient image geo-referencing system.

Nevertheless, DSLR cameras provide a more in-depth photographic data for a plant. For example, as can be seen in Figure 4-41 the plot number (3.58) which was placed next to the plot to verify the geo-referencing algorithm cannot be seen in the image that was captured by webcam due to the intense sunshine. However, the number can be seen in the provided image by DSLR camera because of more advanced lenses and image enhancement algorithms in a DSLR camera.

So if more in-depth data is needed, a DSLR camera can be considered a better choice than a webcam by finding a solution to control all image acquisition steps to eliminate the existing delay. However, in proposed HTPP, photographic data was only used to verify geo-referencing performance and to give an overall intuition of the plot at the time data was collected.

4-6- Summary

To summarize, this chapter provided the results achieved after examining the performance of the developed field-based high-throughput plant phenotyping platform to study a canola nursery consisting of 252 canola plots during summer 2017. Indeed, after introducing the studied field conditions and parameters, the result of evaluating three different methods to create a local map for the field was discussed. It was shown that the optimal approach appears to be using interpolation and estimating the location of different plots in a field according to some known points. Then the result of experiments achieved after using the early generation of the developed HTPP in 2016 was briefly explained. It was discussed why a wireless camera could not meet the requirements for an efficient image acquisition system due to the occurring delay to synchronize GPS data with captured images to provide the possibility of future retrieval.

Most importantly, the result of nine times data collection in nine different days between June 23 and August 18 was explained in five individual sections. It was shown that how the accuracy of data geo-referencing algorithm was verified by exploiting some visible signs. Also, the growth of canola cultivars as a whole population consisting 252 plots as well as in plot level was investigated to clarify the usefulness of the developed HTPP. Particularly, the variation in a plant canopy NDVI, temperature and height during the growth season was explored, and the

provided information can be a resourceful database for plant scientist and breeders to investigate the correlation between different canola traits and the final yield. Moreover, a discussion about the existing challenges for a field-based height measurement trial, and the result of comparing the conducted manual height measurement and the values delivered by ultrasonic sensors was provided. At the end, the quality of captured images using the utilized HD webcams and DSLR cameras was compared, and it was shown that a HD webcam appears to be able to efficiently provide the required RGB images in the developed field-based mobile HTPP.

In the next chapter, conclusion and potential future works will be discussed to enhance the capabilities of the proposed field-based high-throughput plant phenotyping platform.

CHAPTER 5

CONCLUSIONS AND FUTURE WORKS

5-1- Conclusions

The primary objective of this research project was to develop a new mobile platform for field-based high-throughput plant phenotyping. Moreover, it was shown that the proposed plant phenotyping platform could be reliably utilized to phenotype canola cultivars (wheat or other plants with some minor design modification) with high repeatability and accuracy. In fact, canopy height, temperature, and NDVI as well as RGB images of 252 canola plots in a nursery located in Cargill Canada canola research center, were captured through nine field experiments between June-August 2017.

The development of this platform was started with a comprehensive literature review to find out about possible existing designs and their pros and cons. As anticipated, no similar work has been reported for high-throughput phenotyping of canola cultivars in field setting. Most of the existing studies in this area have been done in an indoor setting to explore a particular characteristic of a plant in a controlled condition, or ongoing (not completed) in field setting. Moreover, there are research works conducted to study a limited number of cultivars (such as wheat and cotton) in outdoor configuration with some restrictions. For example, none of the existing field-based plant phenotyping platforms appears to be able to capture RGB images of cultivars at the time of data collection. Additionally, development of a customized and open-end program for data visualization and analysis has not been reported in existing designs. Finally, the knowledge obtained from examination of similar works was extended to be able to develop the proposed platform to study 252 canola plant canopies through nine field experiments.

To gather more evidence about the efficiency of the selected equipment to be used in the developed prototype, a series of indoor tests were conducted at the robotics laboratory, Department of mechanical engineering, University of the Saskatchewan. In fact, the performance of an ultrasonic sensor to measure height of several objects with different shapes was examined. It was found that an ultrasonic sensor could effectively measure the height of different objects including the height of a plant with two considerations. Firstly, the object should be large enough

to reflect ultrasonic signals to achieve an accurate measurement. This means insignificant branches on top of a plant cannot be detected by an ultrasonic sensor, and the height of a plant has to be defined as the distance between the ground and a point on top of a canopy where an enough leaf area can be seen to reflect ultrasonic signals. Secondly, the distance between the tip of an ultrasonic sensor and the ground has to be relatively fixed if a repeatable and accurate height measurement is desired. Also, the performance of three different type of cameras including webcams, DSLR, and wireless cameras was examined to capture RGB images of plant canopies, and it was found that the webcam appears the optimum choice to be used in a field-based mobile phenotyping platform to capture RGB images of plants. The reasons for this verdict can be summarized as fast response time, adequate image quality, convenient data communication, the ability to operate without need of an external power supply, and finally lower cost of a webcam. In fact, it was found that the most time-consuming step in one image acquisition loop is saving an image, and a webcam was found the only camera which offers to be entirely controlled programmatically to minimize the existing delay in synchronization of captured images and GPS data to achieve an accurate geo-referencing algorithm.

After gathering adequate information and performance assessment of the selected equipment, a first generation of the platform with limited features was developed and tested in September 2016. The research was continued with the development of some new programs for data acquisition using a datalogger, autonomous image acquisition, and interactive data visualization. The capabilities of the system was expanded until a reliable version of the platform was developed, and field experiments were started in summer 2017. After conducting several field works to assemble the platform, nine databases in nine different days were collected consisting of plant height, temperature, NDVI and photographic information.

To verify the accuracy and reliability of the developed platform, several verification tests were conducted including comparing the manual height measurements with the height information provided by the ultrasonic sensors. Also, visible signs were used to verify the correctness and accuracy of the proposed data geo-referencing algorithm. As results persisted, the proposed field-based platform can be a reliable asset for breeders, who are in a critical need

to achieve an enriched yield, to precisely study a large-scale field in a short period by high-throughput phenotyping of their desired crop population.

By development of the proposed HTPP in this research, some new features are proposed for the first time which hasn't been offered before. Overall, the most important contributions for this research project can be summarized as below:

1. A new field-based mobile platform consisting of several programs and a measurement system was developed which can be an essential asset for breeders and others to semi-autonomously collect a high volume of data much faster than manual approach. Indeed, only 20 minutes was consumed to scan 252 canola plots using the developed platform (to capture height, temperature, NDVI, and RGB image), while if we assume 10 minutes is needed to manually scan one single plot, the process of data collection with HTP platform is roughly 125 times faster than manual measurement.
2. A Canola nursery comprised of 252 plant canopies was studied for the first time using the developed high-throughput plant phenotyping platform for the first time. Indeed, NDVI, temperature, height and RGB images of all canola plots were captured in nine different days and nine databases were created. Then some primary data analysis were done on the resulting databases to visualize the growth of different plots during the growth season (June – August). In other words, the continuous variation in NDVI, temperature and height of canola cultivars during the growth season were defined. The same approach can be used by breeders for more in-depth statistical analysis of the collected data to create the mathematical models of the data, to define the correlation between different traits, and ultimately to enrich their yield.
3. A modular stand-alone application with an interactive user interface was developed in MATLAB GUI to visualize all collected data/images and future data analysis for the first time in a field-based plant phenotyping platform. In other words, user can explore available data at different spots within a desired plot by clicking on a number of graphical objects drawn on a map. Also, the developed program summarizes all collected data with their corresponding plot number as a single excel file for an all-inclusive statistical analysis. Furthermore, the proposed program with an open-end architecture offers the

possibility of conveniently integrating other MATLAB toolboxes in the current version of the program for advanced data analysis. For example, image acquisition toolbox can be used to determine a plant canopy coverage using the captured images. More capabilities are enlisted as the potential future works in next section.

4. Autonomous image acquisition system was proposed for the first time in a field-based plant phenotyping platform. In other words, images were automatically captured and saved by associating the GPS data as the image name to provide the possibility of future access. None of the existing plant phenotyping platforms are equipped with an autonomous image acquisition feature.
5. The proposed plant phenotyping platform can collect a significant volume of data in a short period of time with minimum human observation because both data acquisition and image acquisition programs are being executed concurrently. Most of the existing plant phenotyping platforms either capture images as a separate process, or they do not offer image acquisition capability at all.
6. Utilized hardware and the developed program for data acquisition is highly flexible for adding more sensors and scanning equipment to the current system to capture more plant characteristics such as humidity, biomass or any other desired parameter.
7. A novel approach was proposed to create a map of a field when an accurate hand-held GPS unit is not accessible. In fact, two equations were derived to define the correlation between the longitude and latitude at two different locations on the earth, and the information captured by a single GPS antenna available on top of a farm vehicle was used to estimate the location of all plots in a field.

5-2- Potential Future Works

There are some possible works to be done as the next steps to improve the performance of the developed field-based plant phenotyping platform. Following are some suggestions in this regard:

1. **Using other MATLAB toolboxes for further analysis and modeling of the collected data and images**. The most important aspect of the proposed data visualization program is utilizing MATLAB as the main programming language to provide the possibility of exploiting a variety of existing toolboxes and functions for further data analysis. For example, image processing toolbox functions can be used to analyze captured images, or Neural Networks toolbox can be used to model phenotypic data or to forecast next year yield according to the available data. Also, a variety of existing functions in MATLAB statistics toolbox can be used for in-depth analysis of the phenotypic database.
2. **Adding more sensors to the current measurement system**. As mentioned earlier, the developed program for data acquisition is highly flexible for adding more 14 single-ended sensors or seven differential sensors and also two more RS232 devices to the system. This capability offers the possibility of capturing more plant characteristics such as humidity, biomass or any other desired trait, as well as environmental parameters such as ambient temperature, light intensity, and the wind speed.
3. **Using a laser distance sensor to continuously measure the distance between the boom and the ground.** As mentioned before, in the current design, the distance between the tip of the sensor and the ground had to be assumed as a relatively fixed number. Otherwise, the accuracy of height measurement will be decreased. If the ground is bumpy, a dedicated laser distance sensor can be attached to the two ends of the boom to continuously measure the distance between the tip of the sensor and the ground, and the measured distance can be incorporated into the height measurements to enhance the accuracy of height measurements.
4. **Adding two more cameras to capture more images of canopies.** In the current design, two cameras are dedicated to capture images of plant canopies from the top view. To obtain more photographic information, two more cameras can be added to the current

image acquisition system to capture images of canopies from the side view as can be seen in Figure 5-1. This enhancement can be a starting point for more advanced image processing, and gradually height of the canopies can be acquired using new images.

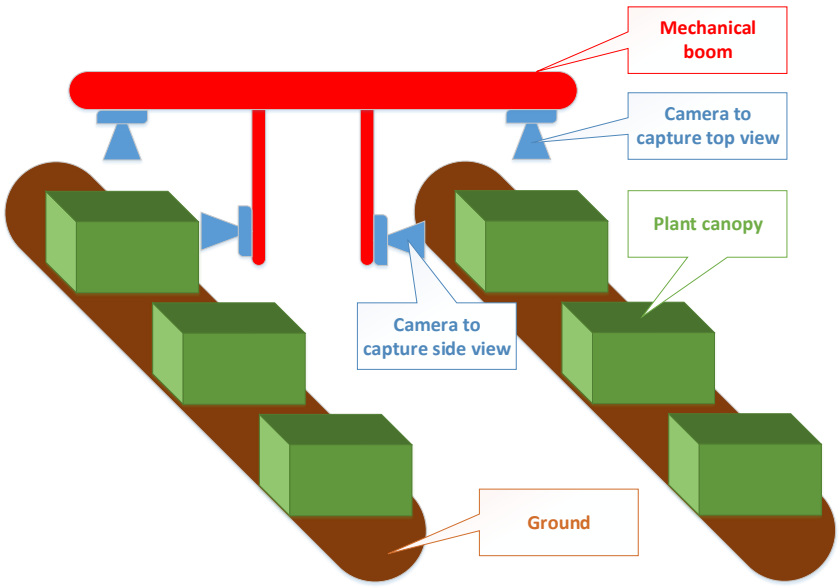

Figure 5-1: Adding two more cameras to capture canopy side view

5. **Conducting data collection in either morning or late afternoon to achieve a better image quality.** It was found that a better image quality can be achieved if data collection is conducted early in the morning or in the evening to eliminate the effect of intense sunshine at noon on the quality of captured images. In other words, intense sunshine at noon can negatively affect the brightness and contrast of an RGB image. However, some primary software filters can be applied on captured images to minimize this effect.
6. **Recording more environmental parameters at the day of data collection.** Recording as much information as possible about the field and environmental condition at the day of data collection such as the location of the sun in the sky, wind direction and the wetness of the ground can be valuable to find out any possible inconsistency in the collected data.

REFERENCES

[1] "United Nations Department of Economics and Social Affairs, Population Division," [Online]. Available: http://www.un.org/en/development/desa/population/.

[2] R. T. Furbank and M. Tester, "Phenomics – technologies to relieve the phenotyping bottleneck," *Trends in Plant Science,* vol. 16, no. 12, 2011.

[3] J. M. Montes, A. E. Melchinger and J. C. Reif, "Novel throughput phenotyping platforms in plant genetic studies," *Trends in Plant Science,* vol. 12, no. 10, pp. 433-436, 2007.

[4] J. N. Cobb, G. DeClerck, A. Greenberg, R. Clark and S. McCouch, "Next-generation phenotyping: requirements and strategies for enhancing our understanding of genotype–phenotype relationships and its relevance to crop improvement," *Theoretical and Applied Genetics,* vol. 126, no. 4, pp. 867-887, 2013.

[5] J. Barker III, N. Zhanga, J. Sharonb, R. Steevesb, X. Wangb, Y. Weia and J. Polandb, "Development of a field-based high-throughput mobile phenotyping platform," *Computers and Electronics in Agriculture,* vol. 122, p. 74–85, March 2016.

[6] [Online]. Available: http://www.ni.com/en-ca/shop/labview.html.

[7] P. Andrade-Sanchez, M. A. Gore and e. al., "Development and evaluation of a Field-Based high-throughput Phenotyping Platform," *Functional Plant Biology,* vol. 41, pp. 68-79, 2014.

[8] M. Gascon, M. Cirach and e. al., "Normalized difference vegetation index (NDVI) as a marker of surrounding greenness in epidemiological studies: The case of Barcelona city," *Urban Forestry & Urban Greening,* vol. 19, pp. 88-94, 2016.

[9] [Online]. Available: www.qgis.org.

[10] L. Busemeyer, D. Mentrup, K. Möller, E. Wunder, K. Alheit, V. Hahn and e. al., "BreedVision — A Multi-Sensor Platform for Non-Destructive Field-Based Phenotyping in Plant Breeding," *sensors,* vol. 13, no. 3, pp. 2830-2847, 2013.

[11] [Online]. Available: https://www.mysql.com/.

[12] [Online]. Available: http://www.navilock.de/produkte/G_60095/merkmale.html?setLanguage=en.

[13] G. Bai, Y. Ge, W. Hussain, P. Baenziger and G. Graef, "A multi-Sensor System for High Throughput Field Phenotyping In Soybean and Wheat Breeding," *Computer and Electronics in Agriculture,* vol. 128, pp. 181-192, 2016.

[14] J. W.White and M. M.Conley, "A Flexible, Low-Cost Cart for Proximal Sensing," *Crop Science,* vol. 53, no. 4, pp. 1646-1649, 2013.

[15] [Online]. Available: https://www.decagon.com/en/canopy/canopy-measurements/spectral-reflectance-sensor-srs/.

[16] A. Ruckelshausen, P. Biber, M. Dorna and e. al., "BoniRob: An autonomous field robot platform for individual plant phenotyping," in *7th European Conference on Precision Agriculture*, 2009.

[17] [Online]. Available: http://gazebosim.org/.

[18] K. D. Hansen, F. Garcia-Ruiz, W. Kazmi and e. al., "An Autonomous Robotic System for Mapping Weeds in Fields," in *2013 IFAC Intelligent Autonomous Vehicles Symposium*, 2013.

[19] L. Ma, M. Li and e. al., "A review of supervised object-based land-cover image classification," *ISPRS Journal of Photogrammetry and Remote Sensing,* vol. 130, p. 277–293, 2017.

[20] Y. Hu and S. Yang, "A knowledge based genetic algorithm for path planning of a mobile robot," in *IEEE International Conference on Robotics and Automation*, New Orleans, LA, USA, 2004.

[21] G. Barmeier and U. Schmidhalter, "High-Throughput Phenotyping of Wheat and Barley Plants Grown in Single or Few Rows in Small Plots Using Active and Passive Spectral Proximal Sensing," *Sensors,* vol. 16, no. 11, 2016.

[22] P. Rischbecka, E. and e. al., "Data fusion of spectral, thermal and canopy height parameters for improved yield prediction of drought stressed spring barley," *European Journal of Agronomy,* vol. 78, p. 44–59, 2016.

[23] T. Bak and H. Jakobsen, "Agricultural Robotic Platform with Four Wheel Steering for Weed Detection," *Biosystems Engineering,* vol. 87, no. 2, pp. 125-136, 2004.

[24] [Online]. Available: http://www.advantech.com/products/pc-104-modules/sub_1-2jklur.

[25] L. Haibo, D. Shuliang, L. Zunmin and Y. Chuijie, "Study and Experiment on a Wheat Precision Seeding Robot," *Journal of Robotics,* vol. 2015, 2015.

[26] H. Wang, Y. Lin, Z. Wang, Y. Yao, Y. Zhang and L. Wu, "Validation of a low-cost 2D laser scanner in development of a more affordable mobile terrestrial proximal sensing system for 3D plant structure phenotyping in indoor environment," *Computers and Electronics in Agriculture,* vol. 140, pp. 180-189, 2017.

[27] [Online]. Available: http://www.lemnatec.com.

[28] N. Fahlgren, M. Feldman and e. al., "A Versatile Phenotyping System and Analytics Platform Reveals Diverse Temporal Responses to Water Availability in Setaria," *Molecular Plant,* vol. 8, no. 10, pp. 1520-1535, 2015.

[29] [Online]. Available: https://www.danforthcenter.org/about/overviewandhistory.

[30] [Online]. Available: http://plantcv.danforthcenter.org/.

[31] [Online]. Available: http://www.lemnatec.com/products/#laboratory.

[32] Y. Ge, G. Bai, V. Stoerger and J. C.Schnable, "Temporal dynamics of maize plant growth, water use, and leaf water content using automated high throughput RGB and hyperspectral imaging," *Computers and Electronics in Agriculture,* vol. 127, pp. 625-632, 2016.

[33] N. Virlet, K. Sabermanesh, P. Sadeghi-Tehran and M. J. Hawkesford, "Field Scanalyzer: An automated robotic field phenotyping platform for detailed crop monitoring," *Functional Plant Biology ,* vol. 44, no. 1, pp. 143-153, 2016.

[34] P. Sadeghi-Tehran, K. Sabermanesh, N. Virlet and M. J. Hawkesford, "Automated Method to Determine Two Critical Growth Stages of Wheat: Heading and Flowering," *Frontiers in Plant Science,* vol. 8, 2017.

[35] A. Muscolo, A. unker, C. Klukas, K. Weigelt-Fischer, D. Riewe and T. Altmann, "Phenotypic and metabolic responses to drought and salinity of four contrasting lentil accessions," *Journal of Experimental Botany,* vol. 66, no. 18, pp. 5467-5480, 2015.

[36] [Online]. Available: https://phenospex.com/products/plant-phenotyping/science-planteye-3d-laser-scanner/.

[37] A. Comar, P. Burger, B. de Solan and e. al., "A semi-automatic system for high throughput phenotyping wheat cultivars in-field conditions: description and first results," *Functional Plant Biology,* vol. 39, no. 11, pp. 914-924, 2012.

[38] J. Svensgaard, T. Roitsch and S. Christensen, "Development of a Mobile Multispectral Imaging Platform for Precise Field Phenotyping," *Agronomy,* vol. 4, no. 3, pp. 322-336, 2014.

[39] J. Montes, F. Technow, B. Dhillon, F. Mauch and A. Melchinger, "High-throughput non-destructive biomass determination during early plant development in maize under field conditions," *Field Crops Research,* vol. 121, no. 2, pp. 268-273, 2011.

[40] J. L. Crain, Y. Wei and e. al., "Development and Deployment of a Portable Field Phenotyping Platform," *crop science,* vol. 56, pp. 965-975, 2016.

[41] D. Rundquist and e. al., "Elements of an Integrated Phenotyping System for Monitoring Crop Status at Canopy Level," *Agronomy,* vol. 4, pp. 108-123, 2014.

[42] [Online]. Available: http://oceanoptics.com/product/usb2000-custom/.

[43] S. Tisn, Y. Serrand, L. Bach and e. al., "Phenoscope: an automated large-scale phenotyping platform offering high spatial homogeneity," *The Plant Journal,* vol. 74, p. 534–544, 2013.

[44] K. A. Nagel, A. Putz and e. al., "GROWSCREEN-Rhizo is a novel phenotyping robot enabling simultaneous measurements of root and shoot growth for plants grown in soil-filled rhizotrons," *Functional Plant Biology,* vol. 39, p. 891–904, 2012.

APPENDIX A- Source Code for the Proposed Data Acquisition Program

This section provides the program developed for CR3000 datalogger to communicate with four ultrasonic sensors, two IR thermometers, two NDVI measurement units and a GPS for data geo-referencing. For a better understanding of this program, refer to the algorithm provided in Figure 3-1 of chapter 3. In fact, the beginning and the end of each block in Figure 3-2 is highlighted in the program below.

```
' Start of Block #1
Public DetectorTC_r, DetectorTK_r, TargetmV_r, m, b, TargetTK_r, TargetTC_r
Public DetectorTC_l, DetectorTK_l, TargetmV_l, TargetTK_l, TargetTC_l
Public USonic_1,USonic_2, USonic_3, USonic_4
Public USonic_1_off,USonic_2_off, USonic_3_off, USonic_4_off
Public GPSData As String * 1000
Public GPS_Data(12) As String *20
Public CC_R As String * 45
Public CC_L As String * 45
'End of Block #1. Start of Block #2
Public mC2 = 167167
Public mC1 = 19747600
Public mC0 = 3774800000
Public bC2 = 6261.61
Public bC1 = 38539.9
Public bC0 = -16067200
'End of Block #2. Start of Block #3
DataTable (July18,1,-1)
        DataInterval (0,250,mSec,10)
  'Sample(1,USonic_1_off,FP2)
        'Sample(1,USonic_2_off,FP2)
        'Sample(1,USonic_3_off,FP2)
        'Sample(1,USonic_4_off,FP2)
        Average(1,TargetTC_r,IEEE4,False)
        Average(1,TargetTC_l,IEEE4,False)
        Sample(1,CC_R,String)
        Sample(1,CC_L,String)
        Sample(1,GPSData,String)
```

```
        Sample(1,USonic_1,FP2)
        Sample(1,USonic_2,FP2)
        Sample(1,USonic_3,FP2)
        Sample(1,USonic_4,FP2)
        'Average(1,DetectorTC_r,IEEE4,False)
        'Average(1,DetectorTC_l,IEEE4,False)
        'Average(1,TargetmV_r,IEEE4,False)
  'Average(1,TargetmV_l,IEEE4,False)
EndTable
'End of Block #3
BeginProg
'Start of Block #4
   SerialOpen (Com3,38400,0,0,100)'GPS
   SerialOpen (Com1,38400,0,0,50)'CCR
   SerialOpen (Com2,38400,0,0,50)'CCL
   SerialFlush (Com1)
   SerialFlush (Com2)
   SerialFlush (Com3)
'End of Block #4
  Scan(250,mSec,0,0)
'Start of Block #5
        SerialIn (CC_R,Com1,1,0,45)
        SerialIn (CC_L,Com2,1,0,45)
  'End of Block #5. Start if Block #6
        VoltDiff(USonic_1_off,1,mV5000,1,false,100,250,1.0,0)
        VoltDiff(USonic_2_off,1,mV5000,2,false,100,250,1.0,0)
        VoltDiff(USonic_3_off,1,mV5000,4,false,100,250,1.0,0)
        VoltDiff(USonic_4_off,1,mV5000,3,false,100,250,1.0,0)
        USonic_1=(0.0949)*(USonic_1_off)-40.686
        USonic_2=(0.0928)*(USonic_2_off)-39.454
        USonic_3=(0.0866)*(USonic_3_off)-36.59
        USonic_4=(0.0848)*(USonic_4_off)-35.551
'End of Block #6. Start of Block #7. Read Thermometers value
        Therm109(DetectorTC_r,1,9,Vx1,0,_60Hz,1.0,0)
        VoltDiff(TargetmV_r,1,mV20,6,True,0,_60Hz,1.0,0)
```

```
        m = mC2 * DetectorTC_r^2 + mC1 * DetectorTC_r + mC0
        b = bC2 * DetectorTC_r^2 + bC1 * DetectorTC_r + bC0
        DetectorTK_r = DetectorTC_r + 273.15
        TargetTK_r = ((DetectorTK_r^4) + m * TargetmV_r + b)^0.25
        TargetTC_r = TargetTK_r - 273.15
            Therm109(DetectorTC_l,1,10,Vx2,0,_60Hz,1.0,0)
            VoltDiff(TargetmV_l,1,mV20,7,True,0,_60Hz,1.0,0)
            m = mC2 * DetectorTC_l^2 + mC1 * DetectorTC_l + mC0
            b = bC2 * DetectorTC_l^2 + bC1 * DetectorTC_l + bC0
            DetectorTK_l = DetectorTC_l + 273.15
            TargetTK_l = ((DetectorTK_l^4) + m * TargetmV_l + b)^0.25
            TargetTC_l = TargetTK_l - 273.15
'End of Block #7. Start of Block #8.
        SerialIn (GPSData,Com3,1,0,100)
'End of Block #8. Start of Block #9.
            CallTable July18
'End of Block #9
            SerialFlush (Com1)
        SerialFlush (Com2)
        SerialFlush (Com3)
    NextScan
EndProg
```

APPENDIX B- Source Code for the Proposed Image Acquisition Program

This section provides the program developed for autonomously capturing RGB images of plant canopies while the phenotyping platform was traversing throughout the field. In fact, two webcams and a GPS was used for image geo-referencing. For a better understanding of this program, refer to the algorithm provided in Figure 3-10 of chapter 3. In fact, the beginning and the end of each block in Figure 3-10 is highlighted in the program below.

```
Dlay=get(handles.edit7,'string');
DDlay=str2num(Dlay);
%% Start of Block #1
if (get(handles.tglcam,'Value') == 1)
   camr=webcam(1);
   caml=webcam(3);
   else
   camr=webcam(3);
   caml=webcam(1);
end
camr.Resolution='1280x720';
caml.Resolution='1280x720';
comnum=get(handles.edit3,'string');
BRate=get(handles.edit6,'string');
BBRate=str2num(BRate);
global s
s=serial(comnum,'BaudRate',BBRate);
fopen(s);
cntr=0;
cntl=0;
camr_img=cell(2500,1);
caml_img=cell(2500,1);
nme_img=cell(2500,1);
 %% End of Block #1. Start of Block #2
for loop_cnt=1:inf
            flushinput(s);
            raw=fscanf(s);
            sz=size(raw);
```

```
            iml=0;
            imr=0;
            if ~isempty(raw) && sz(2)<90 && sz(2)>65
                nme_img{loop_cnt,1}=raw;
            %End of Block #2. Start of Block #3
                iml=snapshot(caml);
              if ~isempty(iml)
              caml_img{loop_cnt}=iml;
              cntl=cntl+1;
              set(handles.cntl,'String',num2str(cntl));
              end
                imr=snapshot(camr);
             if ~isempty(imr)
              camr_img{loop_cnt}= imr;
              cntr=cntr+1;
              set(handles.cntr,'String',num2str(cntr));
             end
           end
           %End of Block #3. Start of Block #4
           pause(DDlay);
           %End of Block #4. Start of Block #5
             if (get(handles.tglloop,'Value') == 1)
                 fclose(s);
                 delete(s)
                 break
              end
            set(handles.stat,'String','In Capturing Loop');
             %End of Block #5
end
 emptyCells_nme = cellfun('isempty', nme_img);
emptyCells_r = cellfun('isempty', nme_img);
emptyCells_l = cellfun('isempty', nme_img);
nme_img(emptyCells_nme) = [];
camr_img(emptyCells_r) = [];
caml_img(emptyCells_l) = [];
```

```
handles.nme_img=nme_img;
handles.camr_img=camr_img;
handles.caml_img=caml_img;
guidata(hObject, handles);
set(handles.stat,'String','Images Are ready To Be Saved. Press save Button Now');
function pushbutton15_Callback(hObject, eventdata, handles)
msgbox('Please wait, images are being saved. This might take few Minutes!')
set(handles.stat,'String','Please wait, images are being saved. This might take few Minutes!');
handles=guidata(hObject);
%Start of Block #8
nme_img=handles.nme_img;
camr_img=handles.camr_img;
caml_img=handles.caml_img;
cntrr=0;
cntll=0;
 camr_sizee=size(camr_img);
caml_sizee=size(caml_img);
nme_sizee=size( nme_img);
 %%End of Block #8. Start of Block #9
if camr_sizee(1)==caml_sizee(1)
   if camr_sizee(1)==nme_sizee(1)
      for i=1:nme_sizee(1)
         [d1 d2 d3 d4 d5 d6 d7 d8 d9 d10 d11 d12 d13 d14 d15]=strread(nme_img{i},'%s %s %s %s %s %s %s %s %s %s
%s %s %s %s %s','delimiter',',');
            tm=size(cell2mat(d1));
            if tm(2)==6
               if cell2mat(d1)=='$GPRMC'
               d4=cell2mat(d4);
               d6=cell2mat(d6);
               d9=cell2mat(d9);
               name_r=sprintf('%s,%s,%s,R.png',d4,d6,d9);
               name_l=sprintf('%s,%s,%s,L.png',d4,d6,d9);
               end
            end
%End of Block #9. Start of Block #10
```

```
        if ~isempty(camr_img{i})
           imwrite(camr_img{i},name_r);
           cntrr=cntrr+1;
           set(handles.rsave,'String',num2str(cntrr));
        end
         if ~isempty(caml_img{i})
           imwrite(caml_img{i},name_l);
           cntll=cntll+1;
           set(handles.lsave,'String',num2str(cntll));
         end
      end
  end
end
%End of Block #10
set(handles.stat,'String','Images are Saved');
msgbox('Images are Saved! Now you can exit the software')
```

APPENDIX C- Source Code for the Proposed Data Visualization Program

This section provides the program developed for visualization of the collected data and images by proposed field-based high-throughput plant phenotyping platform. Because this program consists of several functions for different purposes as was explained in section 3-4 of chapter three, it was tried to break down the whole program into some smaller programs for better understanding.

The following function was developed to draw a map for 252 plots in the studied field. For better understanding of this program, refer to the algorithm provided in Figure 3-16 in chapter three.

```
%Start Block #1
PathName=pwd;
FileName='\FieldMap.csv';
myfile=strcat(PathName,FileName);
if exist('FieldMap.csv','file')
    Plot_Center_Raw = xlsread(myfile);
    else
    [FileName,PathName] = uigetfile({'*.csv';'*.xlsx';'*.xls'},'Unable to find the FieldMap.csv, Please Select the File');
    myfile=strcat(PathName,FileName);
    Plot_Center_Raw = xlsread(myfile);
end
%End Block #1. Start Block#2.
Plot_Center_lat_DD_1=Plot_Center_Raw(:,1);
Plot_Center_lon_DD_1=Plot_Center_Raw(:,2);
Plot_Center_lat_DD_2=Plot_Center_Raw(:,3);
Plot_Center_lon_DD_2=Plot_Center_Raw(:,4);
Plot_Center_lat_DD_3=Plot_Center_Raw(:,5);
Plot_Center_lon_DD_3=Plot_Center_Raw(:,6);
 NR=size(Plot_Center_lat_DD_1);
ss=size(Plot_Center_lon_DD_1);
hold on
%% End Block #2. Start Block #3
%Refer to the figure that shows the location of each sensor and GPS to define following numbers
gps_boom.d1=3.048;
```

```
gps_boom.d2=3.048;
gps_boom.d3=2.1082;
gps_boom.d4=2.1082;
gps_boom.d5=0.254;
gps_boom.d10=0.254;
gps_boom.d6=1.016;
gps_boom.d9=1.016;
gps_boom.d7=0.29464;
gps_boom.d8=0.29464;
gps_boom.th4=atan(gps_boom.d8/gps_boom.d4);
gps_boom.th3=atan((gps_boom.d8+gps_boom.d9)/gps_boom.d4)-gps_boom.th4;
gps_boom.th2=atan((gps_boom.d8+gps_boom.d9+gps_boom.d10)/gps_boom.d4)-gps_boom.th3-gps_boom.th4;
gps_boom.th1=(pi/2)-gps_boom.th2-gps_boom.th3-gps_boom.th4;
gps_boom.th5=atan(gps_boom.d7/gps_boom.d3);
gps_boom.th6=atan((gps_boom.d7+gps_boom.d6)/gps_boom.d3)-gps_boom.th5;
gps_boom.th7=atan((gps_boom.d7+gps_boom.d6+gps_boom.d5)/gps_boom.d3)-gps_boom.th5-gps_boom.th6;
gps_boom.th8=(pi/2)-gps_boom.th5-gps_boom.th6-gps_boom.th7;
gps_boom.l1=(gps_boom.d8+gps_boom.d9+gps_boom.d10)/(sin(gps_boom.th2+gps_boom.th3+gps_boom.th4));
gps_boom.l2=(gps_boom.d8+gps_boom.d9)/(sin(gps_boom.th3+gps_boom.th4));
gps_boom.l3=gps_boom.d8/(sin(gps_boom.th4));
gps_boom.l4=gps_boom.d7/(sin(gps_boom.th5));
gps_boom.l5=(gps_boom.d6+gps_boom.d7)/(sin(gps_boom.th5+gps_boom.th6));
gps_boom.l6=(gps_boom.d5+gps_boom.d6+gps_boom.d7)/(sin(gps_boom.th5+gps_boom.th6+gps_boom.th7));
gps_boom.th1=rad2deg(gps_boom.th1);
gps_boom.th8=rad2deg(gps_boom.th8);
gps_boom.th2=rad2deg(gps_boom.th2);
gps_boom.th7=rad2deg(gps_boom.th7);
gps_boom.th3=rad2deg(gps_boom.th3);
gps_boom.th6=rad2deg(gps_boom.th6);
gps_boom.th4=rad2deg(gps_boom.th4);
gps_boom.th5=rad2deg(gps_boom.th5);
%% End of Block #3. Start of Block #4.
plott.l=6;      %This is length of one plot
plott.h=1.82; % This is width of one plot
Plot_lat_DD_A_1=zeros(ss(1),1);
```

```
Plot_lon_DD_A_1=zeros(ss(1),1);
Plot_lat_DD_B_1=zeros(ss(1),1);
Plot_lon_DD_B_1=zeros(ss(1),1);
Plot_lat_DD_C_1=zeros(ss(1),1);
Plot_lon_DD_C_1=zeros(ss(1),1);
Plot_lat_DD_D_1=zeros(ss(1),1);
Plot_lon_DD_D_1=zeros(ss(1),1);
Plot_lat_DD_A_2=zeros(ss(1),1);
Plot_lon_DD_A_2=zeros(ss(1),1);
Plot_lat_DD_B_2=zeros(ss(1),1);
Plot_lon_DD_B_2=zeros(ss(1),1);
Plot_lat_DD_C_2=zeros(ss(1),1);
Plot_lon_DD_C_2=zeros(ss(1),1);
Plot_lat_DD_D_2=zeros(ss(1),1);
Plot_lon_DD_D_2=zeros(ss(1),1);
Plot_lat_DD_A_3=zeros(ss(1),1);
Plot_lon_DD_A_3=zeros(ss(1),1);
Plot_lat_DD_B_3=zeros(ss(1),1);
Plot_lon_DD_B_3=zeros(ss(1),1);
Plot_lat_DD_C_3=zeros(ss(1),1);
Plot_lon_DD_C_3=zeros(ss(1),1);
Plot_lat_DD_D_3=zeros(ss(1),1);
Plot_lon_DD_D_3=zeros(ss(1),1);
 for cnt=1:ss(1)
   [temp1,temp2]=Boom(Plot_Center_lat_DD_1(cnt),Plot_Center_lon_DD_1(cnt),plott.l/2,(180));
   [Plot_Center_lat_DD_1_A(cnt),Plot_Center_lon_DD_1_A(cnt)]=Boom(temp1,temp2,plott.h/2,(270));
   [Plot_Center_lat_DD_1_B(cnt),Plot_Center_lon_DD_1_B(cnt)]=Boom(temp1,temp2,plott.h/2,(90));
   [temp3,temp4]=Boom(Plot_Center_lat_DD_1(cnt),Plot_Center_lon_DD_1(cnt),plott.l/2,(0));
   [Plot_Center_lat_DD_1_C(cnt),Plot_Center_lon_DD_1_C(cnt)]=Boom(temp3,temp4,plott.h/2,(90));
   [Plot_Center_lat_DD_1_D(cnt),Plot_Center_lon_DD_1_D(cnt)]=Boom(temp3,temp4,plott.h/2,(270));
    [temp1,temp2]=Boom(Plot_Center_lat_DD_2(cnt),Plot_Center_lon_DD_2(cnt),plott.l/2,(180));
   [Plot_Center_lat_DD_2_A(cnt),Plot_Center_lon_DD_2_A(cnt)]=Boom(temp1,temp2,plott.h/2,(270));
   [Plot_Center_lat_DD_2_B(cnt),Plot_Center_lon_DD_2_B(cnt)]=Boom(temp1,temp2,plott.h/2,(90));
   [temp3,temp4]=Boom(Plot_Center_lat_DD_2(cnt),Plot_Center_lon_DD_2(cnt),plott.l/2,(0));
   [Plot_Center_lat_DD_2_C(cnt),Plot_Center_lon_DD_2_C(cnt)]=Boom(temp3,temp4,plott.h/2,(90));
```

```
   [Plot_Center_lat_DD_2_D(cnt),Plot_Center_lon_DD_2_D(cnt)]=Boom(temp3,temp4,plott.h/2,(270));
    [temp1,temp2]=Boom(Plot_Center_lat_DD_3(cnt),Plot_Center_lon_DD_3(cnt),plott.l/2,(180));
   [Plot_Center_lat_DD_3_A(cnt),Plot_Center_lon_DD_3_A(cnt)]=Boom(temp1,temp2,plott.h/2,(270));
   [Plot_Center_lat_DD_3_B(cnt),Plot_Center_lon_DD_3_B(cnt)]=Boom(temp1,temp2,plott.h/2,(90));
   [temp3,temp4]=Boom(Plot_Center_lat_DD_3(cnt),Plot_Center_lon_DD_3(cnt),plott.l/2,(0));
   [Plot_Center_lat_DD_3_C(cnt),Plot_Center_lon_DD_3_C(cnt)]=Boom(temp3,temp4,plott.h/2,(90));
   [Plot_Center_lat_DD_3_D(cnt),Plot_Center_lon_DD_3_D(cnt)]=Boom(temp3,temp4,plott.h/2,(270));
end
%% End of Block #4. Start of Block #5.
lon_1=[Plot_Center_lon_DD_1_A' Plot_Center_lon_DD_1_B' Plot_Center_lon_DD_1_C' Plot_Center_lon_DD_1_D'];
lat_1=[Plot_Center_lat_DD_1_A' Plot_Center_lat_DD_1_B' Plot_Center_lat_DD_1_C' Plot_Center_lat_DD_1_D'];

lon_2=[Plot_Center_lon_DD_2_A' Plot_Center_lon_DD_2_B' Plot_Center_lon_DD_2_C' Plot_Center_lon_DD_2_D'];
lat_2=[Plot_Center_lat_DD_2_A' Plot_Center_lat_DD_2_B' Plot_Center_lat_DD_2_C' Plot_Center_lat_DD_2_D'];
lon_3=[Plot_Center_lon_DD_3_A' Plot_Center_lon_DD_3_B' Plot_Center_lon_DD_3_C' Plot_Center_lon_DD_3_D'];
lat_3=[Plot_Center_lat_DD_3_A' Plot_Center_lat_DD_3_B' Plot_Center_lat_DD_3_C' Plot_Center_lat_DD_3_D'];
 tmp=size(lon_1);
 %% End of Block #5. Start of Block #6
for i=1:tmp(1)
    patch(lon_1(i,:),lat_1(i,:),'g')
    patch(lon_2(i,:),lat_2(i,:),'g')
    patch(lon_3(i,:),lat_3(i,:),'g')
    hold on
end
%% End of Block #6. Start of Block #7
 patch(lon_1(39,:),lat_1(39,:),[100, 30, 22]./255)
 hold on
 patch(lon_1(40,:),lat_1(40,:),[100, 30, 22]./255)
 hold on
 patch(lon_1(79,:),lat_1(79,:),[100, 30, 22]./255)
 hold on
 patch(lon_1(80,:),lat_1(80,:),[100, 30, 22]./255)
 hold on
  patch(lon_2(39,:),lat_2(39,:),[100, 30, 22]./255)
 hold on
```

```
patch(lon_2(40,:),lat_2(40,:),[100, 30, 22]./255)
hold on
patch(lon_2(79,:),lat_2(79,:),[100, 30, 22]./255)
hold on
patch(lon_2(80,:),lat_2(80,:),[100, 30, 22]./255)
hold on
patch(lon_3(39,:),lat_3(39,:),[100, 30, 22]./255)
hold on
patch(lon_3(40,:),lat_3(40,:),[100, 30, 22]./255)
hold on
patch(lon_3(79,:),lat_3(79,:),[100, 30, 22]./255)
hold on
patch(lon_3(80,:),lat_3(80,:),[100, 30, 22]./255)
hold on
%% End of Block #7. Start of Block #8
for t=1:38
   nm=sprintf('1.%d',t) ;
text(lon_1(t,1),lat_1(t,1),nm,'FontWeight','bold','FontSize',13)
end
for t=41:78
   nm=sprintf('1.%d',t+2) ;
text(lon_1(t,1),lat_1(t,1),nm,'FontWeight','bold','FontSize',13)
end
for t=81:88
   tt=t-80;
   nm=sprintf('1.%d',tt) ;
text(lon_1(t,1),lat_1(t,1),nm,'FontWeight','bold','FontSize',13)
end
 for t=1:38
   nm=sprintf('2.%d',t) ;
text(lon_2(t,1),lat_2(t,1),nm,'FontWeight','bold','FontSize',13)
end
for t=41:78
   nm=sprintf('2.%d',t+2) ;
text(lon_2(t,1),lat_2(t,1),nm,'FontWeight','bold','FontSize',13)
```

```
end
for t=81:88
   tt=t-80;
   nm=sprintf('2.%d',tt) ;
text(lon_2(t,1),lat_2(t,1),nm,'FontWeight','bold','FontSize',13)
end
 for t=1:38
   nm=sprintf('3.%d',t) ;
text(lon_3(t,1),lat_3(t,1),nm,'FontWeight','bold','FontSize',13)
end
for t=41:78
   nm=sprintf('3.%d',t+2) ;
text(lon_3(t,1),lat_3(t,1),nm,'FontWeight','bold','FontSize',13)
end
for t=81:88
   tt=t-80;
   nm=sprintf('3.%d',tt) ;
text(lon_3(t,1),lat_3(t,1),nm,'FontWeight','bold','FontSize',13)
end
 xlabel('Longitude','fontweight','bold','FontAngle', 'italic','FontSize',16,'Color',[0 1 0.8])
ylabel('Latitude','fontweight','bold','FontAngle', 'italic','FontSize',16,'Color',[0 1 0.8])
set(gca,'xcolor','w')
set(gca,'ycolor','w')

%% End of Block #8. Start of Block #9
 recLon_1=[Plot_Center_lon_DD_1_A
           Plot_Center_lon_DD_1_B
           Plot_Center_lon_DD_1_C
           Plot_Center_lon_DD_1_D];
  recLon_2=[Plot_Center_lon_DD_2_A
           Plot_Center_lon_DD_2_B
           Plot_Center_lon_DD_2_C
           Plot_Center_lon_DD_2_D];
   recLon_3=[Plot_Center_lon_DD_3_A
           Plot_Center_lon_DD_3_B
```

```
            Plot_Center_lon_DD_3_C
            Plot_Center_lon_DD_3_D];
recLon=[ recLon_1  recLon_2  recLon_3];
 recLat_1=[Plot_Center_lat_DD_1_A
            Plot_Center_lat_DD_1_B
            Plot_Center_lat_DD_1_C
            Plot_Center_lat_DD_1_D];
  recLat_2=[Plot_Center_lat_DD_2_A
            Plot_Center_lat_DD_2_B
            Plot_Center_lat_DD_2_C
            Plot_Center_lat_DD_2_D];
   recLat_3=[Plot_Center_lat_DD_3_A
            Plot_Center_lat_DD_3_B
            Plot_Center_lat_DD_3_C
            Plot_Center_lat_DD_3_D];
recLat=[ recLat_1  recLat_2  recLat_3];
```

At this point a 252 green rectangles are drawn which are the representatives of the location of individual plots in the studied field. The next function is developed to read the phenotypic data file, and to visualize them as some graphical objects. For better understanding of this program, refer to the Figure 3-21 in chapter four.

```
%Start of Block #1
[FileName,PathName] = uigetfile({'*.xlsx';'*.xls'},'Select Collected Data File');
myfile=strcat(PathName,FileName);
[num,txt,Data_Raw]= xlsread(myfile);
s=size(Data_Raw(:,7));
%%End of Block #1. Start of Block #2
for cn=1:s(1)
 gps_raw_temp=strtok(Data_Raw(cn,7),'$');
 gps_temp=size(char(gps_raw_temp));
   if gps_temp(2)>74 &&gps_temp(2)<78
   GPS_Raw(cn,:)=gps_raw_temp;
   T_R(cn,:)=Data_Raw(cn,3);
   T_L(cn,:)=Data_Raw(cn,4);
   CC_R_Raw(cn,:)=Data_Raw(cn,5);
```

```
   CC_L_Raw(cn,:)=Data_Raw(cn,6);
   end
end
%%
%End of Block #2. Start of Block #3
GPS_Raw=GPS_Raw(~cellfun('isempty',GPS_Raw)) ;
T_R=T_R(~cellfun('isempty',T_R)) ;
T_L=T_L(~cellfun('isempty',T_L)) ;
CC_R_Raw=CC_R_Raw(~cellfun('isempty',CC_R_Raw)) ;
CC_L_Raw=CC_L_Raw(~cellfun('isempty',CC_L_Raw)) ;
 a=cellfun('length',CC_R_Raw);
b=cellfun('length',CC_L_Raw);
 ss=size(CC_R_Raw);
 for cnn=1:ss(1)
    if   a(cnn)<28 ||a(cnn)>32
   CC_R_Raw{cnn}=  'nan';
   end
    if   b(cnn)<28 ||b(cnn)>32
   CC_L_Raw{cnn}=  'nan';
   end
end
sz=size(GPS_Raw);
GPS_S=char(GPS_Raw);
CCR_S=char(CC_R_Raw);
CCL_S=char(CC_L_Raw);
 %End of Block #3. Start of Block #4
 GPS1=cell(sz(1),1);
GPS2=cell(sz(1),1);
GPS3=cell(sz(1),1);
GPS4=cell(sz(1),1);
GPS5=cell(sz(1),1);
GPS6=cell(sz(1),1);
GPS7=cell(sz(1),1);
GPS8=cell(sz(1),1);
GPS9=cell(sz(1),1);
```

```
GPS10=cell(sz(1),1);
GPS11=cell(sz(1),1);
GPS12=cell(sz(1),1);
for cnt=1:sz(1)
   [GPS1(cnt,:) GPS2(cnt,:) GPS3(cnt,:) GPS4(cnt,:) GPS5(cnt,:) GPS6(cnt,:) GPS7(cnt,:) GPS8(cnt,:) GPS9(cnt,:)
   GPS10(cnt,:) GPS11(cnt,:) GPS12(cnt,:)]=strread(GPS_S(cnt,:),'%s %s %s %s %s %s %s %s %s %s %s
   %s','delimiter',',');
   %End of Block #4. Start of Block #5
   if CCR_S(cnt)~='n'
   [CCR1(cnt,:) CCR2(cnt,:) CCR3(cnt,:) CCR4(cnt,:) CCR5(cnt,:)]=strread(CCR_S(cnt,:),'%s %s %s %s %s','delimiter',',');
   end
    if CCL_S(cnt)~='n'
   [CCL1(cnt,:) CCL2(cnt,:) CCL3(cnt,:) CCL4(cnt,:) CCL5(cnt,:)]=strread(CCL_S(cnt,:),'%s %s %s %s %s','delimiter',',');
   end
 end
%%End of Block #5. Start of Block #6
GPS4_D=str2double(GPS4);
GPS6_D=str2double(GPS6);
GPS8_D=str2double(GPS8);
GPS9_D=str2double(GPS9);
GPS=[GPS4_D GPS6_D GPS8_D GPS9_D];
CCR1_D=str2double(CCR1);
CCR2_D=str2double(CCR2);
CCR3_D=str2double(CCR3);
CCR4_D=str2double(CCR4);
CCR5_D=str2double(CCR5);
CCL1_D=str2double(CCL1);
CCL2_D=str2double(CCL2);
CCL3_D=str2double(CCL3);
CCL4_D=str2double(CCL4);
CCL5_D=str2double(CCL5);
%% End of Block #6. Start of Block #7
NR=size(GPS(:,1));
Data_lat_DD=zeros(NR(1),1);
Data_lon_DD=zeros(NR(1),1);
```

```
for cnt=1:NR(1)
   if ~(isnan(GPS(cnt,1)) || isnan(GPS(cnt,2)))
      if GPS(cnt,1)>1000 && GPS(cnt,2)>1000
Data_lat_DD(cnt)=((GPS(cnt,1)-5200)/60)+52;
Data_lon_DD(cnt)=(((GPS(cnt,2)-10600)/60)+106)*(-1);
      end
   end
end
Data_lat_DD = Data_lat_DD(Data_lat_DD~=0);
Data_lon_DD = Data_lon_DD(Data_lon_DD~=0);
 %%End of Block #7. Start of Block #8
sss=size(GPS(:,1));
Data_lat_CCR=zeros(sss(1),1);
Data_lon_CCR=zeros(sss(1),1);
Data_lat_CCL=zeros(sss(1),1);
Data_lon_CCL=zeros(sss(1),1);
Data_lat_TR=zeros(sss(1),1);
Data_lon_TR=zeros(sss(1),1);
Data_lat_TL=zeros(sss(1),1);
Data_lon_TL=zeros(sss(1),1);
 for cnt=1:sss(1)
   if GPS(cnt,4)<92 && GPS(cnt,4)>88
      [temp1,temp2]=Boom(Data_lat_DD(cnt),Data_lon_DD(cnt),2.1082,270);
      [Data_lat_CCR(cnt),Data_lon_CCR(cnt)]=Boom(temp1,temp2,2.8,180);
      [Data_lat_TR(cnt),Data_lon_TR(cnt)]=Boom(temp1,temp2,2.292,180);
      elseif GPS(cnt,4)<272 && GPS(cnt,4)>268
      [temp3,temp4]=Boom(Data_lat_DD(cnt),Data_lon_DD(cnt),4,90);
      [Data_lat_CCR(cnt),Data_lon_CCR(cnt)]=Boom(temp3,temp4,2.8,0);
      [Data_lat_TR(cnt),Data_lon_TR(cnt)]=Boom(temp3,temp4,2.292,0);
    end
end
for cnt=1:sss(1)
   if GPS(cnt,4)<92 && GPS(cnt,4)>88
      [temp1,temp2]=Boom(Data_lat_DD(cnt),Data_lon_DD(cnt),2.1082,270);
      [Data_lat_CCL(cnt),Data_lon_CCL(cnt)]=Boom(temp1,temp2,2.8,0);
```

```
    [Data_lat_TL(cnt),Data_lon_TL(cnt)]=Boom(temp1,temp2,2.292,0);
    elseif GPS(cnt,4)<272 && GPS(cnt,4)>268
    [temp3,temp4]=Boom(Data_lat_DD(cnt),Data_lon_DD(cnt),4,90);
    [Data_lat_CCL(cnt),Data_lon_CCL(cnt)]=Boom(temp3,temp4,2.8,180);
    [Data_lat_TL(cnt),Data_lon_TL(cnt)]=Boom(temp3,temp4,2.292,180);
  end
end
%End of Block #8. Start of Block #9
CCR=[Data_lat_CCR Data_lon_CCR CCR1_D CCR2_D CCR3_D CCR4_D CCR5_D GPS(:,3) GPS(:,4)];
CCL=[Data_lat_CCL Data_lon_CCL CCL1_D CCL2_D CCL3_D CCL4_D CCL5_D GPS(:,3) GPS(:,4)];
TRR=cell2mat(T_R);
TLL=cell2mat(T_L);
TR=[Data_lat_TR Data_lon_TR TRR GPS(:,3) GPS(:,4)];
TL=[Data_lat_TL Data_lon_TL TLL GPS(:,3) GPS(:,4)];
temp_Data_lon_CCL=Data_lon_CCL(Data_lon_CCL~=0);
temp_Data_lat_CCL=Data_lat_CCL(Data_lat_CCL~=0);
temp_Data_lon_CCR=Data_lon_CCR(Data_lon_CCR~=0);
temp_Data_lat_CCR=Data_lat_CCR(Data_lat_CCR~=0);
temp_Data_lon_TR=Data_lon_TR(Data_lon_TR~=0);
temp_Data_lat_TR=Data_lat_TR(Data_lat_TR~=0);
temp_Data_lon_TL=Data_lon_TL(Data_lon_TL~=0);
temp_Data_lat_TL=Data_lat_TL(Data_lat_TL~=0);
%End of Block #9. Start of Block #10
plot(temp_Data_lon_CCL,temp_Data_lat_CCL,'or','MarkerSize',15,'MarkerFaceColor','r')
plot(temp_Data_lon_CCR,temp_Data_lat_CCR,'or','MarkerSize',15,'MarkerFaceColor','r')
plot(temp_Data_lon_TR,temp_Data_lat_TR,'or','MarkerSize',15,'MarkerFaceColor','b')
plot(temp_Data_lon_TL,temp_Data_lat_TL,'or','MarkerSize',15,'MarkerFaceColor','b')
%End of Block #10
%%
```

Likewise, importing the collected data file into the visualization program, a function was developed to import captured images of plant canopies which can be explored in the following program. For a better understanding of this program, refer to the algorithm proposed in Figure 3-25 of capture four.

```
%Start of Block #1
```

```
folder_name = uigetdir;
Files = dir([folder_name,'\*.png']);
if isempty(Files)
  Files = dir([folder_name,'\*.jpg']);
end
%End of Block #1. Start of Block #2
imnames={Files.name};
heading=0;
s=size(imnames);
c=char(imnames);
%End of Block #2. Start of Block #3
for cnt=1:s(2)
[dd1(cnt,:) dd2(cnt,:) dd3(cnt,:) dd4(cnt,:)]=strread(c(cnt,:),'%s %s %s %s','delimiter',',');
end
s=size(imnames);
% End of Block #3. Start of Block #4
for cnt=1:s(2)
   if strcmp(dd4(cnt),'R.png ')
      dd4{cnt}='R.png';
   elseif strcmp(dd4(cnt),'L.png ')
      dd4{cnt}='L.png';
   elseif strcmp(dd4(cnt),'R.jpg ')
      dd4{cnt}='R.jpg';
   elseif strcmp(dd4(cnt),'L.jpg ')
      dd4{cnt}='L.jpg';
   end
%End of Block #4. Start of Block #5
   if strcmp(dd4(cnt),'R.png') || strcmp(dd4(cnt),'R.jpg')
   imnames_r(cnt)= imnames(cnt);
   Im_lat_r(cnt)=str2num(char(dd1(cnt)));
   Im_lon_r(cnt)=str2num(char(dd2(cnt)));
   Im_ang_r(cnt)=str2num(char(dd3(cnt)));
   end
   if strcmp(dd4(cnt),'L.png') || strcmp(dd4(cnt),'L.jpg')
   imnames_l(cnt)= imnames(cnt);
```

```
    Im_lat_l(cnt)=str2num(char(dd1(cnt)));
    Im_lon_l(cnt)=str2num(char(dd2(cnt)));
    Im_ang_l(cnt)=str2num(char(dd3(cnt)));
    end
end
imnames_l=imnames_l(~cellfun('isempty',imnames_l))  ;
imnames_r=imnames_r(~cellfun('isempty',imnames_r))  ;
Im_lat_l = Im_lat_l(Im_lat_l~=0);
Im_lon_l = Im_lon_l(Im_lon_l~=0);
Im_lat_r = Im_lat_r(Im_lat_r~=0);
Im_lon_r = Im_lon_r(Im_lon_r~=0);
Im_ang_r = Im_ang_r(Im_ang_r~=0);
Im_ang_l = Im_ang_l(Im_ang_l~=0);
%End of Block #5. Start of Block #6
NR=size(Im_lat_r);
Im_lat_DD_R=zeros(NR(2),1);
Im_lon_DD_R=zeros(NR(2),1);
for cnt=1:NR(2)
    if ~(isnan(Im_lat_r(cnt)) || isnan(Im_lon_r(cnt)))
        if Im_lat_r(cnt)>1000 && Im_lon_r(cnt)>1000
Im_lat_DD_R(cnt)=((Im_lat_r(cnt)-5200)/60)+52;
Im_lon_DD_R(cnt)=(((Im_lon_r(cnt)-10600)/60)+106)*(-1);
        end
    end
end
NR=size(Im_lat_l);
Im_lat_DD_L=zeros(NR(2),1);
Im_lon_DD_L=zeros(NR(2),1);
 for cnt=1:NR(2)
    if ~(isnan(Im_lat_l(cnt)) || isnan(Im_lon_l(cnt)))
        if Im_lat_l(cnt)>1000 && Im_lon_l(cnt)>1000
Im_lat_DD_L(cnt)=((Im_lat_l(cnt)-5200)/60)+52;
Im_lon_DD_L(cnt)=(((Im_lon_l(cnt)-10600)/60)+106)*(-1);
        end
    end
```

```
end
 Im_lat_DD_R = Im_lat_DD_R(Im_lat_DD_R~=0);
Im_lon_DD_R = Im_lon_DD_R(Im_lon_DD_R~=0);
Im_lat_DD_L = Im_lat_DD_L(Im_lat_DD_L~=0);
Im_lon_DD_L = Im_lon_DD_L(Im_lon_DD_L~=0);
%End of Block #6. Start Block #7
sss=size(Im_lon_DD_R);
ssss=size(Im_lon_DD_L);
Im_lat_DD_R_Cam=zeros(sss(1),1);
Im_lon_DD_R_Cam=zeros(sss(1),1);
Im_lat_DD_L_Cam=zeros(ssss(1),1);
Im_lon_DD_L_Cam=zeros(ssss(1),1);
for cnt=1:sss(1)
   if Im_ang_r(cnt)<92 && Im_ang_r(cnt)>88
      [temp1,temp2]=Boom(Im_lat_DD_R(cnt),Im_lon_DD_R(cnt),2.1082,270);
      [Im_lat_DD_R_Cam(cnt),Im_lon_DD_R_Cam(cnt)]=Boom(temp1,temp2,3,180);
      elseif Im_ang_r(cnt)<272 && Im_ang_r(cnt)>268
      [temp3,temp4]=Boom(Im_lat_DD_R(cnt),Im_lon_DD_R(cnt),4,90);
      [Im_lat_DD_R_Cam(cnt),Im_lon_DD_R_Cam(cnt)]=Boom(temp3,temp4,3,0);
    end
 end
 for cnt=1:ssss(1)
    if Im_ang_l(cnt)<92 && Im_ang_l(cnt)>88
       [temp1,temp2]=Boom(Im_lat_DD_L(cnt),Im_lon_DD_L(cnt),2.1082,270);
       [Im_lat_DD_L_Cam(cnt),Im_lon_DD_L_Cam(cnt)]=Boom(temp1,temp2,3,0);
    elseif Im_ang_l(cnt)<272 && Im_ang_l(cnt)>268
       [temp3,temp4]=Boom(Im_lat_DD_L(cnt),Im_lon_DD_L(cnt),4,90);
       [Im_lat_DD_L_Cam(cnt),Im_lon_DD_L_Cam(cnt)]=Boom(temp3,temp4,3,180);
    end
end
%End of Block #7. Start of Block #8
temp_Im_lon_DD_R_Cam=Im_lon_DD_R_Cam(Im_lon_DD_R_Cam~=0);
temp_Im_lat_DD_R_Cam=Im_lat_DD_R_Cam(Im_lat_DD_R_Cam~=0);
temp_Im_lon_DD_L_Cam=Im_lon_DD_L_Cam(Im_lon_DD_L_Cam~=0);
temp_Im_lat_DD_L_Cam=Im_lat_DD_L_Cam(Im_lat_DD_L_Cam~=0);
```

```
plot(temp_Im_lon_DD_R_Cam,temp_Im_lat_DD_R_Cam,'^','MarkerSize',13,'MarkerFaceColor','r')
plot(temp_Im_lon_DD_L_Cam,temp_Im_lat_DD_L_Cam,'^','MarkerSize',13,'MarkerFaceColor','g')
%End of Block #8. Start of Block #9
cam_r=[Im_lon_DD_R_Cam,Im_lat_DD_R_Cam];
cam_l=[Im_lon_DD_L_Cam,Im_lat_DD_L_Cam];
%%End of Block #9
```

At this point, both captured images and collected information for the entire field are loaded into the visualization software, and user can select individual data/image points for precise investigation. So the third function was developed to search into the significant amount of collected data and images to visualize the selected data/image by user. The body of this function can be seen as bellow. For a better understanding of this program, refer to the Figure 3-27 in chapter four.

```
%Start of Block #1
pos = get(0,'userdata');
lon=pos(1);
lat=pos(2);
s0='Data for selected point:';
s1=sprintf('Lon. = %1.8f',lon) ;
s2=sprintf('Lat.  = %1.8f ', lat) ;
 if isempty(lon) || isempty(lat)
    msgbox('Please Select a Data Point First and Then Click on This Button Again')
 end
%%End of block #1. Start of Block #2
 if isfield(handles,'DATA_CCR') && isfield(handles,'DATA_TR')
   CCR=handles.DATA_CCR;
   CCL=handles.DATA_CCL;
   TR=handles.DATA_TR;
   TL=handles.DATA_TL;
 end
 %End of Block #2. Start of Block #3
if isfield(handles,'data_us')
    data_us=handles.data_us;
    data_us_r=handles.data_us_r;
```

```
    data_us_l=handles.data_us_l;
end
%End of Block #3. Start of Block #4
lon_tol=0.0000000001;
lat_tol=0.0000000000001;
if isfield(handles,'data_us')
    US1=data_us( find(abs(data_us_r(:,1)-(lon))<lon_tol   &  abs(data_us_r(:,2)-lat)<lat_tol),1);
    US2=data_us( find(abs(data_us_r(:,3)-(lon))<lon_tol   &  abs(data_us_r(:,4)-lat)<lat_tol),2);
    US3=data_us( find(abs(data_us_l(:,1)-(lon))<lon_tol   &  abs(data_us_l(:,2)-lat)<lat_tol),3);
    US4=data_us( find(abs(data_us_l(:,3)-(lon))<lon_tol   &  abs(data_us_l(:,4)-lat)<lat_tol),4);
    s3=sprintf('US1 = %1.3f mm', US1) ;
    s4=sprintf('US2 = %1.3f mm', US2) ;
    s5=sprintf('US3 = %1.3f mm', US3) ;
    s6=sprintf('US4 = %1.3f mm', US4) ;
end
if isfield(handles,'DATA_TR') && isfield(handles,'DATA_CCR')
    T_R=TR( find(abs(TR(:,2)-(lon))<lon_tol   &  abs(TR(:,1)-lat)<lat_tol),3);
    T_L=TL( find(abs(TL(:,2)-(lon))<lon_tol   &  abs(TL(:,1)-lat)<lat_tol),3);
    T_R_S=TR( find(abs(TR(:,2)-(lon))<lon_tol   &  abs(TR(:,1)-lat)<lat_tol),4);
    T_L_S=TL( find(abs(TL(:,2)-(lon))<lon_tol   &  abs(TL(:,1)-lat)<lat_tol),4);
    T_R_D=TR( find(abs(TR(:,2)-(lon))<lon_tol   &  abs(TR(:,1)-lat)<lat_tol),5);
    T_L_D=TL( find(abs(TL(:,2)-(lon))<lon_tol   &  abs(TL(:,1)-lat)<lat_tol),5);
    s7=sprintf('T_R = %1.3f C', T_R) ;
    s8=sprintf('T_L = %1.3f C', T_L) ;
    s7_S=sprintf('Swather Speed = %1.3f mi/h', T_R_S) ;
    s8_S=sprintf('Swather Speed = %1.3f mi/h', T_L_S) ;
    s7_D=sprintf('Swather Heading = %1.3f Deg.', T_R_D) ;
    s8_D=sprintf('Swather Heading = %1.3f Deg.', T_L_D) ;
end
 if isfield(handles,'DATA_CCR') && isfield(handles,'DATA_TR')
    RE_R=CCR( find(abs(CCR(:,2)-(lon))<lon_tol   &  abs(CCR(:,1)-lat)<lat_tol),3);
    NIR_R=CCR( find(abs(CCR(:,2)-(lon))<lon_tol   &  abs(CCR(:,1)-lat)<lat_tol),4);
    RED_R=CCR( find(abs(CCR(:,2)-(lon))<lon_tol   &  abs(CCR(:,1)-lat)<lat_tol),5);
    NDRE_R=CCR( find(abs(CCR(:,2)-(lon))<lon_tol   &  abs(CCR(:,1)-lat)<lat_tol),6);
    NDVI_R=CCR( find(abs(CCR(:,2)-(lon))<lon_tol   &  abs(CCR(:,1)-lat)<lat_tol),7);
```

```
    CCR_S=CCR( find(abs(CCR(:,2)-(lon))<lon_tol   &  abs(CCR(:,1)-lat)<lat_tol),8);
    CCR_D=CCR( find(abs(CCR(:,2)-(lon))<lon_tol   &  abs(CCR(:,1)-lat)<lat_tol),9);
     s9=sprintf('RE_R = %1.3f ', RE_R) ;
    s10=sprintf('NIR_R = %1.3f ', NIR_R) ;
    s11=sprintf('RED_R = %1.3f ', RED_R) ;
    s12=sprintf('NDRE_R = %1.3f ', NDRE_R) ;
    s13=sprintf('NDVI_R = %1.3f ', NDVI_R) ;
    s12_S=sprintf('Swather Speed = %1.3f mi/h', CCR_S) ;
    s13_D=sprintf('Swather Heading = %1.3f Deg.', CCR_D) ;
     RE_L=CCL( find(abs(CCL(:,2)-(lon))<lon_tol   &  abs(CCL(:,1)-lat)<lat_tol),3);
    NIR_L=CCL( find(abs(CCL(:,2)-(lon))<lon_tol   &  abs(CCL(:,1)-lat)<lat_tol),4);
    RED_L=CCL( find(abs(CCL(:,2)-(lon))<lon_tol   &  abs(CCL(:,1)-lat)<lat_tol),5);
    NDRE_L=CCL( find(abs(CCL(:,2)-(lon))<lon_tol   &  abs(CCL(:,1)-lat)<lat_tol),6);
    NDVI_L=CCL( find(abs(CCL(:,2)-(lon))<lon_tol   &  abs(CCL(:,1)-lat)<lat_tol),7);
    CCL_S=CCL( find(abs(CCL(:,2)-(lon))<lon_tol   &  abs(CCL(:,1)-lat)<lat_tol),8);
    CCL_D=CCL( find(abs(CCL(:,2)-(lon))<lon_tol   &  abs(CCL(:,1)-lat)<lat_tol),9);
    s14=sprintf('RE_L = %1.3f ', RE_L) ;
    s15=sprintf(' NIR_L = %1.3f ', NIR_L) ;
    s16=sprintf('RED_L = %1.3f ', RED_L) ;
    s17=sprintf('NDRE_L = %1.3f ', NDRE_L) ;
    s18=sprintf('NDVI_L = %1.3f ', NDVI_L) ;
    s17_S=sprintf('Swather Speed = %1.3f mi/h', CCL_S) ;
    s18_D=sprintf('Swather Heading = %1.3f Deg.', CCL_D) ;
end
%End of Block #4. Start of Block #5
if isfield(handles,'data_us')
      if ~isempty(US1)
      output_txt = {s0;s1;s2;s3};
      elseif ~isempty(US2)
      output_txt = {s0;s1;s2;s4};
      elseif ~isempty(US3)
      output_txt = {s0;s1;s2;s5};
      elseif ~isempty(US4)
      output_txt = {s0;s1;s2;s6};
      end
```

```
end
 if isfield(handles,'DATA_TR') && isfield(handles,'DATA_CCR')
      if ~isempty(T_R)
      output_txt = {s0;s1;s2;s7_S;s7_D;s7};
      elseif ~isempty(T_L)
      output_txt = {s0;s1;s2;s8_S;s8_D;s8};
      elseif ~isempty(NDVI_R)
      output_txt = {s0;s1;s2;s12_S;s13_D;s13;s9;s10;s11;s12;s13};
      elseif ~isempty(NDVI_L)
      output_txt = {s0;s1;s2;s17_S;s18_D;s18;s14;s15;s16;s17};
      end
end
%End of Block #5. Start of Block #6
      set(handles.txt_d,'String',output_txt)
 %End of Block #6
```

APPENDIX D- Screenshots of the Results Extracted from the Visualization Program

This section is a part of chapter four and provides the screenshots of the results obtained from the developed visualization program to explore into a desired section of the field.

D.1- Part of section 4-5-1-; Result of verifying the accuracy of geo-referencing algorithm by visible signs based-on experiments on June 23, 2017

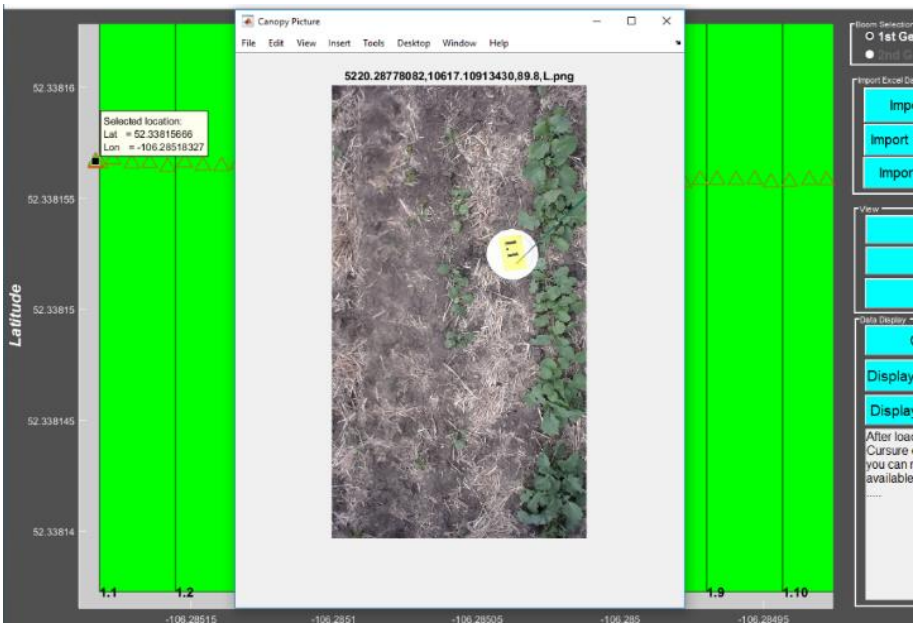

Figure D-1: Plot number 1.1 on June 23, 2017

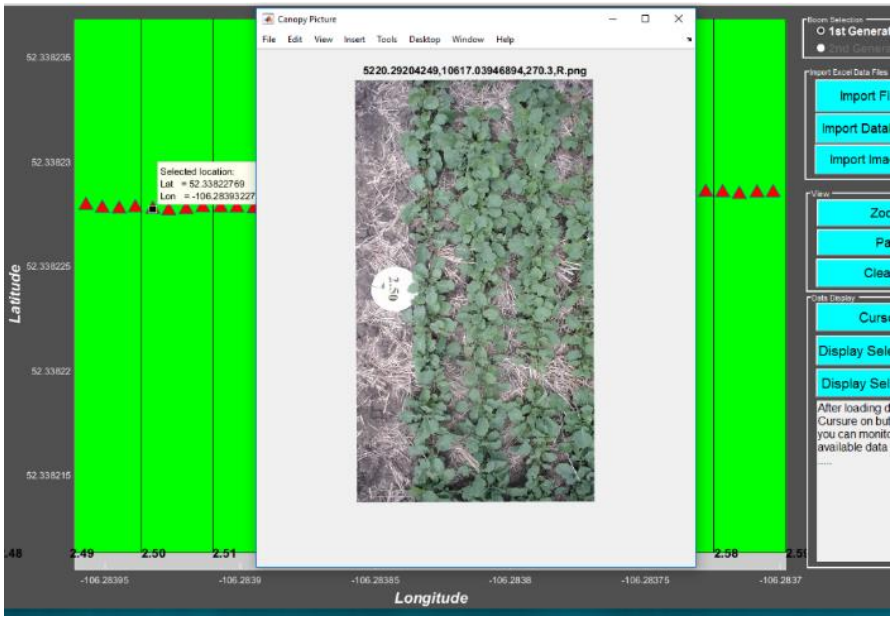

Figure D-2: Plot number 2.50 on June 23, 2017

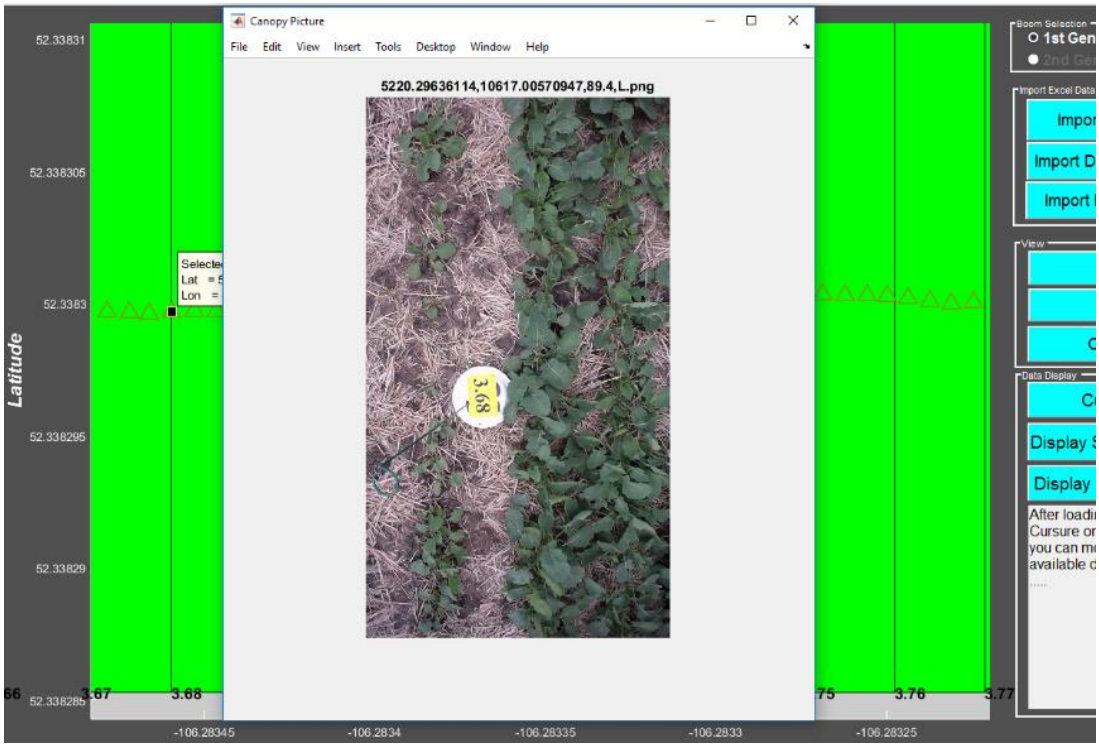

Figure D-3: Plot number 3.68 on June 23, 2017

D.2- Part of section 4-5-1-; Result of verifying the accuracy of geo-referencing algorithm by visible signs based-on experiments on July 13, 2017

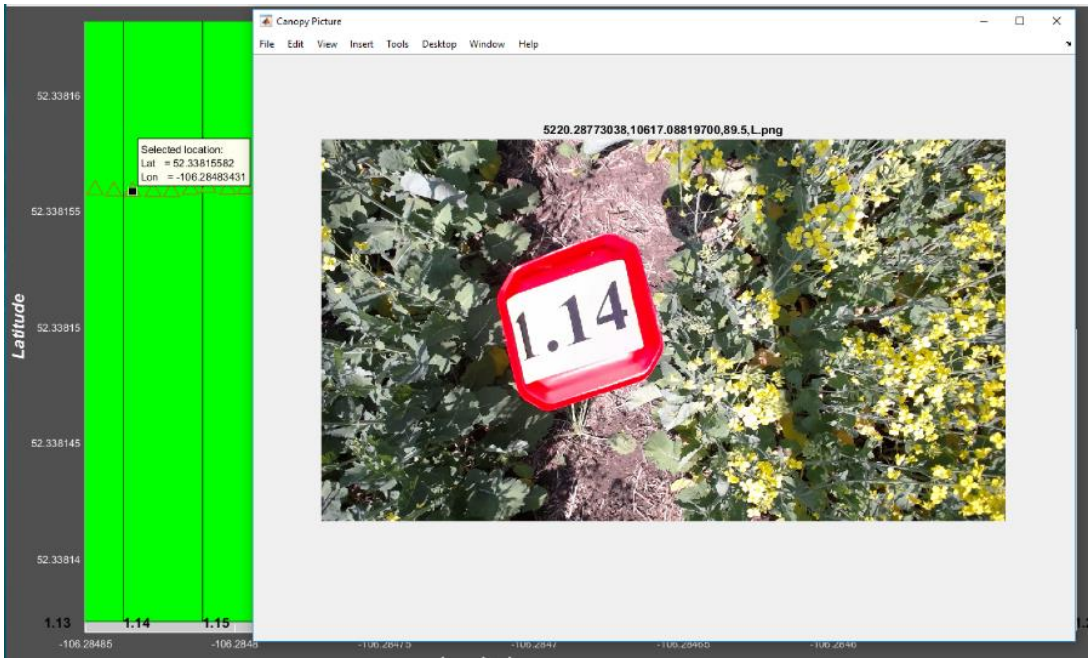

Figure D-4: Plot number 1.14 on July 13, 2017

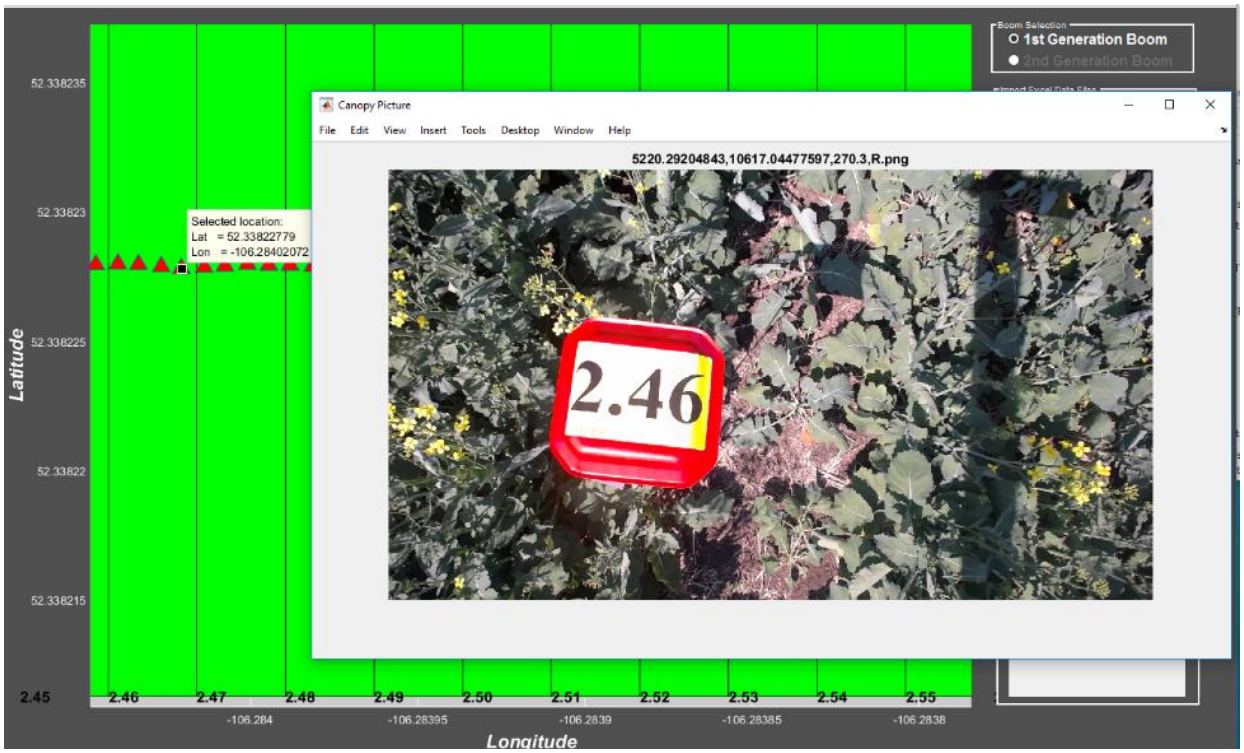

Figure D-5: Plot number 2.46 on July 13, 2017 (Sign was located before the plot)

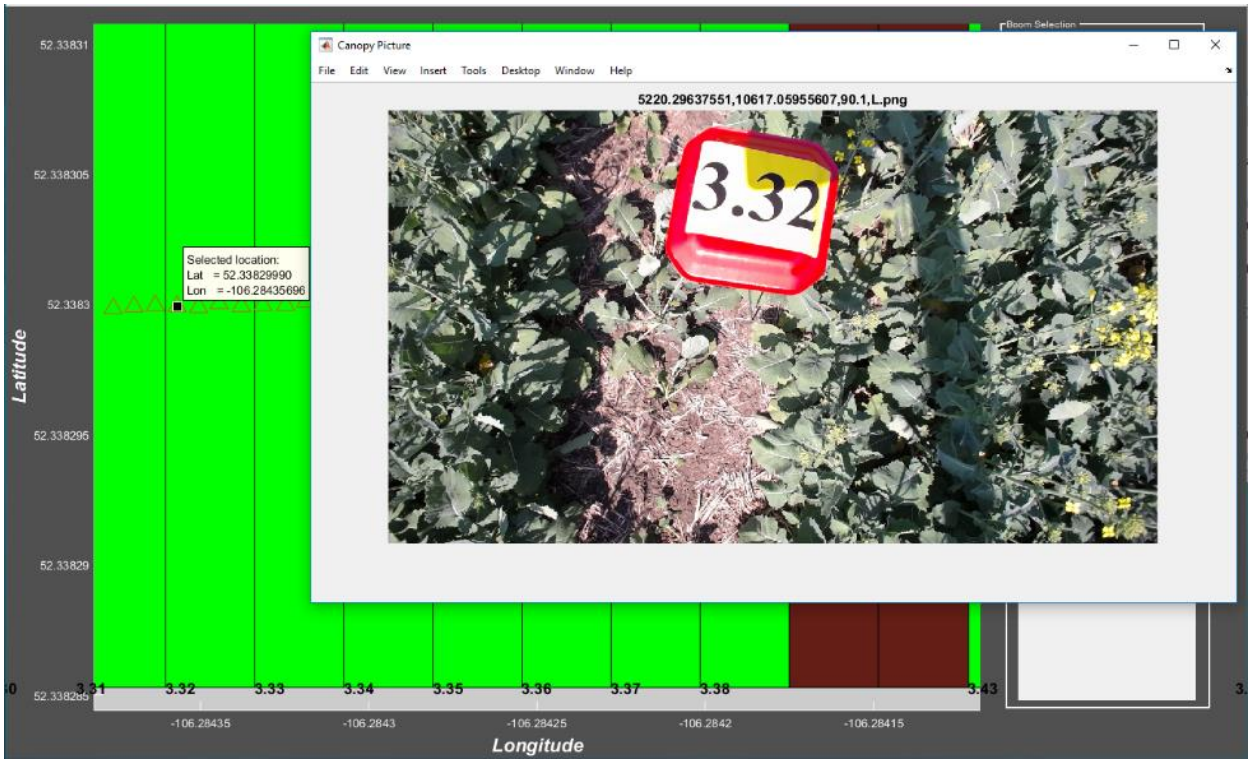

Figure D-6: Plot number 3.32 on July 13, 2017

D.3- Part of section 4-5-1-; Result of verifying the accuracy of geo-referencing algorithm by visible signs based-on experiments on July 25, 2017

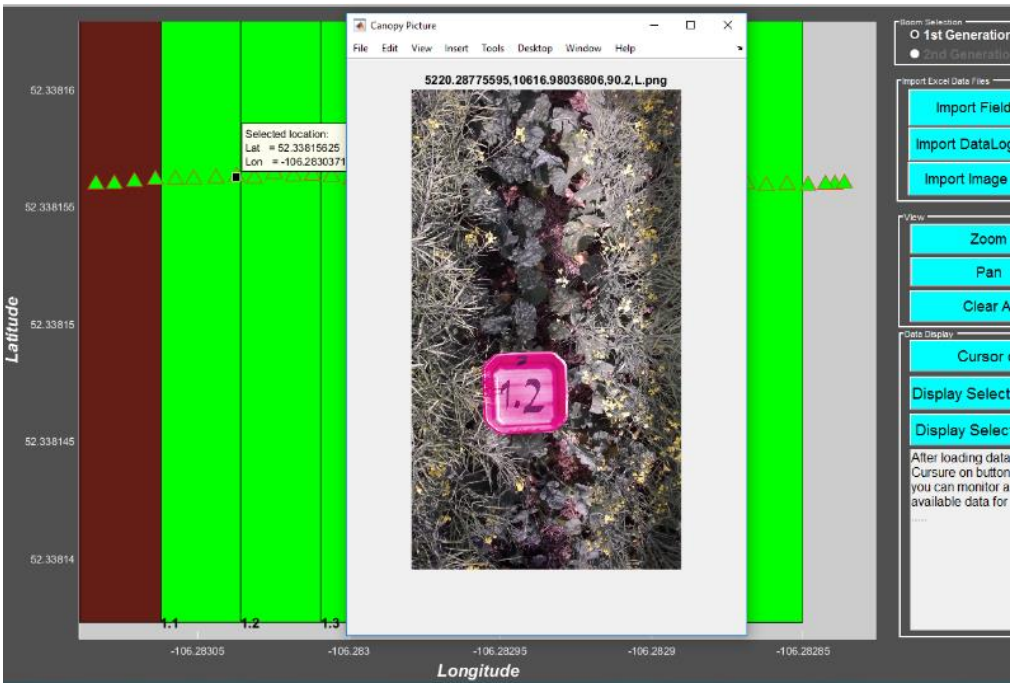

Figure D-7: Plot number 1.2 on July 25, 2017

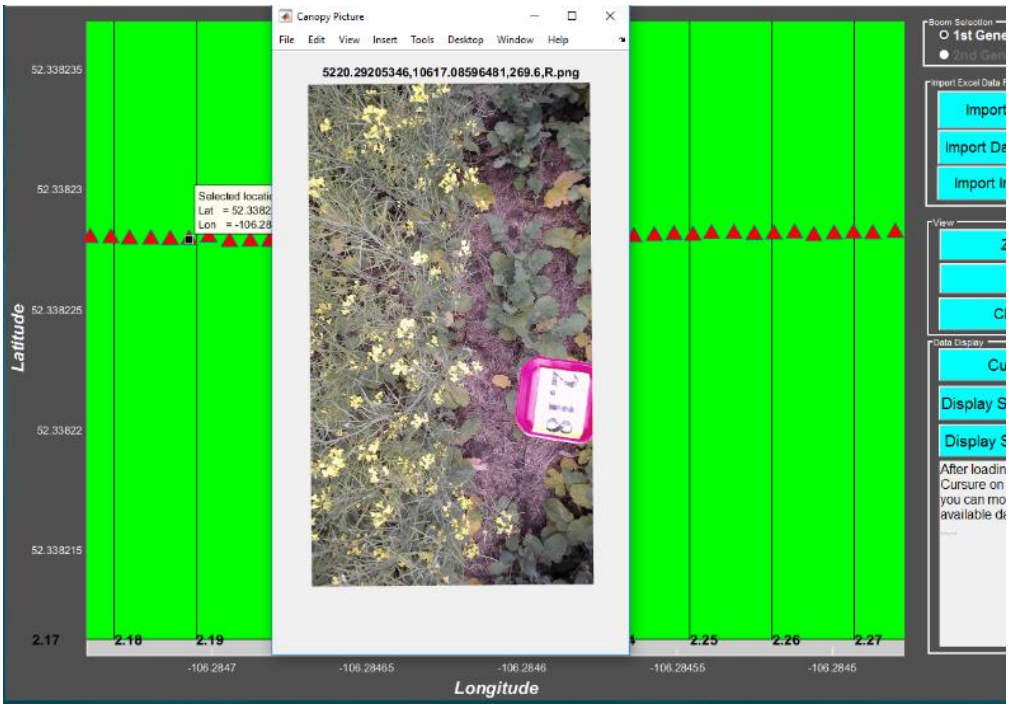

Figure D-8: Plot number 2.18 on July 25, 2017 (Sign was located before the plot)

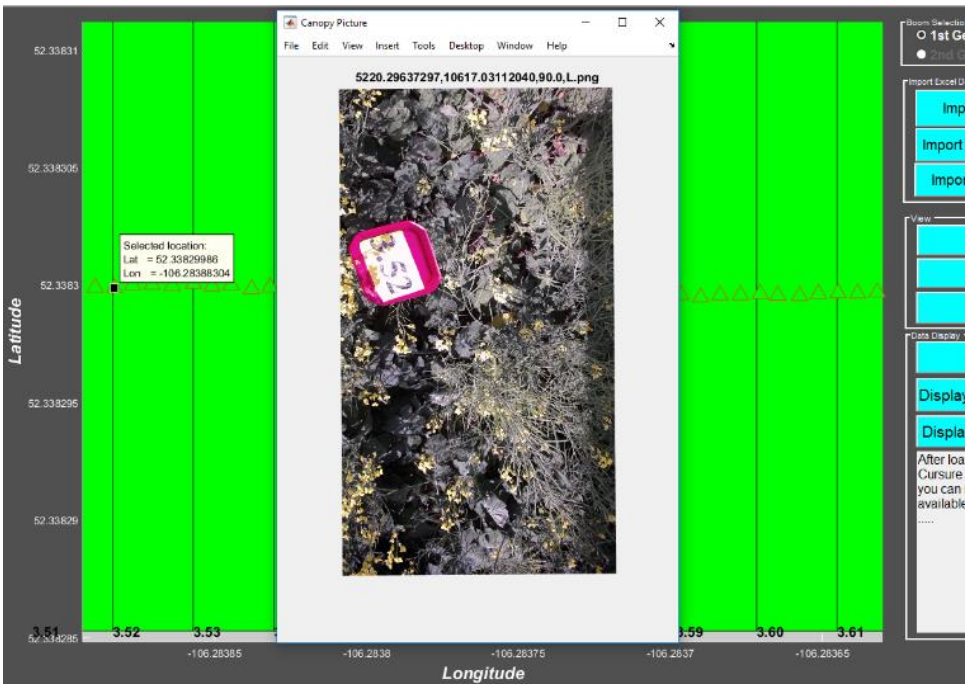

Figure D-9: Plot number 3.52 on July 25, 2017

D.4- Part of section 4-5-1-; Result of verifying the accuracy of geo-referencing algorithm by visible signs based-on experiments on August 2, 2017

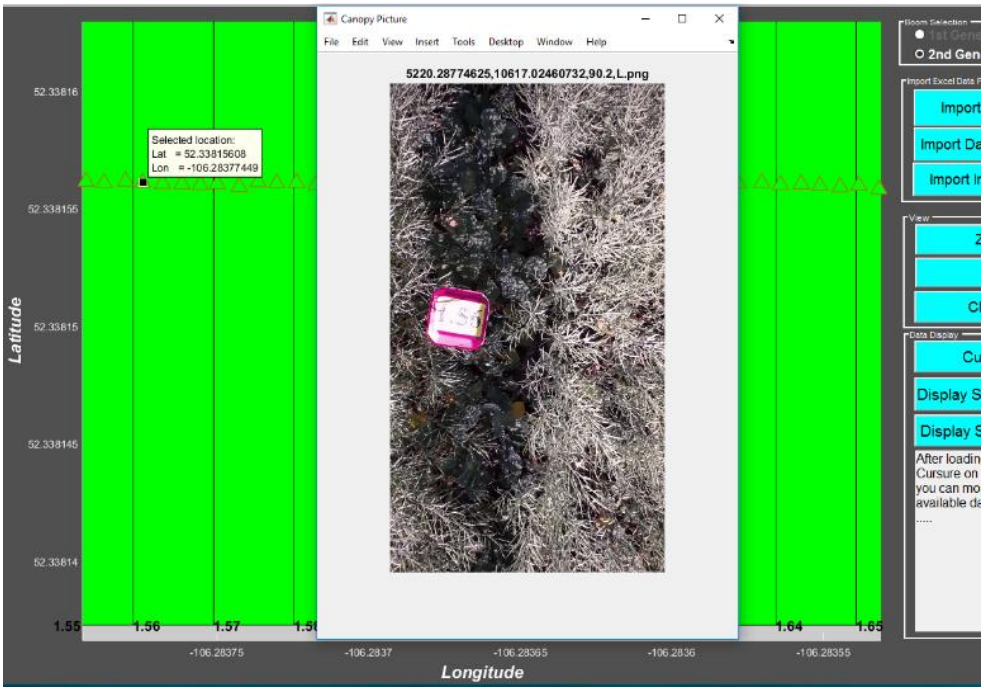

Figure D-10: Plot number 1.56 on August 2, 2017

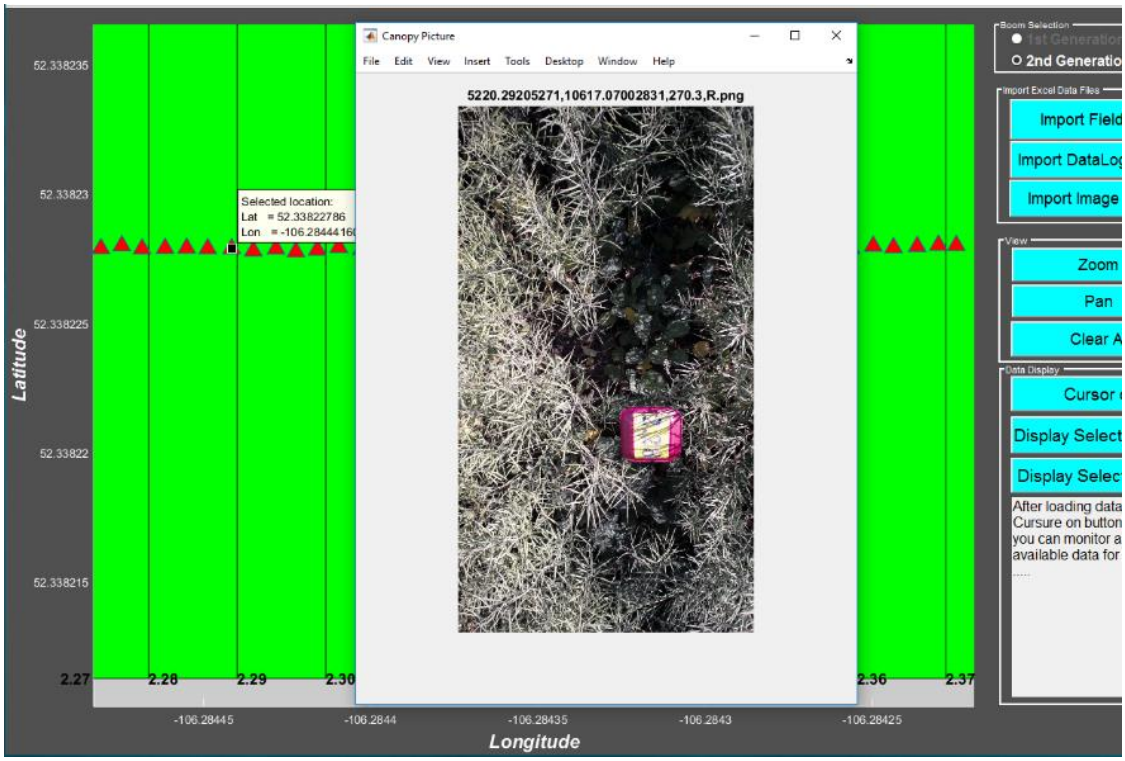

Figure D-11: Plot number 2.28 on August 2, 2017 (Sign was located before the plot)

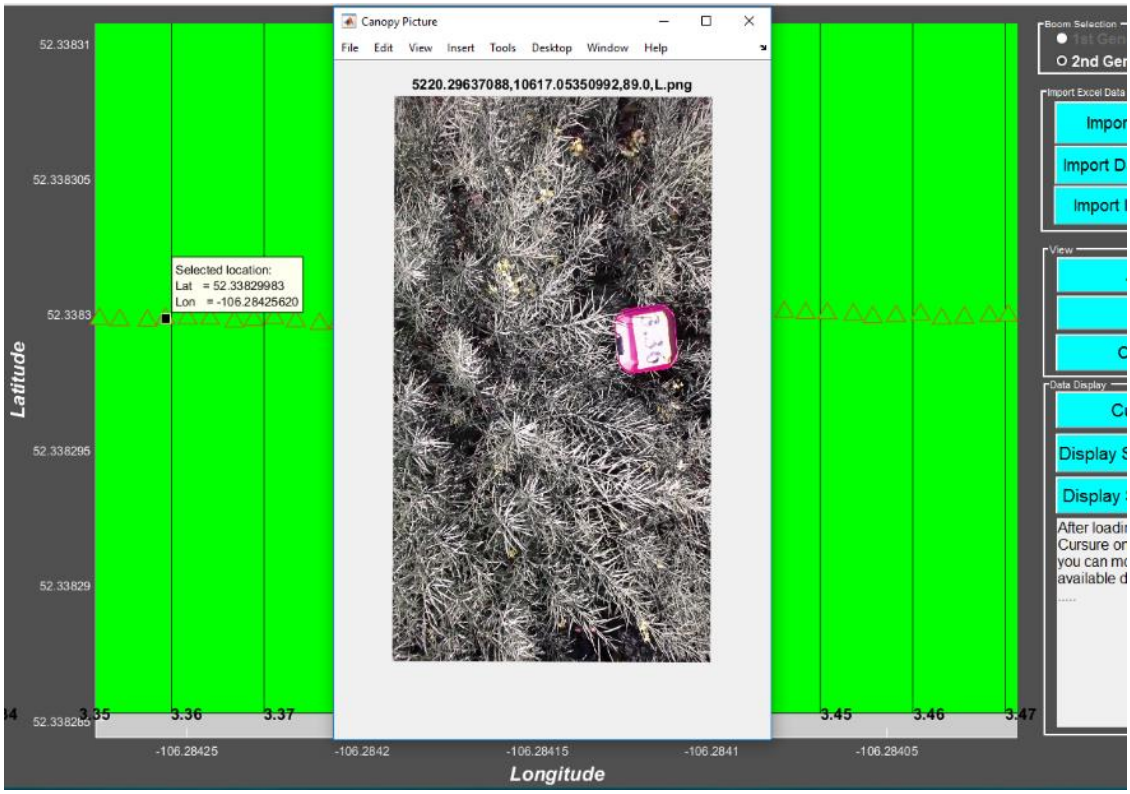

Figure D-12: Plot number 3.36 on August 2, 2017

D.5- Part of section 4-5-3-; Analyzing growth of the plot # 1.75 over summer 2017

Table D-1: Variation of NDVI and temperature of plot # 1.75 during summer 2017

Date	NDVI	Temp (C°)	Ambient Temp (C°) Ref: the weather network	Time of the data collection
June 23, 2017	0.4937	15.1	18.8	15:20 pm
July 4, 2017	0.6799	28.3	27.4	15:50 pm
July 7, 2017	0.7628	23.3	29.8	10:55 am
July 13, 2017	0.5030	27.8	29.3	14:30 pm
July 18, 2017	0.5729	22.3	22.9	14:35 pm
July 25, 2017	0.6672	23.7	25.7	14:45 pm
August 2,2017	0.7264	21.0	24.7	16:30 pm
August 11,2017	0.7001	22.8	27.1	12:05 pm
August 18,2017	0.6368	23.6	27.3	10:20 am

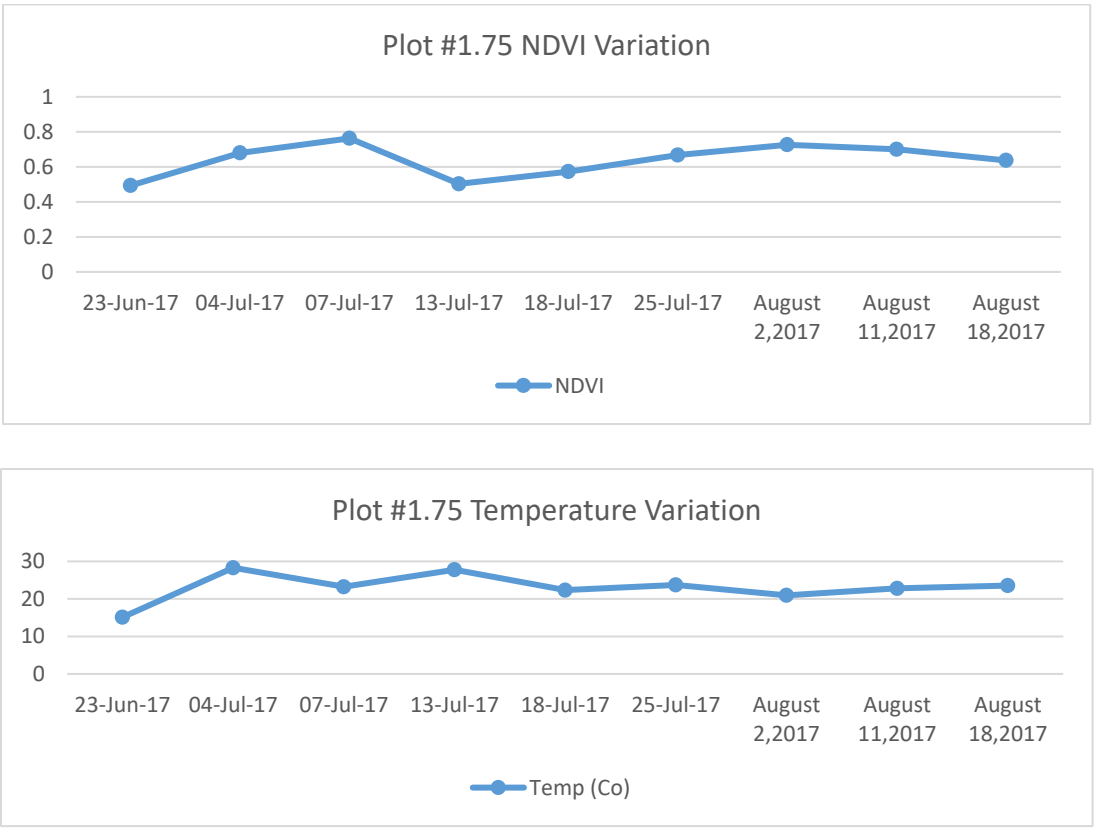

Figure D-13: Variation of NDVI and temperature of plot # 2.30 during summer 2017

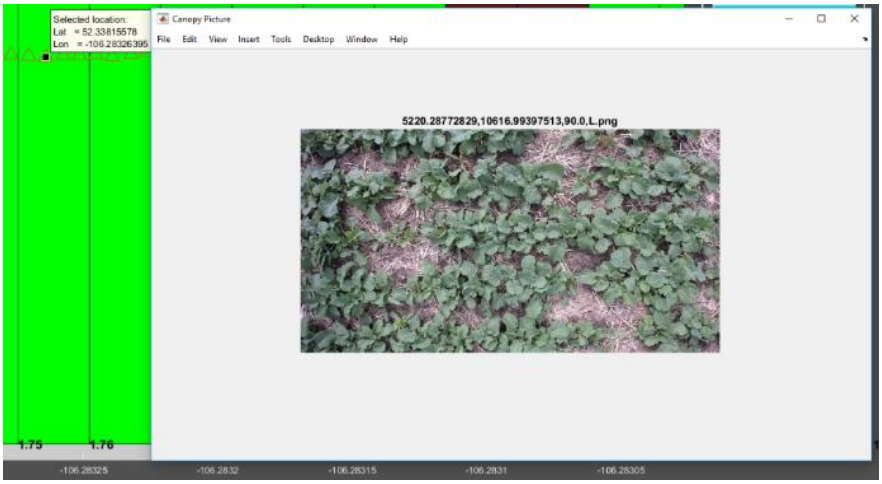

Figure D-14: Plot # 1.75 on June 23

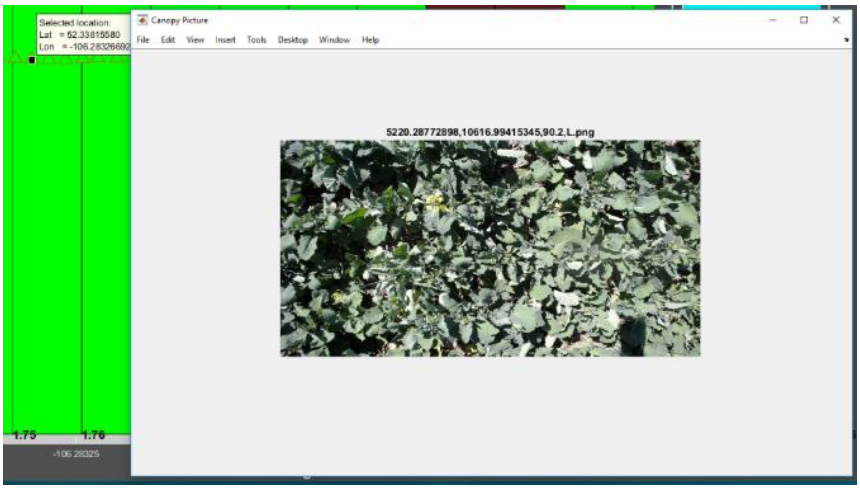

Figure D-15: Plot # 1.75 on July 4

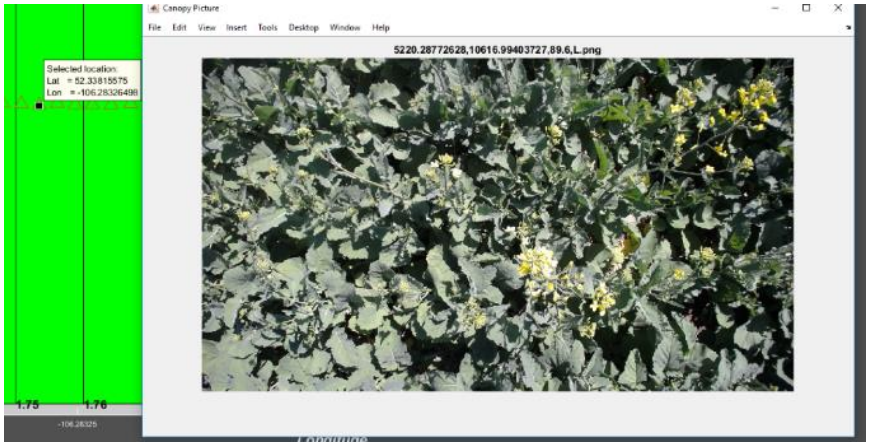

Figure D-16: Plot # 1.75 on July 7

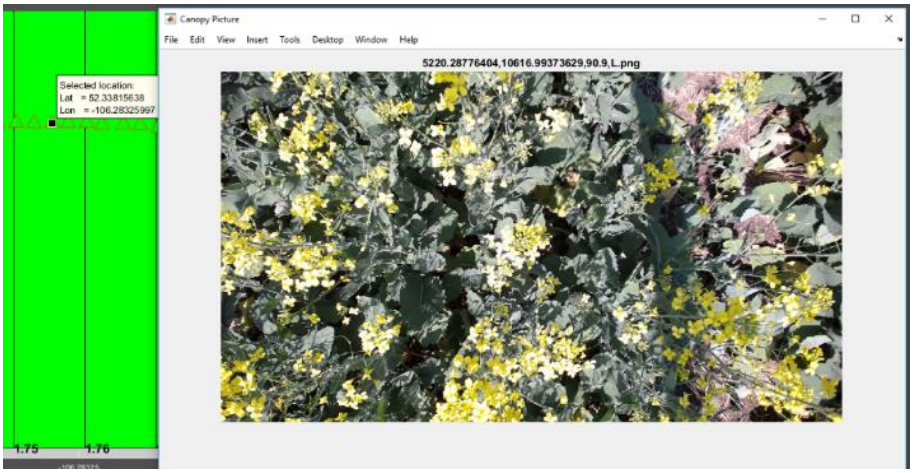

Figure D-17: Plot # 1.75 on July 13

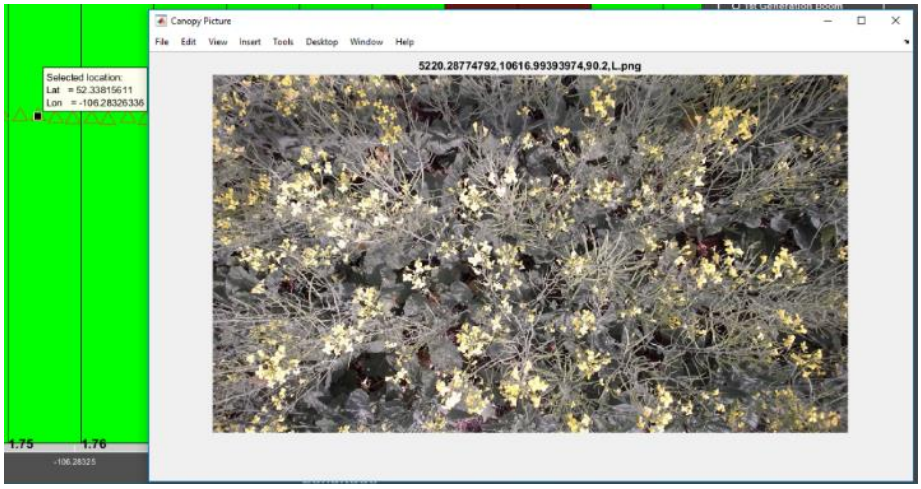

Figure D-18: Plot # 1.75 on July 18

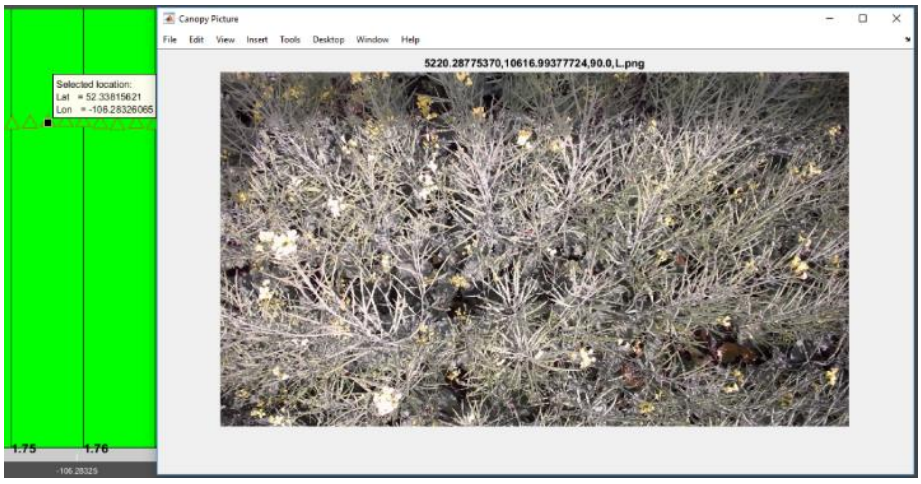

Figure D-19: Plot # 1.75 on July 25

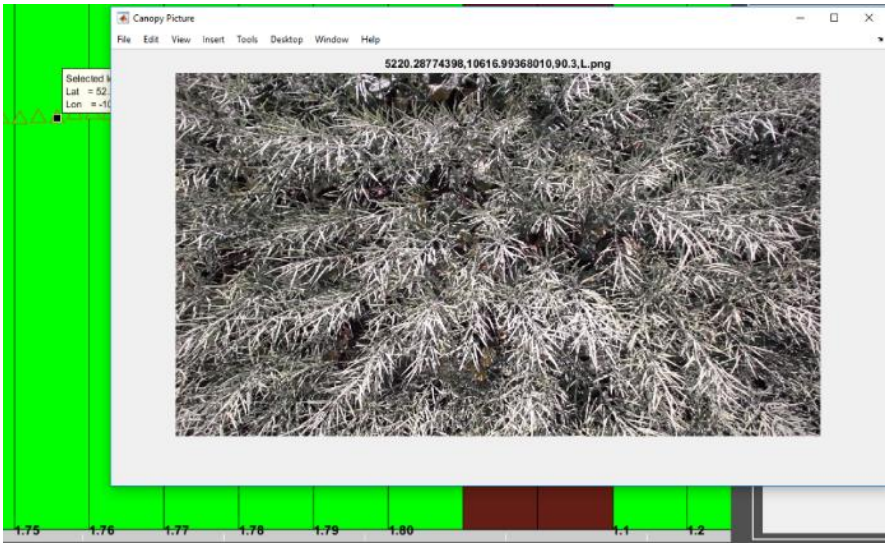

Figure D-20: Plot # 1.75 on August 2

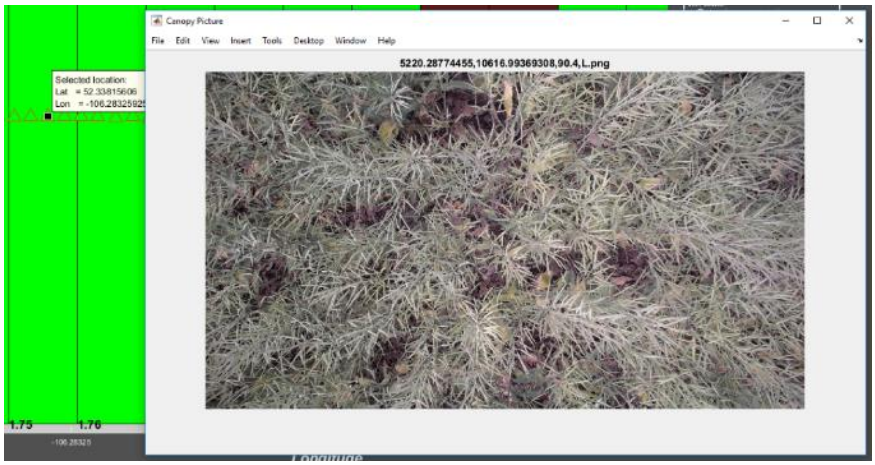

Figure D-21: Plot # 1.75 on August 11

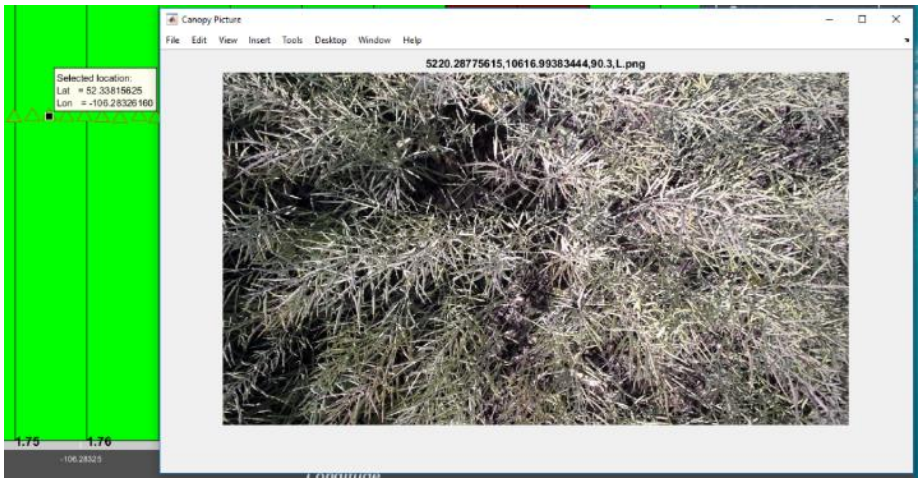

Figure D-22: Plot # 1.75 on August 18

D.6- Part of section 4-5-3-; Analyzing growth of the plot # 2.30 over summer 2017

Table D-2: Variation of NDVI and temperature of plot # 2.30 during summer 2017

Date	NDVI	Temp (C°)	Ambient Temp (C°) Ref: the weather network	Time of the data collection
June 23, 2017	0.3962	19.5	18.8	15:20 pm
July 4, 2017	0.6555	26.6	27.4	15:50 pm
July 7, 2017	0.4848	24.6	29.8	10:55 am
July 13, 2017	0.5714	27.5	29.3	14:30 pm
July 18, 2017	0.5026	20.9	22.9	14:35 pm
July 25, 2017	0.5295	21.9	25.7	14:45 pm
August 2,2017	0.6554	21.1	24.7	16:30 pm
August 11,2017	0.6374	22.0	27.1	12:05 pm
August 18,2017	0.5933	23.4	27.3	10:20 am

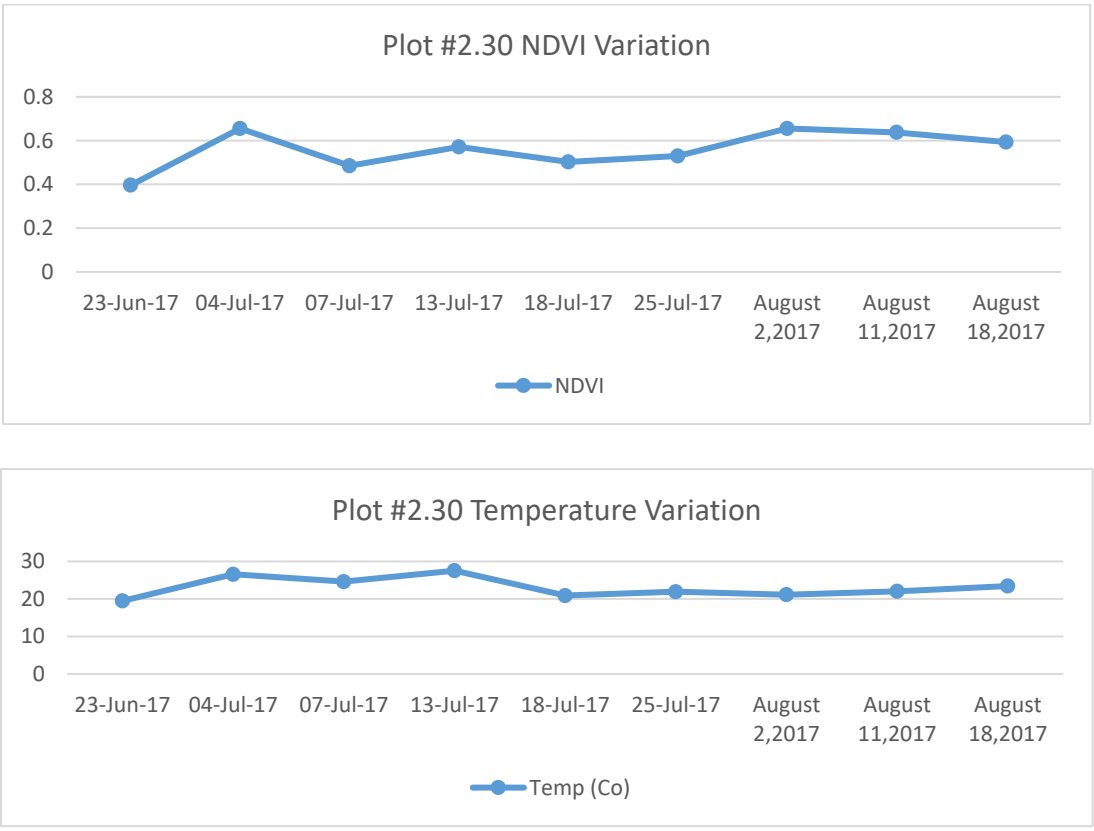

Figure D-23: Variation of NDVI and temperature of plot # 2.30 during summer 2017

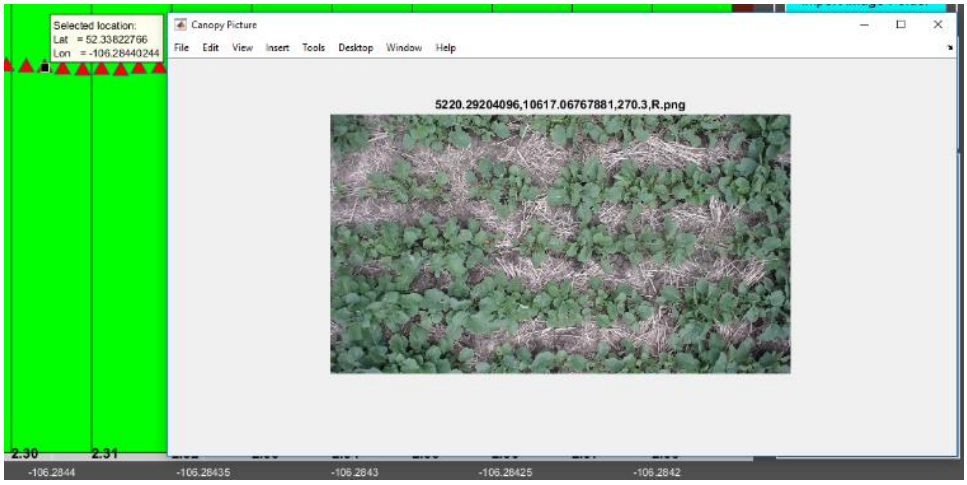

Figure D-24: Plot # 2.30 on June 23

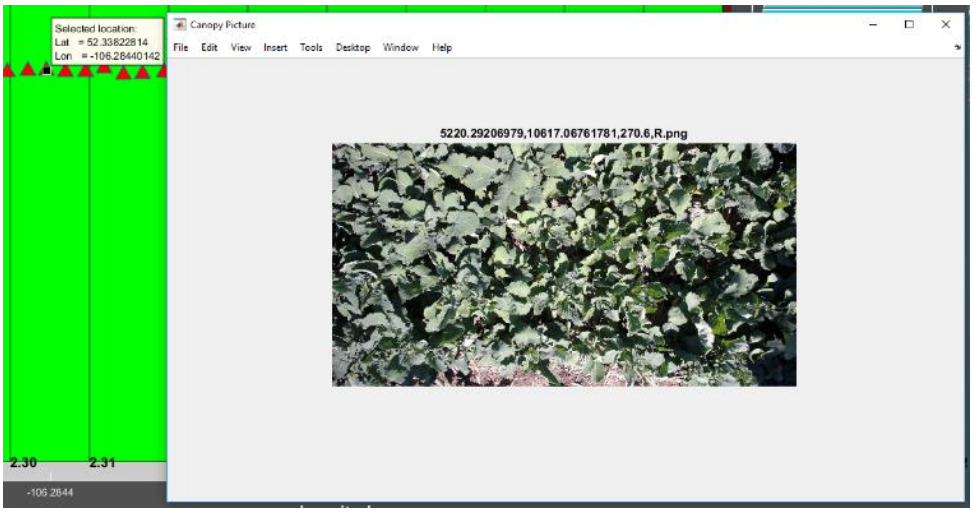

Figure D-25: Plot # 2.30 on July 4

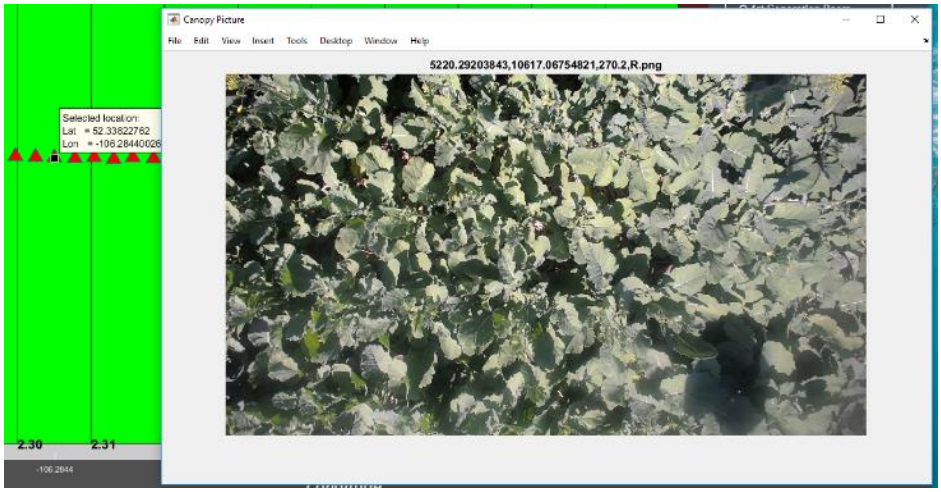

Figure D-26: Plot # 2.30 on July 7

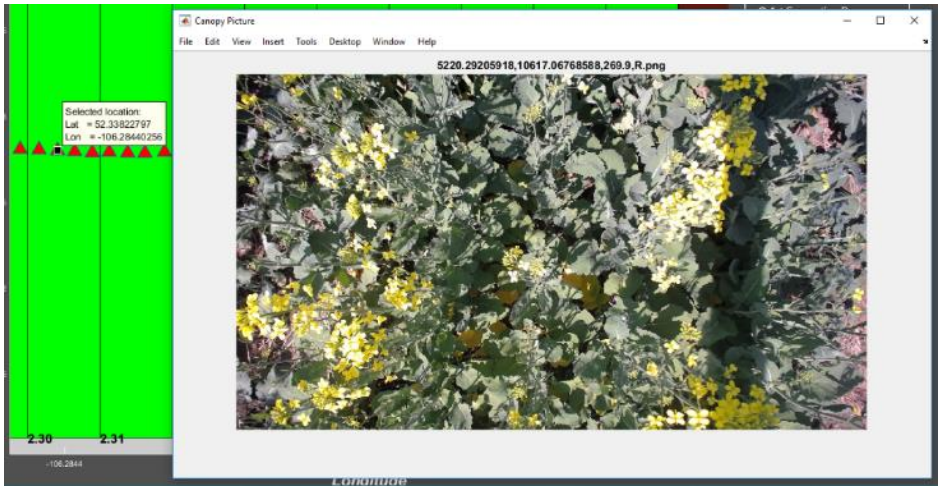

Figure D-27: Plot # 2.30 on July 13

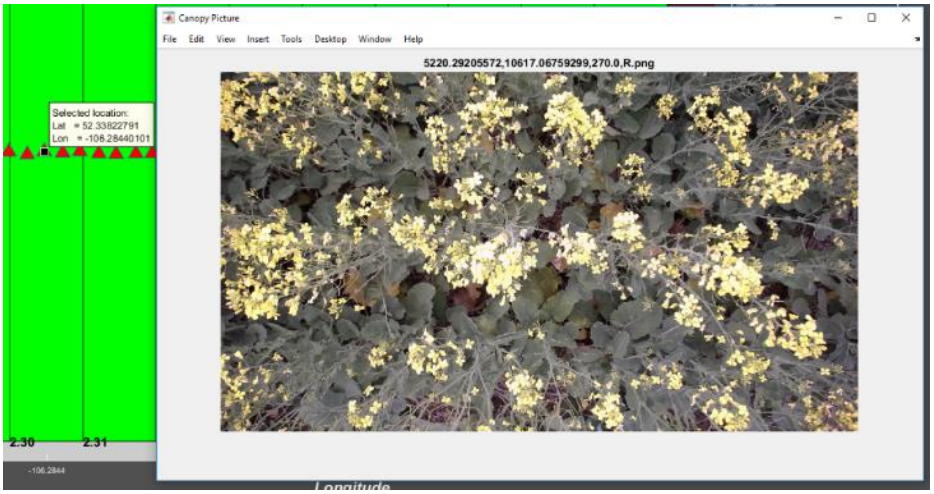

Figure D-28: Plot # 2.30 on July 18

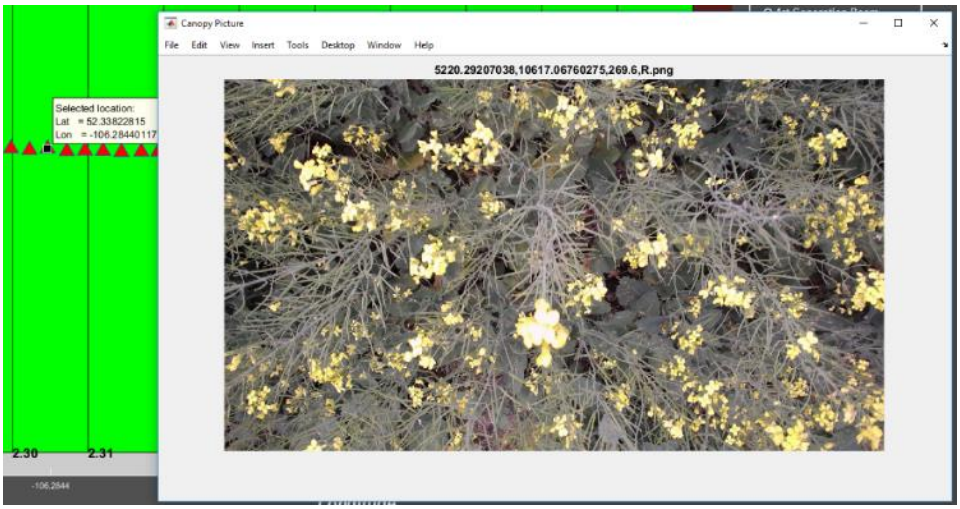

Figure D-29: Plot # 2.30 on July 25

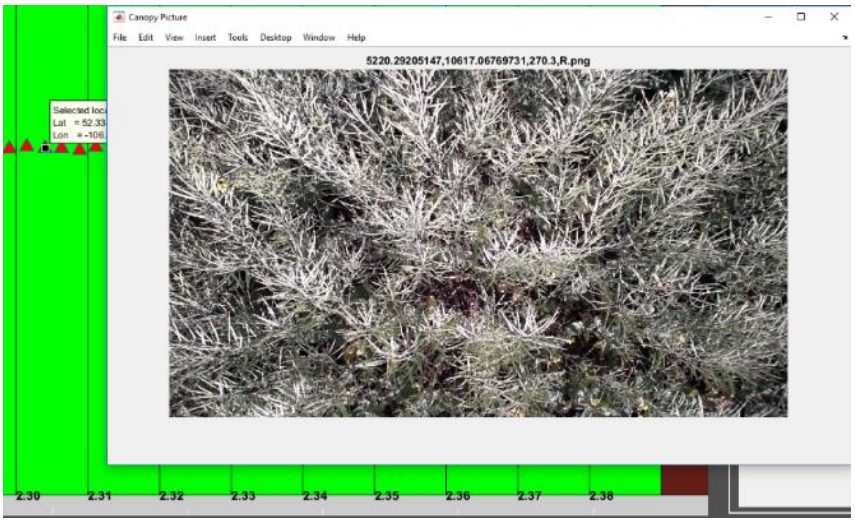

Figure D-30: Plot # 2.30 on August 2

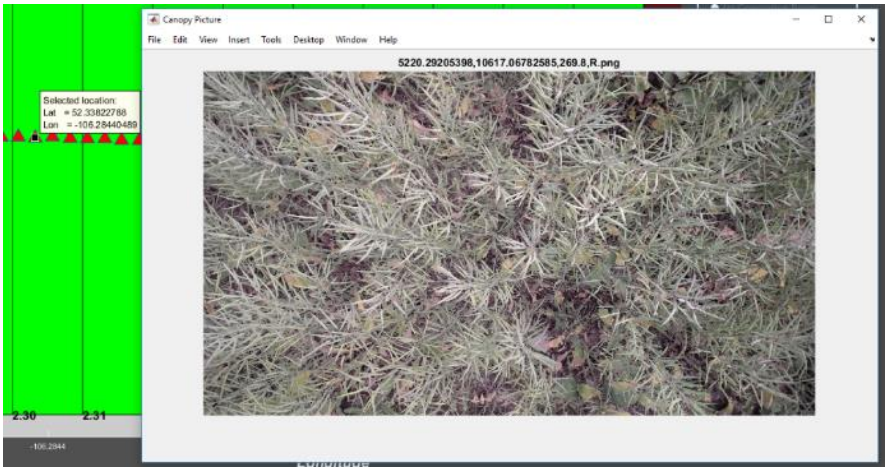

Figure D-31: Plot # 2.30 on August 11

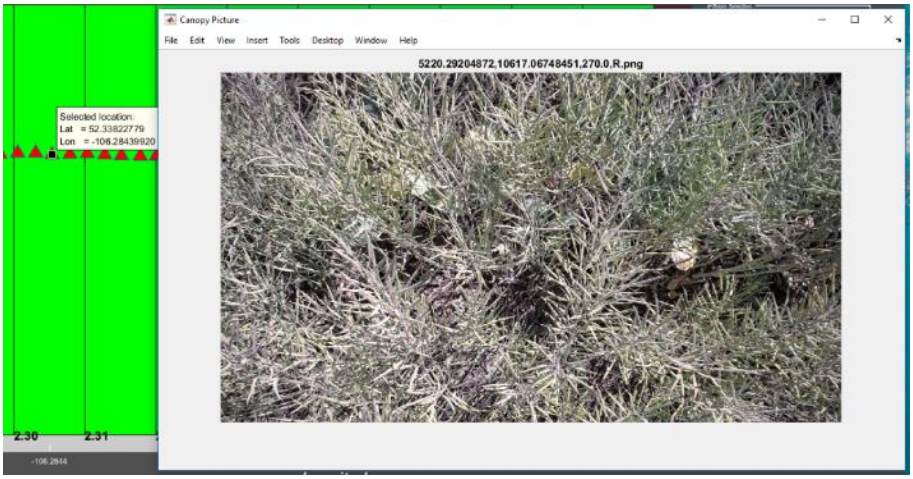

Figure D-32: Plot # 2.30 on August 18

D.7- Part of section 4-5-3-; Analyzing growth of the plot # 2.80 over summer 2017

Table D-3: Variation of NDVI and temperature of plot # 2.80 during summer 2017

Date	NDVI	Temp (C°)	Ambient Temp (C°) Ref: the weather network	Time of the data collection
June 23, 2017	0.5604	17.7	18.8	15:20 pm
July 4, 2017	0.6436	27.7	27.4	15:50 pm
July 7, 2017	0.7006	24.0	29.8	10:55 am
July 13, 2017	0.4297	28.0	29.3	14:30 pm
July 18, 2017	0.5735	24.2	22.9	14:35 pm
July 25, 2017	0.6677	24.7	25.7	14:45 pm
August 2,2017	0.6784	21.1	24.7	16:30 pm
August 11,2017	0.6576	23.3	27.1	12:05 pm
August 18,2017	0.6557	24.6	27.3	10:20 am

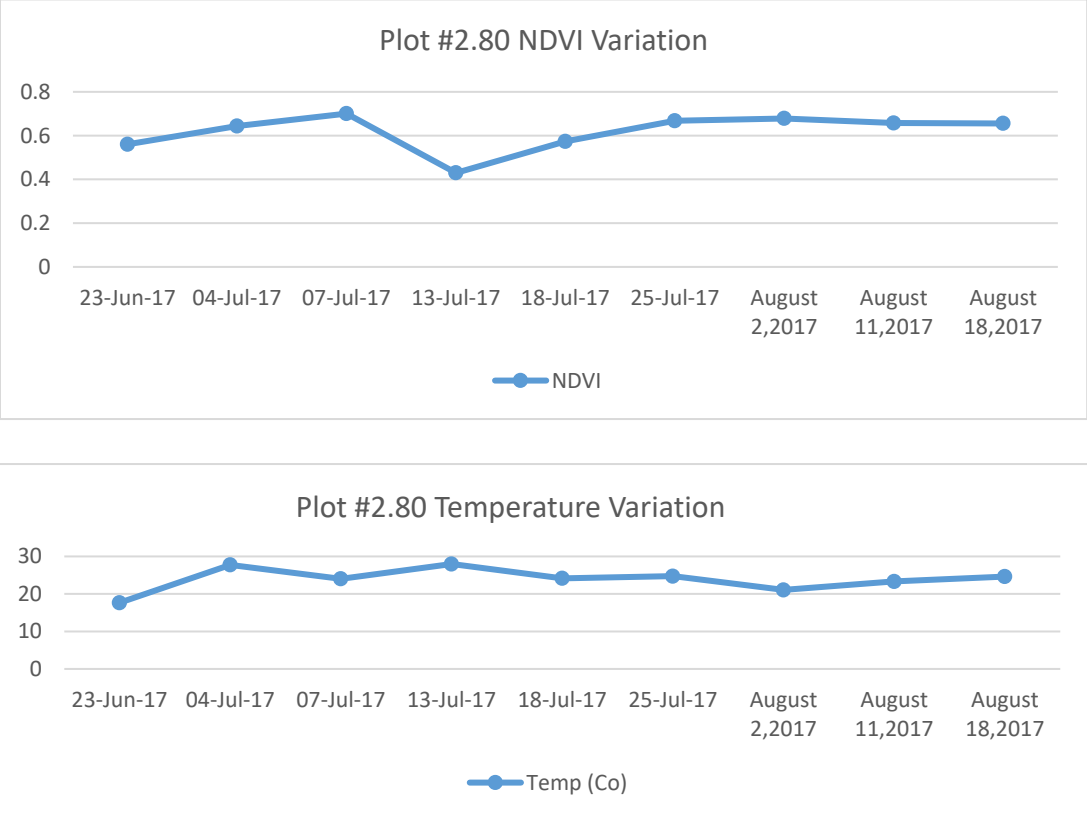

Figure D-33: Variation of NDVI and temperature of plot # 2.80 during summer 2017

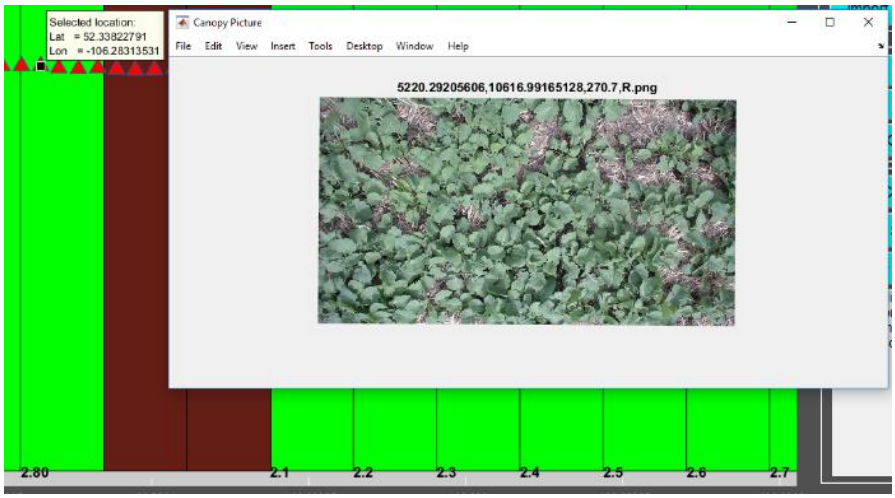

Figure D-34: Plot # 2.80 on June 23

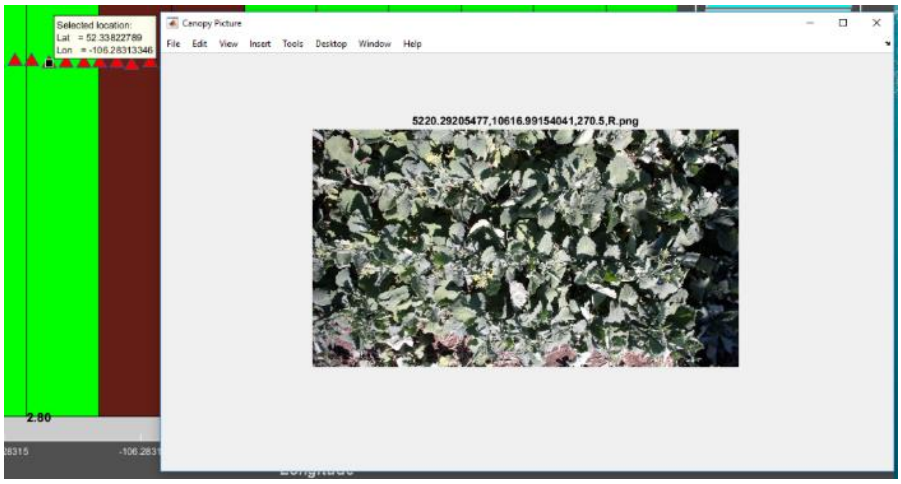

Figure D-35: Plot # 2.80 on July 4

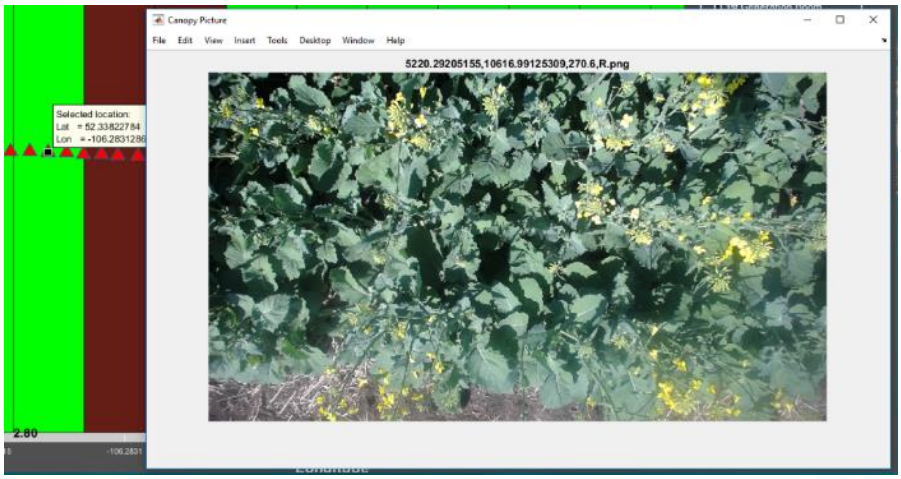

Figure D-36: Plot # 2.80 on July 7

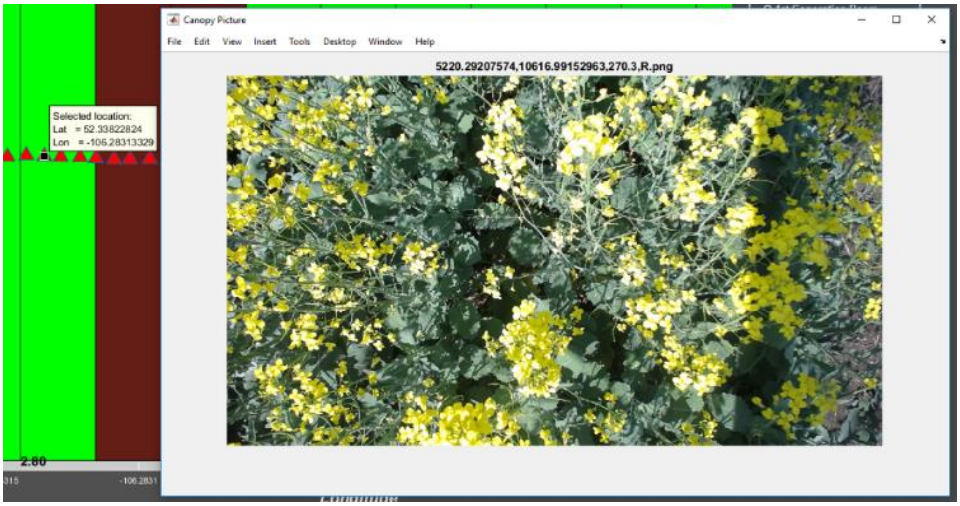

Figure D-37: Plot # 2.80 on July 13

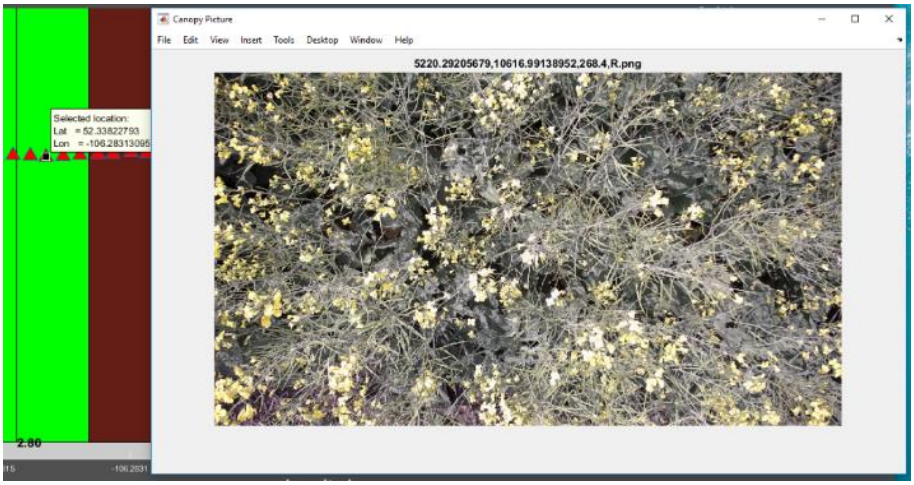

Figure D-38: Plot # 2.80 on July 18

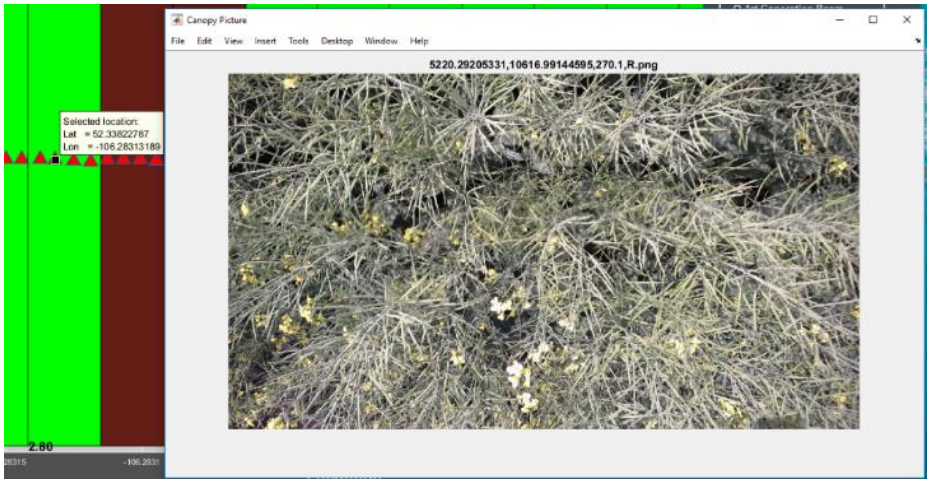

Figure D-39: Plot # 2.80 on July 25

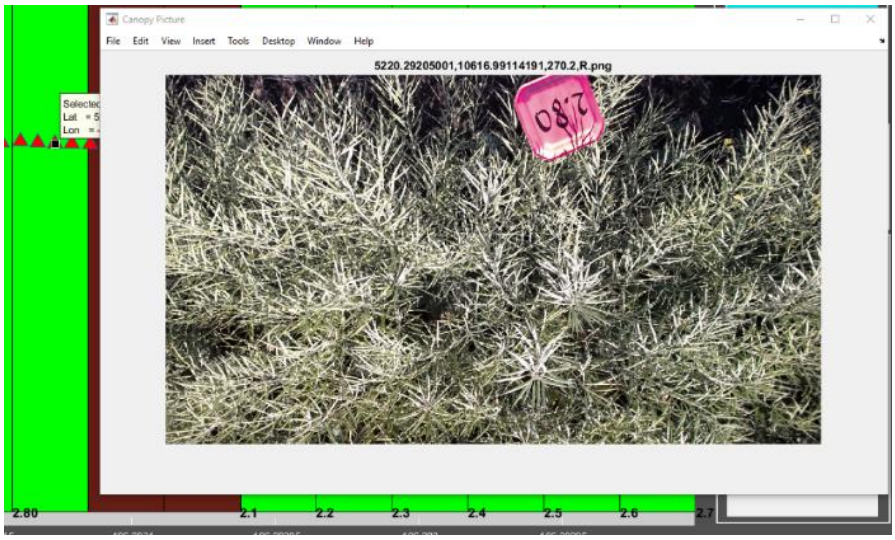

Figure D-40: Plot # 2.80 on August 2

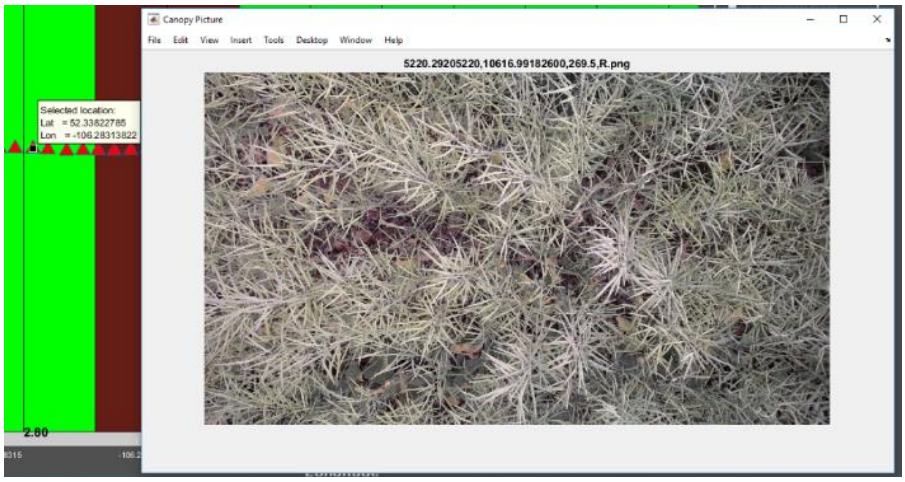

Figure D-41: Plot # 2.80 on August 11

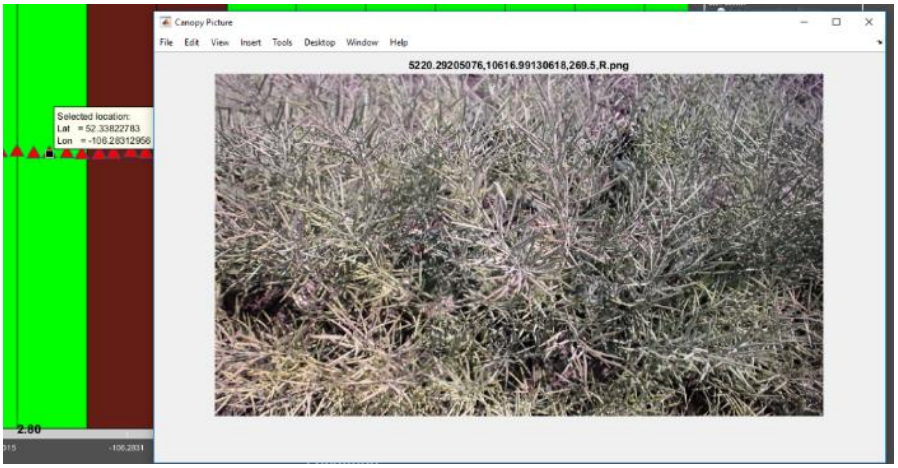

Figure D-42: Plot # 2.80 on August 18

D.8- Part of section 4-5-3-; Analyzing growth of the plot # 3.5 over summer 2017

Table D-4: Variation of NDVI and temperature of plot # 3.5 during summer 2017

Date	NDVI	Temp (C°)	Ambient Temp (C°) Ref: the weather network	Time of the data collection
June 23, 2017	0.3547	19.0	18.8	15:20 pm
July 4, 2017	0.5758	25.2	27.4	15:50 pm
July 7, 2017	0.7377	23.3	29.8	10:55 am
July 13, 2017	0.5239	26.9	29.3	14:30 pm
July 18, 2017	0.5130	18.8	22.9	14:35 pm
July 25, 2017	0.5538	23.2	25.7	14:45 pm
August 2,2017	0.6647	21.8	24.7	16:30 pm
August 11,2017	0.6394	22.1	27.1	12:05 pm
August 18,2017	0.6092	23.9	27.3	10:20 am

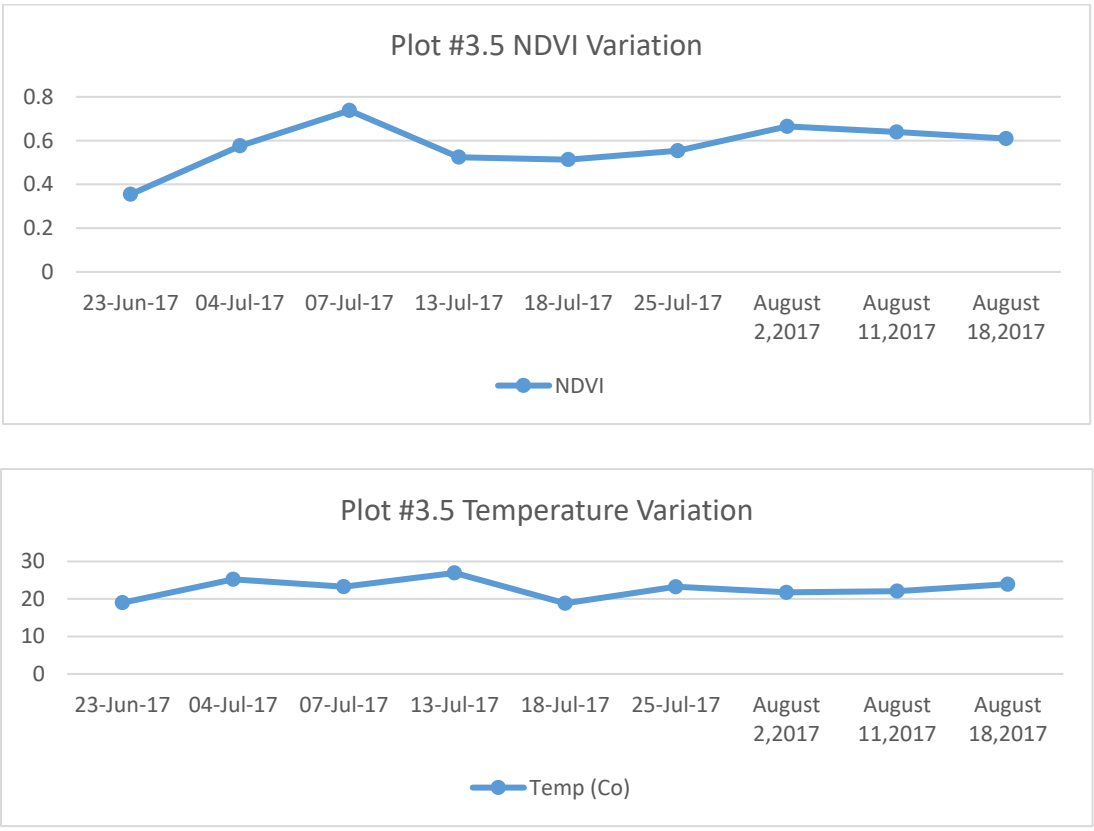

Figure D-43: Variation of NDVI and temperature of plot # 3.5 during summer 2017

Figure D-44: Plot # 3.5 on June 23

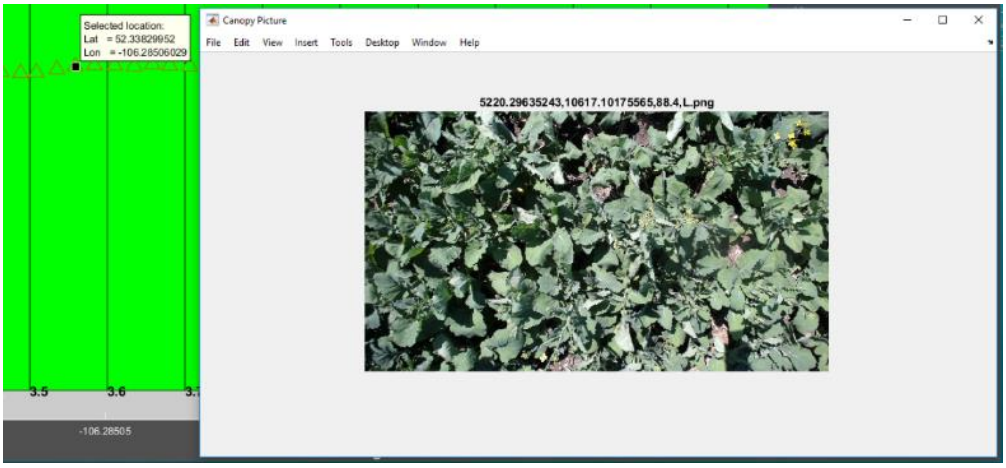

Figure D-45: Plot # 3.5 on July 4

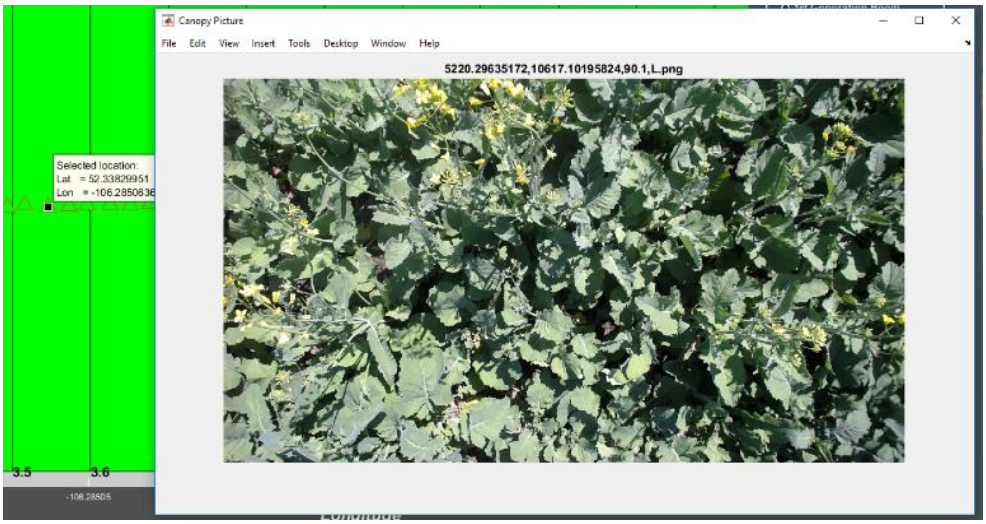

Figure D-46: Plot # 3.5 on July 7

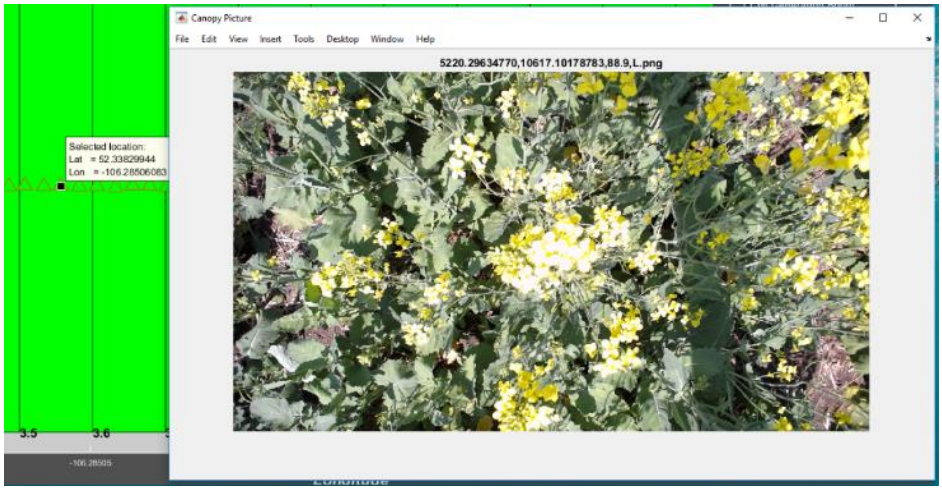

Figure D-47: Plot # 3.5 on July 13

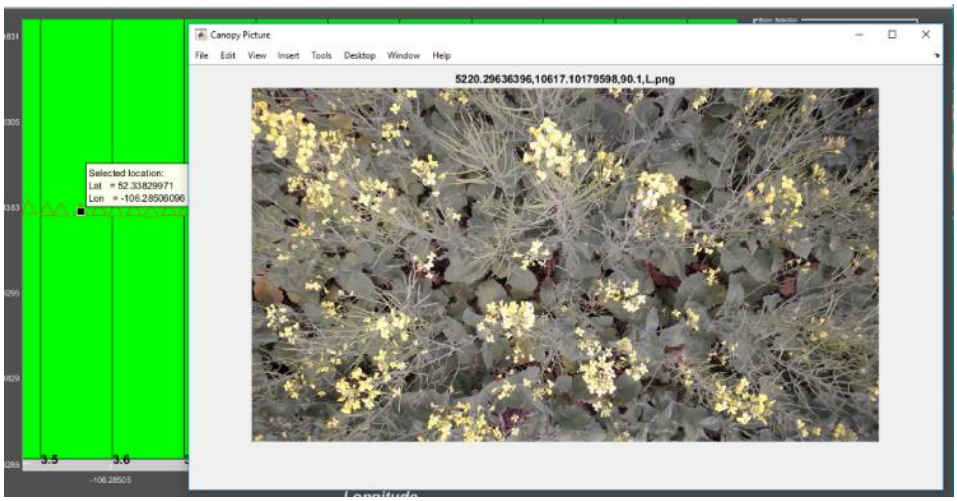

Figure D-48: Plot # 3.5 on July 18

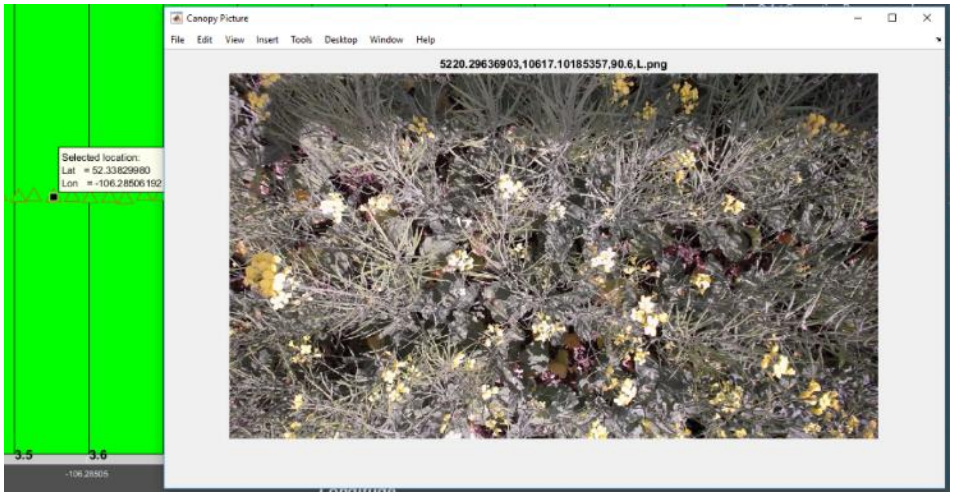

Figure D-49: Plot # 3.5 on July 25

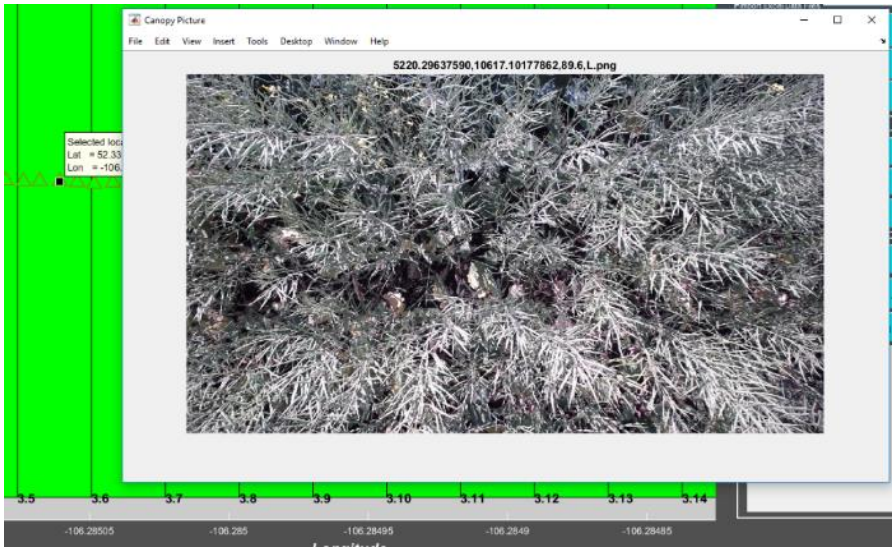

Figure D-50: Plot # 3.5 on August 2

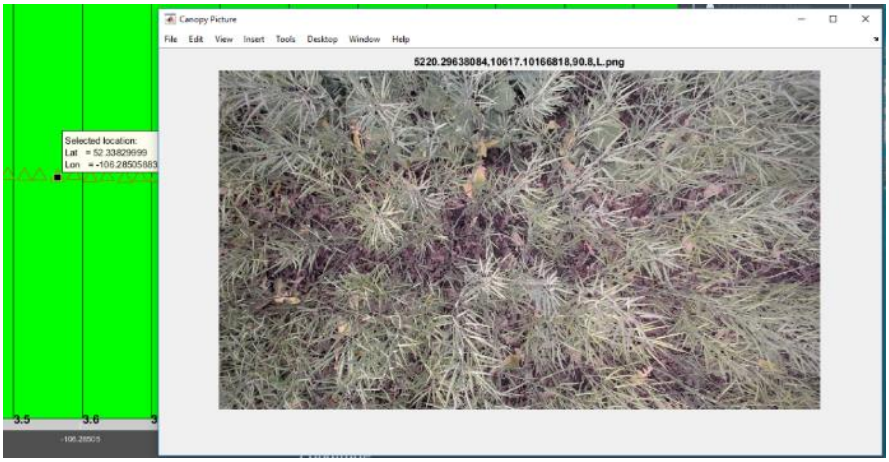

Figure D-51: Plot # 3.5 on August 11

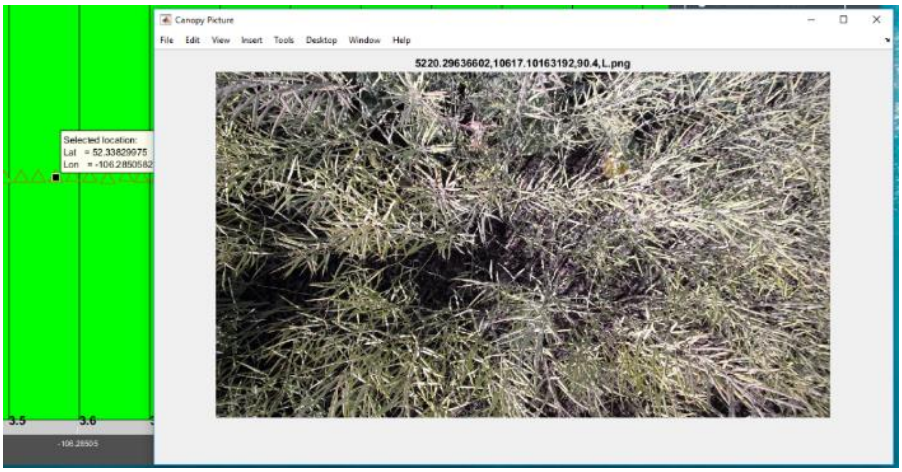

Figure D-52: Plot # 3.5 on August 18

D.9- Part of section 4-5-3-; Analyzing growth of the plot # 3.60 over summer 2017

Table D-5: Variation of NDVI and temperature of plot # 3.60 during summer 2017

Date	NDVI	Temp (C°)	Ambient Temp (C°) Ref: the weather network	Time of the data collection
June 23, 2017	0.3867	20.1	18.8	15:20 pm
July 4, 2017	0.6529	26.3	27.4	15:50 pm
July 7, 2017	0.7381	24.6	29.8	10:55 am
July 13, 2017	0.5554	26.2	29.3	14:30 pm
July 18, 2017	0.5492	20.6	22.9	14:35 pm
July 25, 2017	0.5948	24.3	25.7	14:45 pm
August 2,2017	0.6793	20.5	24.7	16:30 pm
August 11,2017	0.6350	22.2	27.1	12:05 pm
August 18,2017	0.6181	22.3	27.3	10:20 am

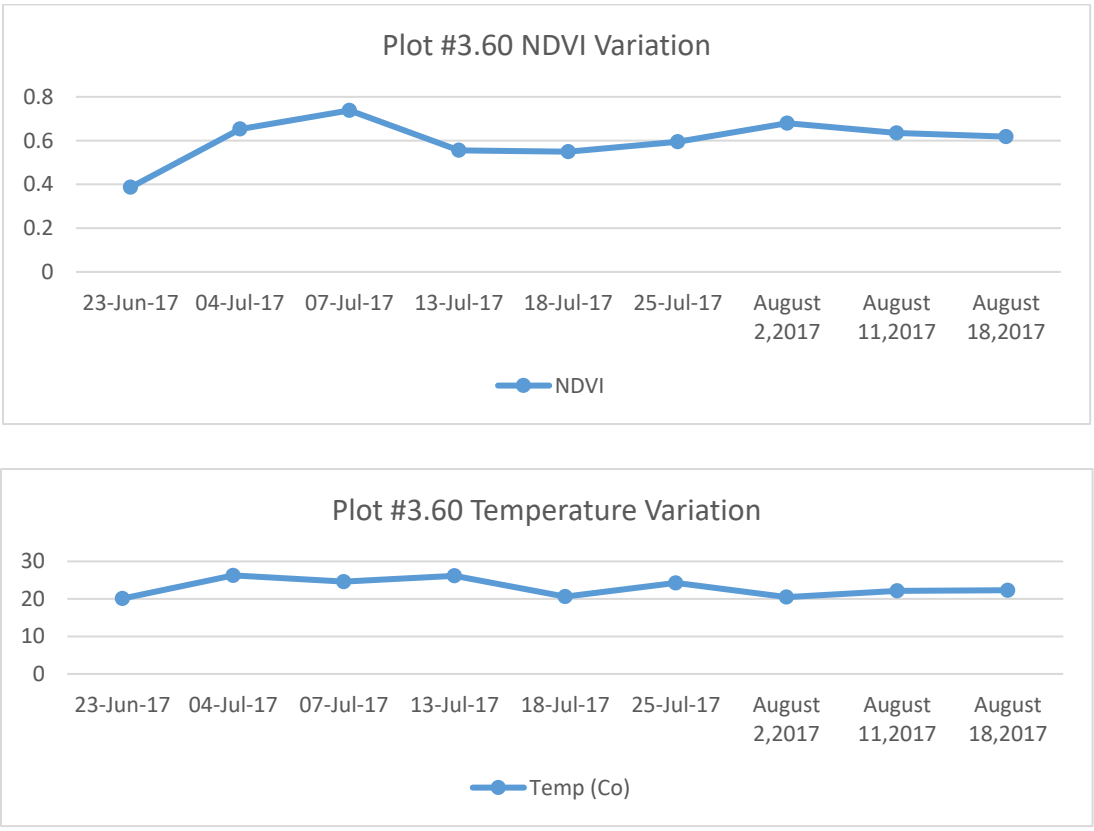

Figure D-53: Variation of NDVI and temperature of plot # 3.60 during summer 2017

Figure D-54: Plot # 3.60 on June 23

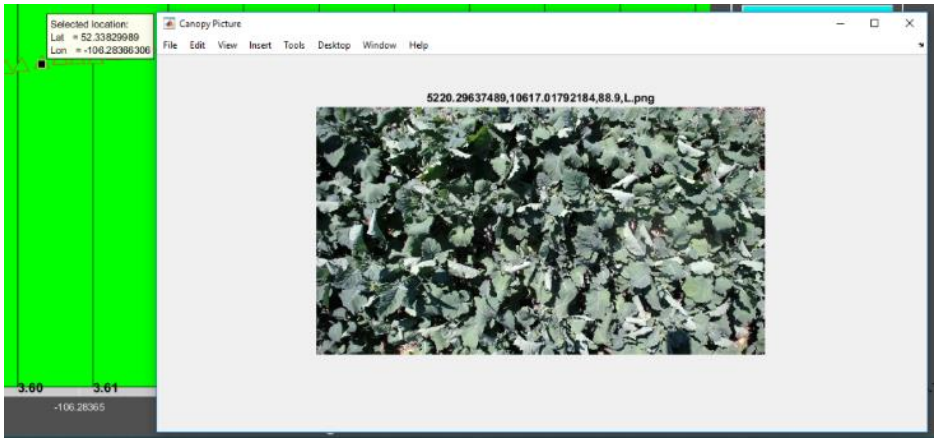

Figure D-55: Plot # 3.60 on July 4

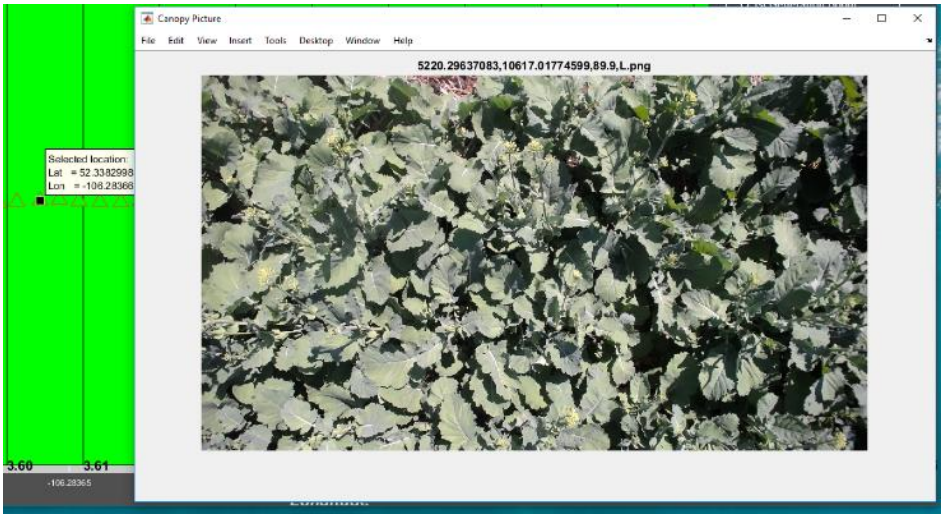

Figure D-56: Plot # 3.60 on July 7

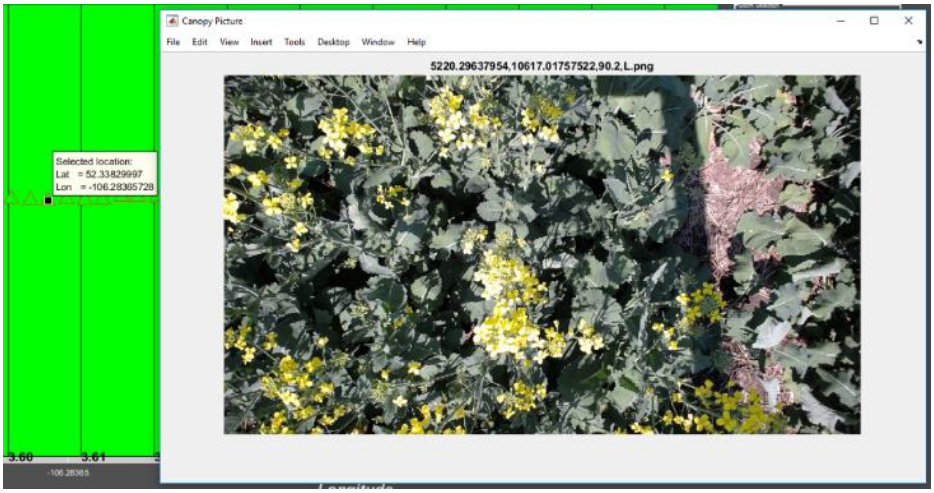

Figure D-57: Plot # 3.60 on July 13

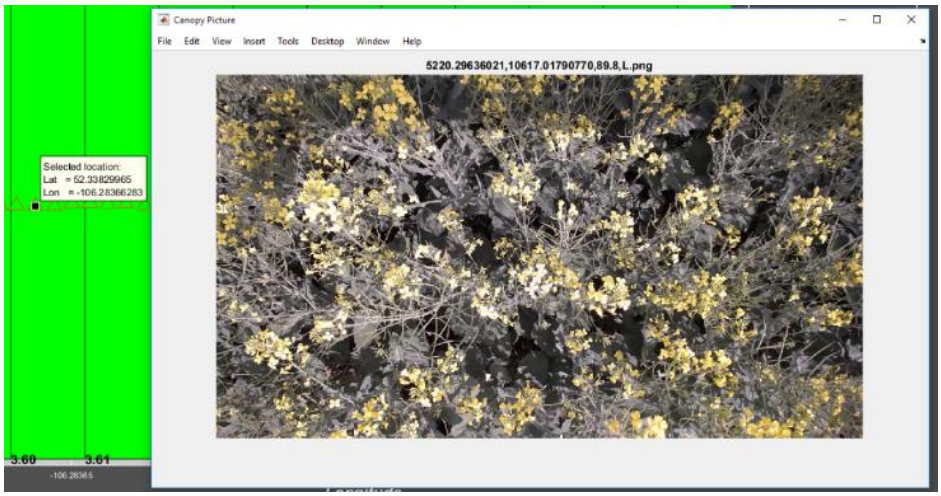

Figure D-58: Plot # 3.60 on July 18

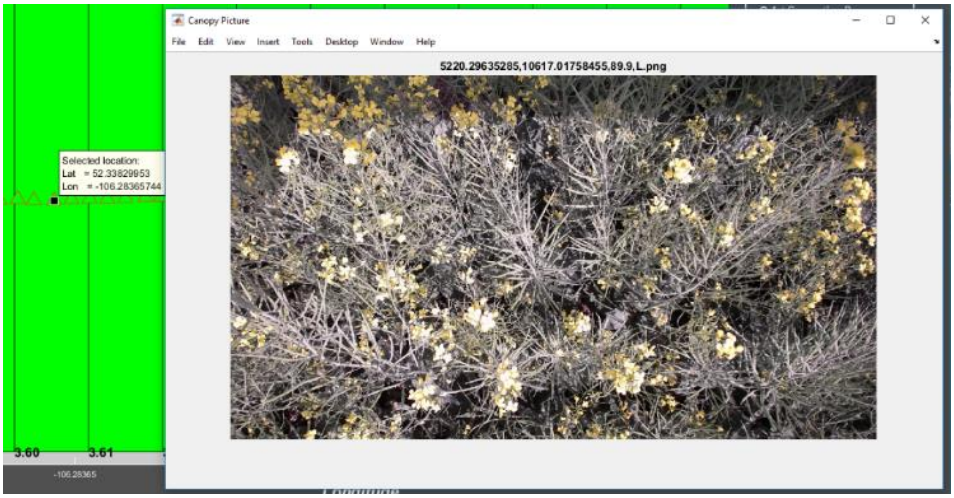

Figure D-59: Plot # 3.60 on July 25

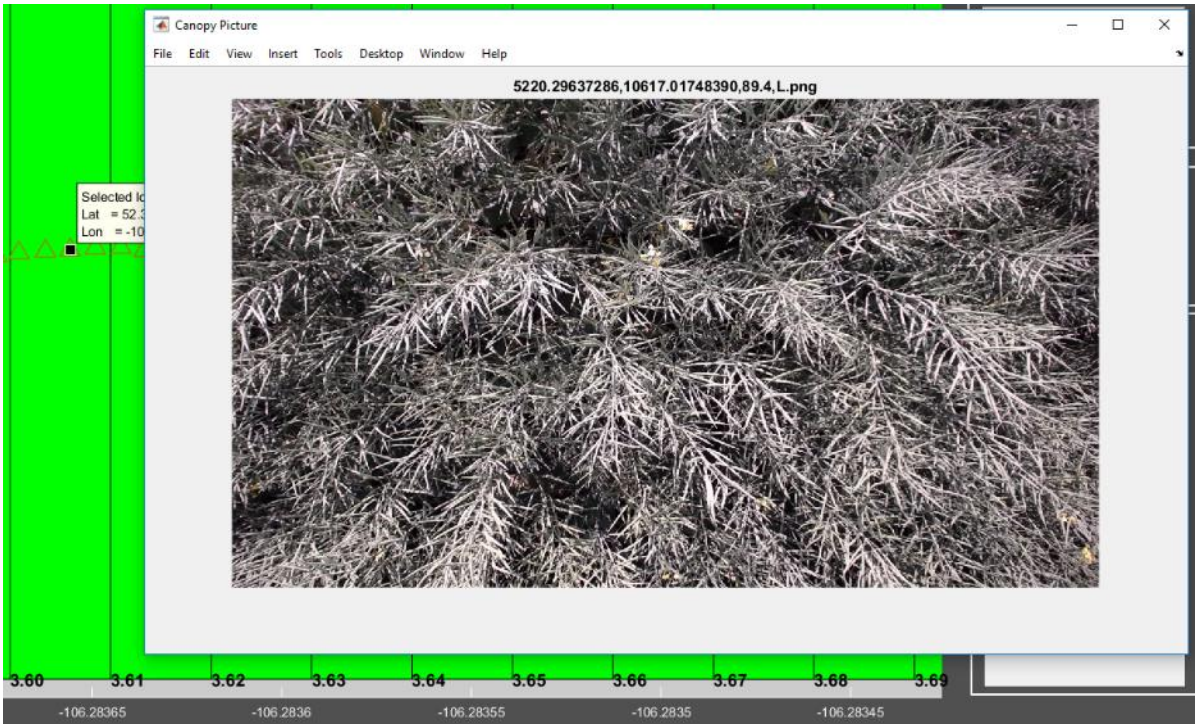

Figure D-60: Plot # 3.60 on August 2

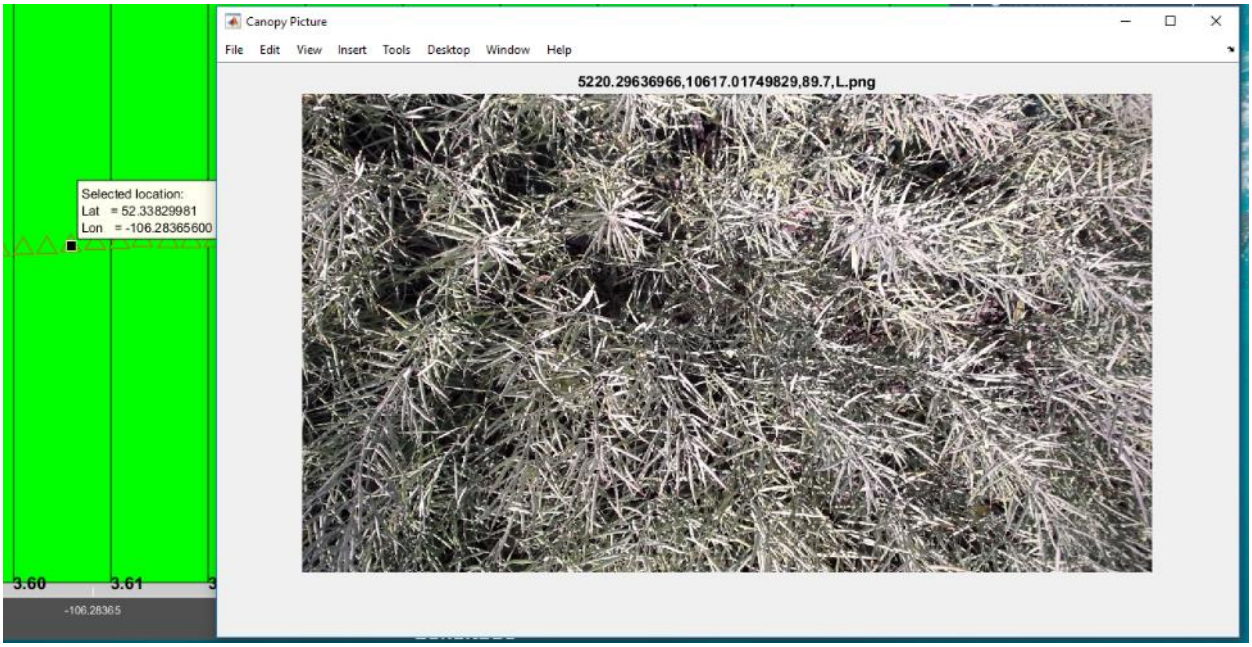

Figure D-61: lot # 3.60 on August 18

D.10- Part of section 4-5-5-; Comparing the quality of captured images by webcams and DSLR cameras for a plot based-on captured data on August 11, 2017

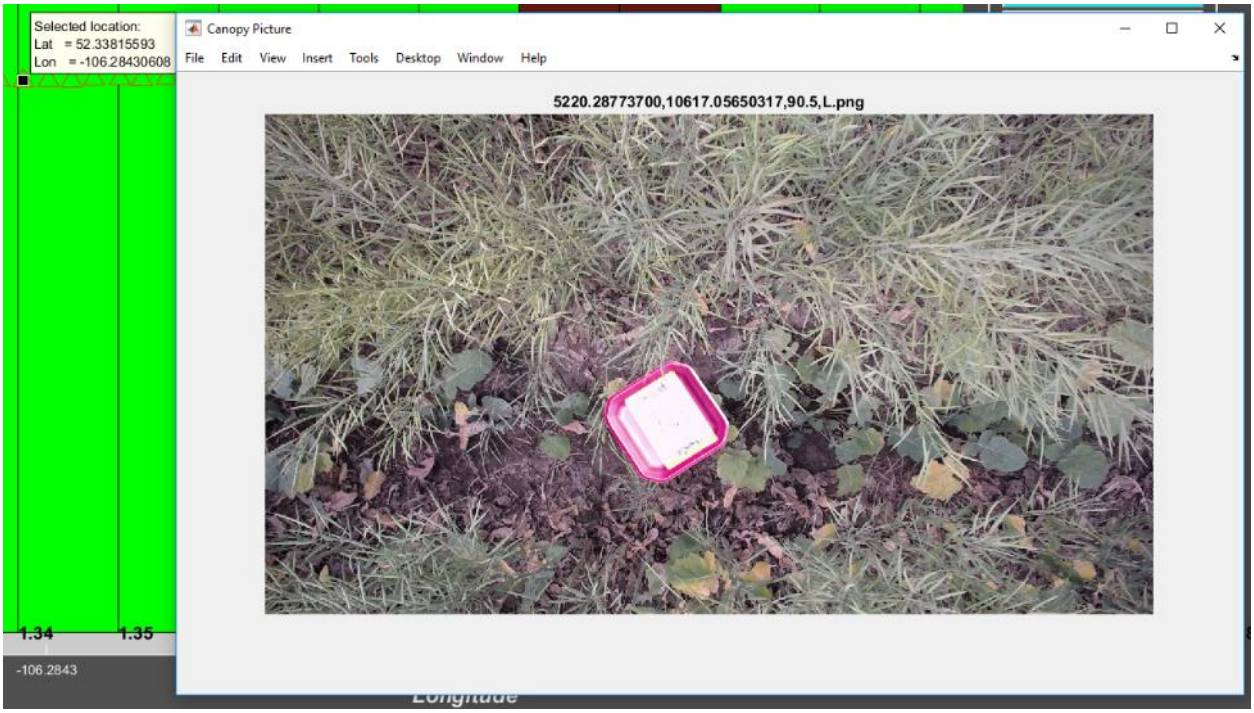

Figure D-62: Webcam Image for plot 1.34

Figure D-63: Canon Image for plot 1.34 (File name: 5220.28774360,10617.05622194,L)

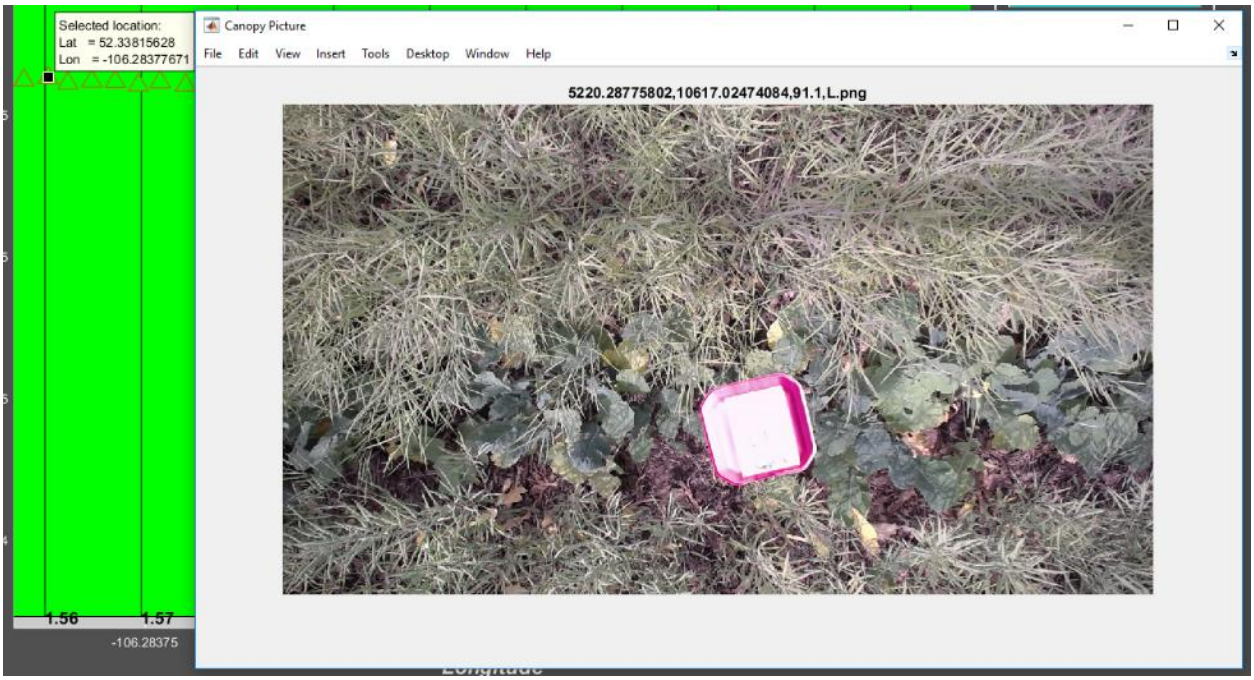

Figure D-64: Webcam Image for plot 1.56

Figure D-65: Canon Image for plot 1.56 (File name: 5220.28774079,10617.02455098,L**)**

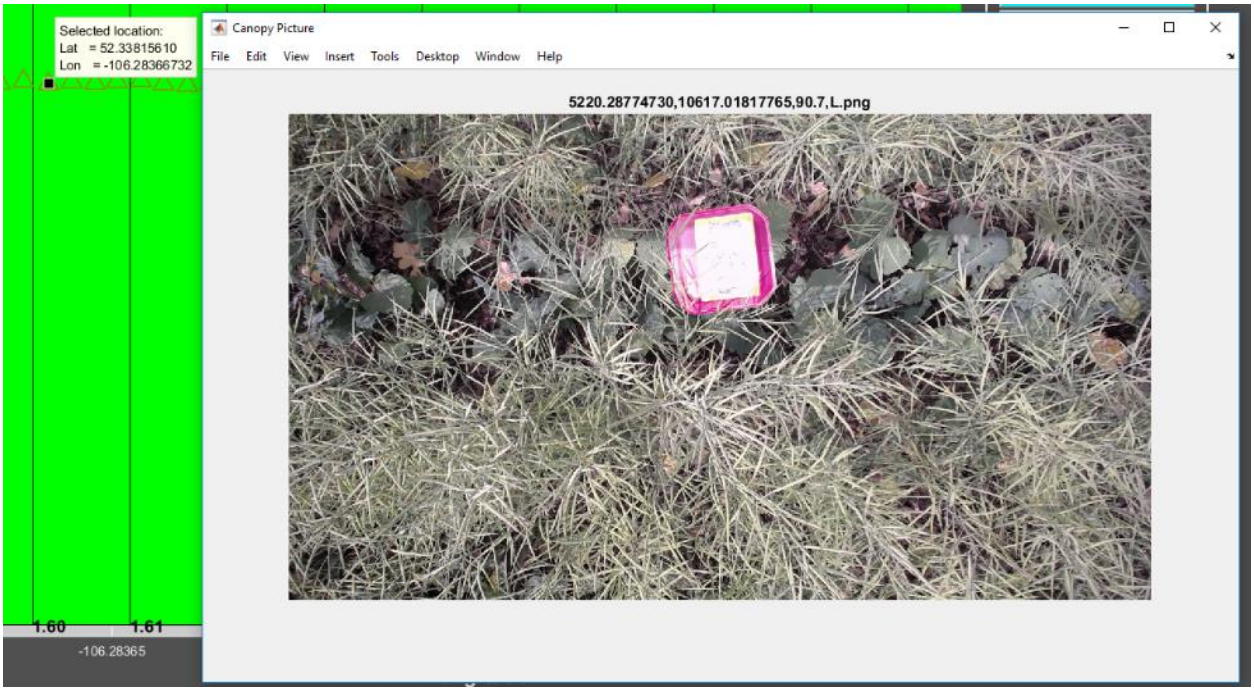

Figure D-66: Webcam Image for plot 1.60

Figure D-67: Canon Image for plot 1.60 (File name: 5220.28773359,10617.01800589,L)

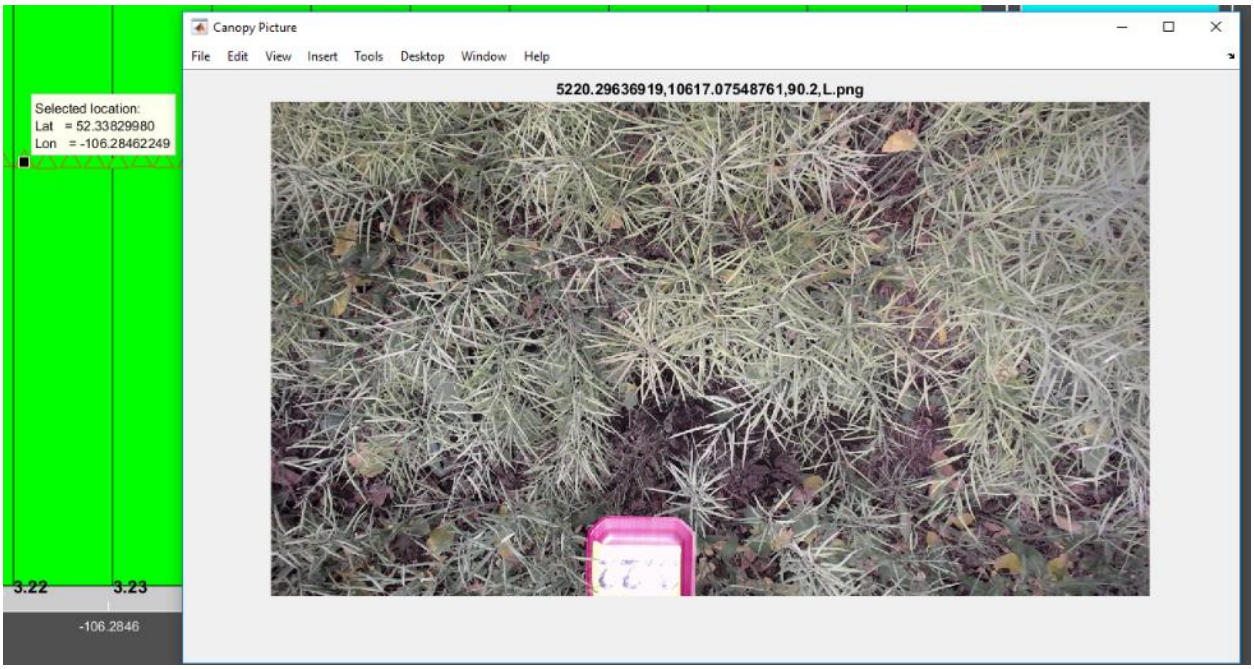

Figure D-68: Webcam Image for plot 3.22

Figure D-69: Canon Image for plot 3.22 (File name: 5220.29635659,10617.06812540,L)

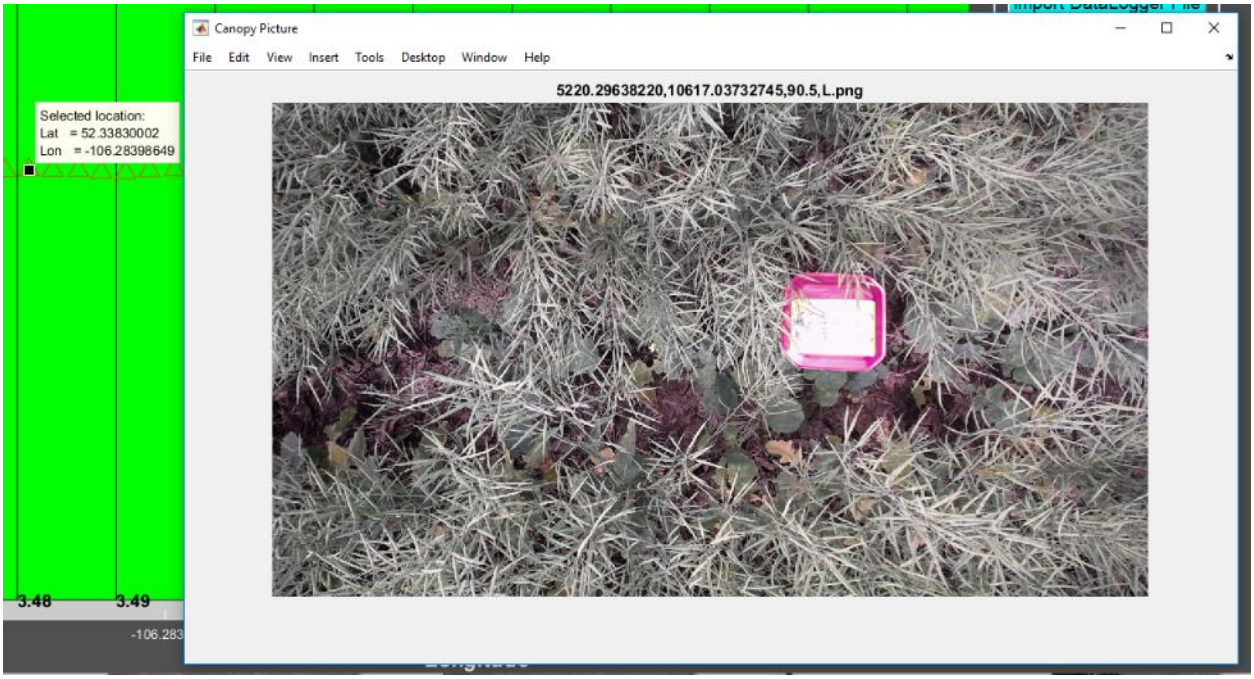

Figure D-70: Webcam Image for plot 3.48

Figure D-71: Canon Image for plot 3.48 (File name: 5220.29637584,10617.03212299,L)

D.11- Part of section 4-5-5-; Comparing the quality of captured images by webcams and DSLR cameras for a plot based-on captured data on August 18, 2017

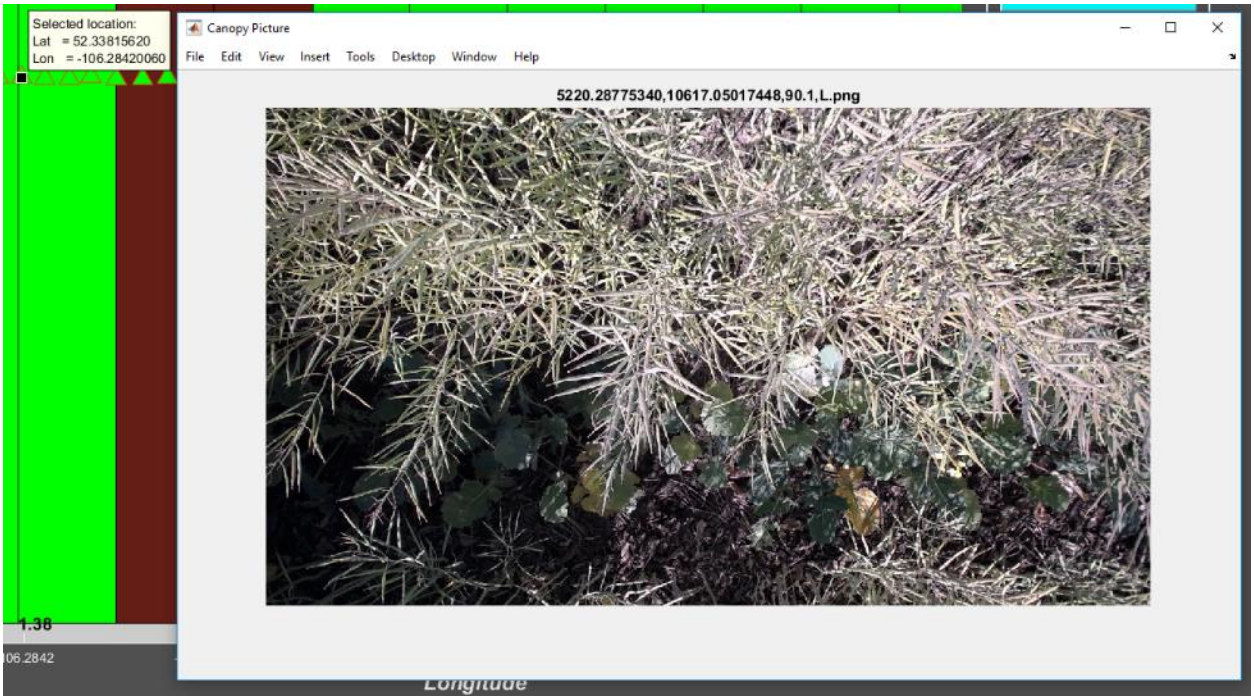

Figure D-72: Webcam Image for plot 1.38

Figure D-73: Canon Image for plot 1.38 (File name: 5220.28774061,10617.05106500,89.3,L)

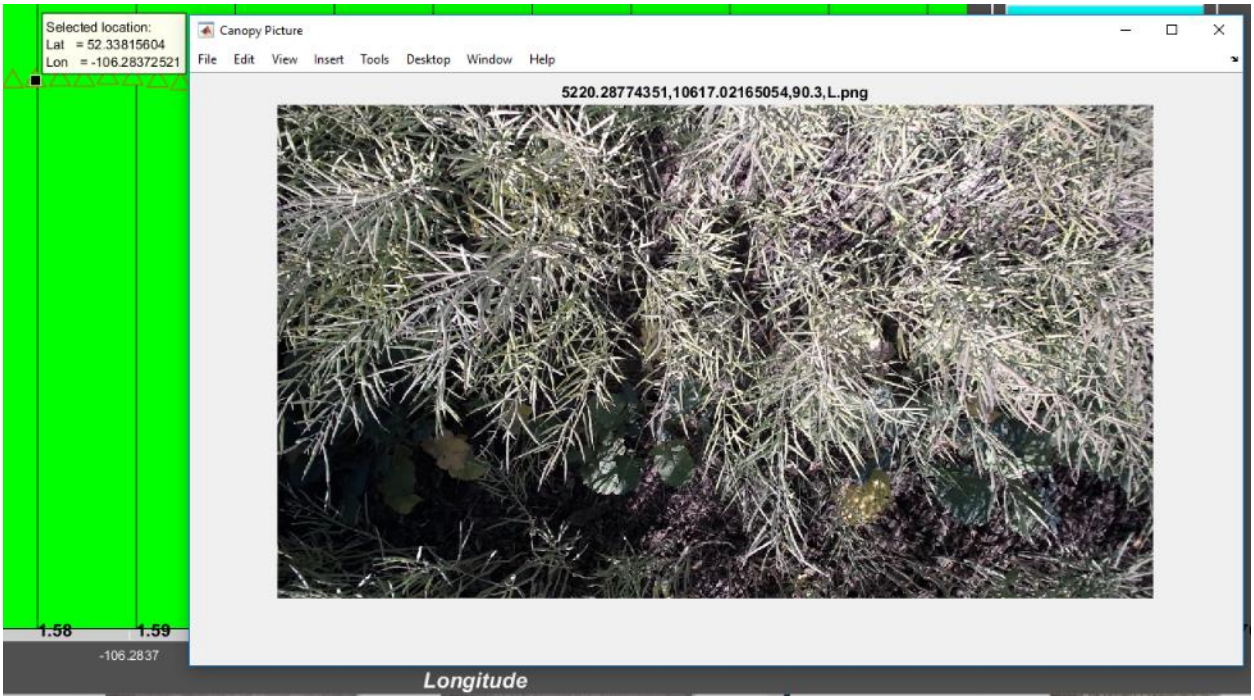

Figure D-74: Webcam Image for plot 1.58

Figure D-75: Canon Image for plot 1.58 (File name: 5220.28774653,10617.02147429,90.4,L)

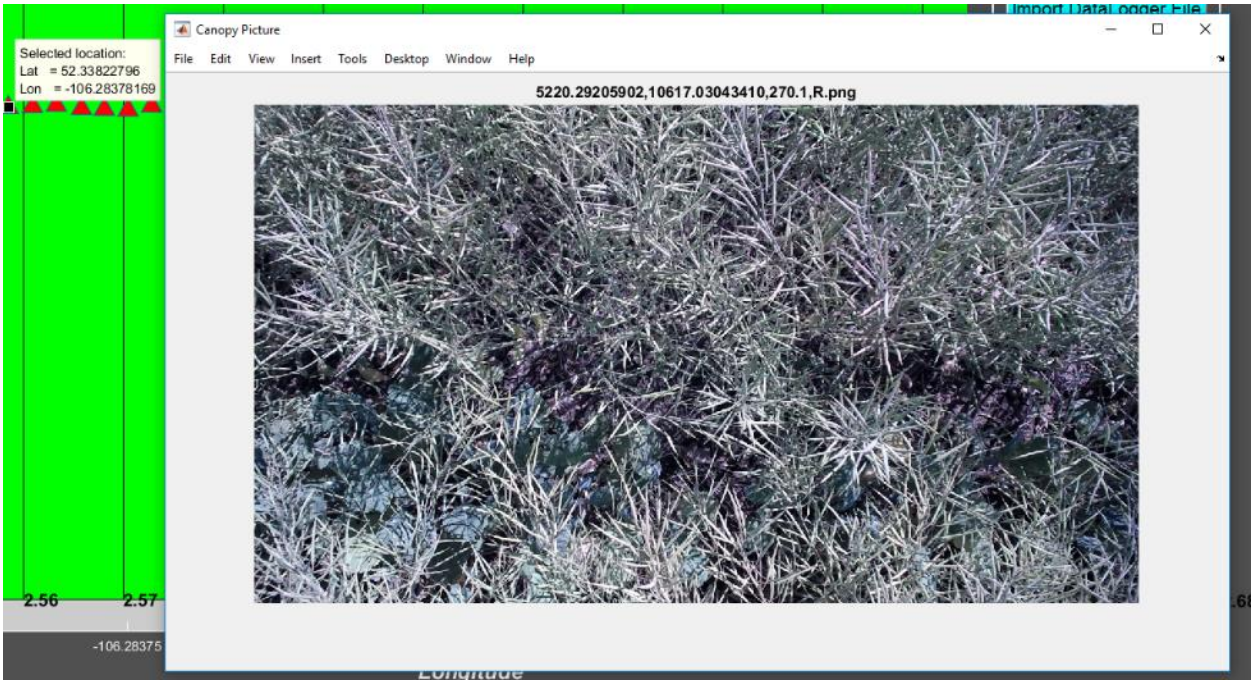

Figure D-76: Webcam Image for plot 2.56

Figure D-77: Canon Image for plot 2.56 (File name: 5220.29206255,10617.04313116,269.9,R)

APPENDIX E - Pictures of Field Tests and Developed HTPP Platform

a) b)

Figure E-1: mechanical boom in a) transportation position and b) data collection position

Figure E-2: Proposed plant phenotyping platform in action

Figure E-3: Assembling mechanical and electrical components of the proposed HTP

Figure E-4: Utilized GPS system in the proposed HTP

Figure E-5: Gathering required information about existing farm vehicles

Figure E-6: Some of team members during field experiments

APPENDIX F- Datasheet of Utilized Equipment [1]

F.1- Campbell Scientific CR3000 datalogger

The CR3000 Micrologger supports complex applications with many sensors. It is fast and powerful enough to handle extended eddy-covariance systems with full energy-balance systems. Multiple CR3000s can be configured as a network or units can be deployed individually. Designed for stand-alone operation in harsh, remote environments. The CR3000 consists of a compact, integrated package with a built-in power supply, a 128-by-64-pixel backlit graphical or eight-line numeric display, and a 16-character keyboard.

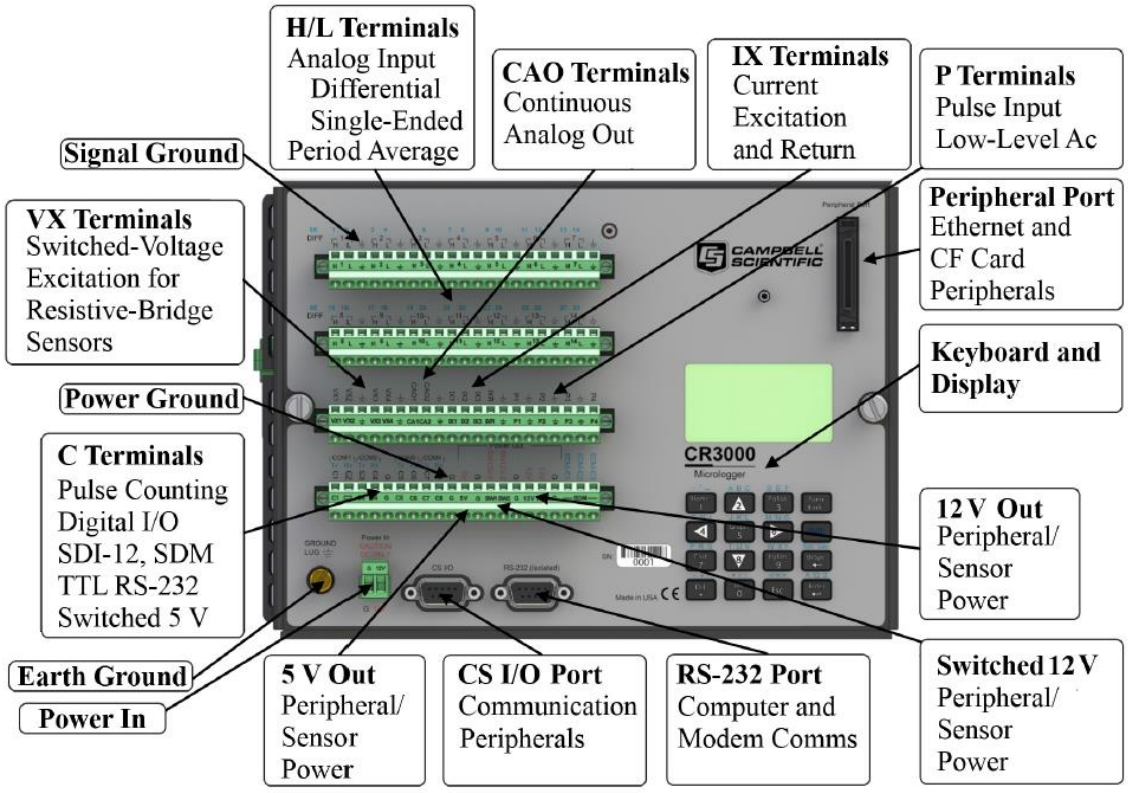

Figure F-1: Pinouts diagram for the utilized datalogger

[1] All datasheets are copied from manufacturers website or their documentations without any modification

Some of the benefits and Features are as follows:

- Ideal applications include eddy covariance, wind profiling, HVAC, weather stations, vehicle testing, air quality, process control, mesonet systems, agriculture, soil moisture, time-domain reflectometry, water quality
- Integrated keyboard and display screen let you program, manually initiate data transfers, and view data, all on site.
- Includes a current excitation channel allowing direct connection of PRTs or other sensors that use a current excitation
- Serial communications with serial sensors and devices supported via I/O port pairs
- Supports PakBus, Modbus, SDI-12, and DNP3 protocols
- Communicates via various options: TCP/IP, email, FTP, web server.
- Gas Discharge Tube (GDT) protected inputs
- 4-MB memory can be expanded with add-on memory systems.
- Flexible power and communication options make it ideal for remote locations.
- Compatible with channel expansion peripherals allowing you to expand your system
- Battery-backed clock that ensures accurate time is maintained while datalogger is disconnected from battery power
- Contains custom ASIC chip that expands pulse count, control port, and serial communications capabilities
- Program with LoggerNet, PC400, or Short Cut to fit your setup
- Collects and stores data and controls peripherals as the brain of your system

Maximum Scan Rate	100 Hz
Analog Inputs	28 single-ended or 14 differential (individually configured)
Pulse Counters	4
Switched Excitation Channels	4 voltage, 3 current
Digital Ports	Certain digital ports can be used to count switch closures. 3 SDM and 8 I/Os or 4 RS-232 COM I/O ports can be paired as transmit and receive for measuring smart serial sensors.
Continuous Analog Outputs	2
Communications/Data Storage Ports	1 CS I/O 1 RS-232 1 parallel peripheral
Switched 12 Volt	2
Input Voltage Range	±5 Vdc
Analog Voltage Accuracy	±(0.04% of reading + offset) at 0° to 40°C
Analog Resolution	0.33 μV
A/D Bits	16
Power Requirements	10 to 16 Vdc
Protocols Supported	PakBus, Modbus, DNP3, FTP, HTTP, XML POP3, SMTP, Telnet, NTCIP, NTP, SDI-12, SDM
CE Compliance Standards to which Conformity Is Declared	IEC61326:2002

Warranty	3 years
Dimensions	24.1 x 17.8 x 7.6 cm (9.5 x 7.0 x 3.0 in.) with low-profile base 24.1 x 17.8 x 11.9 cm (9.5 x 7.0 x 4.7 in.) with alkaline battery base 24.1 x 17.8 x 11.9 cm (9.5 x 7.0 x 4.7 in.) with rechargeable battery base
Weight	1.6 kg (3.6 lb) with low-profile base 3.8 kg (8.3 lb) with alkaline battery base 4.8 kg (10.7 lb) with rechargeable battery base
-NOTE-	Battery bases have different temperature ranges. The rechargeable base option has an operating temperature range of -40° to +60°C. The alkaline base option has a temperature range of -25° to +50°C.
Standard	-25° to +50°C
Extended	-40° to +85°C
Operating System Memory	2 MB flash
CPU Usage, Program Storage & Data Storage	4 MB
Typical Current Drain @ 12 Vdc in Sleep Mode	< 2 mA
Typical Current Drain @ 12 Vdc in Active	3 to 30 mA typical (without RS-232 communication) 17 to 47 mA typical (with RS-232 communication)

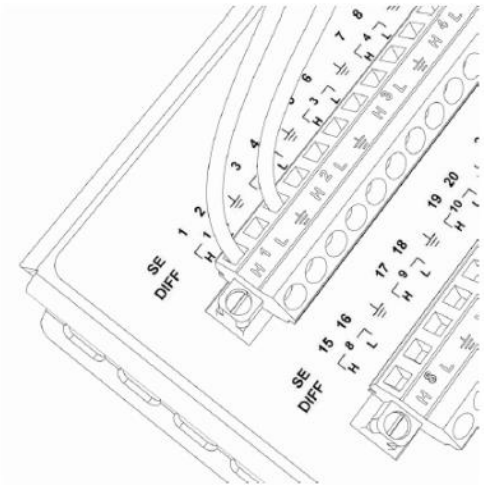

Figure F-2: Analog sensor wired to single-ended channel #1

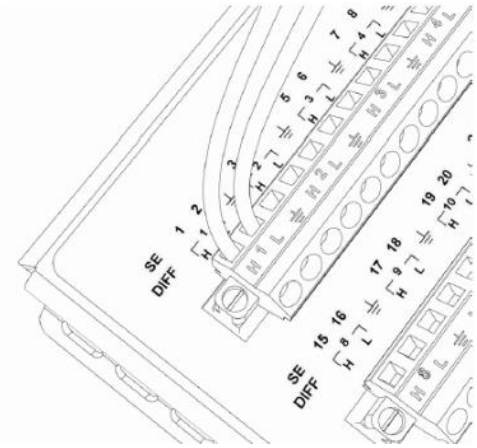

Figure F-3: Analog sensor wired to differential channel #1

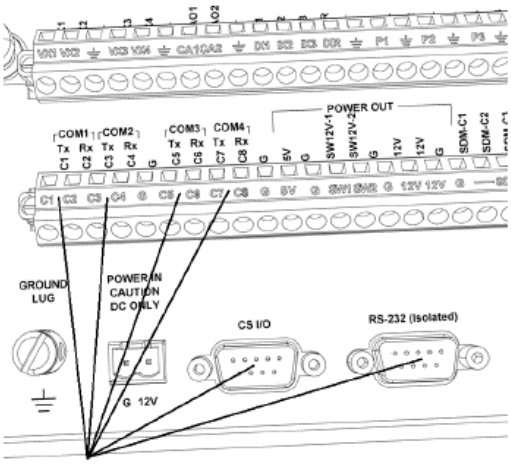

Figure F-4: Terminals Configurable for RS-232 input

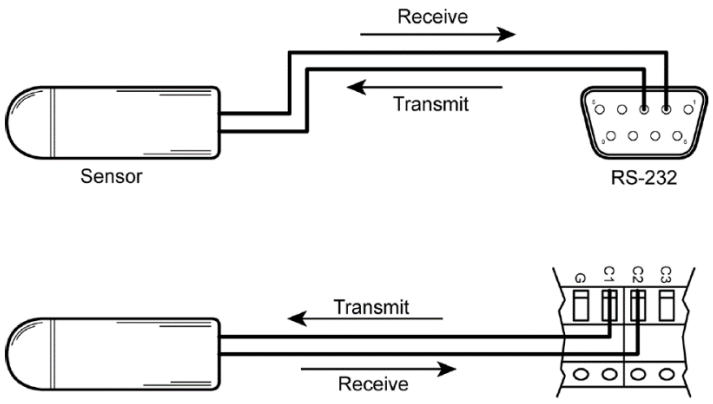

Figure F-5: Use of RS-232 and digital I/O when reading RS-232 devices

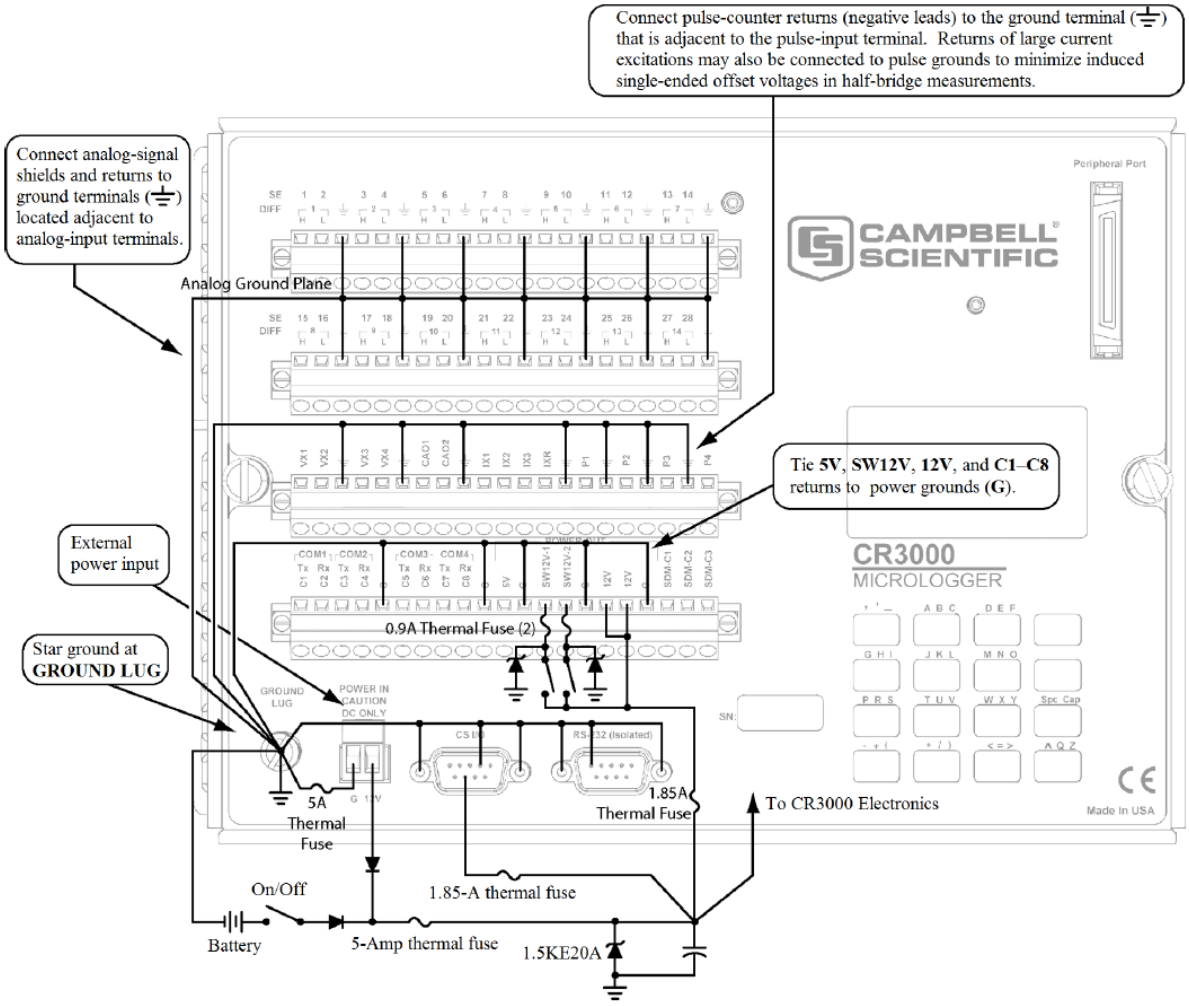

Figure F-6: Schematic of grounds

F.2- Honeywell ultrasonic distance sensor (943-F4Y-2D-1D0-180E)

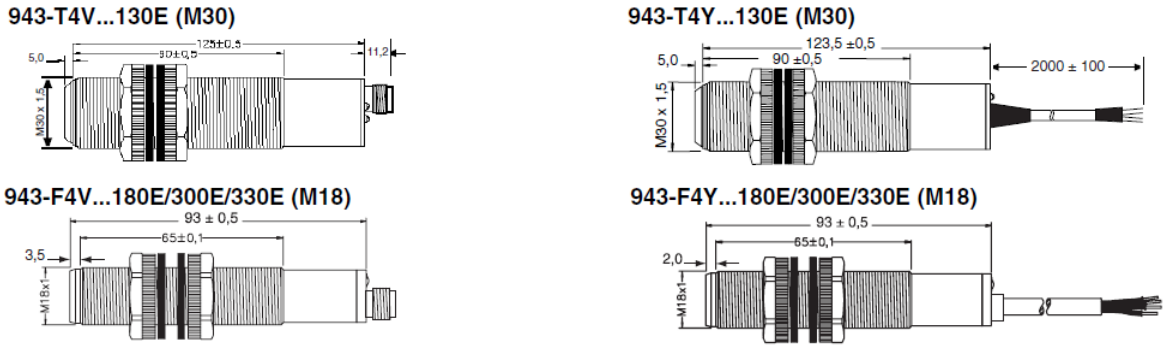

Figure F-7: Dimensions

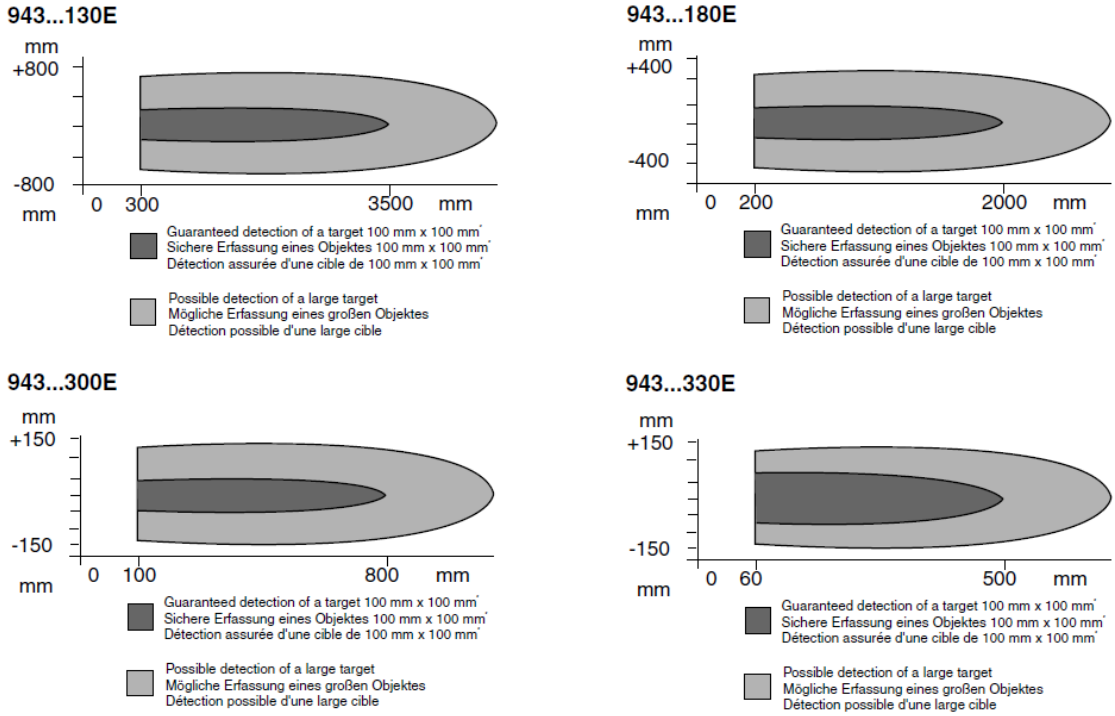

Figure F-8: Detection range

nical Data	Technische Daten	Données techniques	943…130E	943…180E	943…300E	94
tion range	Erfassungsbereich	Portée	300…3500 mm	200…2000 mm	100…800 mm	60
onse time	Ansprechzeit	Temps de réponse	400 ms	250 ms	100 ms	10
er frequency	Trägerfrequenz	Fréquence porteuse	130 kHz	180 kHz	300 kHz	33
angle (°)	Schallkegelöffnung (°)	Angle du faisceau (°)	8			
rity error	Linearitätsfehler	Erreur de linéarité	< 0.3 %			
atability	Wiederholgenauigkeit	Répétabilité	±0.2 %, ±2 mm		±0.2 %, ±1 m	
erature range	Temperaturbereich	Température de service	-15 °C to 70 °C			
erature compensation	Temperaturkompensation	Compensation en température	Yes/Ja/Oui			
ly voltage	Versorgungsspannung	Tension d'alimentation	15 Vdc to 30 Vdc			
ble minimum supply	Mögliche min. Versorgung	Min. alimentation possible	12 Vdc			
nt consumption	Stromaufnahme	Courant consommé	< 40 mA			
gue output	Analogausgänge	Sortie analogique	0…10 V (1C0) / 4…20 mA (1D0)			
t adjustment	Einstellung des Ausgangs	Réglage de la sortie analogique	Teach In			
n In 2 determines 0 V 0 V position	Teach In Der Bereich wird durch P1 and P2 festgelegt	Apprentissage La gamme est défini par les positions P1 et P2	Pin 5/Pink cable			
c housing	Kunststoffgehäuse	Boîtier plastique	M30x1.5	M18x1	M18x1	M1
ng [1]	Schutzart [1]	Etanchéité [1]	IP67			
ector	Steckeranschluss	Connecteur	M12x1 (943-F/T4V) Mating connector not in			
connection	Kabelanschluss	Connection câble	2 m (943-F/T4Y)			

Do not expose head to hot water > 50 °C or water steam.
Den Sensorkopf nicht heißem Wasser > 50 °C oder Wasserdampf aussetzen.
Ne pas mettre en contact continu la tête du capteur avec de l'eau avec une température supérieur à 50 °C ou avec de la vapeur d'eau.

Figure F-9: More technical information for the utilized ultrasonic sensors

F.3- Crop Circle ACS-430 (NDVI sensor)

SPECIFICATIONS

Sensor-to-Canopy Range: Typically 10 in (25 cm) to over 96 in (244 cm)

Field-of-View: ~40 degrees by ~8 degrees

Active Light Source: Modulated polychromatic LED array

Photodetection: Three channel silicon photodiode array

Optical Measurement Bands: 670nm, 730nm and 780nm

ELECTRICAL SPECIFICATIONS

Sample Output Rate: 10 samples per second in autosend mode

Operating Range: 0 to 50 ºC

Communication Interface: RS-485 multi-drop (bidirectional communication); RS-232 (autosend, output only)

RS-232 Serial Communication: 76800, no parity, 8 data bits,1 stop bit (38400, no parity, 8 data bits, 1 stop bit in autosend mode)

Power: 11 to 17V DC @ ~350 mA

EMC Certifications: C-Tick, CE, ISO 14982

MECHANICAL SPECIFICATIONS

Enclosure: Injection molded polycarbonate

Environmental: IP68 for dust and water resistance

Weight: 0.9 lb (430 gm)

Sensor Mount: (2) M6 X 1 threaded holes in base of sensor spaced 1.25 in (3.18 cm)

Dimensions: Width 3.5 in (8.9 cm), Length 7.9 in (20.1 cm), Height 1.9 in (4.8 cm)

Serial/Power Connector: Twelve pin Deutsch, O-ring sealed

ACCESSORIES AND SYSTEM PACKAGES

Crop Circle ACS-430 Handheld System includes: Crop Circle ACS-430, GeoSCOUT X, extension pole apparatus, cables, storage case, charger and user's guide

Crop Circle ACS-430 Mapping System includes: Crop Circle ACS-430, GeoSCOUT X, cables, storage case, mounting plate and user's guide

F.4- Apogee SI_131 IR Thermometer

Analog and digital output options are available. Analog versions include un-amplified and amplified voltage outputs. Digital versions include SDI-12 and ModBus communication protocols. Sensors are also available attached to a hand-held meter with digital readout. Typical Applications are plant canopy temperature measurement for use in plant water status estimation, road surface temperature measurement for determination of icing conditions, and terrestrial surface (soil, vegetation, water, snow) temperature measurement in energy balance studies.

	SI-111	SI-121	SI-131	SI-1H1	SIF-111	SIF-121	SIF-1H1	SI-411	SI-421	SI-431	SI-4H1
Analog Model Output (Difference between Target and Detector)	60 µV per C	40 µV per C	20 µV per C	40 µV per C	15 µV per C	10 µV per C	10 µV per C	-	-	-	-
Input Voltage Requirement Thermistor	2500 mV excitation (typical, other voltages can be used)							-	-	-	-
Analog Output from Thermistor	0 to 2500 mV (typical, depends on input voltage)							-	-	-	-
Digital Input Voltage Requirement	-							4.5 to 24 V DC with current drain of 1.1 mA (quiescent) and 6 mA (transmitting)			
Calibration Uncertainty (-20 to 65 C), when target and detector ΔT are <20 C	0.2 C		0.3 C	0.2 C	0.2 C		0.2 C	0.2 C		0.3 C	0.2 C
Calibration Uncertainty (-40 to 80 C), when target and detector ΔT are >20 C	0.5 C		0.6 C	0.5 C	0.5 C		0.5 C	0.5 C		0.6 C	0.5 C
Measurement Repeatability	Less than 0.05 C										
Long-term Drift	Less than 2 % change in slope per year when germanium filter is maintained in clean condition										
Response Time	0.6 s, time for detector signal to reach 95 % following a step change				0.2, time for detector signal to reach 95 % following a step change			0.6 s, time for detector signal to reach 95% following a step change			
Field of View	22° half angle	18° half angle	14° half angle	32° horizontal half angle; 13° vertical half angle	22° half angle	18° half angle	32° horizontal half angle; 13° vertical half angle	22° half angle	18° half angle	14° half angle	32° horizontal half angle; 13° vertical half angle
Spectral Range	8 to 14 µm; atmospheric window										
Operating Environment	-55 to 80 C; 0 to 100 % relative humidity (non-condensing)										
Dimensions	23 mm diameter, 60 mm length										
Cable	5 m of four conductor, shielded, twisted-pair wire; additional cable available in multiples of 5 m; santoprene rubber jacket (high water resistance, high UV stability, flexibility in clod conditions); pigtail lead wires										
Mass	190 g (with 5 m of lead wire)										
Warranty	4 years against defects in materials and workmanship										

Figure F-10: More technical information of the utilized IR thermometers

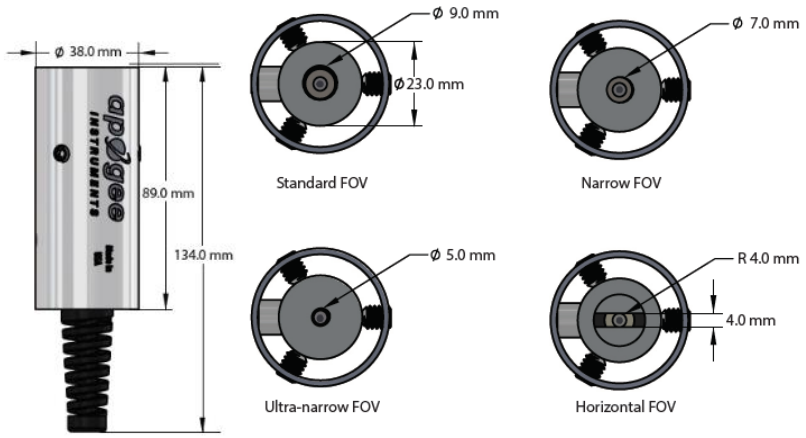

Figure F-11: Dimentions

Spectral response of SI series infrared radiometers. Spectral response (green line) is determined by the germanium filter and corresponds closely to the atmospheric window of 8 -14 μm, minimizing interference from atmospheric absorption/ emission bands (blue line) below 8 μm and above 14 μm. Typical terrestrial surfaces have temperatures that yield maximum radiation emission within the atmospheric window, as shown by the blackbody curve for a radiator at 28 C (red line).

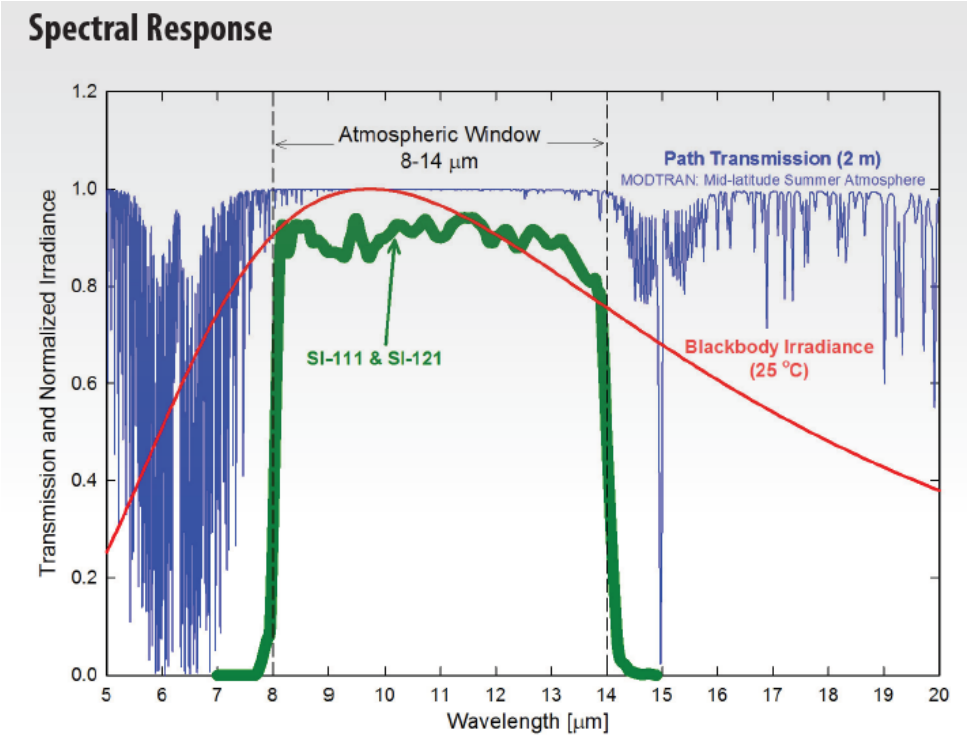

Figure F-12: Spectral response of SI thermometer

F.5- Trimble TMX-2050 GPS display

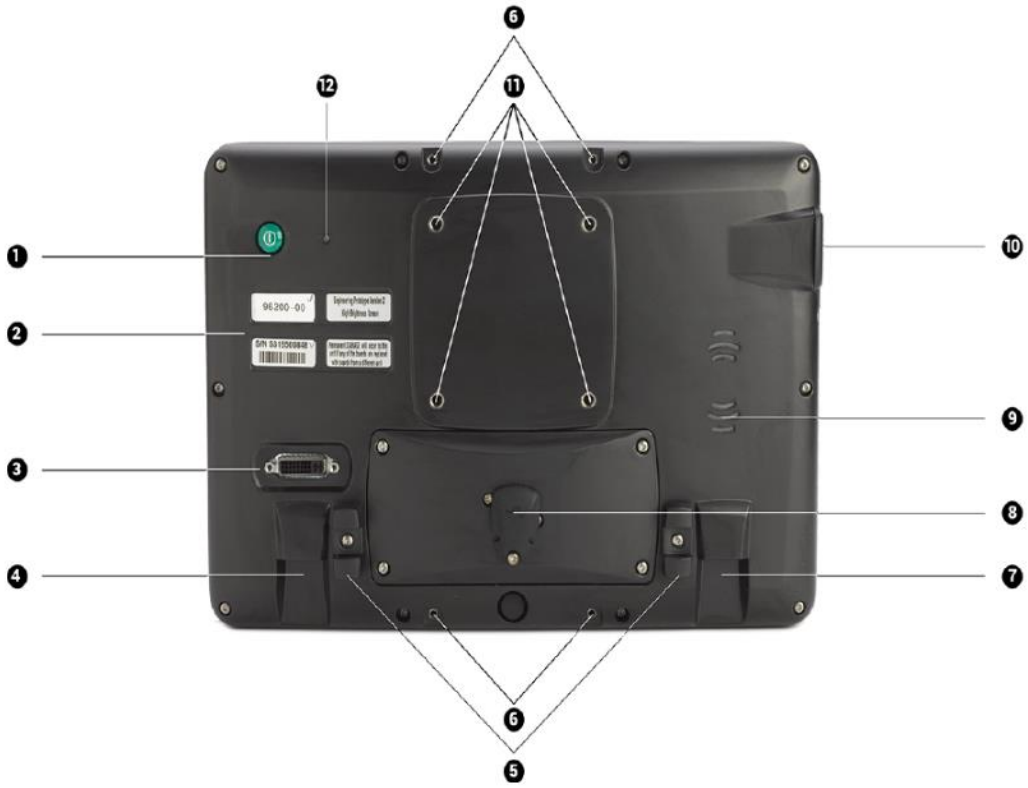

Figure F-13: Back view of the utilized GPS display unit

Item	Name	Explanation
❶	Power button	Powers the TMX-2050 display on or off
❷	Labels with part number and serial number	N/A
❸	Port: DVI / HDMI	For future capability
❹	Jack: TM-200 Module (RJ45)	Socket for connecting to the TM-200 Module
❺	Cable brackets	Holds Trimble Ethernet cables to prevent cable strain
❻	Interior bolts	Location for mounting Field IQ switch box
❼	Jack: CAN (RJ11)	For future capability
❽	Port: USB (rear) with cover	Socket for USB drive to transferring data to and from the TMX-2050 display

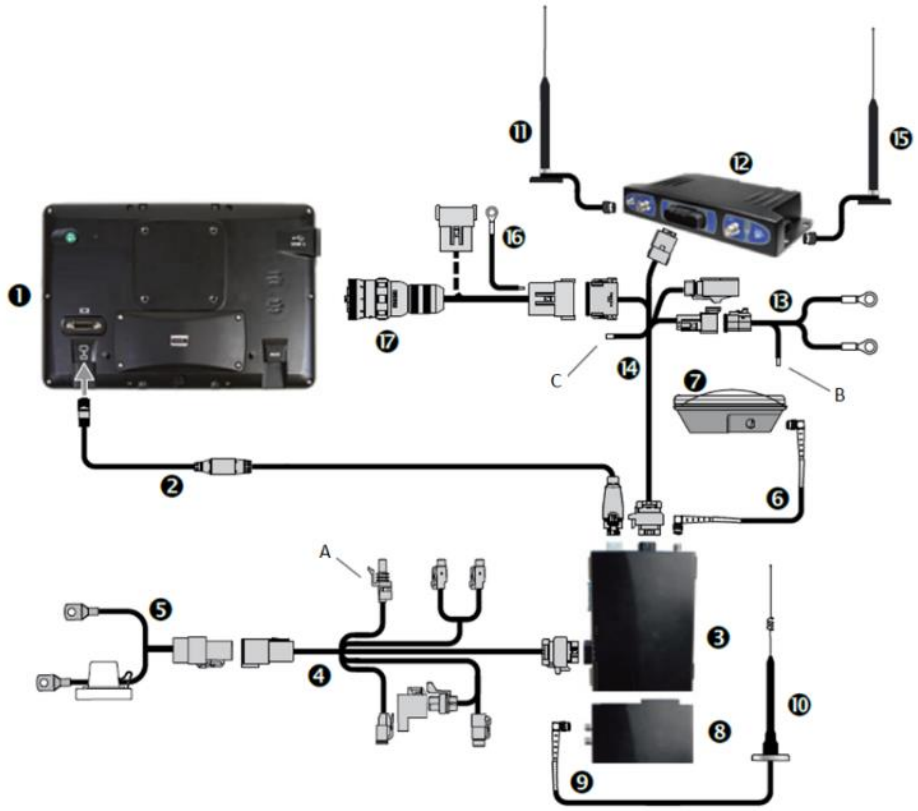

Figure F-14: Wiring diagram for the utilized GPS system

Item	Description	Trimble Part Number
❶	TMX-2050 display and mounting hardware	96700-00
❷	TM-200 Module to TMX-2050 display cable	93843
❸	TM-200 Module	95060-00
❹	DTP to TM-200 Module cable **A**: To vehicle ignition.	92676
❺	Power to DTP cable	92905
❻	GNSS antenna to TM-200 Module cable	50449
❼	AG25 GNSS antenna and mounting hardware	77038-01
❽	AG-815 integrated radio	95080-xx

Item	Description	Trimble Part Number
❾	Radio antenna cable	62120
❿	RTK radio antenna	24253-44 / 24253-46 / 22882-10
⓫	Cellular antenna	72122 and 51227
⓬	DCM-300 modem	80632-xx
⓭	DCM-300 modem to power cable **B**: Connect to ignition source.	94267
⓮	DCM-300 modem to TM-200 Module cable **C**: Connect to chassis ground.	94267
⓯	WiFi antenna for DCM-300 modem	83700-05
⓰	Vehicle Manager CAN adapter, Fleet productivity work input, DCM-300 modem to R terminal on alternator (optional, use if CAN does not have engine hours)	86995 / 87754 / 90147